



**Uniwersytet
Gdański**

Wydział Biologii
Uniwersytetu Gdańskiego

mgr Estera Rintz

**Terapie molekularne w mysich modelach
metabolicznych chorób z grupy
mukopolisacharydoz**

Praca przedstawiona
Radzie Dyscypliny Nauki biologiczne Uniwersytetu Gdańskiego
celem uzyskania stopnia doktora
w dziedzinie nauk ścisłych i przyrodniczych
w dyscyplinie nauki biologiczne

promotorzy:
prof. dr hab. Grzegorz Węgrzyn
Katedra Biologii Molekularnej, Wydział Biologii, Uniwersytet Gdański
prof. dr n. med. Shunji Tomatsu
Szpital dziecięcy Nemours, Wilmington, Delaware, Stany Zjednoczone

GDAŃSK 2024

Wydział Biologii
Uniwersytetu Gdańskiego

MSc. Estera Rintz

Molecular Therapies for Mucopolysaccharidosis in Mouse Models

PhD thesis

presented to the Biological Sciences Discipline Board of the University of
Gdańsk in order to obtain a doctoral degree in the field of exact and natural
sciences in the discipline of biological sciences

supervisors:

Grzegorz Węgrzyn, PhD

Molecular Biology Department, Faculty of Biology,
University of Gdansk

Shunji Tomatsu, MD, PhD

Nemours Children Hospital, Wilmington, Delaware, United States

GDAŃSK 2024

Table of Contents

Summaries.....	5
Summary in English.....	5
Streszczenie po polsku.....	12
References.....	19
Manuscripts included in PhD thesis.....	22
Article no. 1.....	23
Author Contribution to Article no.1.....	34
Article no. 2.....	19
Author Contribution to Article no. 2.....	58
Article no. 3.....	65
Author Contribution to Article no. 3.....	85
Article no. 4.....	90
Author Contribution to Article no. 4.....	112
Article no. 5.....	118
Author Contribution to Article no. 5.....	146
Funding.....	153
Academic achievements.....	154
Scientific articles.....	154
Book chapters.....	158
Scientific Congress.....	158
Research projects as a Primary Investigator.....	160

Summary in English

Mucopolysaccharidoses (MPS) belong to the group of hereditary metabolic diseases where, as a result of a mutation in a gene encoding an enzyme responsible for the breakdown of compounds from the mucopolysaccharide group (glycosaminoglycans, GAG), these compounds accumulate in the cell [1,2]. The process of their degradation in a healthy organism is a sequence reaction of several enzymes, however, when one of them does not function properly, the reaction stops and GAG(s) accumulate(s) in the cells. Depending on which enzyme is inactive, there are 13 types and subtypes of MPS. Many symptoms are common to all or most types and subtypes of MPS, but the most severe are those related to the central nervous system (CNS) and the skeletal system [3]. In both cases, the currently available therapies are not able to overcome the symptoms of the CNS and those related to the skeletal system.

The most commonly used MPS therapy is enzyme replacement therapy (ERT), which uses the active form of the missing enzyme. However, the supply of the missing enzyme is not sufficient in the case of MPS types whose symptoms are expressed in CNS (such as MPS III), because the enzyme does not cross the blood-brain barrier [4,5]. There are also other limitations associated with ERT, including a short half-life of the enzyme, high cost of the therapy, limited impact on avascular tissues and organs, weekly infusions for lifetime [6,7]. Moreover, even though ERT for non-neuronopathic MPS IVA has been approved, it has a limited effect on skeletal abnormalities, which is one of the main symptoms of the disease [8]. Therefore, research into alternative therapeutic approaches for these types of MPS is highly desirable.

One alternative strategy is accelerating the degradation of GAG(s) through autophagy, a lysosomal process that breaks down unnecessary or abnormal macromolecules [9]. Recent discoveries suggested GAGs can be targeted by autophagy, potentially offering a new treatment for diseases involving polysaccharide storage [10]. A key question is how

autophagy can degrade GAGs when a crucial enzyme is impaired. While complete enzyme absence is challenging, many MPS cases have some residual enzyme activity. Enhancing autophagy could boost this residual activity, improving GAG degradation. Additionally, non-specific hydrolases, though low in abundance, might aid GAG removal if autophagy is stimulated. Even if full GAG clearance is not possible due to enzyme deficiencies, degrading secondary storage materials can still benefit patients, as necessary enzymes are present in MPS cell lysosomes [11-Article no.1].

The potential drug for MPS IIIB should also cross the blood-brain barrier and be safe in long-term therapy. It seems that one of the polyphenols, resveratrol, may meet these requirements. Grapes, peanuts, mulberries and black currants are particularly rich in resveratrol. It has multiple biological functions, such as anti-inflammatory, antioxidant and neuroprotective effects. It is a compound that has been widely studied and activates the process of macromolecule degradation through several mechanisms [12]. Due to its pleiotropic mechanism of autophagy induction, ability to cross the blood-brain barrier, and safety profile, resveratrol is a promising candidate for treating neuronopathic forms of MPS [11-Article no.1]. Resveratrol induces autophagy through multiple pathways, including activation of PTEN, AMPK, FoxOs, and TFEB, as well as inhibition of mTOR kinase and the Bcl-2-encoding gene. These mechanisms have been detailed in Rintz et al. 2019 [11-Article no.1]. Thus, I treated MPS IIIB mouse model with resveratrol to improve behavior with reduction in accumulated GAG [13-Article no.2].

A promising alternative therapy for MPS IVA patients is gene therapy. ERT with elosulfase alfa has limited effects on bone growth in MPS IVA (Morquio A syndrome) patients. Hematopoietic stem cell transplantation (HSCT) may offer more benefits, such as improved heart function, bone mineral density, and joint laxity [14], but it also has significant limitations: risk of mortality and morbidity, difficulty in finding donors, post-transplant complications, and

limited impact on bone growth [14,15]. Both ERT and HSCT rely on cross-correction via the mannose-6-phosphate receptor pathway, where lysosomal enzyme-producing cells help enzyme-deficient ones [16]. However, this method struggles to penetrate bone cartilage effectively [15]. Thus, there is a high demand for bone-penetrating agents to treat avascular bone lesions and induce ossification in MPS IVA patients.

C-type natriuretic peptide (CNP) has shown a promise in inducing bone growth by activating the natriuretic peptide receptor B (NPR-B) on chondrocytes [17]. Stimulation of the intracellular molecule cGMP production by CNP activates multiple pathways, resulting in bone growth (for details see ref. [18-Article no.3]). Despite its potential, natural CNP has a short half-life, necessitating frequent injections [19]. Thus, I aimed to improve bone pathology in MPS IVA by combining gene therapy of a small peptide to stimulate growth [20-Article no.4]. With bone growth induction, the next step was to combine two transgenes (*GALNS* and *NPPC*) in AAV system to improve bone growth with reducing GAG accumulation in other tissues [21-Article no.5].

The purposes of this PhD thesis were:

- 1) Determination of the role of resveratrol and the exact molecular mechanism of its action during long-term studies with the MPS IIIB mouse model.**
- 2) Development of an innovative combination gene therapy to improve bone changes in the mouse MPS IVA model.**

Objective 1 - Determination of the role of resveratrol and the exact molecular mechanism of its action during long-term studies effects in with the MPS IIIB mouse model.

Both wild-type and MPS IIIB mice were tested in two groups where water or resveratrol was administered every day for the course of 30 weeks. To test the effectiveness of resveratrol several tests were performed. Behavioral tests were performed. To measure hyperactivity of animals locomotor activity test was performed. Open field test was performed to measure

anxiety in the mouse model. Biochemical and molecular tests were also performed to assess the effects of resveratrol on cells from various organs, especially the brain and liver, where GAG accumulation is at its highest. Urine GAG concentrations (samples were taken at 5, 10, 20 and 30 weeks of age) with Blyscan test. The effect of resveratrol on specific protein levels in terms of the molecular mechanism of autophagy induction by resveratrol was assessed by Western-blot technique.

Among compounds tested *in vitro* (genistein, capsaicin, curcumin, resveratrol, trehalose, and calcitriol), resveratrol showed the greatest effects, specifically reducing levels of heparan sulfate (HS) the GAG which accumulates in Sanfilippo disease. This suggested that the pathological GAG was degraded after autophagy stimulation. Experiments with the MPS IIIB mouse model confirmed resveratrol-mediated activation of otherwise impaired autophagy, normalizing urinary GAG levels and improving behavior in affected animals. These findings supported the proposal of the use of resveratrol as a potential drug for Sanfilippo disease treatment, warranting further research. Resveratrol has also been proposed for other lysosomal storage diseases due to its many biological functions. However, its mechanism of action can be different in various diseases; for example, it showed antioxidant properties in Batten disease models. Resveratrol-mediated activation of autophagy may involve multiple pathways, including mTOR-independent and protein phosphatase 2A-dependent mechanisms. Additionally, behavioral studies with MPS IIIB mice revealed that hyperactivity was reduced after treatment with resveratrol, as was the anxiety level [13 -Article no.2].

Objective 2- Development of an innovative combination therapy to improve bone changes in the mouse MPS IVA model.

MPS IVA mice were tested for monotherapy and combination therapy to see treatment effectiveness. At 4 weeks of age, mice were intravenously administered with a viral vector that contains in its expression cassette a NPPC gene for CNP peptide that activates mouse

growth, the enzyme GALNS, or a combination therapy where the mice were given a mixture of both vectors. From that time animals were measured weekly for the growth effectiveness. To determine the effectiveness of treatment, biochemical and molecular tests were performed, including testing the enzyme activity in the blood, organs and bones. As well as histological slides showing bone pathology and treatment effectiveness. As for the vector copy number determination, I measured the concentration of the CNP peptide in the blood of animals, using the ELISA test. Levels of anti-GALNS antibodies were also measured with ELISA to monitor the immune reaction. The GAG levels was assessed by liquid chromatography with tandem mass spectrometry (LC-MS/MS). Additionally, a specialized computer microtomography examination was used to determine the bone density and structure after treatment.

In the MPS IVA mouse model, I observed an accumulation of mono-sulfated keratan sulfate (KS) in bone, a GAG stored in Morquio disease, together with disorganized column structure of chondrocytes. GALNS enzyme activity was not detected in the tissues and plasma of the MPS IVA mouse model. Although I did not observe significant bone growth abnormalities or skeletal dysplasia, there were tendencies towards increased bone volume and higher bone area in MPS IVA mice, compared to wild-type (WT) control. The study also showed that untreated MPS IVA mice had about 200-times higher mono-KS levels in the liver and 100-times higher mono-KS levels in the lung, compared to WT, with a 30% increase in bone. The mouse models reflect human MPS IVA pathology with no enzyme activity, GAG accumulation, and bone histological changes. However, none of the existing mouse models fully replicate the severe skeletal phenotype seen in humans.

I used an AAV8 vector to express the *NPPC* gene, encoding the CNP peptide, which induced bone growth and reduced KS accumulation in bone. CNP has been shown to stimulate bone growth and regulate GAG synthesis during chondrogenesis. The study demonstrated a decreased KS accumulation and increased chondrocyte proliferation in bone after CNP

treatment of MPS IVA mice. In summary, using an AAV8 vector to express *NPPC* in MPS IVA mice resulted in a high level CNP secretion, bone growth induction, improved bone pathology, and changes in GAG levels. Further research with larger sample sizes and long-term studies is necessary to validate these findings and to develop effective treatments for skeletal dysplasia in MPS IVA patients [20- Article no.4].

The CNP peptide supports cartilage homeostasis and bone formation. Combining two vectors (one for GALNS and one for CNP production) showed promising results, with sustained GALNS activity and reduced KS accumulation, enhancing bone growth without negative outcomes. I observed high GALNS activity and reduced KS levels in blood and tissues after combination treatment, leading to improved bone pathology. The optimal CNP dose is crucial to avoid excessive growth. Biodistribution analysis confirmed the GALNS presence in bone and liver, while NT-proCNP levels correlated with CNP production and growth induction. Combining high doses of AAV8-hNPPC and AAV9-hGALNS vectors yielded the most significant improvements.

In conclusion, co-expressing *GALNS* and *NPPC* genes, especially in separate vectors, enhanced bone growth and GALNS activity. Defining the optimal CNP dose in more extensive studies is essential to avoid overgrowth and adverse effects, moving towards clinical trials. Implementing a microRNA system to control CNP expression may be considered to prevent excessive growth [21- Article no.5].

In summary, this PhD thesis focuses on addressing the challenge of delivering therapeutic agents to hard-to-reach tissues in mouse models of MPS. I propose to use small molecules capable of crossing biological barriers to effectively target these tissues. Specifically, I investigated the potential of resveratrol to cross the blood-brain barrier (BBB) in the treatment of MPS IIIB, and CNP for targeting avascular chondrocytes in MPS IVA. Both therapies demonstrated a significant potential in improving treatment outcomes for mice suffering from

these forms of MPS by enhancing drug delivery to otherwise inaccessible sites within the body. This approach not only aims to improve the efficacy of current treatments but also to pave the way for the development of new therapeutic strategies for MPS and potentially other lysosomal storage disorders.

Streszczenie po polsku

Mukopolisacharydozy (MPS) należą do grupy dziedzicznych chorób metabolicznych, w których, w wyniku mutacji genu kodującego enzym odpowiedzialny za rozkład związków z grupy mukopolisacharydów (glikozaminoglikanów, GAG) [1,2]. Proces ich degradacji w zdrowym organizmie jest sekwencyjną reakcją kilku enzymów, jednak gdy jeden z nich nie funkcjonuje prawidłowo, reakcja zostaje zatrzymana i GAG gromadzą się w komórkach. W zależności od tego, który enzym jest nieaktywny, wyróżnia się 13 typów i podtypów MPS. Wiele objawów jest wspólnych dla większości typów i podtypów MPS, jednak najcięższe dotyczą układu nerwowego (CNS) i układu szkieletowego [3]. Dostępne obecnie terapie są nie skuteczne dla objawów ze strony CNS oraz układu szkieletowego.

Najczęściej stosowaną terapią MPS jest terapia enzymatyczna (ERT), która polega na dostarczaniu aktywnej formy brakującego enzymu. Podawanie brakującego enzymu nie jest wystarczające w przypadku typów MPS, w których główne objawy dotyczą CNS (takich jak MPS III), ponieważ enzym nie przekracza bariery krew-mózg [4,5]. Istnieją również inne ograniczenia związane z ERT, w tym krótki okres półtrwania enzymu, wysoki koszt terapii, ograniczony wpływ na tkanki i narządy beznaczyniowe oraz konieczność cotygodniowych infuzji przez całe życie [6,7]. Ponadto, choć ERT dla nieneuropatycznego typu MPS IVA została zatwierdzona, ma ona ograniczony wpływ na nieprawidłowości szkieletowe, które są jednym z głównych objawów choroby [8]. Dlatego konieczne są badania nad alternatywnymi terapiami dla tych typów MPS.

Jedną z alternatywnych strategii jest przyspieszenie degradacji GAG poprzez indukcję procesu autofagii. Autofagia jest to proces fizjologiczny zachodzący w lizosomach, który rozkłada zbędne lub nieprawidłowe makrocząsteczki w komórce [9]. Ostatnie odkrycia sugerują, że GAG mogą być takimi makrocząsteczkami, co potencjalnie oferuje nowe leczenie dla chorób związanych z magazynowaniem tych polisacharydów [10]. Kluczowe pytanie

brzmi, jak proces autofagii aktywują degradację GAG w przypadku uszkodzenia kluczowego enzymu. Całkowity brak enzymu jest wyzwaniem, wiele przypadków MPS ma pewną resztkową aktywność enzymatyczną. Zwiększenie autofagii mogłoby poprawić tę resztkową aktywność, poprawiając degradację GAG. Dodatkowo, enzymy niespecyficznie degradujące GAG- hydrolazy, choć w niewielkiej ilości, mogą wspomagać usuwanie GAG, jeśli autofagia zostanie pobudzona. Nawet jeśli pełne usunięcie GAG nie jest możliwe ze względu na brak enzymu, degradacja wtórnych materiałów magazynowanych w komórce może przynieść korzyści pacjentom, ponieważ niezbędne enzymy są obecne w lizosomach komórek MPS [11-Artykuł no.1].

Potencjalny lek na MPS IIIB powinien również przekraczać barierę krew-mózg i być bezpieczny w długoterminowej terapii. Wydaje się, że jeden z polifenoli, resweratrol, może spełniać te wymagania. Winogrona, orzeszki ziemne, morwy i czarne porzeczki są szczególnie bogate w resweratrol. Ma on wiele funkcji biologicznych, takich jak działanie przeciwzapalne, przeciwutleniające i neuroprotektoryjne. Jest to związek, który był szeroko badany i aktywuje proces degradacji makrocząsteczek poprzez kilka mechanizmów [12]. Ze względu na pleiotropowy mechanizm indukcji autofagii, zdolność do przenikania przez barierę krew-mózg i profil bezpieczeństwa, resweratrol jest obiecującym kandydatem do leczenia neuronopatycznych form MPS [11-Artykuł nr 1]. Resweratrol indukuje autofagię poprzez wiele ścieżek molekularnych, w tym aktywację PTEN, AMPK, FoxOs i TFEB oraz hamowanie kinazy mTOR i genu kodującego Bcl-2. Te mechanizmy zostały szczegółowo opisane w Rintz et al. 2019 [11-Artykuł nr 1]. Dlatego leczyłam model myszy z MPS IIIB resweratrolem, aby poprawić zachowanie wraz z redukcją zgromadzonych GAG [13-Artykuł nr 2].

Obiecującą alternatywną terapią dla pacjentów z MPS IVA jest terapia genowa. ERT z elosulfazą alfa ma ograniczone efekty na wzrost kości u pacjentów z MPS IVA (zespół Morquio A). Przeszczepienie hematopoetycznych komórek macierzystych (HSCT) może oferować

więcej korzyści niż ERT, takich jak poprawa funkcji serca, gęstości mineralnej kości i elastyczności stawów [14], ale ma również istotne ograniczenia: ryzyko śmiertelności, trudności w znalezieniu dawców, powikłania po przeszczepie i ograniczony wpływ na wzrost kości [14,15]. Zarówno ERT, jak i HSCT opierają się na korekcji krzyżowej za pośrednictwem szlaku receptora mannozo-6-fosforanu, gdzie komórki produkujące enzym lizosomalny pomagają komórkom z deficytem enzymu [16]. Jednak metoda ta ma trudności z przenikaniem do chrząstki stawowej [15]. Dlatego istnieje duże zapotrzebowanie na środki penetrujące kości w celu leczenia beznaczyniowych zmian kostnych i indukcji kostnienia u pacjentów z MPS IVA.

Peptyd natriuretyczny typu C (CNP) indukował wzrost kości poprzez aktywację receptora natriuretycznego peptydu typu B (NPR-B) na chondrocytach w płytce wzrostu kości [17]. Stymulacja cząsteczki wewnątrzkomórkowej cGMP przez CNP aktywuje wiele szlaków, co skutkuje wzrostem kości (szczegóły w ref. [18-Artykuł nr 3]). Mimo swojego potencjału, naturalny CNP ma krótki okres półtrwania, co wymaga częstego podawania pacjentom [19]. Dlatego dążyłam do poprawy patologii kostnej w MPS IVA poprzez wykorzystanie terapii genowej z CNP [20-Artykuł nr 4]. Następnym krokiem było połączenie dwóch transgenów (*GALNS* i *NPPC*) w systemie AAV w celu poprawy wzrostu kości przy jednoczesnym zmniejszeniu akumulacji GAG w innych tkankach [21-Artykuł nr 5].

Celami tej pracy doktorskiej było:

- 1) Określenie roli resweratrolu i dokładnego mechanizmu jego działania na modelu mysim MPS IIIB.**
- 2) Opracowanie innowacyjnej terapii kombinowanej genowej w celu poprawy zmian kostnych w modelu mysim MPS IVA.**

Cel 1 - Określenie roli resweratrolu i dokładnego mechanizmu jego działania na modelu mysim MPS IIIB.

Zarówno myszy typu dzikiego, jak i MPS IIIB były testowane w dwóch grupach, gdzie przez 30 tygodni codziennie podawano im wodę lub resweratrol. Aby sprawdzić skuteczność resweratrolu, przeprowadzono kilka testów. Wykonano testy behawioralne. Test aktywności lokomotorycznej wykonano w celu pomiaru nadpobudliwości zwierząt. Test otwartego pola wykonano w celu pomiaru lęku u myszy. Przeprowadzono również testy biochemiczne i molekularne w celu oceny wpływu resweratrolu na komórki z różnych narządów, zwłaszcza mózgu i wątroby, gdzie akumulacja GAG jest największa. Stężenia GAG w moczu (próbki pobierano w 5, 10, 20 i 30 tygodniu życia myszy) zmierzono testem Blyscan. Wpływ resweratrolu na poziomy specyficznych białek w kontekście molekularnego mechanizmu indukcji autofagii przez resweratrol oceniano techniką Western-blot.

Spośród związków testowanych *in vitro* (genisteina, kapsaicyna, kurkumina, resweratrol, trehaloza i kalcytriol), resweratrol wykazywał największy efekt, szczególnie redukując poziomy siarczanu heparanu (HS), GAG gromadzącego się w chorobie Sanfilippo. Sugerowało to, że poziom HS został zmniejszony po stymulacji autofagii przez resweratrol. Eksperymenty na modelu myszy z MPS IIIB potwierdziły indukcję autofagii resweratrolem, normalizację poziomów GAG w moczu oraz poprawę zachowania u chorych zwierząt. Te wyniki potwierdzają propozycję użycia resweratrolu jako potencjalnego leku na chorobę Sanfilippo, wymagającego dalszych badań. Resweratrol został również zaproponowany do innych chorób magazynowych lizosomalnych ze względu na swoje liczne funkcje biologiczne. Jednak jego mechanizm działania może być różny w różnych chorobach; na przykład, wykazywał właściwości przeciwutleniające w modelach choroby Battena. Indukcja autofagii przez resweratrol może obejmować wiele szlaków, w tym niezależne od mTOR i zależne od fosfatazy białkowej 2A. Dodatkowo, badania behawioralne na myszach z MPS IIIB wykazały, że nadpobudliwość zmniejszyła się po leczeniu resweratrolem, podobnie jak poziom lęku [13 - Artykuł nr 2].

Cel 2 - Opracowanie innowacyjnej terapii kombinowanej w celu poprawy zmian kostnych w modelu mysim MPS IVA.

Myszy z MPS IVA były testowane pod kątem monoterapii i terapii kombinowanej, aby ocenić skuteczność leczenia. W wieku 4 tygodni myszom dożylnie podano wektor wirusowy AAV zawierający gen *NPPC* dla peptydu CNP, który aktywuje wzrost myszy, gen *GALNS* dla enzymu lub terapię kombinowaną, gdzie myszom podano mieszanę obu wektorów. Od tego czasu zwierzęta były mierzone co tydzień w celu oceny skuteczności indukcji wzrostu. Aby ocenić skuteczność leczenia, przeprowadzono testy biochemiczne i molekularne, w tym badanie aktywności enzymatycznej we krwi, narządach i kościach, oraz histologiczne preparaty pokazujące patologię kości i skuteczność leczenia. Do określenia liczby kopii wektora zmierzono stężenie peptydu CNP we krwi zwierząt za pomocą testu ELISA. Poziomy przeciwciał anti-GALNS również mierzono za pomocą testu ELISA w celu monitorowania reakcji immunologicznej. Poziomy GAG oceniano za pomocą chromatografii ciekowej sprzężonej z tandemową spektrometrią mas (LC-MS/MS). Dodatkowo, specjalistyczne badanie mikrotomografii komputerowej było używane do określenia gęstości i struktury kości po leczeniu.

W modelu myszy z MPS IVA zaobserwowałam akumulację monosiarczanowanego siarczanu keratanu (KS) w kości, GAG magazynowanego w chorobie Morquio, wraz z nieuporządkowaną strukturą kolumn chondrocytów. Aktywność enzymu GALNS była nie wykrywalna w tkankach i osoczu myszy z MPS IVA. Choć nie zaobserwowałam znaczących nieprawidłowości wzrostu kości ani dysplazji szkieletowej, zaobserwowano tendencję do zwiększonej objętości kości i większej powierzchni kości u myszy z MPS IVA w porównaniu z kontrolami typu dzikiego (WT). Badanie wykazało również, że nieleczone myszy z MPS IVA miały około 200 razy wyższe poziomy monosiarczanowanego KS w wątrobie i 100 razy wyższe poziomy monosiarczanowanego KS w płucach w porównaniu z WT, z 30% wzrostem w kości.

Modele myszy odzwierciedlają patologię MPS IVA u ludzi z brakiem aktywności enzymu, akumulacją GAG i zmianami histologicznymi kości. Jednak żaden z istniejących modeli myszy nie w pełni odzwierciedla ciężką fenotypową dysplazję szkieletową obserwowaną u ludzi.

Użyłam wektora AAV8 do ekspresji genu *NPPC*, kodującego peptyd CNP, który indukował wzrost kości i zmniejszał akumulację KS w kościach. Badanie wykazało zmniejszoną akumulację KS i zwiększoną proliferację chondrocytów w kości po leczeniu CNP myszy z MPS IVA. Podsumowując, użycie wektora AAV8 do ekspresji *NPPC* u myszy z MPS IVA skutkowało wysokim poziomem sekrecji CNP, indukcją wzrostu kości, poprawą patologii kości i zmianami w poziomach GAG. Dalsze badania z większymi próbkami i długoterminowe badania są niezbędne do potwierdzenia tych wyników i opracowania skutecznych metod leczenia dysplazji szkieletowej u pacjentów z MPS IVA [20-Artykuł nr 4].

Peptyd CNP wspiera homeostazę chrząstki i formowanie kości. Połączenie dwóch wektorów (jeden dla produkcji GALNS i jeden dla produkcji CNP) wykazało obiecujące wyniki, z utrzymującą się aktywnością GALNS i zmniejszoną akumulacją KS, co poprawiało wzrost kości bez negatywnych skutków ubocznych. Zaobserwowałam wysoką aktywność GALNS i zmniejszone poziomy KS we krwi i tkankach po leczeniu kombinowanym, co prowadziło do poprawy patologii kości. Optymalna dawka CNP jest kluczowa, aby uniknąć nadmiernego wzrostu. Analiza biodystrybucji potwierdziła obecność GALNS w kości i wątrobie, podczas gdy poziomy NT-proCNP korelowały z produkcją CNP i indukcją wzrostu. Połączenie wysokich dawek wektorów AAV8-hNPPC i AAV9-hGALNS przyniosło najbardziej znaczące poprawy.

Podsumowując, ko-ekspresja genów *GALNS* i *NPPC*, zwłaszcza w oddzielnych wektorach, zwiększyła wzrost kości i aktywność GALNS. Określenie optymalnej dawki CNP w większych badaniach jest kluczowe, aby uniknąć nadmiernego wzrostu i negatywnych skutków, zmierzając ku badaniom klinicznym. Rozważane może być również wprowadzenie

systemu mikroRNA do kontroli ekspresji CNP w celu uniknięcia nadmiernego wzrostu [21-Artykuł nr 5].

Podsumowując, niniejsza praca doktorska koncentruje się na rozwiązaniu problemu dostarczania środków terapeutycznych do trudno dostępnych tkanek w modelach myszy z MPS. Proponuję użycie małych cząsteczek zdolnych do przenikania przez bariery biologiczne, aby skutecznie dotrzeć do tych tkanek. Konkretnie, zbadalam potencjał resweratrolu do przenikania przez barierę krew-mózg (BBB) w leczeniu MPS IIIB oraz CNP do celowania w beznaczyniowe chondrocyty w MPS IVA. Obie terapie wykazały znaczący potencjał w poprawie wyników leczenia myszy cierpiących na te formy MPS poprzez zwiększenie dostarczania leków do trudno dostępnych miejsc w ciele. To podejście nie tylko ma na celu poprawę skuteczności obecnych terapii, ale także torowanie drogi do opracowania nowych strategii terapeutycznych dla MPS i potencjalnie innych chorób magazynowych lizosomalnych.

References

1. Ballabio A, Gieselmann V. Lysosomal disorders: from storage to cellular damage. *Biochim Biophys Acta*. 2009 Apr;1793(4):684-96. doi: 10.1016/j.bbamcr.2008.12.001. Epub 2008 Dec 8. PMID: 19111581.
2. Muenzer J. (2011) Overview of the mucopolysaccharidoses. *Rheumatology (Oxford)* 50 Suppl 5:v4-12. doi: 10.1093/rheumatology/ker394.
3. Tomatsu S., Lavery, Ch., Giugliani, R., Harmatz, P., Scarpa, M., Węgrzyn, G., Orii, T. (2018). *Mucopolysaccharidoses Update (2 Volume Set)*, Nova science publisher.
4. Beck M. New therapeutic options for lysosomal storage disorders: enzyme replacement, small molecules and gene therapy. *Hum Genet*. 2007 Mar;121(1):1-22. doi: 10.1007/s00439-006-0280-4. Epub 2006 Nov 7. PMID: 17089160.
5. Cimaz R, La Torre F. Mucopolysaccharidoses. *Curr Rheumatol Rep*. 2014 Jan;16(1):389. doi: 10.1007/s11926-013-0389-0. PMID: 24264718.
6. Rintz E, Higuchi T, Kobayashi H, Galileo DS, Węgrzyn G, Tomatsu S. Promoter considerations in the design of lentiviral vectors for use in treating lysosomal storage diseases. *Mol Ther Methods Clin Dev*. 2021 Nov 24;24:71-87. doi: 10.1016/j.omtm.2021.11.007. PMID: 34977274; PMCID: PMC8688940.
7. Kanters TA, van der Ploeg AT, Kruijshaar ME, Rizopoulos D, Redekop WK, Rutten-van Mölken MPMH, Hakkaart-van Roijen L. Cost-effectiveness of enzyme replacement therapy with alglucosidase alfa in adult patients with Pompe disease. *Orphanet J Rare Dis*. 2017 Dec 13;12(1):179. doi: 10.1186/s13023-017-0731-0. PMID: 29237491; PMCID: PMC5729274.
8. Tomatsu S, Alméciga-Díaz CJ, Barbosa H, Montaña AM, Barrera LA, Shimada T, Yasuda E, Mackenzie WG, Mason RW, Suzuki Y, Orii KE, Orii T. Therapies of mucopolysaccharidosis IVA (Morquio A syndrome). *Expert Opin Orphan Drugs*. 2013 Oct 1;1(10):805-818. doi: 10.1517/21678707.2013.846853. PMID: 25419501; PMCID: PMC4238063.
9. Pierzynowska K, Gaffke L, Cyske Z, Puchalski M, Rintz E, Bartkowski M, Osiały M, Pierzynowski M, Mantej J, Piotrowska E, Węgrzyn G. Autophagy stimulation as a promising approach in treatment of neurodegenerative diseases. *Metab Brain Dis*. 2018 Aug;33(4):989-1008. doi: 10.1007/s11011-018-0214-6. Epub 2018 Mar 14. PMID: 29542037; PMCID: PMC6060747.

10. Pierzynowska K, Gaffke L, Podlacha M, Brokowska J, Węgrzyn G. Mucopolysaccharidosis and Autophagy: Controversies on the Contribution of the Process to the Pathogenesis and Possible Therapeutic Applications. *Neuromolecular Med.* 2020 Mar;22(1):25-30. doi: 10.1007/s12017-019-08559-1. Epub 2019 Aug 1. PMID: 31372809; PMCID: PMC7021662.
11. Rintz E, Pierzynowska K, Podlacha M, Węgrzyn G. Has resveratrol a potential for mucopolysaccharidosis treatment? *Eur J Pharmacol.* 2020 Dec 5;888:173534. doi: 10.1016/j.ejphar.2020.173534. Epub 2020 Aug 30. PMID: 32877657. – **Article no. 1 included in PhD thesis**
12. Kou X, Chen N. Resveratrol as a Natural Autophagy Regulator for Prevention and Treatment of Alzheimer's Disease. *Nutrients.* 2017 Aug 24;9(9):927. doi: 10.3390/nu9090927. PMID: 28837083; PMCID: PMC5622687.
13. Rintz E, Podlacha M, Cyske Z, Pierzynowska K, Węgrzyn G, Gaffke L. Activities of (Poly)phenolic Antioxidants and Other Natural Autophagy Modulators in the Treatment of Sanfilippo Disease: Remarkable Efficacy of Resveratrol in Cellular and Animal Models. *Neurotherapeutics.* 2023 Jan;20(1):254-271. doi: 10.1007/s13311-022-01323-7. Epub 2022 Nov 7. PMID: 36344724; PMCID: PMC10119361. - **Article no. 2 included in PhD thesis**
14. Sawamoto K, Álvarez González JV, Piechnik M, Otero FJ, Couce ML, Suzuki Y, Tomatsu S. Mucopolysaccharidosis IVA: Diagnosis, Treatment, and Management. *Int J Mol Sci.* 2020 Feb 23;21(4):1517. doi: 10.3390/ijms21041517. PMID: 32102177; PMCID: PMC7073202.
15. Tomatsu S, Sawamoto K, Alméciga-Díaz CJ, Shimada T, Bober MB, Chinen Y, Yabe H, Montaña AM, Giugliani R, Kubaski F, Yasuda E, Rodríguez-López A, Espejo-Mojica AJ, Sánchez OF, Mason RW, Barrera LA, Mackenzie WG, Orii T. Impact of enzyme replacement therapy and hematopoietic stem cell transplantation in patients with Morquio A syndrome. *Drug Des Devel Ther.* 2015 Apr 1;9:1937-53. doi: 10.2147/DDDT.S68562. PMID: 25897204; PMCID: PMC4389814.
16. Biffi A. Hematopoietic Stem Cell Gene Therapy for Storage Disease: Current and New Indications. *Mol Ther.* 2017 May 3;25(5):1155-1162. doi: 10.1016/j.ymthe.2017.03.025. Epub 2017 Apr 4. PMID: 28389320; PMCID: PMC5417839.
17. Bartels CF, Bükülmez H, Padayatti P, Rhee DK, van Ravenswaaij-Arts C, Pauli RM, Mundlos S, Chitayat D, Shih LY, Al-Gazali LI, Kant S, Cole T, Morton J, Cormier-

Daire V, Faivre L, Lees M, Kirk J, Mortier GR, Leroy J, Zabel B, Kim CA, Crow Y, Braverman NE, van den Akker F, Warman ML. Mutations in the transmembrane natriuretic peptide receptor NPR-B impair skeletal growth and cause acromesomelic dysplasia, type Maroteaux. *Am J Hum Genet.* 2004 Jul;75(1):27-34. doi: 10.1086/422013. Epub 2004 May 14. PMID: 15146390; PMCID: PMC1182004.

18. Rintz E, Węgrzyn G, Fujii T, Tomatsu S. Molecular Mechanism of Induction of Bone Growth by the C-Type Natriuretic Peptide. *Int J Mol Sci.* 2022 May 25;23(11):5916. doi: 10.3390/ijms23115916. PMID: 35682595; PMCID: PMC9180634. - **Article no. 3 included in PhD thesis**
19. Savarirayan R, Irving M, Bacino CA, Bostwick B, Charrow J, Cormier-Daire V, Le Quan Sang KH, Dickson P, Harmatz P, Phillips J, Owen N, Cherukuri A, Jayaram K, Jeha GS, Larimore K, Chan ML, Huntsman Labeled A, Day J, Hoover-Fong J. C-Type Natriuretic Peptide Analogue Therapy in Children with Achondroplasia. *N Engl J Med.* 2019 Jul 4;381(1):25-35. doi: 10.1056/NEJMoa1813446. Epub 2019 Jun 18. PMID: 31269546.
20. Rintz E, Herreño-Pachón AM, Celik B, Nidhi F, Khan S, Benincore-Flórez E, Tomatsu S. Bone Growth Induction in Mucopolysaccharidosis IVA Mouse. *Int J Mol Sci.* 2023 Jun 8;24(12):9890. doi: 10.3390/ijms24129890. PMID: 37373036; PMCID: PMC10298227.- **Article no. 4 included in PhD thesis**
21. Rintz E, Celik B, Fnu N, Herreño-Pachón AM, Khan S, Benincore-Flórez E, Tomatsu S. Molecular therapy and nucleic acid adeno-associated virus-based gene therapy delivering combinations of two growth-associated genes to MPS IVA mice. *Mol Ther Nucleic Acids.* 2024 May 7;35(2):102211. doi: 10.1016/j.omtn.2024.102211. PMID: 38831899; PMCID: PMC11145352. **Article no. 5 included in PhD thesis**

Manuscripts included in PhD thesis

1. **Rintz E**, Pierzynowska K, Podlacha M, Węgrzyn G. Has resveratrol a potential for mucopolysaccharidosis treatment? *Eur J Pharmacol.* 2020 Dec 5;888:173534. doi: 10.1016/j.ejphar.2020.173534
2. **Rintz E**, Podlacha M, Cyske Z, Pierzynowska K, Węgrzyn G, Gaffke L. Activities of (Poly)phenolic Antioxidants and Other Natural Autophagy Modulators in the Treatment of Sanfilippo Disease: Remarkable Efficacy of Resveratrol in Cellular and Animal Models. *Neurotherapeutics.* 2023 Jan;20(1):254-271. doi: 10.1007/s13311-022-01323
3. **Rintz E**, Węgrzyn G, Fujii T, Tomatsu S. Molecular Mechanism of Induction of Bone Growth by the C-Type Natriuretic Peptide. *Int J Mol Sci.* 2022 May 25;23(11):5916. doi: 10.3390/ijms23115916.
4. **Rintz E**, Herreño-Pachón AM, Celik B, Nidhi F, Khan S, Benincore-Flórez E, Tomatsu S. Bone Growth Induction in Mucopolysaccharidosis IVA Mouse. *Int J Mol Sci.* 2023 Jun 8;24(12):9890. doi: 10.3390/ijms24129890.
5. **Rintz E**, Celik B, Fnu N, Herreño-Pachón AM, Khan S, Benincore-Flórez E, Tomatsu S. Molecular therapy and nucleic acid adeno-associated virus-based gene therapy delivering combinations of two growth-associated genes to MPS IVA mice. *Mol Ther Nucleic Acids.* 2024 May 7;35(2):102211. doi: 10.1016/j.omtn.2024.102211.

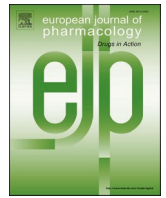
Rintz, E., Pierzynowska, K., Podlacha, M., Węgrzyn, G.
Has resveratrol a potential for mucopolysaccharidosis treatment?
(2020) *European Journal of Pharmacology*. 888:173534.

Impact Factor = 4.432 (2020)

MNISW Punctuation = 70

Contents lists available at [ScienceDirect](https://www.sciencedirect.com)

European Journal of Pharmacology

journal homepage: www.elsevier.com/locate/ejphar

Has resveratrol a potential for mucopolysaccharidosis treatment?

Ester Rintz, Karolina Pierzynowska, Magdalena Podlacha, Grzegorz Węgrzyn*

Department of Molecular Biology, Faculty of Biology, University of Gdansk, Wita Stwosza, 59, 80-308, Gdansk, Poland

ARTICLE INFO

Keywords:

Mucopolysaccharidosis
Trans-Resveratrol
Autophagy
Glycosaminoglycans

ABSTRACT

Mucopolysaccharidoses (MPS) represent a devastating group of lysosomal storage diseases (LSD) affecting approximately 1 in 25,000 individuals, where degradation of glycosaminoglycans (GAG) by lysosomal enzymes is impaired due to mutations causing defects in one of GAG-degrading enzymes. The most commonly used therapy for MPS is enzyme replacement therapy, consisting of application of an active form of the missing enzyme. However, supply of the missing enzyme is not enough in case of MPS types whose symptoms are expressed in central nervous system (CNS), as enzyme does not cross the blood-brain barrier. Moreover, even though enzyme replacement therapy for non-neuronopathic MPS IVA type is approved, it has a limited impact on bone abnormalities, that are one of main symptoms in the disease. Therefore, research into alternative therapeutic approaches for these types of MPS is highly desirable. One such alternative strategy is accelerated degradation of GAG by induction of autophagy. Autophagy is a process of lysosomal degradation of macromolecules that become abnormal or unnecessary for cells. One of the latest discoveries is that GAGs can also be such molecules. Potential drug should also cross blood-brain barrier and be safe in long-term therapy. It seems that one of the polyphenols, resveratrol, can meet the requirements. The mechanism of its action in autophagy stimulation is pleiotropic. Therefore, in this review, we will briefly discuss potential of resveratrol treatment for mucopolysaccharidosis through autophagy stimulation based on research in diseases with similar outcome.

1. Introduction

The group of disorders in which dysfunctions of lysosomal enzymes cause accumulation of various macromolecular compounds in these organelles is known as lysosomal storage diseases (LSDs). There are over 50 classified LSDs while each of them is monogenic, and caused by mutations in a single gene coding for either certain lysosomal hydrolase or another protein crucial for particular lysosomal function, like lysosomal transmembrane trafficking of specific compounds or maturation of complex macromolecules. LSDs are classified according to the kind of deficient protein and nature of accumulated compound(s), like complex carbohydrates, glycosphingolipids, proteins and others. They are exemplified by mucopolysaccharidoses (MPS) (where glycosaminoglycans (GAGs) are accumulated – see section 2 for details), sphingolipidoses (where various sphingolipids cannot be efficiently degraded, like in Gaucher disease and Niemann-Pick diseases), gangliosidoses (characterized with deficiency in degradation of gangliosides, like in Tay-Sachs disease), glycogen storage diseases (Pompe disease and Danon disease) and others. The storage of macromolecules which cannot be efficiently degraded in lysosomes is the first step of the damaging

cascade of secondary effects which lead to dysregulation of the cellular metabolism, followed by dysfunctions of tissues and organs (Ballabio and Gieselmann, 2009; Parkinson-Lawrence et al., 2010).

Vast majority of LSDs are severe diseases, in which high morbidity and mortality is common, with average life span below two decades or even significantly shorter in some conditions (Parkinson-Lawrence et al., 2010). Although LSDs are in the forefront of genetic diseases for which principles of molecular mechanisms are understood, and they are among first inherited metabolic disorders for which specific treatment could be proposed, there are still only relatively few therapeutic options available (Ballabio and Gieselmann, 2009). The currently approved treatments include enzyme replacement therapy (for Gaucher disease, Fabry disease, Pompe disease, mucopolysaccharidoses type I, II, IVA, VI and VII) and substrate reduction therapy (for Gaucher and Niemann-Pick C diseases). Bone marrow and hematopoietic stem cell transplantations are also used for some LSDs in clinical practice, but their efficacies vary considerably between various diseases. Gene therapy is being extensively developed, but it is still at the stage of pre-clinical or early clinical trials at best (Muenzer, 2011; Tomatsu et al., 2018).

One of the newest therapeutic approaches is the accelerated

* Corresponding author.

E-mail address: grzegorz.wegrzyn@biol.ug.edu.pl (G. Węgrzyn).<https://doi.org/10.1016/j.ejphar.2020.173534>

Received 3 June 2020; Received in revised form 26 August 2020; Accepted 28 August 2020

Available online 30 August 2020

0014-2999/© 2020 Elsevier B.V. All rights reserved.

degradation of storage molecules by stimulating the process of autophagy which has been proposed mainly for mucopolysaccharidoses (MPS). Late outcomes suggest that such methodology may be effective in degradation of stored glycosaminoglycans (GAG) as well as secondary storage molecules and improving MPS pathological effects (Pierzynowska et al., 2020).

Autophagy is a process of macromolecules degradation that become abnormal or unnecessary for cells (Pierzynowska et al., 2018a). It was found that accumulated glycosaminoglycans also can be such molecules (Pierzynowska et al., 2020). Potential drug for mucopolysaccharidosis should not only eliminate the primary cause of the disease, i.e. the accumulation of GAG, but also be small enough to cross the blood-brain barrier, which is necessary in the case of neurodegenerative diseases. Moreover, it should be safe for long-term use, because patients will take it for the rest of their lives. A substance that meets the given criteria could therefore be a potential drug in MPS therapy. Attention in this aspect is drawn by one of the compounds belonging to the group of stilbenes, trans-resveratrol.

In this review, we will briefly discuss the potential of resveratrol treatment for mucopolysaccharidosis through autophagy stimulation based on research in diseases with similar outcome.

2. Mucopolysaccharidoses – overview and current treatment

Mucopolysaccharidoses (MPS) belong to the group of lysosomal storage diseases, caused by the lack or low activity of enzymes carrying out glycosaminoglycan (GAG) degradation reactions. GAGs are unbranched multi-sugar chains that play important roles in maintaining connective tissue flexibility and facilitating the binding of various growth factors to their receptors on the cell surface. In a healthy organism, GAG degradation occurs in lysosomes due to activities of several enzymes that sequentially remove individual monosaccharides or chemical groups from GAG chains (Fig. 1). The sequential degradation manner causes that a defect in one of the enzymes prevents all subsequent reactions. Therefore, in the absence of a single enzyme, GAG

degradation stops at a certain stage, and non-degraded molecules accumulate in lysosomes. Due to the defects of individual enzymes, 11 types and subtypes of MPS are distinguished (Tomatsu et al., 2018) (Table 1). Pathways of heparan sulfate and dermatan sulfate (the most commonly occurring stored GAGs in MPS) degradations, with enzymes involved in these processes, are depicted in Fig. 1.

Apart from bone marrow or stem cell transplantation (which, however, gives very limited effectiveness in neurological MPS types), enzyme replacement therapy (ERT) is the most commonly used therapy for MPS, while it is available for only some types of MPS (types I, II, IVA, VI and VII). It consists of supplying the patient with the missing enzyme (Gaffke et al., 2018). This therapy gives good results in the case of somatic symptoms of different types of MPS. However, it is impossible to effectively treat MPS types that affect the central nervous system (CNS), mainly MPS III, because the intravenously administered enzyme does not cross the blood-brain barrier (Banecka-Majkutewicz et al., 2012). On the other hand, there is gene therapy that has been tested recently, and even though it is promising approach for MPS treatment, administration of the viral vector encoding a missing enzyme intravenously required high doses or repeated administration, while when delivered through intra-brain administration, multi-injection is necessary in order to be effective. Other limitation in this method is presence of preexisting antibodies against vector resulting in less effectiveness of the method (Sawamoto et al., 2018). Thus, patients suffering from neuronopathic types of MPS remain without therapy to this day. Moreover, even though enzyme replacement therapy for non-neuronopathic MPS IVA type is approved by FDA, weekly administration of enzyme has a limited impact on bone abnormalities, that are one of main symptom in the disease (Tomatsu et al., 2013).

Due to the lack of therapy for neuronopathic types of MPS, numerous studies are being conducted on potential drugs. Approaches such as substrate reduction therapy, gene therapy, the use of small chemical chaperones, or the use of fusion proteins that could cross the blood-brain barrier are proposed. However, these strategies are either at the experimental stage or do not give the expected results (Gaffke et al., 2018).

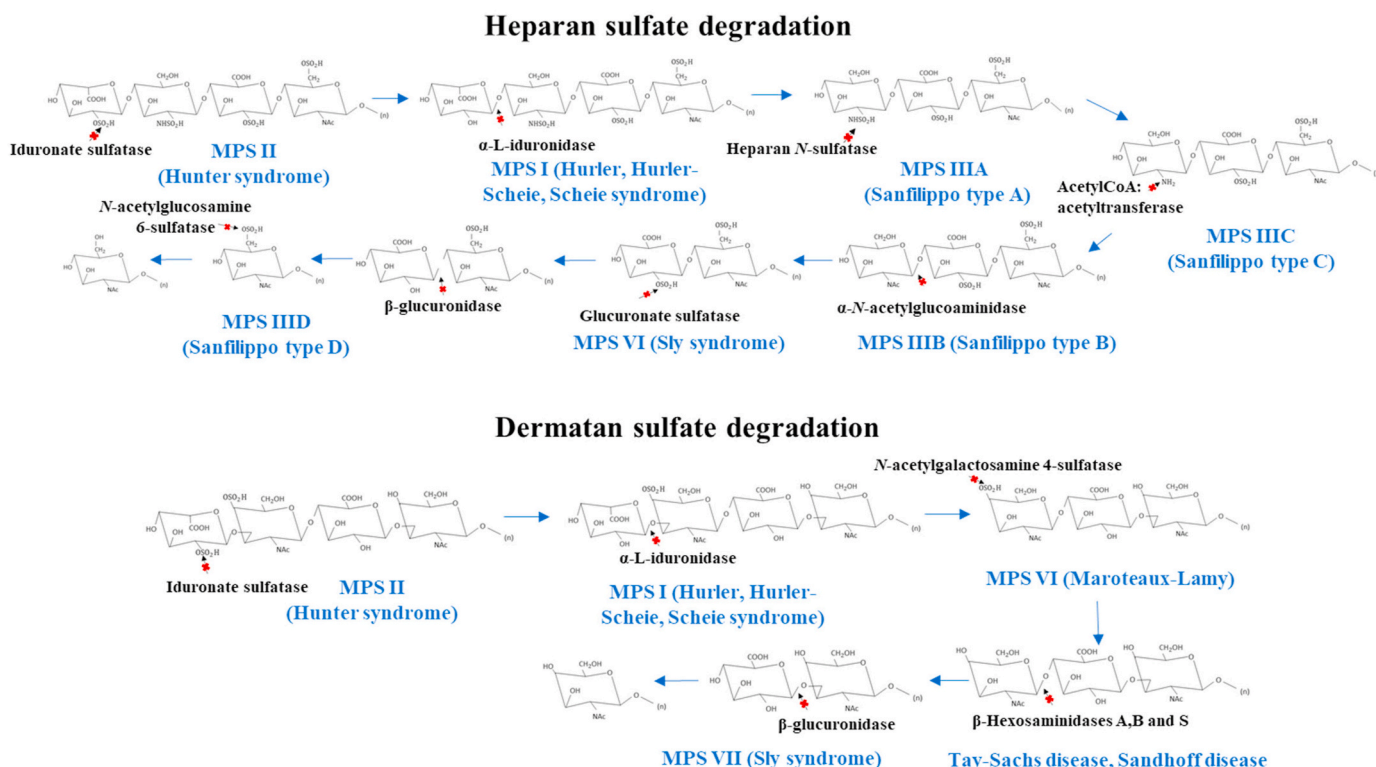


Fig. 1. Pathways of heparan sulfate and dermatan sulfate degradations, with enzymes involved in these processes; based on (Lawrence et al., 2014).

Table 1
Mucopolisaccharidosis types and subtypes; (based on Braunlin et al., 2011).

MPS Type	Eponym	Typical life expectancy if untreated	Defective enzyme	Stored GAG
I ^a	Hurler (H); Hurler-Scheie (H-S); Scheie (S)	H: death in childhood H-S: death in teens or early adulthood S: normal to slightly reduced lifespan	α -L-iduronidase	DS and HS
II ^a	Hunter	rapidly progressing: death < 15 years slowly progressing: death in adulthood	Iduronate 2-sulfatase	DS and HS
IIIA ^a	Sanfilippo type A	death in puberty or early adulthood	Heparan N-sulfatase	HS (secondary DS storage)
IIIB ^a	Sanfilippo type B	death in adulthood	α -N-acetylglucosaminidase	HS (secondary DS storage)
IIIC ^a	Sanfilippo type C		Acetylco: α -glucosaminide acetyltransferase	HS (secondary DS storage)
IIID ^a	Sanfilippo type D		N-acetylglucosamine-6-sulfatase	HS (secondary DS storage)
IVA	Morquio type A	death in childhood	Galactose 6-sulfatase	KS and CS
IVB	Morquio type B	middle age	B- galactosidase	KS
VI	Maroteaux-Lamy	rapidly progressing: death in 2nd-3rd decade slowly progressing: death in 4-5th decade	N-acetylglucosamine-4-sulfatase	DS
VII ^a	Sly	death in infancy- 4th decade	B- glucuronidase	DS, KS and CS
IX	Natowicz	unknown	hyaluronidase	CS

Abbreviations: HS, heparan sulfate; DS- dermatan sulfate; KS- keratan sulfate; CS- chondroitin sulfate.

^a MPS types with neurological impairment.

3. Autophagy induction as a strategy for GAG degradation

Recently, it turned out that a promising therapeutic strategy in the case of neurodegenerative diseases caused by accumulation of macromolecules may be stimulation of macromolecular degradation processes, and one of potential methods is the induction of the autophagy process. Autophagy is a process that is strongly conserved in evolution and occurs in all eukaryotic cells at a low level, and it is activated to a greater extent by the action of various external factors or by the appearance of incorrectly folded macromolecules. Such macromolecules are surrounded by an isolating membrane, which then closes into a vehicle called the autophagosome. This structure then fuses with the lysosome, and the lysosomal enzymes digest its interior into single monomers that can be reused by the cell (Pierzynowska et al., 2018a).

Until recently, the process of autophagy was considered to be a system designed for the degradation of proteins and small cell organelles (Pierzynowska et al., 2018a). A lot of research has confirmed the effectiveness of induction of autophagy activated by natural compounds in improving the phenotypes of Huntington's (Pierzynowska et al., 2018b) and Alzheimer's (Pierzynowska et al., 2019) diseases, and there

are many more such reports (Pierzynowska et al., 2018a). However, autophagy, as a highly non-selective process, could involve degradation of not only proteins but also other accumulated molecules (Pierzynowska et al., 2020). Hence, the hypothesis of its effectiveness in removing accumulated polysaccharides was proposed, and this could successfully become a new therapeutic strategy for the treatment of diseases associated with storage of polysaccharides, including GAG.

The obvious question is how could stimulated autophagy help in degradation of GAGs when one of crucial enzymes involved in this process is impaired. One might presume that this would be difficult if total absence of such an enzyme occurs. However, in many cases of MPS, there is some low, residual activity of the deficient enzyme. Therefore, enhanced autophagy and lysosomal biogenesis may significantly increase the level of this residual activity, thus, improving efficiency of GAG degradation. On the other hand, it has been discussed that apart from specific enzymes which are involved in sequential (through removing chemical moieties or mono-sugars from GAG chains) degradation of GAG, there are also non-specific hydrolases which, although of low abundance and activity, might facilitate GAG removal if significantly stimulated (Banecka-Majkutewicz et al., 2012). Therefore, positive effects of autophagy induction might also be beneficial even in the total absence of activity of one of specific enzymes involved in GAG degradation. Moreover, even if complete GAG clearance cannot be achieved in MPS due to deficiency of particular enzyme, effective degradation of secondary storage materials should still be beneficial for patients, and adequate enzymes are still present in lysosomes of MPS cells (Pierzynowska et al., 2020).

4. Resveratrol

Resveratrol is a nutraceutical belonging to the group of polyphenolic derivatives of stilbene (Fig. 2). Stilbenes are naturally occurring substances that have been found to possess multiple biological activities. Most importantly, stilbenes were characterized as phytoalexins that are known for their ability to microbial and fungal infections resistance in plants, induced by stress or UV light (Kimura, 2003). Stilbene

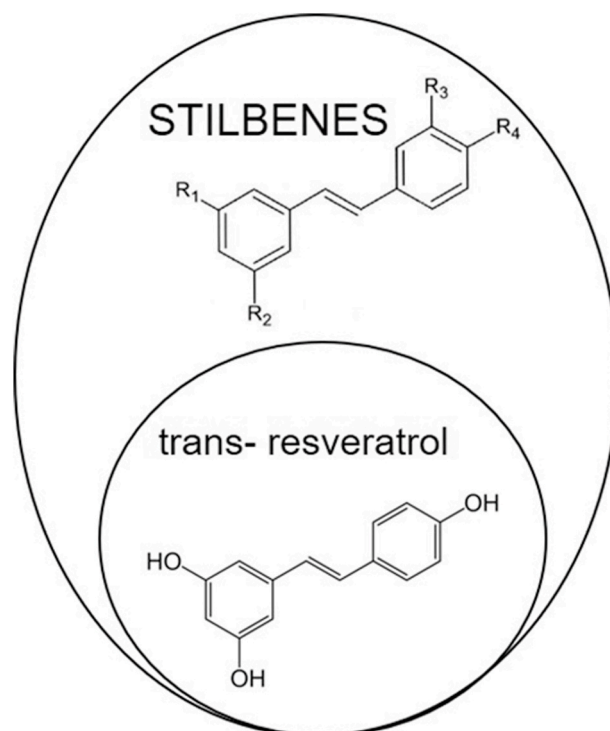


Fig. 2. Resveratrol classification.

compounds are found in the roots, bark, rhizomes and leaves. The main source of stilbene in the diet can be grapes, grape juice, wine, nuts, peanut butter as well as fruits such as mulberry or various species of blueberries. As they contain two benzene rings joined with double bond, they can undergo photoisomerization *cis* or *trans*, but only *trans* isomers of these compounds have considerable biological activities (Makowska-Was and Janeczko, 2008). Among many stilbene compounds, resveratrol (Fig. 2) have been shown to possess various biological functions such as anti-inflammatory, antioxidant, neuroprotective, and many other effects (Kou and Chen, 2017). It was proposed that this single molecule may have so many biological activities as there are over 20 proteins with specific affinities to it (Britton et al., 2015). Therefore, resveratrol is a promiscuous molecule which can interact with many cellular targets, influencing various biological processes (Wu and Hsieh, 2018).

Grapes, peanuts, mulberries and black currants have a particularly high resveratrol content. Stilbene compounds are known for their ability to microbial and fungal infections resistance for plants (Bhullar and Hubbard, 2015; Berman et al., 2017). It is characterized by many biological functions such as anti-inflammatory, antioxidant and neuroprotective effects (Kou and Chen, 2017).

5. Molecular mechanism of autophagy induction by resveratrol

Resveratrol is one of the inducers of autophagy, and the effect of induction of this process is multi-track. The molecular mechanism of this process focuses on the induction of autophagy by: activation of (i) PTEN; (ii) AMPK; (iii) FoxOs; (iv) TFEB; or inhibition of (v) mTOR kinase; (vi) Bcl-2-encoding gene.

Resveratrol regulate PI3K/Akt pathway by stimulating PTEN through androgen receptor inhibition. This negatively regulates transition from PIP2 to PIP3, therefore PIP3 does not interact with PDK1, and Akt is phosphorylated. When Akt is active, it phosphorylates and inactivates FoxOs with transduction from nucleus to cytoplasm (Wang et al., 2010).

Moreover, Park et al. demonstrated that resveratrol directly binds to mTOR kinase, inhibiting its activity by docking onto the ATP-binding pocket of mTOR, and this effect is dependent on the activity of the ULK1 kinase (Park et al., 2016). The ULK1 kinase acts in complex with the Atg13 and FIP200 proteins, and undergo a series of phosphorylation reactions which ultimately lead to the initiation of autophagosome formation (Pierzynowska et al., 2018a). In addition to direct binding to mTOR kinase, it was shown that resveratrol can upregulate transcription factor EB, resulting in induction of lysosome formation and suppression of anti-oxidation (Zhou et al., 2019).

Furthermore, resveratrol has the ability to activate signaling pathways leading to induction of autophagy. It induces autophagy via the JNK1-Beclin-1-PI3K pathway by negatively regulating expression of gene encoding Bcl-2 (Shankar and Srivastava, 2007). The reduced expression level of this gene results in reduced efficiency of the Bcl-2 protein complex formation with the Beclin-1 protein, which then remains free and binds to the class III PI3K protein complex. This leads to rapid stimulation of autophagosome formation (Shankar et al., 2007; Fan et al., 2018; Pierzynowska et al., 2018a; Xu et al., 2018). Resveratrol also induces autophagy by another pathway, AMPK/TSC/mTOR, by affecting the increase in AMP kinase activity. AMP kinase belongs to the group of Ser/Thr kinases. Its gene is mainly expressed in nervous tissue, and is activated mainly by various kinases such as Ca²⁺/CaM-dependent protein kinase β (CaMKK β). Resveratrol is a strong activator of this kinase, which has been shown in both cell and mouse studies. The mechanism by which resveratrol activates AMPK is based on an increase in the intracellular level of Ca²⁺ and promotion of phosphorylation of AMPK at the Thr172 active site, which in turn leads to inhibition of mTOR (Wu et al., 2011; Park et al., 2016; Suvorova and Pospelov, 2019). This affects the phosphorylation modulation, and thus stimulation of the activity of the ULK1-Atg 13-FIP200 complex, which directly leads to the formation of the autophagosome (Chang et al.,

2017; Zhao et al., 2018).

Moreover, AMPK is activated by resveratrol, but exact mechanism of this action is not entirely known. However, it was demonstrated that resveratrol activates AMPK in the presence of liver kinase B1 (LKB1) that is activated by translocation and phosphorylation at T336 and S428. It was also found that resveratrol at high concentration can increase AMP levels that also activates AMPK (Lan et al., 2017). One of the target molecules for AMPK is transcription factor FoxO3a that, when phosphorylated by AMPK, is subsequently translocated into the nucleus where it activates expression of autophagy related genes (Li et al., 2009).

Following this, resveratrol has also direct effect on increasing the expression level of the *SIRT1* gene encoding sirtuin which is an enzyme that belongs to the NAD⁺-dependent deacetylases family. SIRT1 deacetylates histones and nonhistone proteins, including transcription factors, like FoxO3a which is known as one of transcriptional factors up-regulating the autophagy process (Lee, 2019). SIRT1 can be activated by AMPK, causing activation and transduction of the FoxO transcription factor to the nucleus (Ido et al., 2015) what can lead to expression of autophagy related genes. What is more, SIRT1 also modifies PGC-1 α transcription factor by deacetylation which allows transduction of PGC-1 α to the nucleus and activation of genes involved in reduction of oxidative stress by activation of mitochondrial metabolism (Rodgers et al., 2007; Higashida et al., 2013). The SIRT1-regulated pathway can also modulate inflammation-immune function, stress resistance, cell survival and stress resistance. As resveratrol activates SIRT-1, it has many beneficial effects in diseases affected by abnormal metabolic control or inflammation (Salminen and Kaarniranta, 2009; Berman et al., 2017; Zhang et al., 2019). All these mechanisms of resveratrol-dependent autophagy stimulation are shown in Fig. 3.

6. Potential of resveratrol treatment in mucopolysaccharidosis

Depending on the kind of inactive enzyme and stored GAG, 11 types and subtypes of MPS are distinguished. Most of the mucopolysaccharidosis types have similar somatic features due to GAG aggregation, while those with neurological outcome are the most severe forms of the disease. MPS I, II, all forms of III, and VII present cognitive and central nervous system impairment. Those lead to several symptoms including developmental delays, behavioral difficulties, sleep disturbances and dementia (Muenzer, 2011). Moreover, it was found that not only GAGs accumulate in the brain but also p-Tau and β -amyloid are stored in the central nervous system of MPSIIIB mouse model (Martins et al., 2015).

Some of the features of the mucopolysaccharidosis are similar to those in other neurological diseases such as Huntington, Parkinson or Alzheimer diseases. The various mechanisms of action of resveratrol, described above, have been used in experimental therapies for neurodegenerative diseases performed on animal and cellular models.

Resveratrol performance in removing toxic proteins has been tested in models of many diseases involving protein aggregation (Wu et al., 2011). Exemplary studies performed on the cellular model of Huntington's disease (HD) (neuroblastoma SH-SY5Y) have shown that resveratrol, by inducing the process of autophagy, facilitates the degradation of mutant huntingtin, which protects cells against dopamine-induced toxicity (Vidoni et al., 2018). Moreover, resveratrol prevented early neuronal dysfunction phenotypes in a transgenic *Caenorhabditis elegans* model expressing mutant polyglutamine (Parker et al., 2005). A lot of studies showed efficacy of resveratrol in protection against mutant polyglutamine-mediated cell death in striatal neuronal cultures isolated from the HdhQ111 knock-in mice model of HD (Parker et al., 2005). Moreover, oral administration of resveratrol reversed motor and cognitive impairments induced by 3-nitropropionic acid in mice, another model for neurotoxicity and HD (Pasinetti et al., 2011).

The use of resveratrol in studies on Parkinson's disease (PD) indicated that in mouse neuroblastoma cells (N2a line) the number of alpha-synuclein aggregates decreased, while the viability of the tested cells increased (Gautam et al., 2017; Pierzynowska et al., 2018a). Studies on

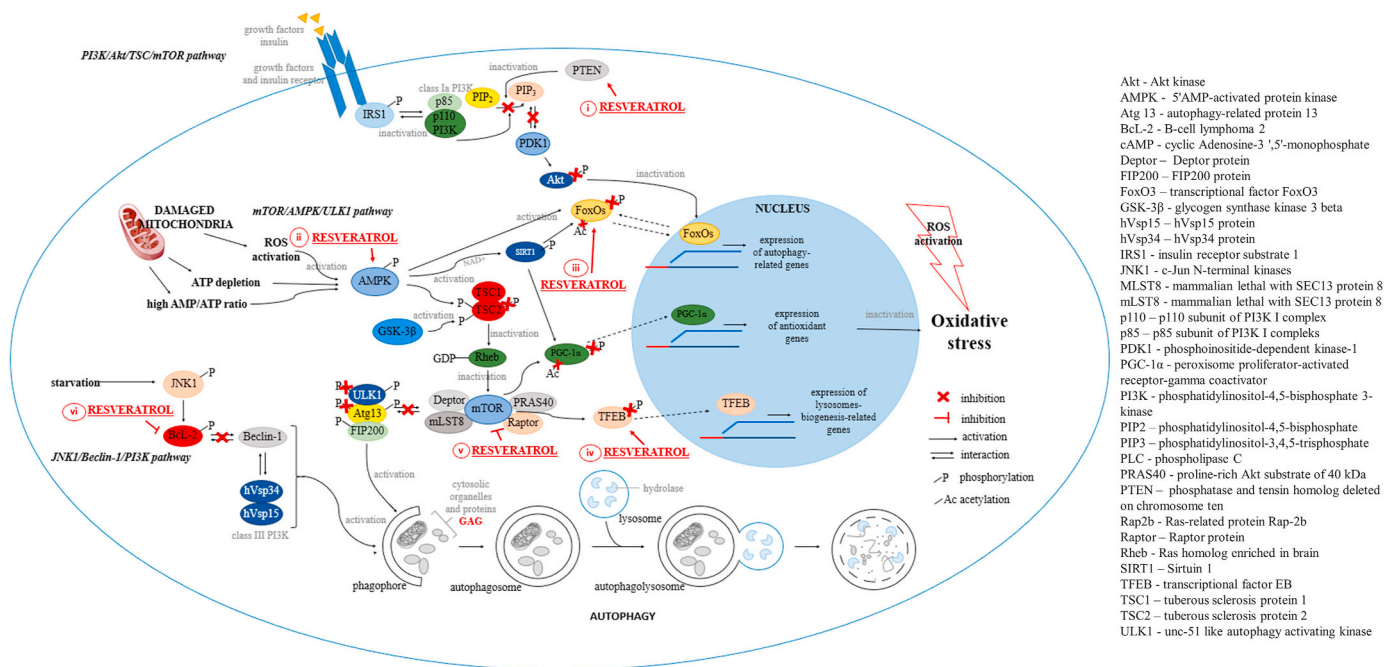


Fig. 3. Mechanisms of autophagy induction by resveratrol: activation of (i) PTEN; (ii) AMPK; (iii) FoxOs; (iv) TFEB; or inhibition of (v) mTOR kinase; (vi) Bcl-2-encoding gene.

the use of resveratrol for the treatment of PD have also been conducted in mouse models (induced by MPTP, 1-methyl-4-phenyl-1,2,3,6-tetrahydropyridine) and primary fibroblasts from patients. Although these studies ended with positive effects, the topic of autophagy as a mechanism of action of resveratrol was not discussed there, and these studies focused rather on the role of non-coding RNA molecules in improving the disease phenotype (Xia et al., 2019) or its impact on mitochondrial functions (Ferretta et al., 2014). These and other studies on the use of resveratrol in PD focused on the mechanism associated with the improvement of cellular energy disorders or with the reduction of ROS levels which is thought to be the cause of neuronal death (Andrade et al., 2018).

Neuroprotective effects of resveratrol have also been shown in a lot of models of Alzheimer's disease (AD), where an improvement in animals behavior, and increased survival of in vitro cultured cells (representing various cellular models of AD) have also been noted as a consequence of the stimulation of SIRT1, AMPK and mTOR signal pathways leading to decrease in amyloids levels (Sawda et al., 2017; Gomes et al., 2018; Zhou et al., 2019). Moreover, recent studies have shown that resveratrol together with exercise can also prevent aberrations in cardiac function and aortic elastin morphology in mouse model of Alzheimer's disease (Esfandiarei et al., 2019). Low estrogen level is associated with more severe and rapid development of AD in women, also indicating a decrease in neuronal activity and enhanced Aβ aggregation. After resveratrol administration in mouse model of AD, oxidative stress and progression of the disease were ameliorated, as were enhanced estrogen levels (Kong et al., 2019). In addition, the latest studies have shown that resveratrol mediates cleavage of amyloid β1-42 peptide into smaller peptides in SH-SY5Y human neuroblastoma cells (Al-Edresi et al., 2020).

It was also demonstrated that resveratrol can attenuate hypoxia-induced neuronal cell death. First, this compound revealed neuroprotection in neural cells subjected to hypoxia conditions by modulation of oxidative stress, inflammatory reactions, apoptosis and cell death through influencing the TRPM2 channel which is otherwise activated during hypoxia (Akyuva and Naziroğlu, 2020). Moreover, resveratrol reduces the hypoxia-related oxidative stress through facilitating translocation of the DJ-1 protein from cytoplasm to mitochondria which

maintain proper functions of these organelles and prevents their damage by the oxidative stress (Zhou et al., 2020).

In the animal model of amyotrophic lateral sclerosis (ALS), resveratrol therapy led to delayed disease onset, preserved motoneuron function, relieve muscle atrophy, and improvement mitochondrial function of muscle fibers (Wang et al., 2011; Mancuso et al., 2014; Song et al., 2014). All these studies focused on investigating the role of SIRT1 activation in this phenomenon and were performed on SOD1 (G93A) ALS mice. Resveratrol also activates mitophagy, as demonstrated by studies on the mouse model of Duchenne muscular dystrophy, where, among others, cardiomyopathy in animals has been reduced by its long-term administration (Kuno et al., 2018). All examples given above are summarized in Table 2.

The examples described above are only some of the reports indicating the positive effect of resveratrol on cells and animal organisms that are models of human neurological diseases. It is noteworthy, however, that the mechanism of resveratrol activity studied by various research teams focused only slightly on the activation of autophagy, and used rather different properties of this compound. The models used sometimes did not allow to study the effect of this compound at the level of storage macromolecules at all, because they do not always reflect the cause of the disease (3-nitropropionic acid in HD and MPTP in PD).

Apart from neurodegeneration, severe symptoms appear in virtually all organs and systems in all MPS types. Many of them affect patient's daily life, which can be exemplified by cardiovascular disorders. In fact, cardiac manifestation has been shown probably due to primary GAG storage that leads to perturbation of valves, heart muscle, and vessels (particularly the coronary arteries). Level of cardiac failure depends on MPS type and enzyme defects. MPS I, II, and VI have the most severe cardiac involvement. Progression of cardiac manifestation worsen with patients age (Boffi et al., 2018). Several studies indicated that resveratrol interferes with several processes involved in the pathophysiology of cardio-vascular diseases. Recent studies performed on mice have shown that resveratrol is inhibitor of immunoproteasome activity and due to that, it can attenuate cardiac hypertrophy after pressure overload. The mechanism of this action depends on inhibition of PTEN degradation that leads to inactivation of AKT/mTOR and activation of AMPK signals (Chen et al., 2019). Other studies on ovariectomized mice have shown

Table 2
Potential of resveratrol treatment in mucopolysaccharidosis suggested on the basis of its effects in other diseases.

Disease	Used model	Concentration/ Dose	Some features of the disease	Effects of resveratrol treatment	Probable mechanism of resveratrol action	Similar outcome in MPS
Huntington disease	SH-SY5Y cells hyper-expressing the mutant polyglutamines	100 μ M	accumulation of toxic protein – mutant huntingtin;	protecting cells from dopamine toxicity (Vidoni et al., 2018)	autophagy induction (LC3-II protein), decreasing the level of reactive oxygen species (ROS)	accumulation of GAG, cognitive disorder (Ballabio and Gieselmann, 2009), sleep disturbances (Berger et al., 2012)
	<i>C. elegans</i> model expressing mutant polyglutamines	10 μ M	movement, cognitive and behavioral disorder	prevented early neuronal dysfunction (Parker et al., 2005; Pasinetti et al., 2011)	<i>SIRT1</i> activation	
	striatal neuronal cultures isolated from the HdhQ111 knock-in mouse model	N/A		decreasing mutant huntingtin level; protection against mutant polyglutamine-mediated cell death (Parker et al., 2005; Pasinetti et al., 2011)	<i>SIRT1</i> activation	
	Huntington's disease-like mouse model (induced by 3-nitropropionic acid)	5 and 10 mg/kg		reversion of 3-nitropropionic acid-induced motor and cognitive impairment (Pasinetti et al., 2011)	decreasing the level of reactive oxygen species (ROS)	
Parkinson disease	MPTP mouse model	50 mg/kg/day	accumulation of toxic protein – alpha-synuclein; motor symptoms; sleep disorders, genitourinary problems (Chaudhuri et al., 2006)	partly offsetting the effect of mptp (Xia et al., 2019)	modulation of ncRNA in regulation of disease-related genes	accumulation of GAG (Ballabio and Gieselmann, 2009), sleep disturbances (Berger et al., 2012), epileptic seizures (Scarpa et al., 2017);
	primary fibroblast cultures from patients with early-onset disease	25 μ M		positive regulation of energetic homeostasis (Ferretta et al., 2014)	AMP kinase and <i>SIRT1</i> activation, decreasing ROS levels, increasing biogenesis of mitochondria	
Alzheimer disease	over 50 reports on studies with mice, cells and other models of the disease	from 150 mg to 1000 mg daily in clinical trials	accumulation of toxic protein – ptau and β -amyloid; disturbed sleep; obsessive, repetitive or impulsive behavior; aphasia)	positive effects on animal behavior, cell viability and levels of toxic proteins (Zhou et al., 2019)	stimulation of <i>SIRT1</i> , AMP kinase and mTOR signal pathways	accumulation of GAG (Ballabio and Gieselmann, 2009), MPSIII: Dementia (Muenzer, 2011), accumulation of pTau, and β -amyloid in MPSIIIB mouse model (Martins et al., 2015)
Amyotrophic lateral sclerosis	SOD1 (G93A) ALS mice	160 mg/food kg	accumulation of toxic protein – superoxide dismutase; movement disorder	delaying disease onset and preservation lower and upper motoneuron function (Mancuso et al., 2014)	AMP kinase and <i>SIRT1</i> activation	accumulation of GAG (Ballabio and Gieselmann, 2009)
	SOD1 (G93A) ALS mice	25 mg/kg/day		attenuation of motor neurons' loss, relieve muscle atrophy, and improvement of mitochondrial functions in muscle fibers (Song et al., 2014; Wang et al., 2011)	<i>SIRT1</i> activation	
Cardiovascular diseases	hypertensive mice	10 mg/kg/day	hypertension	reduced pathological cardiac remodeling and dysfunction; moreover, it decreased oxidative stress, inflammation, fibrosis and apoptosis (Gupta et al., 2014)	<i>SIRT1</i> activation; eNOS activation; increased $^{*}NO$ production; improve flow-mediated vasodilation in animal models (Bonnefont-Rousselot, 2016)	coronary artery narrowing and/or occlusion (all types of MPS), cardiac valve thickening (MPS I, II, VI) (Scarpa et al., 2017); cardiomyopathy (MPS I, MPS VI) (Ribeiro et al., 2014); hypertension (Boffi et al., 2018)
	hypertensive rats and angiotensin-II infused mice	1 mg/kg/day and 18 mg/kg/day	hypertension	RES to reverse cardiac hypertrophy and contractile dysfunction (Rimbaud et al., 2011; Chan et al., 2011)		hypertension; left ventricle hypertrophy (Braunlin et al., 2011)
	rat	~146 mg Resv/kg/day	left ventricle hypertrophy	inhibited left ventricle hypertrophy (Dolinsky et al., 2015)	AMP kinase activation (Bonnefont-Rousselot, 2016)	
	induced MI in mice via left coronary artery occlusion	5 or 50 mg/kg/day	myocardial ischemia	left ventricle ejection fraction (LVEF) was significantly reduced (Kanamori et al., 2013)	activation of eNOS and vascular endothelial growth factor (VEGF) by decreasing oxidative stress; Autophagy induction through activation of AMPK and/or <i>SIRT1</i> in the	

(continued on next page)

Table 2 (continued)

Disease	Used model	Concentration/ Dose	Some features of the disease	Effects of resveratrol treatment	Probable mechanism of resveratrol action	Similar outcome in MPS
Liver diseases	pressure overload-induced hypertrophic mice model	25 and 50 mg/kg/day	cardiac hypertrophy	attenuates cardiac hypertrophy after pressure overload	cardiomyocyte; induction of autophagy by activation of mTOR in the rat myocardium (Bonnetfont-Rousselot, 2016)	
	ovariectomized mice	N/A	ischemic heart	improved cardiac contractile function in estrogen-deficient mice and reduced LDH release, restored mitochondrial function	inhibition of PTEN degradation that led to inactivation of AKT/mTOR and activation of AMPK signals (Chen et al., 2019)	
	cardiac-specific SIRT1 knockout mice	25 mg/kg/day	cardiac hypertrophy and dysfunction, insulin resistance, and abnormal glucose metabolism	reverse impaired mitochondrial biogenesis, high glucose and function in cardiomyocytes	AMP kinase and SIRT1 activation (Meng et al., 2016)	
	murine models of hepatic iron-overload	320 mg/kg/day	hepatosplenomegaly, increased oxidative stress, hepatic fibrosis, and inflammation	correction of hepatosplenomegaly, increased oxidative stress, hepatic fibrosis, and inflammation, and a pro-apoptotic state	activation of SIRT1 through PGC-1 α -mediated mitochondrial regulation (Ma et al., 2017)	hepatosplenomegaly (Tomatsu et al., 2018)
	high-fat diet (HFD)-induced nonalcoholic fatty liver disease in mice	30 mg/kg/day	high levels of nonesterified fatty acids (NEFA), inflammation, and hepatic steatosis	decreases the inflammatory level by inhibiting NF- κ B pathway and improving hepatic steatosis	acetylation of FoxO 1 in association with increased SIRT1 levels which together with its pleotropic antioxidant properties (Das et al., 2016)	fatty lipids accumulation (Tomatsu et al., 2018)
	high-fat diet (HFD)-induced nonalcoholic fatty liver disease in offspring rats	50 mg/kg/day	Fatty liver accumulation	protective effects on lipid metabolism, regulation of oxidative stress and apoptosis	AMP kinase and SIRT1 activation (Tian et al., 2016)	
Rheumatology diseases	high-fat diet (HFD)-induced nonalcoholic fatty liver disease in rats	100 mg/kg/day	hepatic steatosis	improved lipid metabolism, enhanced antioxidant capacity, and restored mitochondrial respiratory chain activities	Induction of PKA/AMPK/PPAR α signaling pathway (Huang et al., 2020)	
	acute antigen-induced inflammatory arthritis rat model	12.5 mg/kg/day	Knee joint swelling, oxidative stress, especially oxidative DNA damage	reduced knee swelling and histological score of synovial tissue	decrease in PCNA, CD68, CD3, marker indicating DNA damage (Riveiro-Naveira et al., 2016)	joint stiffness and contractures (Morishita and Petty, 2011)
	collagen-induced inflammatory arthritis model in rats	20 mg/kg/day	cartilage and bone destructions	ameliorated the clinical and histopathological (perisynovial inflammation and cartilage-bone destruction)	inhibition of Src tyrosine kinase, STAT3, and Wnt/ β -catenin signaling pathway (Oz et al., 2018)	
	acute antigen-induced inflammatory arthritis rat model	12,5 mg/kg/day	synovial hyperplasia, knee joint swelling chemokines and oxidative damage	decreased inflammation	autophagy induction (LC3-II protein, p62 protein, Beclin-1) (Fernandez-Rodriguez et al., 2019)	

effects of RSV on ischemic heart. Administration of resveratrol improved cardiac contractile function in estrogen-deficient mice and reduced lactate dehydrogenase (LDH) release. Moreover, those studies indicated that resveratrol can restore mitochondrial functions (Meng et al., 2016). Other approaches to determine whether resveratrol can improve heart failure were assessed in a hypertensive rat model. Treatment with RSV indicated that survival and reduction in body weight can be improved, as can be cardiac dysfunction evaluated by echocardiography. In that study mitochondrial mass and biogenesis were preserved, and mitochondrial fatty acid oxidation and expression of PPAR α (peroxisome proliferator-activated receptor α) were protected by resveratrol

(Rimbaud et al., 2011). Resveratrol also reversed impaired mitochondrial biogenesis and function, as well as high glucose levels in cardiomyocytes of cardiac-specific SIRT1 knockout mice by activation of SIRT1 through PGC-1 α -mediated mitochondrial regulation (Ma et al., 2017).

GAG accumulation leading to enlargement of organs such as hepatomegaly or hepatosplenomegaly is recognized as one of the first symptoms in MPS pathogenesis (Tomatsu et al., 2018). Moreover, other liver disturbances have been shown as elevated activities of alanine aminotransferase (ALT) and aspartate aminotransferase (AST) in mucopolysaccharidosis patients with MPSIIIA that could be caused by

liver storage of GAGs (Krawiec et al., 2014). The pathological process of growth of cells of liver and spleen is not understood, as it can be directly caused by GAG storage or by dysregulation of cell growth expression factors. Transcriptional analysis indicated that cell growth process was dysregulated in MPS cells in comparison to healthy cells (Rintz et al., 2020). Accumulating evidence suggests that resveratrol is beneficial for liver-associated diseases, such as hepatic iron-overload and/or non-alcoholic fatty liver disease (NAFLD). Hepatic iron-overload, linked with hepatosplenomegaly, increased oxidative stress, hepatic fibrosis, inflammation, and a pro-apoptotic activities. Studies with murine models of hepatic iron-overload have shown that resveratrol therapy corrected all the mouse hepatic related symptoms (Das et al., 2016). What is more, inflammation plays a crucial role in accumulation of fatty acids in liver. Mice fed with high fat diet had high concentration of pro-inflammatory cytokines TNF- α , IL-6, and IL-1 β in blood as well as over-induced NF- κ B inflammatory pathway. Treatment with resveratrol ameliorated these changes, and decreased the inflammatory level by inhibiting NF- κ B pathway and improving hepatic steatosis (Tian et al., 2016). Recent studies on application and treatment in NAFLD, performed on rats, indicated that resveratrol improved hepatic steatosis (induced by high-fat diet) in rats by different way, i.e. through induction of PKA/AMPK/PPAR α signaling pathway. Moreover, resveratrol inhibited PA-induced lipid accumulation in HepG2 cells (Huang et al., 2020). On the other hand, nonalcoholic fatty liver disease can develop in prenatal stages as well as with high-fat diet. Therefore, treatment with resveratrol was tested on male rat offspring on different diets – normal diet, maternal high-fat diet and postnatal high fat diet. Administration of resveratrol prevented NAFLD, with protective effects on lipid metabolism, regulation of oxidative stress and apoptosis. What was found is that resveratrol actions were via renin-angiotensin system, increasing SIRT1 and leptin expression, and decreasing angiotensinogen and renin, ACE1, and AT1R mRNA in liver cells in rats (Tiao et al., 2018).

Other MPS symptoms are musculoskeletal manifestations that are common in all forms of the disease. Some symptoms, like joint stiffness and muscle contractures, may imitate different conditions, such as inflammatory arthritis, which may lead to misdiagnosis. Hence, early diagnosis is crucial for MPS treatment (Morishita and Petty, 2011). The latest research suggests that resveratrol can be beneficial as potential agent to suppress inflammation of collagen-induced arthritis in a mouse model. Studies performed on induced rat model of arthritis have shown that after resveratrol treatment for 8 weeks before induction, symptoms like knee swelling and histological score of synovial tissue were significantly reduced. Moreover, there was a decrease in PCNA, CD68, CD3 as well in marker indicating DNA damage (Riveiro-Naveira et al., 2016). Other studies with the same model and type of administration indicated that autophagy process can be activated by resveratrol in addition with reduced serum levels of interleukin (IL)-1 β levels, C-reactive protein (CRP) and prostaglandin E2 (PGE2). Autophagy induction was measured by increased level of LC3-II marker, compared with non-treated animals. Moreover, other autophagy marker p62, that indicates autophagic degradation dysfunction, was inhibited by resveratrol treatment. While LC3-II and p62 were ameliorated, Beclin 1 protein that is associated with autophagosome formation did not change, suggesting that autophagy can be activated by other pathway in this case (Fernandez-Rodriguez et al., 2019).

Other approach was to test resveratrol effectiveness in inhibition of Wnt/ β -catenin signaling pathway. Wnt/ β -catenin signaling pathway was found to be important in joint/cartilage destructions in rheumatoid arthritis. It also plays a significant role in cell differentiation, limb development and joint formation. Due to that, collagen-induced arthritis rat model was treated with resveratrol. After resveratrol treatment, clinical and histopathology-related inflammation and cartilage-bone destruction changes were ameliorated. Mechanism of this action was probably due to inhibition of Wnt/ β -catenin signaling pathway through decreasing Wnt5a mRNA expression as well as inhibiting Src kinases that are factors involved in the activation of inflammatory cells. What is

more, Src kinases are responsible for activation of transcriptional factor STAT3, what triggers progression and severity of rheumatoid arthritis. After resveratrol treatment, STAT3 mRNA expression was also decreased comparing to non-treated group (Oz et al., 2018).

The only research reported so far with the use of resveratrol in MPS was conducted with a *Drosophila melanogaster* model (MPS type VII). The experiments have shown that resveratrol improved animal behavior and crossed the blood-brain barrier in flies (Bar et al., 2018). However, this model does not reflect the actual cause of the disease, GAG storage, thus, effects of resveratrol on GAG storage remains unknown.

When considering that potential effects of resveratrol on GAG storage and secondary or tertiary disorders related to MPS can be due to autophagy stimulation, one should also consider putative limitations. Potentially the most dangerous side effect could be overstimulation of autophagy which might result in destruction of normal cellular components, as indicated previously (Pierzynowska et al., 2020; Pierzynowska et al., 2018a). Nevertheless, since resveratrol has been demonstrated to be safe and well tolerated in many experiments on animals and even in human clinical trials (discussed in earlier sections of this article), such a potential danger might be considered rather unlikely.

It is also necessary to consider an optimal dose for potential treatment of MPS with resveratrol. Since different doses were used for various models of different diseases (as summarized in Table 2), it is clear that when testing resveratrol in MPS, dose optimization will be necessary.

7. Conclusions

Although mucopolysaccharidoses are monogenic diseases, they are complex disorders, as multiple cascade systems are involved in their pathogenesis. Therefore, these diseases are difficult to treat, particularly their neuronopathic forms, and new therapies should lead to improvement in patient's life. One might assume that novel therapeutic strategies for MPS should be focused not only on reduction of GAG level but also on ameliorating whole spectrum of cellular processes, causing reduction of symptoms. Resveratrol appears as a potential candidate for a drug which might be useful in therapies for MPS. This compound can induce autophagy which has recently been suggested as a way to improve physiology of MPS cells. Moreover, it reveals other beneficial activities, like antioxidative and anti-inflammatory properties. Encouraging results of studies on the use of resveratrol in other diseases, including neurodegenerative disorders, suggest that further investigations of the use of this compound in treatment of MPS models are substantiated.

Funding

This work was supported by National Science Center (501100004281%20:) (Poland) (project grant no. 2019/35/N/NZ2/00505) and The Sanfilippo Foundation (Poland) (project no. 21/01/2019).

Author contributions

ER conceptualization, writing - original draft, visualization. KP collectioning the data, writing - review & editing. MP collectioning the data, visualization. GW writing - review & editing, supervision.

Declaration of competing interest

The authors declare that they have no known competing financial interests or personal relationships that could have appeared to influence the work reported in this paper.

References

- Akyuva, Y., Naziroğlu, M., 2020. Resveratrol attenuates hypoxia-induced neuronal cell death, inflammation and mitochondrial oxidative stress by modulation of TRPM2 channel. *Sci. Rep.* 10, 6449. <https://doi.org/10.1038/s41598-020-63577-5>.
- Al-Edressi, S., Alsalahat, I., Freeman, S., Aojula, H., Penny, J., 2020. Resveratrol-mediated cleavage of amyloid β 1-42 peptide; potential relevance to Alzheimer's disease. *Neurobiol. Aging*. <https://doi.org/10.1016/j.neurobiolaging.2020.04.012>.
- Andrade, S., Ramalho, M.J., do, C., Pereira, M., Loureiro, J.A., 2018. Resveratrol brain delivery for neurological disorders prevention and treatment. *Front. Pharmacol.* 9, 1261. <https://doi.org/10.3389/fphar.2018.01261>.
- Ballabio, A., Gieselmann, V., 2009. Lysosomal disorders: from storage to cellular damage. *Biochim. Biophys. Acta* 1793 (4), 684–696. <https://doi.org/10.1016/j.bbamer.2008.12.001>.
- Banecka-Majkutewicz, Z., Jakóbkiewicz-Banecka, J., Gabig-Cimińska, M., Węgrzyn, A., Węgrzyn, G., 2012. Putative biological mechanisms of efficiency of substrate reduction therapies for mucopolysaccharidoses. *Arch. Immunol. Ther. Exp.* 60 (6), 461–468. <https://doi.org/10.1007/s00005-012-0195-9>.
- Bar, S., Prasad, M., Datta, R., 2018. Neuromuscular degeneration and locomotor deficit in a Drosophila model of mucopolysaccharidosis VII is attenuated by treatment with resveratrol. *Dis. Model Mech* 11 (11). <https://doi.org/10.1242/dmm.036954>, 036954.
- Berger, K.I., Fagondes, S.C., Giugliani, R., Hardy, K.A., Lee, K.S., McArdle, C., Scarpa, M., Tobin, M.J., Ward, S.A., Rapoport, D.M., 2012. Respiratory and sleep disorders in mucopolysaccharidosis. *J. Inher. Metab. Dis.* 36 (2), 201–210. <https://doi.org/10.1007/s10545-012-9555-1>.
- Berman, A.Y., Motechin, R.A., Wiesenfeld, M.Y., Holz, M.K., 2017. The therapeutic potential of resveratrol: A review of clinical trials. *Npj Precision Oncology* 1, 35. <https://doi.org/10.1038/s41698-017-0038-6>.
- Bhullar, K.S., Hubbard, B.P., 2015. Lifespan and health span extension by resveratrol. *Biochim. Biophys. Acta* 1852 (6), 1209–1218. <https://doi.org/10.1016/j.bbdis.2015.01.012>.
- Boffi, L., Russo, P., Limongelli, G., 2018. Early diagnosis and management of cardiac manifestations in mucopolysaccharidoses: a practical guide for paediatric and adult cardiologists. *Ital. J. Pediatr.* 44 (S2). <https://doi.org/10.1186/s13052-018-0560-3>.
- Bonnefont-Rousselot, D., 2016. Resveratrol and cardiovascular diseases. *Nutrients* 8 (5), 250. <https://doi.org/10.3390/nu8050250>.
- Braunlin, E.A., Harmatz, P.R., Scarpa, M., Furlanetto, B., Kampmann, C., Loehr, J.P., Ponder, K.P., Roberts, C.W., Howard, M.R., Giugliani, R., 2011. Cardiac disease in patients with mucopolysaccharidosis: presentation, diagnosis and management. *J. Inher. Metab. Dis.* 34 (6), 1183–1197. <https://doi.org/10.1007/s10545-011-9359-8>.
- Britton, R.G., Kovoor, C., Brown, K., 2015. Direct molecular targets of resveratrol: identifying key interactions to unlock complex mechanisms. *Ann. N. Y. Acad. Sci.* 1348 (1), 124–133. <https://doi.org/10.1111/nyas.12796>.
- Chan, V., Fenning, A., Iyer, A., Hoey, A., Brown, L., 2011. Resveratrol improves cardiovascular function in DOCA-salt hypertensive rats. *Curr. Pharmaceut. Biotechnol.* 12 (3), 429–436. <https://doi.org/10.2174/138920111794480552>.
- Chang, C.H., Lee, C.Y., Lu, C.C., Tsai, F.J., Hsu, Y.M., Tsao, J.W., Juan, Y.N., Chiu, H.Y., Yang, J.S., Wang, C.C., 2017. Resveratrol-induced autophagy and apoptosis in cisplatin-resistant human oral cancer CAR cells: a key role of AMPK and Akt/mTOR signaling. *Int. J. Oncol.* 50 (3), 873–882. <https://doi.org/10.3892/ijo.2017.3866>.
- Chaudhuri, K.R., Healy, D.G., Schapira, A.H., 2006. Non-motor symptoms of Parkinson's disease: Diagnosis and management. *Lancet Neurol.* 5 (3), 235–245. [https://doi.org/10.1016/s1474-4422\(06\)70373-8](https://doi.org/10.1016/s1474-4422(06)70373-8).
- Chen, C., Zou, L.-X., Lin, Q.-Y., Yan, X., Bi, H.-L., Xie, X., Wang, S., Wang, Q.-S., Zhang, Y.-L., Li, H.-H., 2019. Resveratrol as a new inhibitor of immunoproteasome prevents PTEN degradation and attenuates cardiac hypertrophy after pressure overload. *Redox Biol.* 20, 390–401. <https://doi.org/10.1016/j.redox.2018.10.021>.
- Das, S.K., DesAulniers, J., Dyck, J.R.B., Kassiri, Z., Oudit, G.Y., 2016. Resveratrol mediates therapeutic hepatic effects in acquired and genetic murine models of iron-overload. *Liver Int.* 36 (2), 246–257. <https://doi.org/10.1111/liv.12893>.
- Dolinsky, V.W., Soltys, C.L., Rogan, K.J., Chan, A.Y., Nagendran, J., Wang, S., Dyck, J.R., 2015. Resveratrol prevents pathological but not physiological cardiac hypertrophy. *J. Mol. Med. (Berl.)* 93, 413–425. <https://doi.org/10.1007/s00109-014-1220-8>.
- Esfandiari, M., Hoxha, B., Talley, N.A., Anderson, M.R., Alkhouli, M.F., Squire, M.A., Eckman, D.M., Babu, J.R., Lomaschuk, G.D., Broderick, T.L., 2019. Beneficial effects of resveratrol and exercise training on cardiac and aortic function and structure in the 3xTg mouse model of Alzheimer's disease. *Drug Des. Dev. Ther.* 13, 1197–1211. <https://doi.org/10.2147/dddt.s196119>.
- Fan, Y., Chiu, J.-F., Liu, J., Deng, Y., Xu, C., Zhang, J., Li, G., 2018. Resveratrol induces autophagy-dependent apoptosis in HL-60 cells. *BMC Canc.* 18 (1). <https://doi.org/10.1186/s12885-018-4504-5>.
- Fernandez-Rodriguez, J.A., Almonte-Becerril, M., Ramil-Gomez, O., Viñas, S., Hermida-Carballo, L., Vela-Anero, A., Concha, A., Camacho-Encina, M., Blanco, F.J., Lopez-Armas, M.J., 2019. Resveratrol-enhanced autophagic flux reduces severity of experimental rheumatoid arthritis. *Osteoarthritis Cartilage* 27, S474–S475. <https://doi.org/10.1016/j.joca.2019.02.521>.
- Ferretta, A., Gaballo, A., Tanzarella, P., Piccoli, C., Capitano, N., Nico, B., Annesse, T., Paola, M.D., Dell'aquila, C., De Mari, M., Ferranini, E., Bonifati, V., Pacelli, C., Cocco, T., 2014. Effect of resveratrol on mitochondrial function: implications in parkin-associated familial Parkinson's disease. *Biochim. Biophys. Acta* 1842 (7), 902–915. <https://doi.org/10.1016/j.bbdis.2014.02.010>.
- Gaffke, L., Pierzynowska, K., Piotrowska, E., Węgrzyn, G., 2018. How close are we to therapies for Sanfilippo disease? *Metab. Brain Dis.* 33 (1), 1–10. <https://doi.org/10.1007/s11011-017-0111-4>.
- Gautam, S., Karmakar, S., Batra, R., Sharma, P., Pradhan, P., Singh, J., Kundu, B., Chowdhury, P.K., 2017. Polyphenols in combination with β -cyclodextrin can inhibit and disaggregate α -synuclein amyloids under cell mimicking conditions: A promising therapeutic alternative. *Biochim. Biophys. Acta Protein Proteomics* 1865 (5), 589–603. <https://doi.org/10.1016/j.bbapap.2017.02.014>.
- Gomes, B.A.Q., Silva, J.P.B., Romeiro, C.F.R., dos Santos, S.M., Rodrigues, C.A., Gonçalves, P.R., Sakai, J.T., Santos Mendes, P.F., Pompeu Varela, E.L., Monteiro, M. C., 2018. Neuroprotective mechanisms of resveratrol in Alzheimer's disease: Role of SIRT1. *Oxid. Med. Cell Longev.* 1, 15. <https://doi.org/10.1155/2018/8152373>.
- Gupta, P.K., DiPette, D.J., Supowit, S.C., 2014. Protective effect of resveratrol against pressure overload-induced heart failure. *Food Sci. Nutr.* 2 (3), 218–229. <https://doi.org/10.1002/fsn.392>.
- Higashida, K., Kim, S.H., Jung, S.R., Asaka, M., Holloszy, J.O., Han, D.H., 2013. Effects of resveratrol and SIRT1 on PGC-1 α activity and mitochondrial biogenesis: a reevaluation. *PLoS Biol.* 11 (7), e1001603. <https://doi.org/10.1371/journal.pbio.1001603>.
- Huang, Y., Lang, H., Chen, K., Zhang, Y., Gao, L., Ran, L., Yi, L., Mi, M., Zhang, Q., 2020. Resveratrol protects against nonalcoholic fatty liver disease by improving lipid metabolism and redox homeostasis via the PPAR α pathway. *Appl. Physiol. Nutr. Metab.* 45, 227–239. <https://doi.org/10.1139/apnm-2019-0057>.
- Ido, Y., Duranton, A., Lan, F., Weikel, K.A., Breton, L., Ruderman, N.B., 2015. Resveratrol prevents oxidative stress-induced senescence and proliferative dysfunction by activating the AMPK-FOXO3 cascade in cultured primary human keratinocytes. *PLoS One* 10 (2), e0115341. <https://doi.org/10.1371/journal.pone.0115341>.
- Kanamori, H., Takemura, G., Goto, K., Tsujimoto, A., Ogino, A., Takeyama, T., Kawaguchi, T., Watanabe, T., Morishita, K., Kawasaki, M., Mikami, A., Fujiwara, T., Fujiwara, H., Seishima, M., Minatoguchi, S., 2013. Resveratrol reverses remodeling in hearts with large, old myocardial infarctions through enhanced autophagy-activating AMP kinase pathway. *Am. J. Pathol.* 182 (3), 701–713. <https://doi.org/10.1016/j.ajpath.2012.11.009>.
- Kimura, Y., 2003. Prevention of cancer chemotherapy drug-induced adverse reaction, antitumor and antimetastatic activities by natural products. In: Atta-ur-Rahman (Ed.), *Studies in Natural Products Chemistry*, Part 1, 28. Elsevier Science, pp. 559–586. [https://doi.org/10.1016/S1572-5995\(03\)80149-7](https://doi.org/10.1016/S1572-5995(03)80149-7).
- Kong, D., Yan, Y., He, X.-Y., Yang, H., Liang, B., Wang, J., He, Y., Ding, Y., Yu, H., 2019. Effects of resveratrol on the mechanisms of antioxidants and estrogen in Alzheimer's disease. *BioMed Res. Int.* 1, 8. <https://doi.org/10.1155/2019/8983752>.
- Kou, X., Chen, Ni., 2017. Resveratrol as a natural autophagy regulator for prevention and treatment of Alzheimer's disease. *Nutrients* 9 (9), 927. <https://doi.org/10.3390/nu9090927>.
- Krawiec, P., Pac-Kożuchowska, E., Melges, B., Mroczkowska-Juchkiewicz, A., Skomra, S., Pawłowska-Kamieniak, A., Kominek, K., 2014. From hypertransaminasemia to mucopolysaccharidosis IIIA. *Ital. J. Pediatr.* 40 (1). <https://doi.org/10.1186/s13052-014-0097-z>.
- Kuno, A., Hosoda, R., Sebori, R., Hayashi, T., Sakuragi, H., Tanabe, M., Horio, Y., 2018. Resveratrol ameliorates mitophagy disturbance and improves cardiac pathophysiology of dystrophin-deficient mdx mice. *Sci. Rep.* 8 (1). <https://doi.org/10.1038/s41598-018-33930-w>.
- Lan, F., Weikel, K.A., Cacicado, J.M., Ido, Y., 2017. Resveratrol-induced AMP-activated protein kinase activation is cell-type dependent: Lessons from basic research for clinical application. *Nutrients* 9 (7), 751. <https://doi.org/10.3390/nu9070751>.
- Lawrence, R., Brown, J.R., Lorey, F., Dickson, P.I., Crawford, B.E., Esko, J.D., 2014. Glycan-based biomarkers for mucopolysaccharidoses. *Mol. Genet. Metab.* 111 (2), 73–83. <https://doi.org/10.1016/j.ymgme.2013.07.016>.
- Lee, I.H., 2019. Mechanisms and disease implications of sirtuin-mediated autophagic regulation. *Exp. Mol. Med.* 51 (9), 1–11. <https://doi.org/10.1038/s12276-019-0302-7>.
- Li, X.-N., Song, J., Zhang, L., LeMaire, S.A., Hou, X., Zhang, C., Shen, Y.H., 2009. Activation of the AMPK-FOXO3 pathway reduces fatty acid-induced increase in intracellular reactive oxygen species by upregulating thioredoxin. *Diabetes* 58 (10), 2246–2257. <https://doi.org/10.2337/db08-1512>.
- Ma, S., Feng, J., Zhang, R., Chen, J., Han, D., Li, X., Yang, B., Li, X., Fan, M., Li, C., Tian, Z., Cao, F., 2017. SIRT1 activation by resveratrol alleviates cardiac dysfunction via mitochondrial regulation in diabetic cardiomyopathy mice. *Oxid. Med. Cell Longev.* 1, 15. <https://doi.org/10.1155/2017/4602715>.
- Makowska-Was, J., Janeczko, Z., 2008. *Stilbeny pochodzenia naturalnego, część I. Rośliny lecznicze w Polsce i na świecie* 2 (14).
- Mancuso, R., del Valle, J., Modol, L., Martínez, A., Granado-Serrano, A.B., Ramirez-Núñez, O., Pallás, M., Portero-Otin, M., Osta, R., Navarro, X., 2014. Resveratrol improves motoneuron function and extends survival in SOD1G93A ALS mice. *Neurotherapeutics* 11 (2), 419–432. <https://doi.org/10.1007/s13311-013-0253-y>.
- Martins, C., Hülková, H., Dridi, L., Dormoy-Raclet, V., Grigoryeva, L., Choi, Y., Langford-Smith, A., Wilkinson, F.L., Ohmi, K., DiCristo, G., Hamel, E., Ausseil, J., Cheillan, D., Moreau, A., Svobodová, E., Hájková, Z., Tesarova, M., Hansiková, H., Bigger, B.W., Hřebíček, M., Pshchetsky, A.V., 2015. Neuroinflammation, mitochondrial defects and neurodegeneration in mucopolysaccharidosis III type C mouse model. *Brain* 138 (2), 336–355. <https://doi.org/10.1093/brain/awu355>.
- Meng, Z., Jing, H., Gan, L., Li, H., Luo, B., 2016. Resveratrol attenuated estrogen-deficient-induced cardiac dysfunction: Role of AMPK, SIRT1, and mitochondrial function. *Am J Transl Res* 8 (6), 2641–2649. <https://doi.org/10.1186/1745-7581-8-2641>.
- Morishita, K., Petty, R.E., 2011. Musculoskeletal manifestations of mucopolysaccharidoses. *Rheumatology* 50 (Suppl. 5), v19–v25. <https://doi.org/10.1093/rheumatology/ker397>.
- Muenzer, J., 2011. Overview of the mucopolysaccharidoses. *Rheumatology (Oxford)* 50 (5), 4–12. <https://doi.org/10.1093/rheumatology/ker394>.

- Oz, B., Yildirim, A., Yolbas, S., Celik, Z.B., Etem, E.O., Deniz, G., Akin, M., Abidin Akar, Z., Karatas, A., Koca, S.S., 2018. Resveratrol inhibits Src tyrosine kinase, STAT3, and Wnt signaling pathway in collagen induced arthritis model. *Biofactors* 45 (1), 69–74. <https://doi.org/10.1002/biof.1463>.
- Park, D., Jeong, H., Lee, M.N., Koh, A., Kwon, O., Yang, Y.R., Ryu, S.H., 2016. Resveratrol induces autophagy by directly inhibiting mTOR through ATP competition. *Sci. Rep.* 6 (1), 21772. <https://doi.org/10.1038/srep21772>.
- Parker, J.A., Arango, M., Abderrahmane, S., Lambert, E., Tourette, C., Catoire, H., Néri, C., 2005. Resveratrol rescues mutant polyglutamine cytotoxicity in nematode and mammalian neurons. *Nat. Genet.* 37 (4), 349–350. <https://doi.org/10.1038/ng1534>.
- Parkinson-Lawrence, E.J., Shandala, T., Prodoehl, M., Plew, R., Borlace, G.N., Brooks, D. A., 2010. Lysosomal storage disease: Revealing lysosomal function and physiology. *Physiology* 25, 102–115. <https://doi.org/10.1152/physiol.00041.2009>.
- Pasinetti, G.M., Wang, J., Marambaud, P., Ferruzzi, M., Gregor, P., Knable, L.A., Ho, L., 2011. Neuroprotective and metabolic effects of resveratrol: Therapeutic implications for Huntington's disease and other neurodegenerative disorders. *Exp. Neurol.* 232 (1), 1–6. <https://doi.org/10.1016/j.expneurol.2011.08.014>.
- Pierzynowska, K., Gaffke, L., Cyske, Z., Puchalski, M., Rintz, E., Bartkowski, M., Węgrzyn, G., 2018a. Autophagy stimulation as a promising approach in treatment of neurodegenerative diseases. *Metab. Brain Dis.* 33 (4), 989–1008. <https://doi.org/10.1007/s11011-018-0214-6>.
- Pierzynowska, K., Gaffke, L., Hać, A., Mantej, J., Niedziałek, N., Brokowska, J., Węgrzyn, G., 2018b. Correction of Huntington's disease phenotype by genistein-induced autophagy in the cellular model. *NeuroMolecular Med.* 20 (1), 112–123. <https://doi.org/10.1007/s12017-018-8482-1>.
- Pierzynowska, K., Podlacha, M., Gaffke, L., Majkutewicz, I., Mantej, J., Węgrzyn, A., Osiały, M., Myślińska, D., Węgrzyn, G., 2019. Autophagy-dependent mechanism of genistein-mediated elimination of behavioral and biochemical defects in the rat model of sporadic Alzheimer's disease. *Neuropharmacology* 148, 332–346. <https://doi.org/10.1016/j.neuropharm.2019.01.030>.
- Pierzynowska, K., Gaffke, L., Podlacha, M., Brokowska, J., Węgrzyn, G., 2020. Mucopolysaccharidosis and autophagy: Controversies on the contribution of the process to the pathogenesis and possible therapeutic applications. *NeuroMolecular Med.* 22 (1), 25–30. <https://doi.org/10.1007/s12017-019-08559-1>.
- Ribeiro, E.M., Brusius-Facchin, A.C., Leistner-Segal, S., da Silva, C.A.B., Schwartz, I.V., 2014. Cardiac disease as the presenting feature of mucopolysaccharidosis type IIIA: A case report. *Mol. Genet. Metab. Rep.* 1, 422–424. <https://doi.org/10.1016/j.ymgmr.2014.09.003>.
- Rimbaud, S., Ruiz, M., Piquereau, J., Mateo, P., Fortin, D., Vekslar, V., Garnier, A., Ventura-Clapier, R., 2011. Resveratrol improves survival, hemodynamics and energetics in a rat model of hypertension leading to heart failure. *PLoS One* 6 (10), e26391. <https://doi.org/10.1371/journal.pone.0026391>.
- Rintz, E., Gaffke, L., Podlacha, M., Brokowska, J., Cyske, Z., Węgrzyn, G., Pierzynowska, K., 2020. Transcriptomic changes related to cellular processes with particular emphasis on cell activation in lysosomal storage diseases from the group of mucopolysaccharidoses. *Int. J. Mol. Sci.* 21 (9), 3194. <https://doi.org/10.3390/ijms21093194>.
- Riveiro-Naveira, R.R., Valcárcel-Ares, M.N., Almonte-Becerril, M., Vaamonde-García, C., Loureiro, J., Hermida-Carballo, L., López-Peláez, E., Blanco, F.J., López-Armeda, M. J., 2016. Resveratrol lowers synovial hyperplasia, inflammatory markers and oxidative damage in an acute antigen-induced arthritis model. *Rheumatology* 55 (10), 1889–1900. <https://doi.org/10.1093/rheumatology/kew255>.
- Rodgers, J.T., Lerin, C., Gerhart-Hines, Z., Puigserver, P., 2007. Metabolic adaptations through the PGC-1 α and SIRT1 pathways. *FEBS (Fed. Eur. Biochem. Soc.) Lett.* 582 (1), 46–53. <https://doi.org/10.1016/j.febslet.2007.11.034>.
- Salminen, A., Kaamiranta, K., 2009. SIRT1: Regulation of longevity via autophagy. *Cell. Signal.* 21 (9), 1356–1360. <https://doi.org/10.1016/j.cellsig.2009.02.014>.
- Sawamoto, K., Chen, H.-H., Alcegica-Dıaz, C.J., Mason, R.W., Tomatsu, S., 2018. Gene therapy for mucopolysaccharidoses. *Mol. Genet. Metab.* 123 (2), 59–68. <https://doi.org/10.1016/j.ymgme.2017.12.434>.
- Sawda, C., Moussa, C., Turner, R.S., 2017. Resveratrol for Alzheimer's disease. *Ann. N. Y. Acad. Sci.* 1403 (1), 142–149. <https://doi.org/10.1111/nyas.13431>.
- Scarpa, M., Lourenço, C.M., Amartino, H., 2017. Epilepsy in mucopolysaccharidosis disorders. *Mol. Genet. Metab.* 122, 55–61. <https://doi.org/10.1016/j.ymgme.2017.10.006>.
- Shankar, S., Chen, Q., Siddiqui, I., Sarva, K., Srivastava, R.K., 2007. Sensitization of TRAIL-resistant LNCaP cells by resveratrol (3, 4', 5 tri-hydroxystilbene): molecular mechanisms and therapeutic potential. *J. Mol. Signal.* 2 <https://doi.org/10.1186/1750-2187-2-7>.
- Shankar, S., Srivastava, R., 2007. Involvement of Bcl-2 family members, phosphatidylinositol 3'-kinase/AKT and mitochondrial p53 in curcumin (diferulolylmethane)-induced apoptosis in prostate cancer. *Int. J. Oncol.* 30 (4), 905–918. <https://doi.org/10.3892/ijo.30.4.905>.
- Song, L., Chen, L., Zhang, X., Li, J., Le, W., 2014. Resveratrol ameliorates motor neuron degeneration and improves survival in SOD1G93A mouse model of amyotrophic lateral sclerosis. *BioMed Res. Int.* 1–10. <https://doi.org/10.1155/2014/483501>.
- Suvorova, I.I., Pospelov, V.A., 2019. AMPK/ULK1-dependent autophagy as a key mTOR regulator in the context of cell pluripotency. *Cell Death Dis.* 10 (4), 260. <https://doi.org/10.1038/s41419-019-1501-9>.
- Tian, Y., Ma, J., Wang, W., Zhang, L., Xu, J., Wang, K., Li, D., 2016. Resveratrol supplement inhibited the NF- κ B inflammation pathway through activating AMPK α -SIRT1 pathway in mice with fatty liver. *Mol. Cell. Biochem.* 422 (1–2), 75–84. <https://doi.org/10.1007/s11010-016-2807-x>.
- Tiao, M.-M., Lin, T.-J., Yu, H.-R., Sheen, J.-M., Lin, I.-C., Lai, Y.-J., Tain, Y.-L., Huang, L.-T., Tsai, C.-C., 2018. Resveratrol ameliorates maternal and post-weaning high-fat diet-induced nonalcoholic fatty liver disease via renin-angiotensin system. *Lipids Health Dis.* 17 (1), 178. <https://doi.org/10.1186/s12944-018-0824-3>.
- Tomatsu, S., Alcegica-Dıaz, C.J., Barbosa, H., Montano, A.M., Barrera, L.A., Shimada, T., Eriko, Y., Mackenzie, W.G., Mason, R.W., Suzuki, Y., Orii, K.E., Orii, T., 2013. Therapies of mucopolysaccharidosis IVA (Morquio A syndrome). *Expert Opinion on Orphan Drugs* 1 (10), 805–818. <https://doi.org/10.1517/21678707.2013.846853>.
- Tomatsu, S., Lavery, Ch, Giugliani, R., Harmatz, P., Scarpa, M., Węgrzyn, G., Orii, T., 2018. Mucopolysaccharidoses Update (2 Volume Set). Nova Science Publisher.
- Vidoni, C., Secomandi, E., Castiglioni, A., Melone, M.A.B., Isidoro, C., 2018. Resveratrol protects neuronal-like cells expressing mutant Huntingtin from dopamine toxicity by rescuing ATG4-mediated autophagosome formation. *Neurochem. Int.* 117, 174–187. <https://doi.org/10.1016/j.neuint.2017.05.013>.
- Wang, J., Zhang, Y., Tang, L., Zhang, N., Fan, D., 2011. Protective effects of resveratrol through the up-regulation of SIRT1 expression in the mutant hSOD1-G93A-bearing motor neuron-like cell culture model of amyotrophic lateral sclerosis. *Neurosci. Lett.* 503 (3), 250–255. <https://doi.org/10.1016/j.neulet.2011.08.047>.
- Wang, Y., Romigh, T., He, X., Orloff, M.S., Silverman, R.H., Heston, W.D., Eng, C., 2010. Resveratrol regulates the PTEN/AKT pathway through androgen receptor-dependent and -independent mechanisms in prostate cancer cell lines. *Hum. Mol. Genet.* 19 (22), 4319–4329. <https://doi.org/10.1093/hmg/ddq354>.
- Wu, J.M., Hsieh, T.-Ch., 2018. Resveratrol: State-of-the-art science and health applications - actionable targets and mechanisms of resveratrol. *World Scientific* 348, 80–100.
- Wu, Y., Li, X., Zhu, J.X., Xie, W., Le, W., Fan, Z., Jankovic, J., Pan, T., 2011. Resveratrol-activated AMPK/SIRT1/Autophagy in cellular models of Parkinson's disease. *Neurosignals* 19 (3), 163–174. <https://doi.org/10.1159/000328516>.
- Xia, D., Sui, R., Zhang, Z., 2019. Administration of resveratrol improved Parkinson's disease-like phenotype by suppressing apoptosis of neurons via modulating the MALAT1/miR-129/SNCA signaling pathway. *J. Cell. Biochem.* 120 (4), 4942–4951. <https://doi.org/10.1002/jcb.27769>.
- Xu, K., Liu, X., Ke, Z., Yao, Q., Guo, S., Liu, C., 2018. Resveratrol modulates apoptosis and autophagy induced by high glucose and palmitate in cardiac cells. *Cell. Physiol. Biochem.* 46 (5), 2031–2040. <https://doi.org/10.1159/000489442>.
- Zhang, T., Chi, Y., Ren, Y., Du, C., Shi, Y., Li, Y., 2019. Resveratrol reduces oxidative stress and apoptosis in podocytes via sir2-related enzymes, Sirtuins 1 (SIRT1)/ Peroxisome proliferator-activated receptor γ Co-activator 1 α (PGC-1 α) Axis. *Med. Sci. Mon. Int. Med. J. Exp. Clin. Res.* 25, 1220–1231. <https://doi.org/10.12659/MSM.911714>.
- Zhao, H., Han, L., Jian, Y., Ma, Y., Yan, W., Chen, X., Xu, H., Li, L., 2018. Resveratrol induces apoptosis in human melanoma cell through negatively regulating Erk/PKM2/Bcl-2 axis. *OncoTargets Ther.* 11, 8995–9006. <https://doi.org/10.2147/OTT.S186247>.
- Zhou, T.T., Wang, X.-Y., Huang, J., Deng, Y.-Z., Qiu, L.-J., Liu, H.-Y., Xing-Wang, Xu, Zhao-Xia Ma, B.S., Lei Tang, M.D., Chen, H.-P., 2020. Mitochondrial translocation of DJ-1 is mediated by Grp75. *J. Cardiovasc. Pharmacol.* 75 (4), 305–313. <https://doi.org/10.1097/fjc.0000000000000805>.
- Zhou, X., Yang, J., Zhou, M., Zhang, Y., Liu, Y., Hou, P., Zeng, X., Yi, L., Mi, M., 2019. Resveratrol attenuates endothelial oxidative injury by inducing autophagy via the activation of transcription factor EB. *Nutr. Metab.* 16, 42. <https://doi.org/10.1186/s12986-019-0371-6>.

Authors Contribution

Oświadczenie o wkładzie w publikację

Oświadczam, że mój wkład w publikację:

Rintz E, Pierzynowska K, Podlacha M, Węgrzyn G. Has resveratrol a potential for mucopolysaccharidosis treatment? Eur J Pharmacol. 2020 Dec 5;888:173534. doi: 10.1016/j.ejphar.2020.173534. Epub 2020 Aug 30. PMID: 32877657.

polegał na:

- kierowaniu projektem Preludium 18;
- zaplanowanie koncepcji pracy przeglądowej;
- napisanie wstępnej pracy przeglądowej;
- przeglądzie literatury;
- poprawienie ostatecznej wersji manuskryptu;
- udziale w dyskusji z recenzentami.



Uniwersytet Gdański
Katedra Biologii Molekularnej
mgr Estera Rintz

Oświadczenie o wkładzie w publikację

Oświadczam, że mój wkład w publikację:

Rintz E, Pierzynowska K, Podlacha M, Węgrzyn G. Has resveratrol a potential for mucopolysaccharidosis treatment? Eur J Pharmacol. 2020 Dec 5;888:173534. doi: 10.1016/j.ejphar.2020.173534. Epub 2020 Aug 30. PMID: 32877657.

polegał na:

1. udziale w przeglądzie literatury;
2. udziale w przygotowaniu manuskryptu publikacji;
3. udziale w dyskusji z recenzentami.



Dr hab. Magdalena Podlacha
Katedra Biologii Molekularnej
Wydział Biologii
Uniwersytet Gdański

Gdańsk, 25.04.2024

Oświadczenie o wkładzie w publikację

Oświadczam, że mój wkład w publikację:

Rintz E, Pierzynowska K, Podlacha M, Węgrzyn G. Has resveratrol a potential for mucopolysaccharidosis treatment? Eur J Pharmacol. 2020 Dec 5;888:173534. doi: 10.1016/j.ejphar.2020.173534. Epub 2020 Aug 30. PMID: 32877657.

polegał na:

1. udziale w przygotowaniu manuskryptu publikacji;
2. udziale w dyskusji z recenzentami.



Prof. dr hab. Grzegorz Węgrzyn
Katedra Biologii Molekularnej
Wydział Biologii
Uniwersytet Gdański

Gdańsk, 29.05.2024

Oświadczenie o wkładzie w publikację

Oświadczam, że mój wkład w publikację:

Rintz E, Pierzynowska K, Podlacha M, Węgrzyn G. Has resveratrol a potential for mucopolysaccharidosis treatment? Eur J Pharmacol. 2020 Dec 5;888:173534. doi: 10.1016/j.ejphar.2020.173534. Epub 2020 Aug 30. PMID: 32877657.

polegał na opiece nad Panią Esterą Rintz oraz udziale w przygotowaniu ostatecznej wersji manuskryptu i wysłaniu jej do czasopisma.

KIEROWNIK
KATEDRY BIOLOGII MOLEKULARNEJ

prof. dr hab. Grzegorz Węgrzyn

prof. dr hab. Grzegorz Węgrzyn

Rintz, E., Podlacha, M., Cyske, Z., Pierzynowska, K., Wegrzyn, G.,
Gaffke, L. (2023)

Activities of (Poly)phenolic Antioxidants and Other Natural
Autophagy Modulators in the Treatment of Sanfilippo Disease:
Remarkable Efficacy of Resveratrol in Cellular and Animal Models.
Neurotherapeutics. 20(1):254-271.

Impact Factor = 5.7 (2023)

MNISW Punctuation = 140



Activities of (Poly)phenolic Antioxidants and Other Natural Autophagy Modulators in the Treatment of Sanfilippo Disease: Remarkable Efficacy of Resveratrol in Cellular and Animal Models

Estera Rintz¹ · Magdalena Podlacha¹ · Zuzanna Cyske¹ · Karolina Pierzynowska¹ · Grzegorz Węgrzyn¹ · Lidia Gaffke¹

Accepted: 22 October 2022
© The Author(s) 2022

Abstract

Sanfilippo disease, caused by mutations in the genes encoding heparan sulfate (HS) (a glycosaminoglycan; GAG) degradation enzymes, is a mucopolysaccharidosis (MPS), which is also known as MPS type III, and is characterized by subtypes A, B, C, and D, depending on identity of the dysfunctional enzyme. The lack of activity or low residual activity of an HS-degrading enzyme leads to excess HS in the cells, impairing the functions of different types of cells, including neurons. The disease usually leads to serious psychomotor dysfunction and death before adulthood. In this work, we show that the use of molecules known as dietary (poly)phenolic antioxidants and other natural compounds known as autophagy activators (genistein, capsaicin, curcumin, resveratrol, trehalose, and calcitriol) leads to accelerated degradation of accumulated HS in the fibroblasts of all subtypes of MPS III. Both the cytotoxicity tests we performed and the available literature data indicated that the use of selected autophagy inducers was safe. Since it showed the highest effectivity in cellular models, resveratrol efficacy was tested in experiments with a mouse model of MPS IIIB. Urinary GAG levels were normalized in MPS IIIB mice treated with 50 mg/kg/day resveratrol for 12 weeks or longer. Behavioral tests indicated complete correction of hyperactivity and anxiety in these animals. Biochemical analyses indicated that administration of resveratrol caused autophagy stimulation through an mTOR-independent pathway in the brains and livers of the MPS IIIB mice. These results indicate the potential use of resveratrol (and possibly other autophagy stimulators) in the treatment of Sanfilippo disease.

Keywords Autophagy inducers · Resveratrol · Sanfilippo disease · Novel therapy

Introduction

Sanfilippo disease (mucopolysaccharidosis type III or MPS III) belongs to a group of lysosomal storage diseases (LSDs) caused by mutations leading to the accumulation of a glycosaminoglycan (GAG): heparan sulfate (HS) [1]. In MPS III, one of the following genes encoding HS-degrading enzymes is pathologically mutated: the *SGSH* gene (encoding N-sulfatase heparan), *NAGLU* gene (encoding α -N-acetylglucosaminidase), *HGSNAT* gene (encoding acetyl-CoA: α -glucosaminide acetyltransferase), and *GNS* gene

(encoding N-acetylglucosamine-6-sulfatase), resulting in one of the 4 subtypes of the disease, MPS III A, B, C, and D, respectively [2]. The pathways of HS degradation, enzymes involved in this process, and MPS types/subtypes caused by deficiencies of specific enzymes are presented in Fig. 1.

MPS III is a neuronopathic mucopolysaccharidosis [3]. Patients affected by this disease present with a set of common traits that include developmental delay, sleep disturbances, aggressive behavior, cognitive decline, hyperactivity, and seizures [4]. These symptoms sometimes appear at the age of a few months, but they are usually evident when an affected child is a few years old. Because these symptoms are not unique to MPS III, this disease is often misdiagnosed in its early stages [5]. The expected lifespan of Sanfilippo disease patients is approximately 2 decades [1].

Despite various attempts to develop a therapy for Sanfilippo disease, no treatment has been shown to be effective in patients to date [6]. In fact, although many encouraging

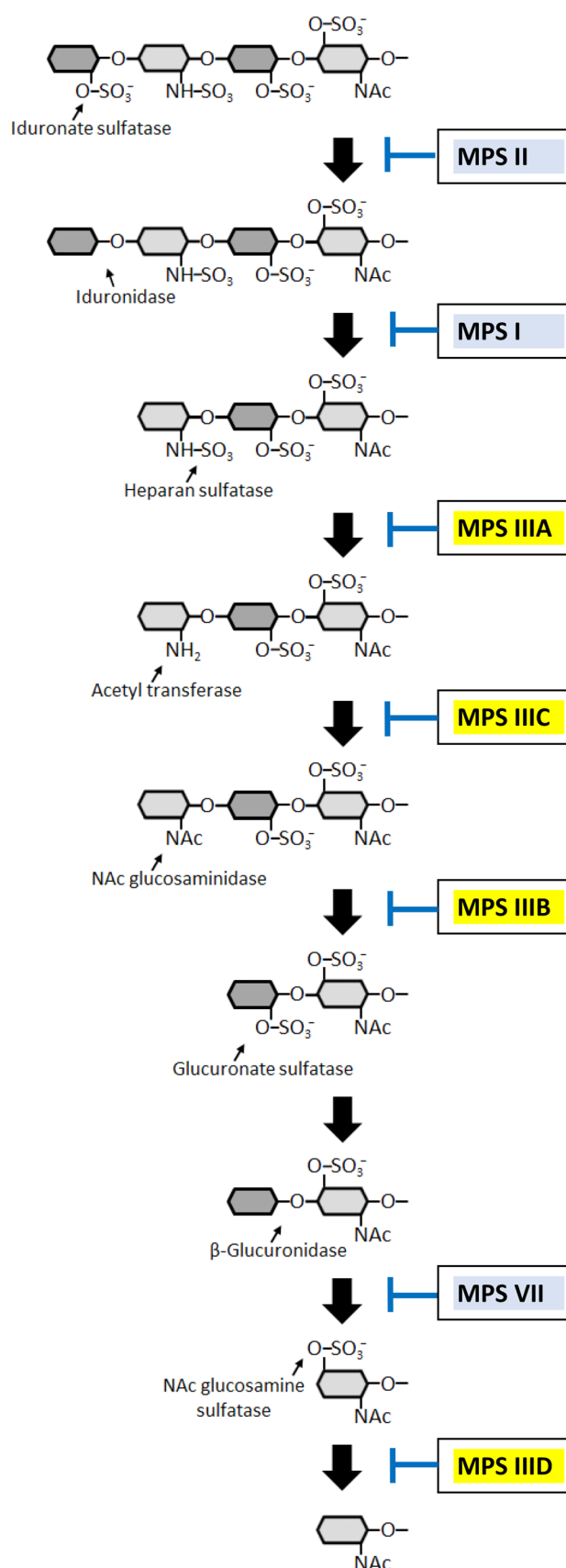
✉ Lidia Gaffke
lidia.gaffke@ug.edu.pl

¹ Department of Molecular Biology, Faculty of Biology, University of Gdansk, Wita Stwosza 59, 80-308 Gdansk, Poland

Fig. 1 The pathway of heparan sulfate (HS) degradation. The HS molecule consists of repeated polysaccharide fragments composed of the following mono-sugars: 2-O-sulfo- α -L-iduronic acid, 2-deoxy-2-sulfamido- α -D-glucopyranosyl, 2-O-sulfo-glucuronic acid, and 2-deoxy-2-acetamido- α -D-glucopyranosyl sulfate. Enzymes involved in the sequential steps of HS degradation are indicated with arrows showing the specific reactions they catalyze. As a result of deficiency in any one of these enzymes, the degradation process is halted at a specific stage (symbolized by blunt-ended lines), causing the accumulation of undegraded HS-derivative and the development of symptoms corresponding to an MPS type/subtype (marked in boxes). The disease subtypes with accumulated HS as the only primary molecule stored in excess are commonly grouped into the MPS III (Sanfilippo disease) A, B, C, and D subtypes (marked in yellow), based on ref. [1] with modifications

results of various therapeutic approaches have been reported in preclinical trials (including enzyme replacement therapy, gene therapy, substrate reduction therapy, and others [7–9]), no therapy has been approved for MPS III [10]. Severe neurodegeneration is a major obstacle in the development of an effective therapy for this disease, as it is challenging to find an efficient way to deliver potential drugs, especially large molecules, to the brain [6]. Moreover, recent studies have indicated that although HS storage is the major pathomechanism of the disease, secondary processes, including the dysregulated expression of hundreds of genes encoding proteins involved in the structures and functions of various cellular organelles, as well as different cellular processes (such as metabolic processes, cell communication, signal transduction, cell development, movement of subcellular components, and the cell cycle), may significantly influence the pathomechanisms of Sanfilippo disease, hindering the development of effective therapies [11–14]. Recent failures in the clinical improvements of MPS III patients participating in clinical trials with different kinds of therapies, such as gene therapy [15], enzyme replacement therapy [16, 17], and substrate reduction therapy [18], have confirmed the great challenge to finding an effective therapy for Sanfilippo disease [19].

In this light, novel therapeutic approaches to MPS III are highly desirable. Autophagy is a highly conserved process in all eukaryotic cells, functioning at a low level and activated largely by the action of various external factors or by incorrectly folded macromolecules. A macromolecule destined for degradation is encompassed by an insulating membrane, forming a vesicle called an autophagosome. An autophagosome fuses with a lysosome, and lysosomal enzymes digest the macromolecules in the autophagolysosome, forming single monomers that can be reused by the cell [20]. Induction of autophagy has been proposed as a promising therapeutic strategy for neurodegenerative diseases associated with protein aggregation (such as Huntington's disease, Alzheimer's disease, and Parkinson's disease), as stimulated removal of



these toxic structures might restore cellular homeostasis [21]. However, autophagy has rarely been evaluated as an MPS III treatment strategy, although suggestions about its possible effectiveness have been published [22–26]. However, autophagy is not limited to the degradation of proteins; in fact, it is a poorly selective process and can remove stored carbohydrates such as GAG. Therefore, the broad spectrum of neurodegenerative diseases might be considered when assessing autophagy-related treatments. Nevertheless, any potential pharmacological treatment of a genetic disease is necessarily a long-term strategy; therefore, a putative drug must be safe for long-term use. Unfortunately, most strong exogenous autophagy activators are deleterious to cells when used for a long time; therefore, they are not appropriate candidates for treatments against genetic diseases [27]. Hence, in our studies, we have focused on natural compounds that are safe for patients to use long-term and that effectively stimulate autophagy [28].

In this study, we asked whether pharmacological stimulation of autophagy by naturally occurring molecules can accelerate the degradation of stored GAG in MPS III. In this work, we tested the following known phenolic compounds and other natural autophagy stimulators: capsaicin [29, 30], curcumin [31–33], resveratrol [34, 35], trehalose (the only autophagy stimulator previously reported to be a potential drug for MPS III treatment) [22, 36, 37], and calcitriol [38, 39]. Since resveratrol showed the greatest capacity to reduce the amount of stored GAG (HS) in all subtypes of MPS III, as demonstrated in experiments with fibroblast cultures, this compound was chosen for further study with a mouse model of MPS IIIB. These experiments allowed us to test a recently proposed hypothesis suggesting that resveratrol might be a potential therapeutic agent in the treatment of MPS [40]. Our results confirmed the high potential of natural autophagy inducers, especially resveratrol, in the treatment of Sanfilippo disease, as assessed in experiments with cell and animal models.

Methods

Cell Cultures

Lines of fibroblasts derived from patients suffering from Sanfilippo disease types A, B, C, and D, as well as a control cell line of human fibroblasts (the HDFa line), were assessed. MPS III fibroblasts were purchased from the NIGMS Human Genetic Cell Repository at the Coriell Institute for Medical Research (this Institute provides all documentation related to bioethical issues). The following cell lines were used: HDFa — control fibroblasts derived from a healthy person; MPS IIIA — fibroblasts (NIGMS Cat No. GM00879) from a Caucasian, 3-year-old, female patient with mutations in the

SGSH gene: c.G1351A/G746A (p.Glu447Lys/p.Arg245His); MPS IIIB — fibroblasts (NIGMS Cat No. GM00156) from a 7-year-old Caucasian male patient with mutations in the *NAGLU* gene: c.C1876T/C1876T (p.Arg626Ter/p.Arg626Ter); MPS IIIC — fibroblasts (NIGMS Cat No. GM05157) from an 8-year-old male patient of unknown race with mutations in the *HGSNAT* gene and diagnosed on the basis of estimated urinary GAG levels and the activity of the corresponding enzyme in plasma; MPS IIID — fibroblasts (NIGMS Cat No. GM05093) from a 7-year-old Asian–Indian male patient with mutations in the *GNS* gene: c.C1063T/C1063T (p.Arg355Ter/p.Arg355Ter). Cells (passages 6–17) were cultured in flasks with DMEM (Thermo Fisher Scientific Inc., Paisley, UK) supplemented with 10% FBS (Thermo Fisher Scientific Inc., Paisley, UK) and a 1% antibiotic/antimycotic solution (Sigma–Aldrich Co. LLC., St. Louis, USA) at 37 °C in a humidified atmosphere with 5% CO₂.

Reagents

Genistein (99% purity; #446–72-0) was purchased from the Pharmaceutical Research Institute in Warsaw (Poland). It was dissolved in DMSO to obtain stock solutions of 30, 60, and 100 mM; these solutions were stored at –20 °C. Capsaicin (≥99% purity; #M2028) was purchased from Sigma–Aldrich, USA. It was dissolved in DMSO to obtain stock solutions of 10, 50, or 100 mM; these solutions were stored at –20 °C. Curcumin (Cay81025) was purchased from Cayman Chemical, USA. It was dissolved in DMSO to obtain stock solutions of 10, 30, and 80 mM; these solutions were stored at –20 °C. Resveratrol (#T1558) was purchased from TargetMol (USA). It was dissolved in DMSO to obtain stock solutions of 20, 80, and 160 mM; these solutions were prepared and stored at –20 °C. Trehalose (Cay20517) was purchased from Cayman Chemical, USA. It was dissolved in distilled water to obtain a stock solution of 1 M; this solution was stored at –20 °C. Calcitriol (#C0225000) was purchased from Sigma–Aldrich, USA. It was dissolved in 96% ethanol to obtain stock solutions of 10, 50, and 100 mM; these solutions were stored at –20 °C. Thiazolyl blue tetrazolium bromide (98% purity; #M2128) was purchased from Sigma–Aldrich. MTT was dissolved in PBS (4 mg/ml) and stored at 4 °C.

Cell Viability Assay

Cells (3×10^3) were seeded in the wells of 96-well plates and allowed to attach overnight. They were then treated with either DMSO, distilled water or 96% ethanol (control cells) or increasing concentrations of the test compound for 24 h. Then, 25 µl of MTT (3-(4,5-dimethylthiazol-2-yl)-2,5-diphenyltetrazolium bromide) solution (4 mg/ml) was

added to each well. Following a 3-h incubation at 37 °C, formazan crystals that formed in living cells were dissolved in 100 µl of DMSO. Absorbance was measured at 570 nm and 660 nm (the reference wavelengths) with a Victor3 microplate reader.

Measurement of Glycosaminoglycan (GAG) Levels in Fibroblasts

For the determination of GAG levels in fibroblasts, 1×10^5 cells were seeded in each well of a 6-well plate, and they were allowed to attach overnight. The cells were then treated with either DMSO, distilled water, or 96% ethanol (control cells) or increasing concentrations of the test compound for 24 h and collected in tubes via trypsinization. The level of GAG in the cells was measured using a Glycosaminoglycan Assay Blyscan kit (Biocolor Ltd., Carrickfergus, UK) following the manufacturer's instructions.

Levels of heparan sulfate (HS) in fibroblasts were estimated using extracts from cells treated with lysis buffer (1% Triton X-100, 0.5 mM EDTA, 150 mM NaCl, and 50 mM Tris, pH 7.5) and the dot-blot procedure with a PVDF membrane (IPFL00010, Millipore). Briefly, cell extracts were fixed to the membrane using a dot-blot apparatus (Bio-Rad, Hercules, CA, USA). The membrane was blocked with 5% nonfat dry milk in PBST buffer and incubated with a primary mouse anti-HS antibody (NBP-2–23,523, Novus) overnight at 4 °C. Then, the membrane was washed with PBST and incubated with a secondary anti-mouse antibody coupled with peroxidase (#A9044, Sigma Aldrich, USA) for 1 h at room temperature. Following treatment with a chemiluminescent HRP substrate (Merck, Darmstadt, Germany) solution, the membrane was exposed to X-ray film. The intensities of the dots were analyzed with QuantityOne software. The values were normalized to the total protein amount as determined by Ponceaus S staining.

Animals

The B6.129S6-Naglu^{tm1Efn/J} mouse model of MPS IIIB (*Naglu*^{-/-}) was used (JAX stock #003,827, purchased from Jackson Laboratories (Sacramento, CA, USA)). MPS IIIB mice were backcrossed with C57BL/6 J (WT) mice. Each group of mice consisted of six males ($n=6$). This size of each group was calculated via power analysis, which indicates the number of animals ($n=6$) to include in each experimental group to achieve an $\alpha=5\%$ as the significance level for a statistical test with a power of 95%. All animal procedures were approved by the Local Ethics Committee for Animal Experiments in Bydgoszcz (application approval no. BUD13/2020) and carried out according to the guidelines of the European Communities Council Directive (2010/63/

UE). The mice were housed with a 12/12-h light/dark cycle and with food and water provided ad libitum.

Administration of Resveratrol or Water to Mice

Resveratrol was administered to mice by an orogastric probe once per day. The dose was 50 mg/kg mouse weight/day, and the duration of the treatment was 22 weeks (starting when the mice were 8 weeks old). Stock volumes of resveratrol suspension in water were prepared in such a way that a single dose administered to a mouse was 0.1 ml or lower. The control group of mice received 0.1 ml of distilled water administered by orogastric probe, exactly as resveratrol treatment of the mice, every day.

Determination of Urinary GAG Levels

Urine samples were collected using commercially available hydrophobic sand (LabSand, Coastline Global, Palo Alto, CA) at four time points: when the mice reached 5, 10, 20, and 30 weeks of age. The material was collected at a fixed time between 10:00 a.m. and 12:00 a.m. This method is much less stressful for the animals than the use of metabolic cages, and it reduces the influence of additional factors that can interfere with the evaluation of the parameters of interest. In brief, a portion of hydrophobic sand was poured into the bottom of a cage measuring 15.2 cm \times 25.4 cm with a surface area of 386 cm². The mice were individually placed in the cage and prepared for testing. Prior to urine sampling, the animals had no access to water or food (for 2 h), but their movement was not restricted in any way. Due to the special properties of the sand used, the urine samples stayed on the surface and were easily collected with a pipette. Samples of mouse urine were prepared for measurements by making serial dilutions (with a final sample volume of 0.1 ml) to obtain values that could be compared to a calibration curve obtained using known GAG concentrations. GAG levels were measured using a commercial kit (a BlyscanTM Glycosaminoglycan Assay, Biocolor Ltd., Carrickfergus, UK).

Behavioral Tests

The locomotion of the mice was measured with an actometer. Experiments were performed as described previously [41]. The numbers of horizontal, vertical, and ambulatory movements within a time period were measured.

Anxiety-related locomotion activity was investigated in an open field. Previously described experimental procedures were employed [41]. The following parameters were measured for each investigated mouse: freezing and exploratory activity; the total amount of time spent in inner/outer squares; the total number of inner/outer squares entered by

the animal; the number of lines crossed; and the frequency of mouse entry with all four paws in an inner/outer arena.

All behavioral analyses were recorded using EthoVision XT 10 software (Noldus, Wageningen, the Netherlands). However, the results were not solely based on the automated analysis performed with this software, as each video was additionally reviewed by the experimenter to detect atypical behavior. Despite the fact that certain types of reactions seem contradictory, the observations indicated that the MPS IIIB mice exhibited hyperactivity that was very chaotic in nature, as these behaviors were interrupted with episodes of immobility and other deviations from the pattern observed in the treated or control mice.

Determination of Protein Levels by Western Blotting

Relative levels of selected proteins in the brains and livers of mice were measured by Western blot experiments using a WES system (WES — Automated Western blots with Simple Western; ProteinSimple, San Jose, CA, USA). Mice were euthanized at 30 weeks of age with Morbital (2 ml/kg). After separation from organs, tissue samples were homogenized in IG buffer (0.9% NaCl, 0.5% Triton X-100, 0.1% SDS, 1% sodium deoxycholate, 5 mM EDTA, and 50 mM Tris-HCl pH 7.5) and prepared as described previously [41]. Proteins were separated in a WES system using the 12–230 kDa separation module with 8 × 25 capillary cartridges (#SM-W004; ProteinSimple, San Jose, CA, USA). Specific proteins were detected with the following antibodies: anti-SQSTM1/P62 mouse antibody (#sc-48402, Santa Cruz Biotechnology, Santa Cruz, CA, USA), anti-Beclin-1 rabbit antibody (#D40C5, Cell Signaling Technology, Danvers, MA, USA), anti-PI3 kinase class III rabbit antibody (#D9A5, Cell Signaling Technology, Danvers, MA, USA), anti-TFEB rabbit antibody (#D207D, Cell Signaling Technology, Danvers, MA, USA), anti-S6K rabbit antibody (#9202; Cell Signaling Technology, Danvers, MA, USA), anti-phospho-p70 S6 kinase (Thr389) anti-rabbit antibody (#9205, Cell Signaling Technology, Danvers, MA, USA), anti-4ebp1 rabbit antibody (#9452, Cell Signaling Technology, Danvers, MA, USA), and anti-phospho-4E-BP1 (Thr37/46) rabbit antibody (#9459, Cell Signaling Technology, Danvers, MA, USA). For the detection procedure, secondary antibodies (either anti-mouse or anti-rabbit), which were included in an anti-mouse detection module (#DM-002, ProteinSimple, San Jose, CA, USA) or an anti-rabbit detection module (#DM-001, ProteinSimple, San Jose, CA, USA), were used. The total protein level, determined using a total protein detection module for chemiluminescence (#DM-TP01, ProteinSimple, San Jose, CA, USA), was used as the loading control. Quantification of the results was performed using the software included in the WES system.

For the measurement of LAMP-2 and LC3-II levels, the classical Western blot procedure was employed using an anti-LAMP-2 mouse antibody (H4B4, #sc-18822, Santa Cruz Biotechnology, Santa Cruz, CA, USA) and anti-LC3 mouse antibody (G-4, #sc-398822, Santa Cruz Biotechnology, Santa Cruz, CA, USA). In these experiments, the GAPDH protein level, as measured with an anti-GAPDH rabbit antibody (14C10, #2118 Cell Signaling Technology, Danvers, MA, USA), was used as the control. The performance of classical Western blotting was necessary because certain proteins, including the LC3-II form, are not effectively separated with the WES system, as indicated in the guidelines for studies on autophagy [42]. The results were quantified via densitometry.

Statistical Analysis

The values are presented as the mean ± SD or SEM. For statistical analysis of the results, SPSS 21.0 (SPSS Inc., Amonk, USA) software was used. All parameters for in vitro experiments were analyzed via two-way ANOVA and Tukey's post hoc test or the Kruskal–Wallis and Dunn test. The choice of a test was dictated by the fulfillment of two basic assumptions indicating the appropriate use of a parametric analysis. When the distribution of the results was normal and the variances were homogeneous, a two-way ANOVA was performed. When on or both one of these assumptions were not met, a nonparametric analysis was performed. The differences were considered statistically significant when $p < 0.05$.

Results

Toxicity of the Tested Compounds to MPS III Fibroblasts

We aimed to test the effectivity of select dietary (poly) phenolic antioxidants and certain other natural compounds known to activate autophagy in the treatment of cells derived from patients suffering from all subtypes of Sanfilippo disease (MPS III). In the first step, we tested whether these compounds induced cytotoxicity in the MPS fibroblasts.

An MTT assay was used in experiments with MPS IIIA, IIIB, IIIC, and IIID fibroblasts and all the tested compounds: genistein (used as a positive control, which had been previously demonstrated to decrease the levels of GAG by acting as both a negative regulator of the synthesis of these compounds and an autophagy stimulator), capsaicin, curcumin, resveratrol, trehalose, and calcitriol. The concentration ranges of all tested compounds were chosen on the basis of previously published results, indicating that, at these levels, these treatments stimulate autophagy efficiently [29–39].

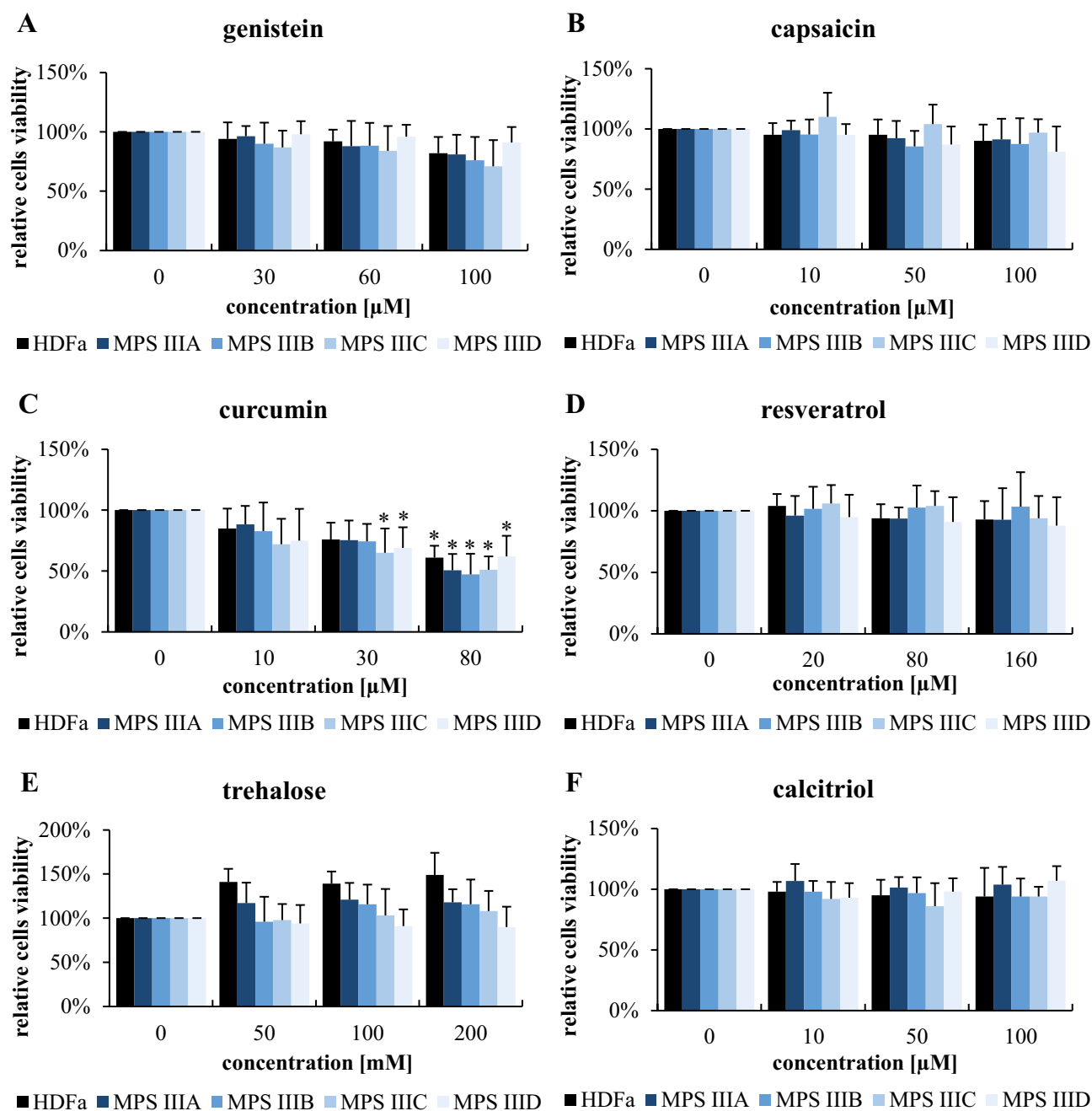


Fig. 2 Viability of control (HDFa) and MPS III (subtypes A-D) fibroblasts treated with various compounds at the indicated concentrations for 24 h, as estimated by MTT test. The results obtained at time 0 were considered to indicate 100% viability. Each column represents

the mean value of three independent experiments, and error bars indicate the standard deviation. Asterisks indicate significant differences ($p < 0.05$) between the results at time 0 and other time points

We found that most of these molecules did not affect the viability of the MPS III cell lines or the HDFa cell controls, when used in the concentration ranges previously reported as standards for in vitro experiments (Fig. 2). A significant decrease in cell viability was found only in the presence of curcumin at 30 and 80 μM (Fig. 2).

Reduction in GAG Levels by the Tested Compounds

Since deficiency in the activity of one of the enzymes involved in GAG degradation is a primary cause of an MPS, we evaluated whether treatment of MPS III cells with the tested compounds results in the reduced accumulation of

GAG. Concentrations of GAG were determined by performing Blyscan assays, which indicated any increase in the amounts of GAG in MPS III cells relative to those in the HDFa control cells (when compared to the control cell line, the GAG levels were increased 2.3-, 3.2-, 4.1-, and 2.2-fold in the MPS IIIA, IIIB, IIIC, and IIID fibroblasts, respectively). Genistein has been used as a positive control for the tested

molecules, which was previously demonstrated to cause a reduction in GAG levels in MPS cells due to its activity as an indirect inhibitor of GAG synthesis and stimulator of lysosomal biogenesis [43–47]. As expected, when applied at concentrations of 60 or 100 μM for 48 h, this natural polyphenol (acting as an antioxidant) caused a significant decrease in GAG levels in all subtypes of MPS III (Fig. 3). Interestingly,

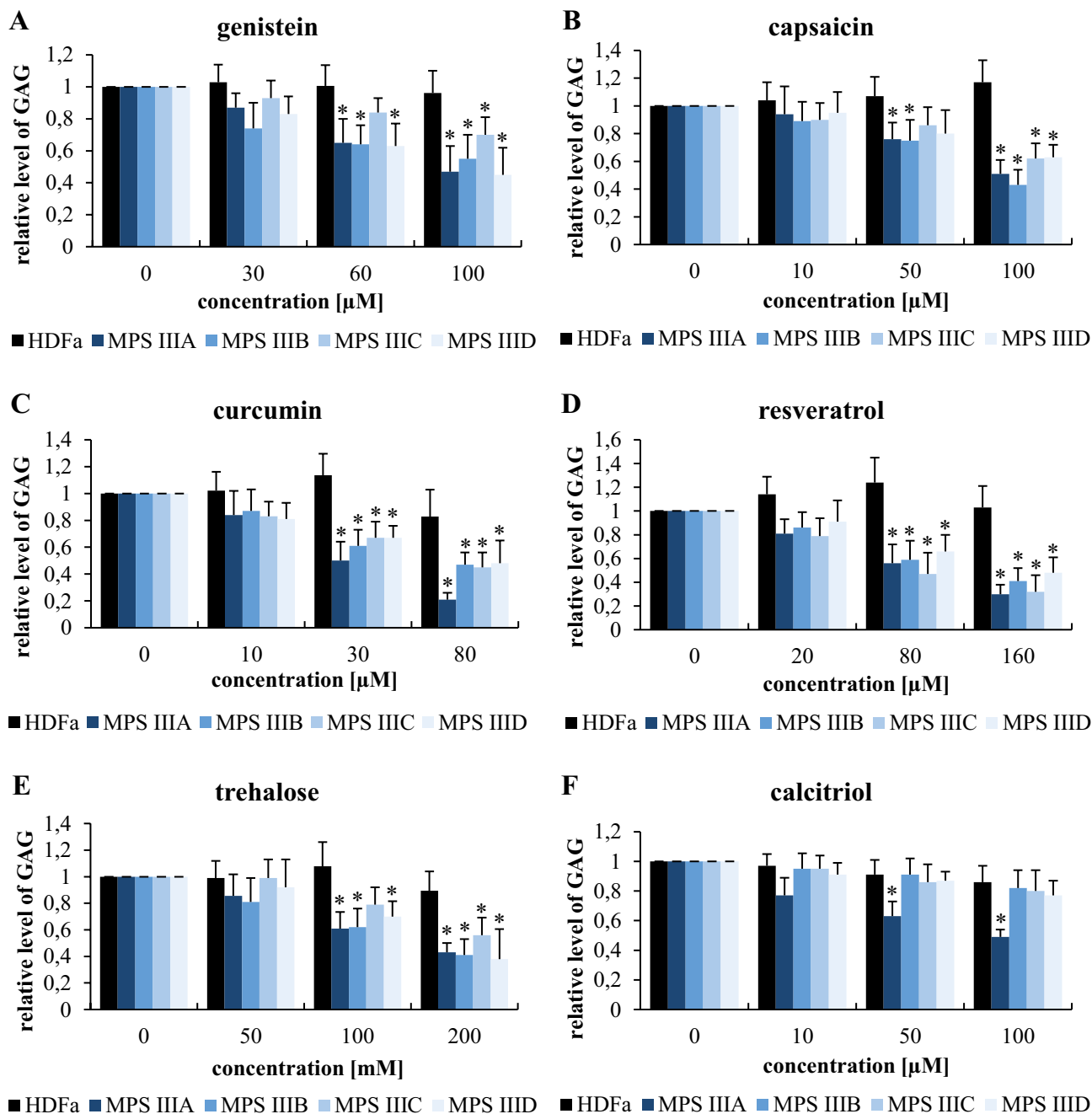


Fig. 3 Relative GAG levels in control (HDFa) and MPS fibroblasts treated with various compounds at the indicated concentrations for 24 h, as assessed by the Blyscan assay. The results obtained at time 0 were considered to be 1 for each separate cell line. Each column represents

the mean value of three independent experiments, and error bars indicate the standard deviation. Asterisks indicate significant differences ($p < 0.05$) between the results at time 0 and other time points

similar effects were observed for all the tested compounds, although the reduction in GAG levels was especially pronounced in experiments with curcumin, trehalose, and resveratrol, and was less pronounced with calcitriol (Fig. 3). However, since curcumin showed some negative effects on cell viability (see Fig. 2) and because the effects of trehalose on MPS IIIB mice had been reported previously [22], resveratrol was chosen for further and more detailed studies.

Resveratrol-Mediated Reduction of HS Levels in MPS III Cells

Since HS is the primary GAG stored in MPS III (secondary dermatan sulfate storage has also been reported in Sanfilippo disease [48]), we have tested the efficiency of resveratrol in the reduction of HS levels in fibroblasts derived from patients suffering from all subtypes of MPS III. A specific anti-HS antibody was employed, and the concentrations of HS in the extracts of fibroblasts were estimated using a dot-blot procedure. When assessing basic levels of HS in untreated fibroblasts, the concentrations of GAG were increased by factors of 4.8, 3.4, 3.7, and 3.2 in MPS IIIA, IIIB, IIIC, and IIID, respectively, relative to control cells

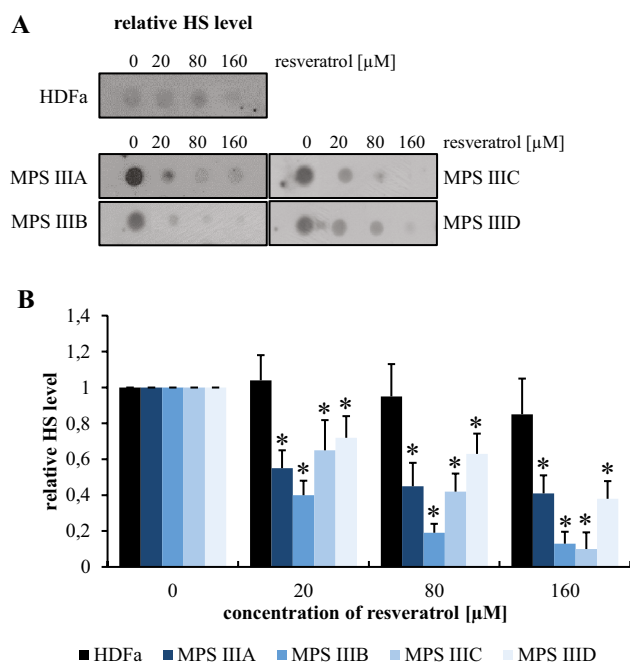


Fig. 4 HS levels in control (HDFa) and MPS fibroblasts treated with resveratrol at the indicated concentrations for 24 h, as assessed by the dot-blot assay with a specific anti-HS antibody. Panel **A** indicates representative results, while panel **B** shows the quantitation of the results in (A). In panel **B**, the results obtained at time 0 were considered to be 1 for each separate cell line. Each column represents the mean value of three independent experiments, and error bars indicate the standard deviation. Asterisks indicate significant differences ($p < 0.05$) between the results at time 0 and other time points

(HDFa) (Fig. 3A). Treatment with resveratrol at concentrations of 20, 80, and 160 μM for 48 h resulted in significant decreases in HS levels in all subtypes of Sanfilippo disease cells, and a dose–response correlation was observed (Fig. 4B). These results indicated that resveratrol was effective in clearing HS from MPS III cells in vitro, pointing to its therapeutic potential in the treatment of Sanfilippo disease. Therefore, in the next step, we tested the efficacy of resveratrol in an experimental therapy of mouse models of MPS IIIB.

Resveratrol-Mediated Reduction in Urinary GAG Levels in MPS IIIB Mice

To test the effects of resveratrol on the course of Sanfilippo disease, we used a mouse model of MPS IIIB. The animals were allocated into 4 groups: wild-type (WT; *Naglu*^{+/+}) mice treated with water (W), wild-type mice treated with resveratrol (RSV; 50 mg/kg/day), MPS IIIB (*Naglu*^{-/-}) mice treated with water (W), and MPS IIIB mice treated with resveratrol (RSV; 50 mg/kg/day) (Fig. 5A). The dose of 50 mg/kg/day was chosen

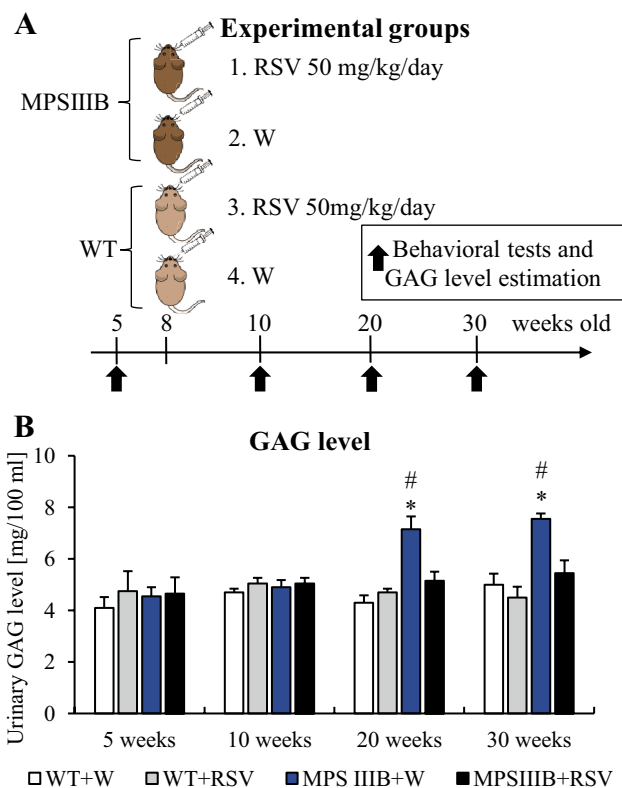


Fig. 5 Scheme of the animal experiments (A) and effects of resveratrol (RSV) on urinary GAG levels in MPS IIIB mice (B). The results shown in panel **B** are presented as the mean values \pm SEMs. Statistically significant differences obtained for a particular group ($n = 6$) are marked with (*), which indicates $p < 0.05$ vs. WT+W (wild type with water), or (#), which indicates $p < 0.05$ vs. MPS IIIB+RSV (MPS IIIB treated with resveratrol)

as the concentrations of resveratrol on the basis of our in vitro experiments, which caused an effective reduction in GAG levels (as determined by the molecular mass of resveratrol, which is equal to 228.25 g/mol, and assuming ~50% bioavailability of the orally administered compound). Both water and resveratrol were administered orally. The treatment was initiated in mice 8 weeks old and was conducted until the mice were 30 weeks old. Measurements of the levels of urinary GAG and behavioral tests were performed at weeks 5, 10, 20, and 30 (Fig. 5A).

Levels of GAG in urine were found to be similar in both WT and MPS III B mice at weeks 5 and 10, with or without resveratrol treatment. However, MPS III mice not treated with an investigated compound showed increased urinary GAG concentrations at weeks 20 and 30 (Fig. 5B). Treatment with resveratrol at 50 mg/kg/day normalized the levels of urinary GAG (the GAG concentrations were indistinguishable from those measured in the urine of wild-type mice, as shown in Fig. 5B). These results indicated that this polyphenol was effective, causing a significant reduction in or the complete clearance of urinary GAG in MPS III mice. Therefore, we asked whether this molecule can

positively influence the behavior of mouse models of Sanfilippo disease.

Effects of Resveratrol on the Behavior of MPS III B Mice

As behavioral problems are the most pronounced symptoms in Sanfilippo disease [1], we aimed to investigate the effects of resveratrol on the behavior of MPS III B mice. Hyperactivity and anxiety-related changes are characteristic of patients suffering from this disease, as well as of corresponding animal models [2–4]; therefore, we performed experiments allowing us to assess the movements and fear-related activities of the mouse models.

Using an actometer, we measured different kinds of movement, including vertical, horizontal, and ambulatory movements (Fig. 6A). All kinds of movements were significantly more frequent in the water-treated MPS III B mice than in the WT animals that were 10 weeks older or older (Fig. 6). However, the treatment of mice with Sanfilippo disease B with resveratrol at a dose of 50 mg/kg/day resulted in the

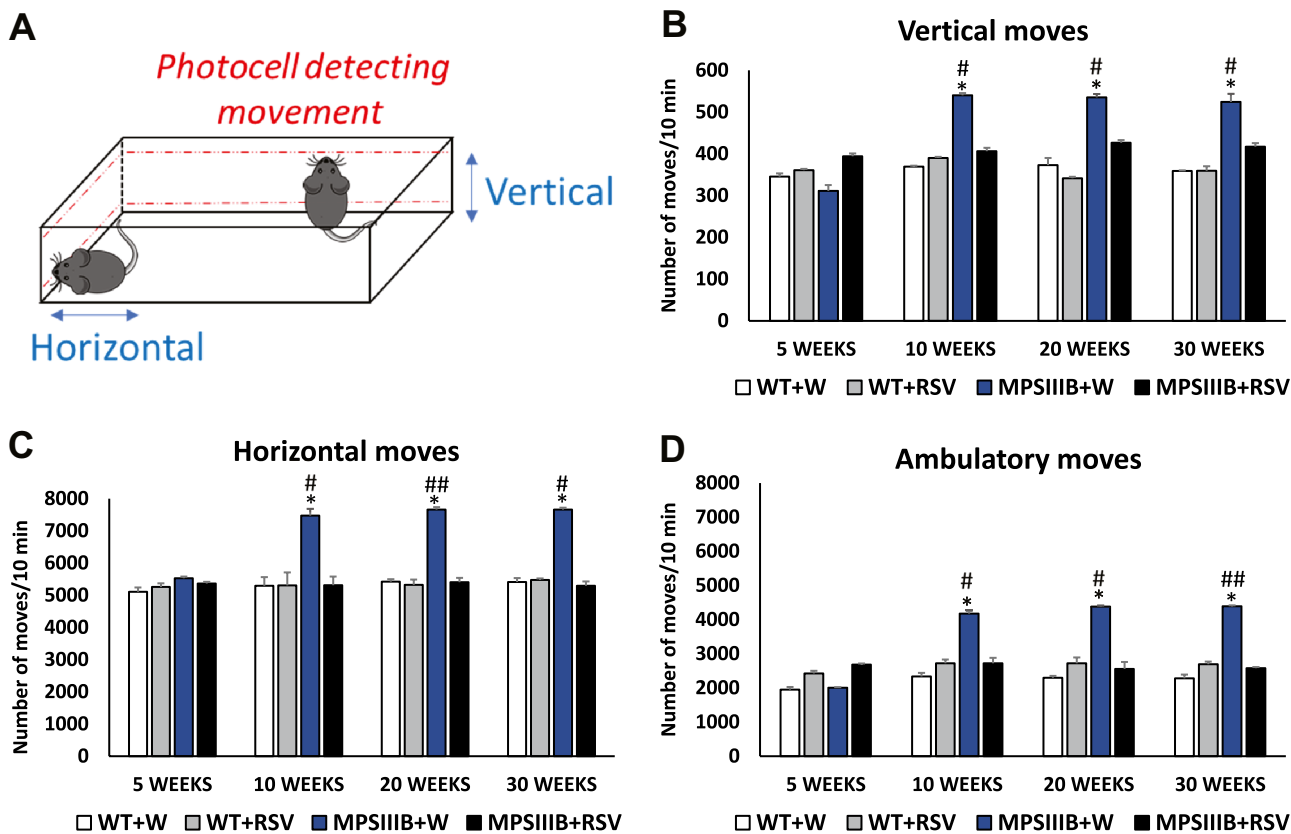


Fig. 6 Normalization of hyperactivity in MPS III B mice after resveratrol (RSV) treatment. Schematic representation of the actometer used for measuring animal movements via photocell detection is shown in panel (A). The numbers of vertical (B), horizontal (C), and ambulatory (D) movements in a 10-min period are presented.

The data represent the mean values ± SEMs. Statistically significant differences obtained for each group (n=6) are marked with (*), which indicates $p < 0.05$ vs. WT+W (wild type with water), or (#) and (##), which indicate $p < 0.05$ and $p < 0.01$, respectively, vs. MPS III B + RSV (MPS III B treated with resveratrol)

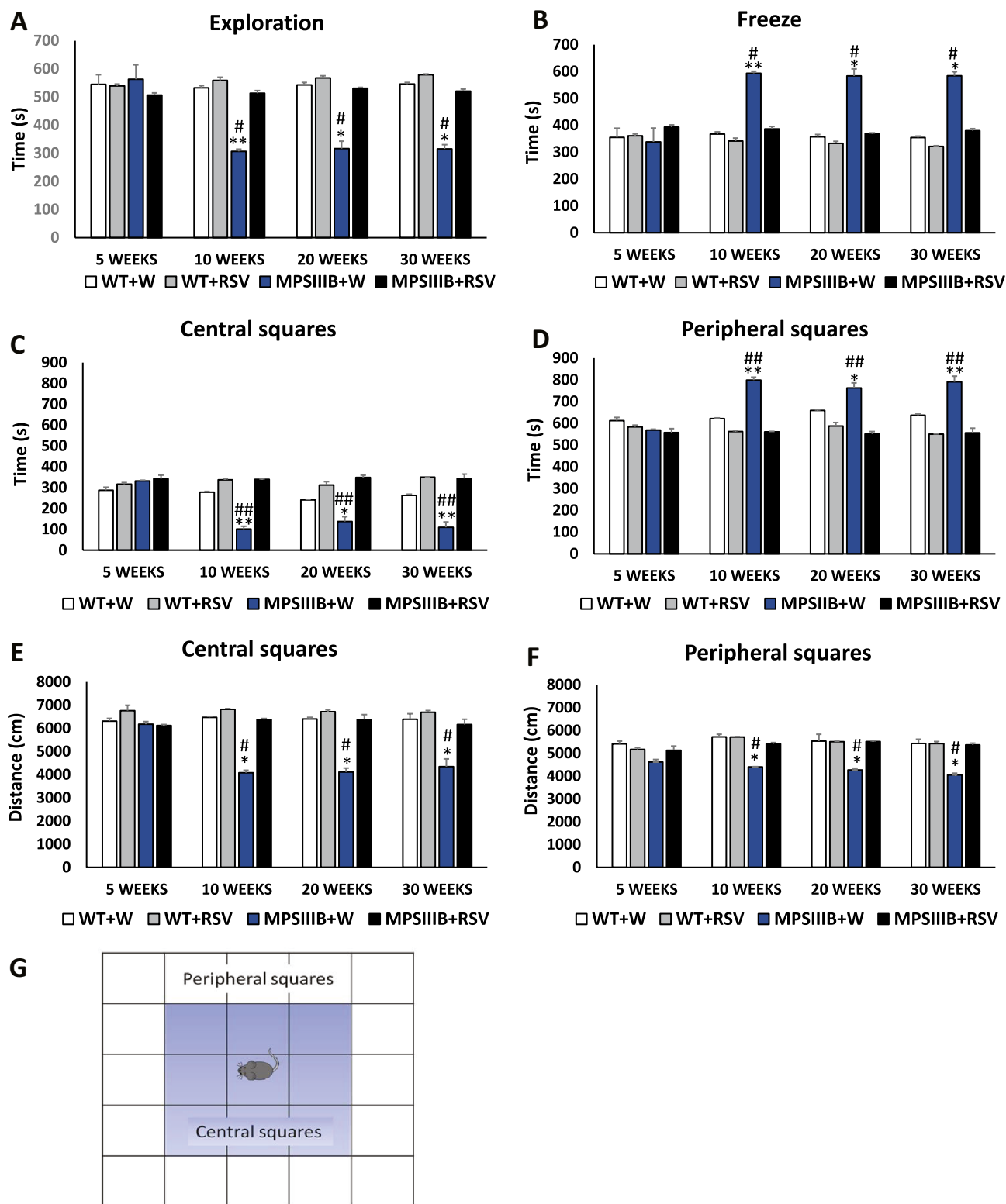


Fig. 7 Normalization of anxiety-related behavior in MPS IIIB mice after resveratrol (RSV) treatment. The time spent in exploration (A), freezing (B), central (C), and peripheral (D) squares during the 15-min measurement was determined. The distance traveled in central (E) and peripheral (F) squares over 15 min was measured. A schematic of the open field test is shown in panel (G). Data represent the

mean values \pm SEMs. Statistically significant differences obtained for each group ($n=6$) are marked with (*) and (**), which indicate $p < 0.05$ and $p < 0.01$, respectively, vs. WT+W (wild type with water), or (#) and (##), which indicate $p < 0.05$ and $p < 0.01$, respectively, vs. MPS IIIB + RSV (MPS IIIB treated with resveratrol)

complete attenuation of all types of aberrant movements (Fig. 6). Therefore, these results indicated that resveratrol attenuated the hyperactivity in MPS IIIB mice. Moreover, these effects were observed as soon as 2 weeks after the initial administration of this compound (treatment was initiated at the age of 8 weeks, while significant improvement was evident at the age of 10 weeks and later, as demonstrated in Fig. 6).

Performing an open-field test, we estimated fear-related changes in animal behavior. Since anxiety disorders are characteristic of both MPS III (all subtypes) patients and MPS IIIB mice, experiments based on this test were used to measure of these abnormalities. Various parameters were measured to assess animal behavior in the open field, including time of exploration, time of freezing, time spent in central squares, time spent in peripheral squares, distance traveled in central squares, and distance traveled in peripheral squares. The scheme of the experiment is shown in Fig. 7G.

When water-treated animals were investigated, abnormalities in all of the above-listed parameters measured in the open-field test were found in the MPS IIIB mice but not the WT mice (Fig. 7A–F). However, administration of resveratrol normalized all the behavioral functions that had been estimated using this test (Fig. 7). Again, the attenuation of the hyperactive behaviors was evident at the age of 10 weeks, at which time the resveratrol-treated MPS IIIB mice were behaviorally undistinguishable from the WT animals, while the behaviors of water-treated Sanfilippo type B mice were significantly different from those of the control animals for all the measured parameters (Fig. 7). These results demonstrated that resveratrol was a very efficient in correcting behavioral abnormalities in the mouse models of Sanfilippo disease used in this study.

Resveratrol Induces Autophagy in the Brains and Livers of MPS IIIB Mice

To test whether resveratrol can induce autophagy, we determined the levels of protein markers during autophagy. When comparing relative concentrations of the p62 protein, significantly higher levels were found in the brains and livers of untreated MPS IIIB mice compared to those in to wild-type animals. No significant differences in Beclin-1 levels were detected (Fig. 8). These results indicated that autophagy was impaired in the MPS IIIB mice without a specific treatment. Administration of resveratrol at 50 mg/kg/day for 22 days resulted in a significant decrease in the p62 level in two tested organs of the MPS IIIB mice, demonstrating enhanced autophagy relative to that in the water-treated Sanfilippo mice (Fig. 8). This conclusion was corroborated by the significantly higher levels of LAMP-2 and LC3-II proteins in the brains of the MPS

IIIB mice treated with resveratrol compared to those in the untreated animals (Fig. 9).

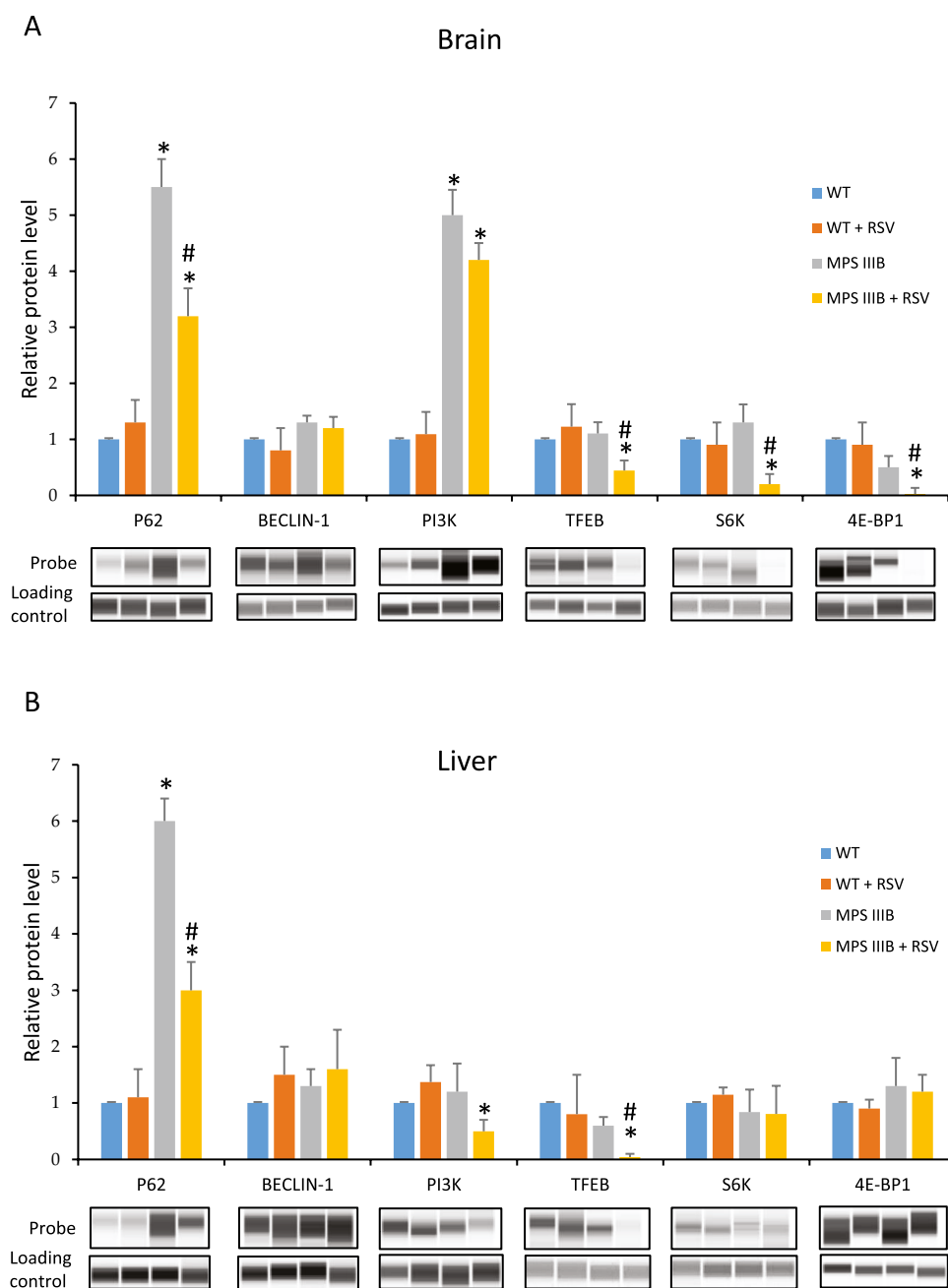
Previous studies indicated that resveratrol can stimulate autophagy through an mTOR-independent pathway (for a review, see ref. [27]). We found that PI3K levels were decreased, and the levels of mTOR kinase substrates (TFEB, S6K, and 4E-BP1) were either decreased or unchanged in the resveratrol-treated MPS IIIB mice compared to the water-treated MPS IIIB animals (Fig. 8). These results confirmed that in these animals, resveratrol-induced autophagy proceeded independent of the mTOR pathway.

Discussion

Sanfilippo disease (MPS III) is a severe inherited metabolic disorder that causes devastating changes in the central nervous system and a significantly shortened lifespan (which is limited to approximately two decades) [1]. Although four different genetic defects leading to deficiency of different enzymes cause this disease, the general symptoms are similar in subtypes A, B, C, and D, but the course of the disease and level of severity may vary [2]. Many therapies developed for this disease have been tested, but despite remarkable successes in preclinical experiments, the clinical trials performed to date did not indicate sufficient efficacy to abolish or even alleviate most of the symptoms. These failure treatments included enzyme replacement therapy [16, 17], gene therapy [15], and substrate reduction therapy [18, 49]. Therefore, there is an urgent need to develop a method for the efficient treatment of MPS III patients. In this study, we tested previously proposed hypotheses [23, 27, 31, 40] suggesting that stimulation of the autophagy process, especially with natural compounds, might be beneficial in the treatment of Sanfilippo disease.

In this study, several natural (poly)phenols or other natural autophagy stimulators, also known for their antioxidative activities, were tested in both cell and animal models. As a positive control, genistein was used because it reduces the synthesis of GAG [43–45] and stimulates lysosomal biogenesis [47]. Genistein has been demonstrated by various groups to slow the production of GAG in cultured fibroblasts [43, 45], and some studies showed an increase in GAG synthesis in chondrocytes [50]. The discrepancy among studies has been suggested to be due to different effects of genistein on GAG levels in different types of cells [51]. Nevertheless, experiments with animal models of MPS II and MPS IIIB demonstrated the efficacy of this isoflavone in reducing GAG levels and attenuating abnormal behavior [46, 52], but these benefits have not been observed in MPS I mice [53]. In fact, several clinical experiments and trials have been conducted to test the efficacy of genistein in the treatment of

Fig. 8 Levels of autophagy-related proteins in the brains (A) and livers (B) of wild-type mice treated with water (WT) or resveratrol at 50 mg/kg/day (WT + RSV) and MPS III B mice (analogous to the MPS III B and MPS III B + RSV groups). The data represent the mean values \pm SDs. Statistically significant differences obtained for each group ($n=6$) are marked with (*), which indicates $p < 0.05$ vs. WT (wild type with water), or (#), which indicates $p < 0.05$ vs. MPS III B + RSV (MPS III B treated with resveratrol). Representative blots with the tested proteins (probe) and loading controls (total protein assessed using the total protein detection module for chemiluminescence compared with the WES system) are presented below the corresponding columns

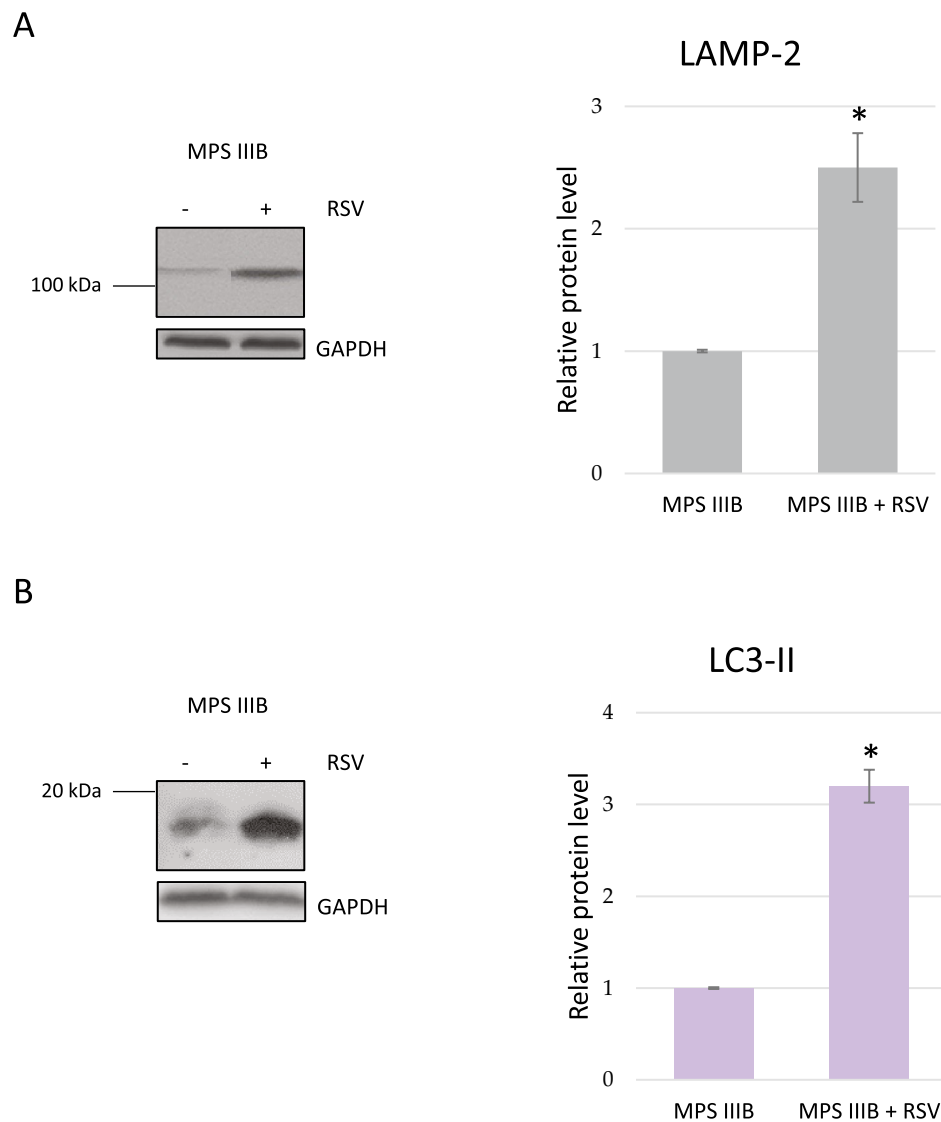


MPS patients (different types), but contradictory results have been reported, indicating either significant attenuation of symptoms [54–57] or a lack of considerable clinical benefit [18, 58–60]. One might assume that these ostensibly discrepancies may be due to the various sources of genistein used (which may influence the bioavailability of this compound in humans), different patient age ranges (younger patients might respond better to treatment) or the different tests that were performed to assess drug efficacy (the results of psychological and cognitive tests for this disease are especially difficult to interpret). The multiple effects of genistein indicate how difficult it is to unequivocally estimate the efficacy

of a drug for MPS. Therefore, extensive studies, both pre-clinical and clinical, are required to analyze each potential therapeutic method proposed to be treat this disease.

In the experiments presented in this report, we used known natural autophagy stimulators, capsaicin [29, 30], curcumin [31–33], resveratrol [34, 35], trehalose [36, 37], and calcitriol [39]. Cytotoxic effects were observed only at high concentrations of curcumin (30 and 80 μ M) (Fig. 2), indicating the general safety of the investigated compounds in MPS III cells. Moreover, a significant decrease in GAG levels was observed after treatment of cells obtained from patients with one of each subtype of

Fig. 9 Levels of LAMP-2 (A) and LC3-II (B) proteins in the brains of MPS IIIIB mice treated with water (minus (-) or MPS IIIIB) or resveratrol at 50 mg/kg/day (plus (+) or MPS IIIIB + RSV). Representative blots (obtained using the classical Western blotting procedure) are shown in the left panels, and the quantified results are presented in the right panels as the mean values \pm SDs. Statistically significant differences obtained for each group ($n=6$) are marked with (*), which indicates $p < 0.05$ vs. MPS IIIIB (i.e., MPS IIIIB with water)



MPS III with each tested molecules (Fig. 3). The positive effects of trehalose on MPS IIIIB mice, due to the induction of autophagy, had been previously demonstrated [22], and the results of our experiments with cell models of all Sanfilippo disease subtypes corroborated this discovery. Among the tested compounds, resveratrol exerted the greatest effects (Fig. 3), and we confirmed its efficacy in the specific reduction in HS levels (Fig. 4). Unaffected HS levels in control (HFDa) cells (Fig. 4) may indicate that GAG molecules present at normal concentrations did not undergo accelerated decay via autophagy. If this is the case, pathological GAG is degraded after autophagy stimulation. In fact, resveratrol-mediated activation of the impaired autophagy pathway were confirmed in experiments with MPS IIIIB mouse models (Fig. 8), which were also used in experiments on the effects of this compound in vivo. Unexpectedly, we found that resveratrol

normalized urinary GAG levels (Fig. 5) and attenuated all tested abnormal behaviors in the affected animals (Figs. 6 and 7). These results provide proof of principle for considering natural autophagy stimulators, especially resveratrol, potential drugs for Sanfilippo disease treatment. This possibility reveals a new direction for further studies focused on developing a therapeutic procedure based on the use of these compounds. In fact, resveratrol appears to possess properties that result in reduced GAG (including HS) levels in MPS cells and in mouse urine, and it also attenuated the abnormal behaviors of Sanfilippo subtype B mice. Therefore, it seems that the recently published proposal suggesting that resveratrol may be potential treatment of mucopolysaccharidosis (especially Sanfilippo disease) [40] is substantiated.

Notably, resveratrol has been previously proposed as a compound that is potentially useful in the treatment of

other lysosomal storage diseases. In studies on neuronal ceroid lipofuscinosis (also called Batten disease), resveratrol was found to increase the NAD⁺/NADH ratio and levels of ATP, p-AMPK, PGC-1 α , and SIRT1, whereas decreased levels of p-S6K1 were observed in cell and mouse models of this disease treated with this compound [61]. Interestingly, we observed a reduction in the regulatory factor p-S6K1 in the brains of MPS IIIB mice treated with resveratrol (Fig. 8). An increased lifespan was reported for mouse models of neuronal ceroid lipofuscinosis [61], and we demonstrated improved behavior in animals. Notably, it has been proposed that resveratrol may act on neuronal ceroid lipofuscinosis by improving adaptive energy metabolism [61]. We propose that activation of autophagy is the major mechanism of this compound in MPS III, although a possible influence on cell metabolism cannot be excluded. Other beneficial effects of resveratrol have been reported in for a lymphoblast model of Batten disease; however, the study suggested that the action of this compound action was due mainly to its antioxidant properties [62]. Furthermore, subsequent experiments on the mouse *Ppt1*-knockout model demonstrated a reduction in T_H17 cells, IL-17A, and MMPs and an elevation in the levels of tight junction proteins after administration of resveratrol, and improved blood–brain-barrier integrity was observed under these conditions [63]. Therefore, resveratrol likely functions via different mechanisms to attenuate various abnormal cellular functions in Batten disease and possibly in other lysosomal storage diseases.

Another interesting mechanism of action of resveratrol was reported for Pompe disease (a Type II glycogen storage disease). When a leaky splicing mutation in the *GAA* gene was the cause of this disease, treatment with resveratrol resulted in an increase in the level of normally spliced mRNA, but the mechanism of this phenomenon remains unknown [64].

Beneficial effects of resveratrol have also been reported for Gaucher disease, a lysosomal storage disorder caused by deficiency of glucocerebrosidase. In Gaucher disease patient-derived fibroblasts, treatment with resveratrol caused a reduction in the storage of glucosylceramides [65] and enhanced the viability of these cells [66]. These outcomes were correlated with decreased levels of the apoptotic factors AIF, Bax, and cleaved caspase-3. On the other hand, the concentrations of ACAT1, E3BP, and CS were increased in resveratrol-treated cells [65, 66]. Interestingly, the possible involvement of autophagy modulation induced by resveratrol has been suggested in studies on mutants in the *Drosophila GBA1* gene (encoding glucocerebrosidase) [67]. An analogous *Drosophila* model bearing mutations in the *CG2135* gene, thus resembling human MPS VII (Sly disease), was used in experiments that demonstrated reduced neuromuscular pathology and restored motor functions after resveratrol administration [68]. Various

potential mechanisms of action of this compound have been proposed, including antioxidant, anti-inflammatory, cellular energy homeostasis-controlling, and autophagy-modulating activities, but the true mechanism(s) remains to be elucidated. Intriguingly, in a murine model of Krabbe disease (caused by the deficiency of galactosyl-ceramidase), rapamycin (a strong activator of autophagy), but not resveratrol, partially restored the levels of autophagy markers that had been dysregulated [69]. Interestingly, excessive accumulation of p62 has been observed in the neurons of mice with Krabbe disease [63], similar to an outcome observed in MPS IIIB mice in our study (Fig. 8). Notably, resveratrol treatment resulted in a decrease in p62 levels in our model but not in the previous study (Fig. 8 and ref. [69]). These results indicate that the action of resveratrol may be different in different lysosomal storage diseases. Moreover, a recently published article indicated that (in contrast to previous reports [27, 34, 35] and the results presented in this work (Fig. 8), demonstrating stimulation of autophagy via resveratrol mediated through mTOR-independent pathways) this compound activated the autophagy process mediated by protein phosphatase 2A-dependent dephosphorylation of TFE3, a transcription activator that enhances the expression of genes encoding lysosomal proteins, which are inactive when phosphorylated by mTOR [70]. Therefore, the mechanisms of action of resveratrol may be even more complex than those identified to date.

In our behavioral studies, we noted an additional interesting observation: the hyperactive phenotype was generally not associated with neurodegeneration. Indeed, when we detected hyperactivity in untreated MPS IIIB mice (at 10 weeks), mouse brain GAG levels were low. Thus, the motor hyperactivity observed in these mice was not necessarily due solely to GAG accumulation. Reports in the literature indicated that a number of histological changes identified long before GAG levels were found to be elevated in the CNS. MPS IIIB mice accumulate the ganglioside GM2 and, more importantly, the ganglioside GM3 in brain cells. The consequences of these accumulated gangliosides in lysosomes and the cell membrane lead to extensive and not yet fully understood neuropathological changes. Moreover, the characteristic vacuolization of lysosomes that contain aggregates and deposits was detected in the brains of MPS IIIB mice as young as 6 weeks of age, and this vacuolization increased with disease progression [71]. Further indicators of an ongoing disease process in the brain were changes detected at an early stage, such as microglial activation, astrogliosis, or an extensive and intense inflammatory process. These histopathological changes clearly correlate with the clinical picture, which consists of a shortened life expectancy, as well as a number of behavioral abnormalities, including aberrant anxiety responses and locomotion activity levels, which have been previously detected in an open field test [71]. Therefore, although in our experiments performed

with 10-week-old MPS IIIB mice with brain GAG levels that did not exceed those observed in other groups, GAG likely accumulated in specific brain areas, leading to specific deviation from the typical behavioral pattern, and at an early stage of the disease, these increased GAG levels likely resulted in the described behavioral changes, including hyperactivity, episodes of immobility, and increased anxiety responses.

However, the results of other recent studies performed with a mouse model of MPS IIIA indicated that autistic-like behavior is caused by the increased proliferation of mesencephalic dopamine neurons not lysosomal dysfunction [72]. Notably, these outcomes are characteristic of children suffering from Sanfilippo disease [5, 73, 74]; hence, the mechanisms underlying to storage disorders are likely to be similar (or the same) in mice and humans. Detailed experiments with a mouse MPS IIIA model suggested that pathological modulation of dopamine activity can be a result of altered HS function, not elevated GAG levels [72]. This possible connection was corroborated by the results presented in our study with MPS IIIB mice. Hyperactivity and increased vertical movements seemed to mimic autistic behavior, and we observed these movements before observing significant accumulation of GAG. Therefore, these results may reflect the same or a similar mechanisms of neuropathology in the MPS IIIA and IIIB subtypes, which are not necessarily simple consequences of excessive GAG storage. Hence, changes in both the expression of many genes and the pathways of various cellular processes in MPS cells as reported recently [11–14, 75] might contribute to the pathomechanisms of Sanfilippo disease, which differ from the direct consequences of the accumulation of GAG (or, more precisely, that of HS).

Considering resveratrol as a potential drug for treating MPS III, a neurodegenerative disease, it is worth noting that this compound has been found to cross the blood–brain barrier [76]. However, recent quantitative studies indicated that resveratrol crossing this barrier was relatively inefficient, at a few percentage points [77]. Therefore, various attempts to increase the efficiency of resveratrol delivery to the brain (such as those proposed recently [78, 79]) may be especially important to the development of a true therapy based on this compound.

Notably, considerable literature data have supported the ability of resveratrol not only to remove toxic protein aggregates in a variety of disease models but also to confer protection, as reviewed recently [40]. For example, resveratrol conferred protection against early neuronal dysfunction observed in a transgenic *Caenorhabditis elegans* model expressing mutant polyglutamine. Many studies have confirmed the high potential of resveratrol protecting striatal

neurons from death and progressive neurodegeneration resulting from mutant polyglutamine accumulation in a mouse model of Huntington's disease [40]. The neuroprotective properties of resveratrol have also been confirmed in Alzheimer's disease models, where it has been shown to enhance memory processes, as well as increase cell survival, through the stimulation of SIRT1-, AMPK-, and mTOR-dependent pathways, leading to a reduction in amyloid levels [40]. Therefore, it is likely that resveratrol can exert similar effects on patients with MPS III.

Conclusions

Natural dietary (poly)phenols and other natural autophagy stimulators, known also for their antioxidant activity, efficiently reduced the levels of GAG in fibroblasts derived from patients suffering from all subtypes of Sanfilippo disease. Resveratrol normalized urinary GAG levels and attenuated abnormal behaviors in MPS IIIB model mice, supporting further studies on this compound as a possible drug for treating Sanfilippo disease. Autophagy stimulation appeared to be a mechanism of action of resveratrol in ameliorating MPS IIIB pathology; however, other functions of this molecule (such as its antioxidative effects) cannot be excluded, especially when considering its multiple biochemical functions.

Supplementary Information The online version contains supplementary material available at <https://doi.org/10.1007/s13311-022-01323-7>.

Acknowledgements The authors thank Julian Guzowski for assistance with some experiments.

Required Author Forms Disclosure forms provided by the authors are available with the online version of this article.

Funding This research was funded by the National Science Center, Poland (grant no. 2018/29/N/NZ2/00802 to L.G., and grant no. 2019/35/N/NZ2/00505 to E.R.) and by Fundacja Sanfilippo, Poland (grant 21.01.2019 to G.W.).

Declarations

Conflict of Interest The authors declare no competing interests.

Open Access This article is licensed under a Creative Commons Attribution 4.0 International License, which permits use, sharing, adaptation, distribution and reproduction in any medium or format, as long as you give appropriate credit to the original author(s) and the source, provide a link to the Creative Commons licence, and indicate if changes were made. The images or other third party material in this article are included in the article's Creative Commons licence, unless indicated otherwise in a credit line to the material. If material is not included in the article's Creative Commons licence and your intended use is not permitted by statutory regulation or exceeds the permitted use, you will need to obtain permission directly from the copyright holder. To view a copy of this licence, visit <http://creativecommons.org/licenses/by/4.0/>.

References

1. Węgrzyn G, Pierzynowska K, Jakobkiewicz-Banecka J, et al. Mucopolysaccharidosis type III: clinical features, biochemistry, diagnosis, genetics, and treatment. In: Mucopolysaccharidoses Update; Tomatsu S, Lavery C, Giugliani R, Hermatz P, Scarpa M, Węgrzyn G, Orii T, Eds. Nova Publishers: Hauppauge, NY, USA, 2018; Volume 1, pp. 211–233.
2. Pierzynowska K, Rintz E, Gaffke L, et al. Mucopolysaccharidosis type III (Sanfilippo disease) subtypes A, B, C, D: molecular mechanism and therapeutic effect. In: Tomatsu S, Lavery C, Giugliani R, Hermatz P, Scarpa M, Węgrzyn G, Orii T, editors., et al., Mucopolysaccharidoses Update. Hauppauge, NY, USA: Nova Publishers; 2018. p. 51–101.
3. Heon-Roberts R, Nguyen ALA, Pshzhetsky AV. Molecular bases of neurodegeneration and cognitive decline, the major burden of Sanfilippo disease. *J Clin Med.* 2020;9:344. <https://doi.org/10.3390/jcm9020344>.
4. Benetó N, Vilageliu L, Grinberg D, Canals I. Sanfilippo syndrome: molecular basis, disease models and therapeutic approaches. *Int J Mol Sci.* 2020;21:7819. <https://doi.org/10.3390/ijms21217819>.
5. Wijburg FA, Węgrzyn G, Burton BK, Tylki-Szymańska A. Mucopolysaccharidosis type III (Sanfilippo syndrome) and misdiagnosis of idiopathic developmental delay, attention deficit/hyperactivity disorder or autism spectrum disorder. *Acta Paediatr.* 2013;102:462–70.
6. Gaffke L, Pierzynowska K, Piotrowska E, Węgrzyn G. How close are we to therapies for Sanfilippo disease? *Metab Brain Dis.* 2018;33:1–10.
7. Noh H, Lee JI. Current and potential therapeutic strategies for mucopolysaccharidoses. *J Clin Pharm Ther.* 2014;39:215–24.
8. De Pasquale V, Sarogni P, Pistorio V, et al. Targeting heparan sulfate proteoglycans as a novel therapeutic strategy for mucopolysaccharidoses. *Mol Ther Methods Clin Dev.* 2018;10:8–16. <https://doi.org/10.1016/j.omtm.2018.05.002>.
9. Hollak CE, Wijburg FA. Treatment of lysosomal storage disorders: successes and challenges. *J Inherit Metab Dis.* 2014;37:587–98.
10. Yilmaz BS, Davison J, Jones SA, Baruteau J. Novel therapies for mucopolysaccharidosis type III. *J Inherit Metab Dis.* 2021;44:129–47. <https://doi.org/10.1002/jimd.12316>.
11. Gaffke L, Pierzynowska K, Podlacha M, et al. Underestimated aspect of mucopolysaccharidosis pathogenesis: global changes in cellular processes revealed by transcriptomic studies. *Int J Mol Sci.* 2020;21:1204.
12. Rintz E, Gaffke L, Podlacha M, et al. Transcriptomic changes related to cellular processes with particular emphasis on cell activation in lysosomal storage diseases from the group of mucopolysaccharidoses. *Int J Mol Sci.* 2020;21:3194.
13. Gaffke L, Pierzynowska K, Krzelowska K, Piotrowska E, Węgrzyn G. Changes in expressions of genes involved in the regulation of cellular processes in mucopolysaccharidoses as assessed by fibroblast culture-based transcriptomic analyses. *Metab Brain Dis.* 2020;35:1353–60.
14. Gaffke L, Pierzynowska K, Rintz E, Cyske Z, Giecwicz I, Węgrzyn G. Gene expression-related changes in morphologies of organelles and cellular component organization in mucopolysaccharidoses. *Int J Mol Sci.* 2021;22:2766.
15. Tardieu M, Zerah M, Gougeon ML, et al. Intracerebral gene therapy in children with mucopolysaccharidosis type IIIB syndrome: an uncontrolled phase 1/2 clinical trial. *Lancet Neurol.* 2017;16:712–20. [https://doi.org/10.1016/S1474-4422\(17\)30169-2](https://doi.org/10.1016/S1474-4422(17)30169-2).
16. Wijburg FA, Whitley CB, Muenzer J, et al. Intrathecal heparan-N-sulfatase in patients with Sanfilippo syndrome type A: a phase IIb randomized trial. *Mol Genet Metab.* 2019;126:121–30. <https://doi.org/10.1016/j.ymgme.2018.10.006>.
17. Whitley CB, Vijay S, Yao B, et al. Final results of the phase 1/2, open-label clinical study of intravenous recombinant human N-acetyl-alpha-d-glucosaminidase (SBC-103) in children with mucopolysaccharidosis IIIB. *Mol Genet Metab.* 2019;126:131–8. <https://doi.org/10.1016/j.ymgme.2018.12.003>.
18. Ghosh A, Rust S, Langford-Smith K, et al. High dose genistein in Sanfilippo syndrome: a randomised controlled trial. *J Inherit Metab Dis.* 2021;44:1248–62. <https://doi.org/10.1002/jimd.12407>.
19. Pearse Y, Iacovino M. A cure for Sanfilippo syndrome? A summary of current therapeutic approaches and their promise. *Med Res Arch.* 2020;8. <https://doi.org/10.18103/mra.v8i2.2045>.
20. Saha S, Panigrahi DP, Patil S, Bhutia SK. Autophagy in health and disease: a comprehensive review. *Biomed Pharmacother.* 2018;104:485–95. <https://doi.org/10.1016/j.biopha.2018.05.007>.
21. Ajoobabady A, Aslkhodapasandhokmabad H, Henninger N, et al. Targeting autophagy in neurodegenerative diseases: from molecular mechanisms to clinical therapeutics. *Clin Exp Pharmacol Physiol.* 2021;48:943–53. <https://doi.org/10.1111/1440-1681.13500>.
22. Lotfi P, Tse DY, Di Ronza A, et al. Trehalose reduces retinal degeneration, neuroinflammation and storage burden caused by a lysosomal hydrolase deficiency. *Autophagy.* 2018;14:419–1434. <https://doi.org/10.1080/15548627.2018.1474313>.
23. Pierzynowska K, Gaffke L, Podlacha M, Brokowska J, Węgrzyn G. Mucopolysaccharidosis and autophagy: controversies on the contribution of the process to the pathogenesis and possible therapeutic applications. *Neuromolecular Med.* 2020;22:25–30. <https://doi.org/10.1007/s12017-019-08559-1>.
24. Monaco A, Fraldi A. Protein aggregation and autophagy dysfunction: new lessons from mucopolysaccharidoses. *Autophagy.* 2021;17:3875–6. <https://doi.org/10.1080/15548627.2021.1961076>.
25. De Pasquale V, Caterino M, Costanzo M, Fedele R, Ruoppolo M, Pavone LM. Targeted metabolomic analysis of a mucopolysaccharidosis IIIB mouse model reveals an imbalance of branched-chain amino acid and fatty acid metabolism. *Int J Mol Sci.* 2020;21:4211. <https://doi.org/10.3390/ijms21124211>.
26. Schiattarella GG, Cerulo G, De Pasquale V, et al. The murine model of mucopolysaccharidosis IIIB develops cardiopathies over time leading to heart failure. *PLoS ONE.* 2015;10:e0131662. <https://doi.org/10.1371/journal.pone.0131662>.
27. Pierzynowska K, Gaffke L, Cyske Z, et al. Autophagy stimulation as a promising approach in treatment of neurodegenerative diseases. *Metab Brain Dis.* 2018;33:989–1008.
28. Stacchiotti A, Corsetti G. Natural compounds and autophagy: allies against neurodegeneration. *Front Cell Dev Biol.* 2020;8:555409. <https://doi.org/10.3389/fcell.2020.555409>.
29. Lin YT, Wang HC, Hsu YC, Cho CL, Yang MY, Chien CY. Capsaicin induces autophagy and apoptosis in human nasopharyngeal carcinoma cells by downregulating the PI3K/AKT/mTOR pathway. *Int J Mol Sci.* 2017;18:1343. <https://doi.org/10.3390/ijms18071343>.
30. Chu H, Li M, Wang X. Capsaicin induces apoptosis and autophagy in human melanoma cells. *Oncol Lett.* 2019;17:4827–34. <https://doi.org/10.3892/ol.2019.10206>.
31. He HJ, Xiong X, Zhou S, et al. Neuroprotective effects of curcumin via autophagy induction in 6-hydroxydopamine Parkinson's models. *Neurochem Int.* 2022;155:105297. <https://doi.org/10.1016/j.neuint.2022.105297>.
32. Musial C, Siedlecka-Kroplewska K, Kmiec Z, Gorska-Ponikowska M. Modulation of autophagy in cancer cells by dietary polyphenols. *Antioxidants.* 2021;10:123. <https://doi.org/10.3390/antiox10010123>.
33. Tu Z, Jiang X, Li Y, et al. Curcumin promotes the survival of ischemic random skin flaps via autophagy. *Am J Transl Res.* 2021;13:1337–51.
34. Pang K, Li B, Tang Z, et al. Resveratrol inhibits hypertrophic scars formation by activating autophagy via the miR-4654/Rheb axis. *Mol Med Rep.* 2020;22:3440–52. <https://doi.org/10.3892/mmr.2020.11407>.

35. Fernández-Rodríguez JA, Almonte-Becerril M, Ramil-Gómez O, et al. Autophagy activation by resveratrol reduces severity of experimental rheumatoid arthritis. *Mol Nutr Food Res*. 2021;65:e2000377. <https://doi.org/10.1002/mnfr.202000377>.
36. Abokyi S, Shan SW, To CH, Chan HH, Tse DY. Autophagy upregulation by the TFEB inducer trehalose protects against oxidative damage and cell death associated with NRF2 inhibition in human RPE cells. *Oxid Med Cell Longev*. 2020;2020:5296341. <https://doi.org/10.1155/2020/5296341>.
37. Jeong SJ, Stitham J, Evans TD, et al. Trehalose causes low-grade lysosomal stress to activate TFEB and the autophagy-lysosome biogenesis response. *Autophagy*. 2021;11:1–13. <https://doi.org/10.1080/15548627.2021.1896906>.
38. Chen L, Zhou K, Chen H, Li S, Lin D, Zhou D. Calcitriol promotes survival of experimental random pattern flap via activation of autophagy. *Am J Transl Res*. 2017;9:3642–53.
39. Yuan F, Xu Y, You K, Zhang J, Yang F, Li YX. Calcitriol alleviates ethanol-induced hepatotoxicity via AMPK/mTOR-mediated autophagy. *Arch Biochem Biophys*. 2021;697:108694. <https://doi.org/10.1016/j.abb.2020.108694>.
40. Rintz E, Pierzynowska K, Podlacha M, Węgrzyn G. Has resveratrol a potential for mucopolysaccharidosis treatment? *Eur J Pharmacol*. 2020;888:173534.
41. Pierzynowska K, Podlacha M, Gaffke L, et al. Autophagy-dependent mechanism of genistein-mediated elimination of behavioral and biochemical defects in the rat model of sporadic Alzheimer's disease. *Neuropharmacology*. 2019;148:332–46. <https://doi.org/10.1016/j.neuropharm.2019.01.030>.
42. Kliensky DJ, Abdel-Aziz AK, Abdelfatah S, et al. Guidelines for the use and interpretation of assays for monitoring autophagy (4th edition). *Autophagy*. 2021;17:1–382. <https://doi.org/10.1080/15548627.2020.1797280>.
43. Piotrowska E, Jakóbkiewicz-Banecka J, Barańska S, et al. Genistein-mediated inhibition of glycosaminoglycan synthesis as a basis for gene expression-targeted isoflavone therapy for mucopolysaccharidoses. *Eur J Hum Genet*. 2006;14:846–52. <https://doi.org/10.1038/sj.ejhg.5201623>.
44. Jakóbkiewicz-Banecka J, Piotrowska E, Narajczyk M, Barańska S, Węgrzyn G. Genistein-mediated inhibition of glycosaminoglycan synthesis, which corrects storage in cells of patients suffering from mucopolysaccharidoses, acts by influencing an epidermal growth factor-dependent pathway. *J Biomed Sci*. 2009;16:26. <https://doi.org/10.1186/1423-0127-16-26>.
45. Arfi A, Richard M, Gandolphe C, Scherman D. Storage correction in cells of patients suffering from mucopolysaccharidoses types IIIA and VII after treatment with genistein and other isoflavones. *J Inherit Metab Dis*. 2010;33:61–7. <https://doi.org/10.1007/s10545-009-9029-2>.
46. Friso A, Tomanin R, Salvalaio M, Scarpa M. Genistein reduces glycosaminoglycan levels in a mouse model of mucopolysaccharidosis type II. *Br J Pharmacol*. 2010;159:1082–91. <https://doi.org/10.1111/j.1476-5381.2009.00565.x>.
47. Moskot M, Montefusco S, Jakóbkiewicz-Banecka J, et al. The phytoestrogen genistein modulates lysosomal metabolism and transcription factor EB (TFEB) activation. *J Biol Chem*. 2014;289:17054–69. <https://doi.org/10.1074/jbc.M114.555300>.
48. Lamanna WC, Lawrence R, Sarrazin S, Esko JD. Secondary storage of dermatan sulfate in Sanfilippo disease. *J Biol Chem*. 2011;286:6955–62. <https://doi.org/10.1074/jbc.M110.192062>.
49. Guffon N, Bin-Dorel S, Decullier E, Paillet C, Guitton J, Foulhoux A. Evaluation of miglustat treatment in patients with type III mucopolysaccharidosis: a randomized, double-blind, placebo-controlled study. *J Pediatr*. 2011;159:838–44. <https://doi.org/10.1016/j.jpeds.2011.04.040>.
50. Kingma SD, Wagemans T, IJlst L, Wijburg FA, van Vlies N. Genistein increases glycosaminoglycan levels in mucopolysaccharidosis type I cell models. *J Inherit Metab Dis*. 2014;37:813–21. <https://doi.org/10.1007/s10545-014-9703-x>.
51. Lan Y, Li X, Liu X, et al. Genistein enhances or reduces glycosaminoglycan quantity in a cell type-specific manner. *Cell Physiol Biochem*. 2018;47:1667–81. <https://doi.org/10.1159/000490985>.
52. Malinowska M, Wilkinson FL, Langford-Smith KJ, et al. Genistein improves neuropathology and corrects behaviour in a mouse model of neurodegenerative metabolic disease. *PLoS ONE*. 2010;5:e14192. <https://doi.org/10.1371/journal.pone.0014192>.
53. Kingma SD, Wagemans T, IJlst L, et al. Adverse effects of genistein in a mucopolysaccharidosis type I mouse model. *N JIMD Rep*. 2015;23:77–83. https://doi.org/10.1007/8904_2015_432.
54. Piotrowska E, Jakóbkiewicz-Banecka J, Tylki-Szymanska A, et al. Genistin-rich soy isoflavone extract in substrate re-reduction therapy for Sanfilippo syndrome: an open-label, pilot study in 10 pediatric patients. *Curr Ther Res Clin Exp*. 2008;69:166–79. <https://doi.org/10.1016/j.curtheres.2008.04.002>.
55. Piotrowska E, Jakóbkiewicz-Banecka J, Maryniak A, et al. Two-year follow-up of Sanfilippo disease patients treated with a genistein-rich isoflavone extract: assessment of effects on cognitive functions and general status of patients. *Med Sci Monit*. 2011;17:CR196–202. <https://doi.org/10.12659/msm.881715>.
56. Marucha J, Tylki-Szymańska A, Jakóbkiewicz-Banecka J, et al. Improvement in the range of joint motion in seven patients with mucopolysaccharidosis type II during experimental gene expression-targeted isoflavone therapy (GET IT). *Am J Med Genet A*. 2011;155A:2257–62. <https://doi.org/10.1002/ajmg.a.34146>.
57. Malinová V, Węgrzyn G, Narajczyk M. The use of elevated doses of genistein-rich soy extract in the gene expression-targeted isoflavone therapy for Sanfilippo disease patients. *JIMD Rep*. 2012;5:21–5. https://doi.org/10.1007/8904_2011_87.
58. Delgadillo V, O'Callaghan MDM, Artuch R, Montero R, Pineda M. Genistein supplementation in patients affected by Sanfilippo disease. *J Inherit Metab Dis*. 2011;34:1039–44. <https://doi.org/10.1007/s10545-011-9342-4>.
59. de Ruijter J, Valstar MJ, Narajczyk M, et al. Genistein in Sanfilippo disease: a randomized controlled crossover trial. *Ann Neurol*. 2012;71:110–20. <https://doi.org/10.1002/ana.22643>.
60. Kim KH, Dodsworth C, Paras A, Burton BK. High dose genistein aglycone therapy is safe in patients with mucopolysaccharidoses involving the central nervous system. *Mol Genet Metab*. 2013;109:382–5. <https://doi.org/10.1016/j.ymgme.2013.06.012>.
61. Wei H, Zhang Z, Saha A, et al. Disruption of adaptive energy metabolism and elevated ribosomal p-S6K1 levels contribute to INCL pathogenesis: partial rescue by resveratrol. *Hum Mol Genet*. 2011;20:1111–21. <https://doi.org/10.1093/hmg/ddq555>.
62. Yoon DH, Kwon OY, Mang JY, et al. Protective potential of resveratrol against oxidative stress and apoptosis in Batten disease lymphoblast cells. *Biochem Biophys Res Commun*. 2011;414:49–52. <https://doi.org/10.1016/j.bbrc.2011.09.019>.
63. Saha A, Sarkar C, Singh SP, et al. The blood-brain barrier is disrupted in a mouse model of infantile neuronal ceroid lipofuscinosis: amelioration by resveratrol. *Hum Mol Genet*. 2012;21:2233–44. <https://doi.org/10.1093/hmg/dd038>.
64. Dardis A, Zanin I, Zampieri S, et al. Functional characterization of the common c.-32–13T>G mutation of GAA gene: identification of potential therapeutic agents. *Nucleic Acids Res*. 2014;42:1291–302. <https://doi.org/10.1093/nar/gkt987>.
65. Yoo S, Kim JB. Anti-apoptotic and beneficial metabolic activities of resveratrol in type II Gaucher disease. *Biol Pharm Bull*. 2015;38:913–8. <https://doi.org/10.1248/bpb.b14-00712>.
66. Seo CH, Kim JB. Therapeutic potential of resveratrol in type I Gaucher disease. *Phytother Res*. 2015;29:835–9. <https://doi.org/10.1002/ptr.5304>.
67. Dasari SK, Schejter E, Bialik S, et al. Death by over-eating: the Gaucher disease associated gene GBA1, identified in a screen for

- mediators of autophagic cell death, is necessary for developmental cell death in *Drosophila* midgut. *Cell Cycle*. 2017;16:2003–10. <https://doi.org/10.1080/15384101.2017.1380134>.
68. Bar S, Prasad M, Datta R. Neuromuscular degeneration and locomotor deficit in a *Drosophila* model of mucopolysaccharidosis VII is attenuated by treatment with resveratrol. *Dis Model Mech*. 2018;11:dmm036954. <https://doi.org/10.1242/dmm.036954>.
 69. Del Grosso A, Angella L, Tonazzini I, et al. Dysregulated autophagy as a new aspect of the molecular pathogenesis of Krabbe disease. *Neurobiol Dis*. 2019;129:195–207. <https://doi.org/10.1016/j.nbd.2019.05.011>.
 70. Shao R, Shi J, Du K, et al. Resveratrol promotes lysosomal function via ER calcium-dependent TFEB activation to ameliorate lipid accumulation. *Biochem J*. 2021;478:1159–73. <https://doi.org/10.1042/BCJ20200676>.
 71. Heldermon CD, Hennig AK, Ohlemiller KK, et al. Development of sensory, motor and behavioral deficits in the murine model of Sanfilippo syndrome type B. *PLoS ONE*. 2007;2:e772. <https://doi.org/10.1371/journal.pone.0000772>.
 72. De Risi M, Tufano M, Alvino FG, et al. Altered heparan sulfate metabolism during development triggers dopamine-dependent autistic-behaviours in models of lysosomal storage disorders. *Nat Commun*. 2021;12:3495. <https://doi.org/10.1038/s41467-021-23903-5>.
 73. Wiśniewska K, Wolski J, Gaffke L, Cyske Z, Pierzynowska K, Węgrzyn G. Misdiagnosis in mucopolysaccharidoses. *J Appl Genet*. 2022;63:475–95. <https://doi.org/10.1007/s13353-022-00703-1>.
 74. Cyske Z, Anikiej-Wiczenbach P, Wisniewska K, Gaffke L, Pierzynowska K, Mański A, Węgrzyn G. Sanfilippo syndrome: optimizing care with a multidisciplinary approach. *J Multidiscip Healthc*. 2022;15:2097–110. <https://doi.org/10.2147/JMDH.S362994>.
 75. Cyske Z, Gaffke L, Pierzynowska K, Węgrzyn G. Complex changes in the efficiency of the expression of many genes in monogenic diseases, mucopolysaccharidoses, may arise from significant disturbances in the levels of factors involved in the gene expression regulation processes. *Genes*. 2022;13:593. <https://doi.org/10.3390/genes13040593>.
 76. Wang Q, Xu J, Rottinghaus GE, Simonyi A, Lubahn D, Sun GY, Sun AY. Resveratrol protects against global cerebral ischemic injury in gerbils. *Brain Res*. 2002;958:439–47. [https://doi.org/10.1016/s0006-8993\(02\)03543-6](https://doi.org/10.1016/s0006-8993(02)03543-6).
 77. Shimazu R, Anada M, Miyaguchi A, Nomi Y, Matsumoto H. Evaluation of blood-brain barrier permeability of polyphenols, anthocyanins, and their metabolites. *J Agric Food Chem*. 2021;69:11676–86. <https://doi.org/10.1021/acs.jafc.1c02898>.
 78. Andrade S, Ramalho MJ, Pereira MDC, Loureiro JA. Resveratrol brain delivery for neurological disorders prevention and treatment. *Front Pharmacol*. 2018;9:1261. <https://doi.org/10.3389/fphar.2018.01261>.
 79. Katekar R, Thombre G, Riyazuddin M, Husain A, Rani H, Praveena KS, Gayen JR. Pharmacokinetics and brain targeting of trans-resveratrol loaded mixed micelles in rats following intravenous administration. *Pharm Dev Technol*. 2020;25:300–7. <https://doi.org/10.1080/10837450.2019.1680690>.

Publisher's Note Springer Nature remains neutral with regard to jurisdictional claims in published maps and institutional affiliations.

Authors Contribution

Oświadczenie o wkładzie w publikację

Oświadczam, że mój wkład w publikację:

Rintz, E., Podlacha, M., Cyske, Z., Pierzynowska, K., Wegrzyn, G., Gaffke, L. (2023) Activities of (Poly)phenolic Antioxidants and Other Natural Autophagy Modulators in the Treatment of Sanfilippo Disease: Remarkable Efficacy of Resveratrol in Cellular and Animal Models. *Neurotherapeutics*. 20(1):254-271.

polegał na:

- kierowaniu projektem Preludium 18;
- udziale w planowaniu badań;
- udziale w przeprowadzeniu eksperymentów na myszach;
- analizie eksperymentów przeprowadzonych na myszach;
- przygotowaniu figur z eksperymentów przeprowadzonych na myszach;
- udziale w przygotowaniu manuskryptu publikacji;
- udziale w dyskusji z recenzentami.



Uniwersytet Gdański
Katedra Biologii Molekularnej
mgr Estera Rintz

Dr hab. Magdalena Podlacha
Katedra Biologii Molekularnej
Wydział Biologii
Uniwersytet Gdański

Gdańsk, 25.04.2024

Oświadczenie o wkładzie w publikację

Oświadczam, że mój wkład w publikację:

Rintz, E., Podlacha, M., Cyske, Z., Pierzynowska, K., Wegrzyn, G., Gaffke, L. (2023) Activities of (Poly)phenolic Antioxidants and Other Natural Autophagy Modulators in the Treatment of Sanfilippo Disease: Remarkable Efficacy of Resveratrol in Cellular and Animal Models. *Neurotherapeutics*. 20(1):254-271.

polegał na:

1. Przeprowadzaniu eksperymentów na myszach;
2. Udziale w analizie eksperymentów przeprowadzonych na myszach;
3. Udziale w przygotowaniu manuskryptu publikacji;
4. Udziale w dyskusjach nad manuskrytem.



Wydział Biologii
Katedra Biologii Molekularnej
dr hab. Magdalena Podlacha

Oświadczenie o wkładzie w publikację

Oświadczam, że mój wkład w publikację:

Rintz, E., Podlacha, M., Cyske, Z., Pierzynowska, K., Wegrzyn, G., Gaffke, L. (2023) Activities of (Poly)phenolic Antioxidants and Other Natural Autophagy Modulators in the Treatment of Sanfilippo Disease: Remarkable Efficacy of Resveratrol in Cellular and Animal Models. *Neurotherapeutics*. 20(1):254-271.

polegał na:

1. udziale w analizie żywotności pod wpływem różnych induktorów autofagii;
2. udziale w detekcji białek markerowych dla procesu autofagii;
3. udziale w dyskusji nad manuskrytem.



Wydział Biologii
Katedra Biologii Molekularnej

mgr Zuzanna Cyske

Oświadczenie o wkładzie w publikację

Oświadczam, że mój wkład w publikację:

Rintz, E., Podlacha, M., Cyske, Z., Pierzynowska, K., Wegrzyn, G., Gaffke, L. (2023) Activities of (Poly)phenolic Antioxidants and Other Natural Autophagy Modulators in the Treatment of Sanfilippo Disease: Remarkable Efficacy of Resveratrol in Cellular and Animal Models. *Neurotherapeutics*. 20(1):254-271.

polegał na:

1. udziale w planowaniu badań;
2. udziale w wizualizacji wyników;
3. udziale w przygotowaniu manuskryptu publikacji;
4. udziale w dyskusji z recenzentami.

 Wydział Biologii
Katedra Biologii Molekularnej
Karolina Pierzynowska
dr hab. Karolina Pierzynowska
profesor uczelni

Prof. dr hab. Grzegorz Węgrzyn
Katedra Biologii Molekularnej
Wydział Biologii
Uniwersytet Gdański

Gdańsk, 29.05.2024

Oświadczenie o wkładzie w publikację

Oświadczam, że mój wkład w publikację:

Rintz, E., Podlacha, M., Cyske, Z., Pierzynowska, K., Węgrzyn, G., Gaffke, L. (2023) Activities of (Poly)phenolic Antioxidants and Other Natural Autophagy Modulators in the Treatment of Sanfilippo Disease: Remarkable Efficacy of Resveratrol in Cellular and Animal Models. *Neurotherapeutics*. 20(1):254-271.

polegał na kierowaniu projektem, udziale we wspólnej z innymi autorami analizie i interpretacji wyników oraz udziale w przygotowaniu ostatecznej wersji manuskryptu.

KIEROWNIK
KATEDRY BIOLOGII MOLEKULARNEJ



prof. dr hab. Grzegorz Węgrzyn
prof. dr hab. Grzegorz Węgrzyn

Oświadczenie o wkładzie w publikację

Oświadczam, że mój wkład w publikację:

Rintz, E., Podlacha, M., Cyske, Z., Pierzynowska, K., Wegrzyn, G., Gaffke, L. (2023)
Activities of (Poly)phenolic Antioxidants and Other Natural Autophagy Modulators in the
Treatment of Sanfilippo Disease: Remarkable Efficacy of Resveratrol in Cellular and
Animal Models. *Neurotherapeutics*. 20(1):254-271.

polegał na:

1. kierowaniu projektem Preludium 15;
2. udziale w zaplanowaniu badań;
3. analizie żywotności pod wpływem różnych induktorów autofagii;
4. analizie poziomu siarczanu heparanu (Dot-blotting);
5. analizie poziomu białek markerowych procesu autofagii w tkankach myszy (Western-blotting) i przygotowaniu stosowanych figur;
6. przygotowaniu manuskryptu publikacji;
7. udziale w dyskusji z recenzentami (przygotowanie odpowiedzi na recenzję oraz ostatecznej wersji manuskryptu publikacji).

 Wydział Biologii
Katedra Biologii Molekularnej
Dr hab. Lidia Gaffke

Rintz, E., Węgrzyn, G., Fujii, T., Tomatsu, S. (2022)
Molecular Mechanism of Induction of Bone Growth by the C-Type
Natriuretic Peptide. *International Journal of Molecular Sciences*.
23(11):5916.

Impact Factor = 5.6 (2022)

MNISW Punctuation = 140



Review

Molecular Mechanism of Induction of Bone Growth by the C-Type Natriuretic Peptide

Estera Rintz^{1,2}, Grzegorz Węgrzyn¹, Toshihito Fujii³ and Shunji Tomatsu^{2,4,*} 

¹ Department of Molecular Biology, Faculty of Biology, University of Gdansk, 80-308 Gdansk, Poland; estera.rintz@ug.edu.pl (E.R.); grzegorz.wegrzyn@ug.edu.pl (G.W.)

² Skeletal Dysplasia Research Lab, Nemours Children's Health, 1600 Rockland Rd., Wilmington, DE 19899, USA

³ Department of Diabetes, Endocrinology, and Nutrition, Kyoto University Hospital, Kyoto 606-8507, Japan; tfujii@kuhp.kyoto-u.ac.jp

⁴ Department of Pediatrics, Thomas Jefferson University, Philadelphia, PA 19107, USA

* Correspondence: shunji.tomatsu@nemours.com; Tel.: +1-302-298-7336; Fax: +1-302-651-6888

Abstract: The skeletal development process in the body occurs through sequential cellular and molecular processes called endochondral ossification. Endochondral ossification occurs in the growth plate where chondrocytes differentiate from resting, proliferative, hypertrophic to calcified zones. Natriuretic peptides (NPTs) are peptide hormones with multiple functions, including regulation of blood pressure, water-mineral balance, and many metabolic processes. NPTs secreted from the heart activate different tissues and organs, working in a paracrine or autocrine manner. One of the natriuretic peptides, C-type natriuretic peptide-, induces bone growth through several mechanisms. This review will summarize the knowledge, including the newest discoveries, of the mechanism of CNP activation in bone growth.

Keywords: natriuretic peptide; growth plate; chondrocyte cell; bone growth; molecular mechanism



Citation: Rintz, E.; Węgrzyn, G.; Fujii, T.; Tomatsu, S. Molecular Mechanism of Induction of Bone Growth by the C-Type Natriuretic Peptide. *Int. J. Mol. Sci.* **2022**, *23*, 5916. <https://doi.org/10.3390/ijms23115916>

Academic Editor: Chih-Hsin Tang

Received: 12 April 2022

Accepted: 21 May 2022

Published: 25 May 2022

Publisher's Note: MDPI stays neutral with regard to jurisdictional claims in published maps and institutional affiliations.



Copyright: © 2022 by the authors. Licensee MDPI, Basel, Switzerland. This article is an open access article distributed under the terms and conditions of the Creative Commons Attribution (CC BY) license (<https://creativecommons.org/licenses/by/4.0/>).

1. Introduction

The skeletal development process in the body occurs through sequential cellular and molecular processes called endochondral ossification. Only craniofacial bones and clavicles are not developed through endochondral ossification [1]. Endochondral ossification occurs in the growth plate where chondrocytes differentiate from resting (reserve), proliferative, hypertrophic, to calcified zones. Differentiated chondrocytes construct a cartilage extracellular matrix (ECM) through the upregulation of proteolytic enzyme production (matrix metalloproteinases). Together with the vascular endothelial growth factor, this process induces degradation of cartilage matrix components inducing vascularization. Eventually, cartilage will be replaced with mature bone tissue. Differentiation of growth plate cartilage is regulated by several factors, including hormones, growth factors, and components of the cartilage ECM [2].

Natriuretic peptides (NPTs) are peptide hormones with multiple functions, including the regulation of blood pressure, water-mineral balance, and many metabolic processes [3]. NPTs secreted from the heart (the cardiac atria and ventricles-ANP and BNP; vascular endothelium-CNP) activate different tissues and organs, working in a paracrine or autocrine manner. The first NPT was discovered as atrial NPT (ANP) in 1981, secreted from the cardiac atria and ventricles [4]. From that time, eight NPTs have been described: ANP, B-type natriuretic peptide (BNP), C-type NPT (CNP), D-type NPT (DNP), urodilatin, urogauylin, osteocrin, myocardin, and musclin [3]. The functions of three main peptides (ANP, BNP, and CNP) were investigated in detail.

The peptides mentioned above can be used to diagnose heart or pulmonary diseases (Table 1). Various cellular factors stimulate the expression of genes coding for ANP, BNP, and CNP, and the secretion of these peptides. In the case of patients with heart failure,

levels of particular forms of ANP (proANP/ γ -ANP, β -ANP) or BNP (uncleaved proBNP, mature BNP, and N-terminal proBNP) increased compared to healthy controls. Precursors of the peptides are proteolytically degraded to their active forms, acting in tissues and organs [5]. Moreover, a decrease in the levels of NPTs and an increase in the receptor level that degrades the peptides (NPR-C) have been associated with diet and physical activity [6].

Table 1. Natriuretic peptides used in diagnosis and treatment.

NTPs	NTPs Used for Diagnosis/Evaluation		NTPs Tested for Diseases as a Treatment
	Final Peptide	Pro-form of the Peptide	
ANP	Heart failure [7–10] Cancer [11] Type-2 diabetes [12] Chronic renal failure [13]	Heart failure [10,14] Insulin resistance [15,16] Obesity [17]	Heart failure [18–22] Cardioprotective effects during surgery [23–30] Renal failure [31–36] Colorectal cancer [37] Forearm vasculature [37] Acute kidney injury [38] Lipid mobilization [39] Pulmonary vasorelaxant [40]
BNP	Heart failure [10,41–53] Acute dyspnea [54] Asthma [55] Type 2 diabetes [56] Cancer [11] Chronic renal failure [13] Obesity [17,57] Chronic kidney disease [58,59] SARS-CoV-2 [60] Atrial fibrillation [61] Hemodialysis patients [62] Diabetic nephropathy [63]	Heart failure [48,64–69] Type 2 diabetes [70,71] Obesity [17,72] Chronic kidney disease [58] Cardiac function [73] Stroke [73]	Forearm vasculature [37] Pulmonary vasorelaxant [40] Myocardial infarction [74,75]
CNP	Heart failure [47,76]	Heart failure [64] Growth failure [77]	Heart failure (CNP fused to DNP) [78] Renal failure [79,80] Achondroplasia [81,82] Anxiety [83]

There are three known NPT receptors: NPT receptor-A (NPR-A; also called NPR1 or GC-A), NPT receptor-B (NPR -B; another way NPR2 or GC-B), and NPT receptor-C (NPR-C; also called NPR3 or GC-C). ANP and BNP are ligands for NPR-A, while CNP activates NPR-B. NPR-C receptor is responsible for the degradation and internalization of circulating NPTs within the cell [84]. NPRs catalyze the synthesis of cyclic guanosine-3',5'-monophosphate (cyclic GMP; cGMP), known as the internal mediator for most effects of NPTs.

CNP structure differs from ANP and BNP in the second cysteine, lacking further C-terminal extension [85]. CNP is released by endothelial cells, cardiomyocytes, and fibroblasts and regulates the function of the cardiovascular system together with ANP and BNP [86]. However, CNP function not only affects the cardiovascular system but also governs bone growth [87–91]. Interestingly, the mechanism of CNP action can be different depending on the cell type. CNP activates ossification and calcification in bone cells, while in the valvular interstitial cells, those processes are inhibited by the CNP peptide [92]. The same pattern is observed with osteoblast and myofibroblast differentiation, where those processed are activated in bone cells and inhibited in the valvular interstitial cells with CNP treatment [92].

Some previous reviews explained CNP peptide and its bone mechanism, but still questions remain unanswered. This review will summarize our knowledge, including the newest discoveries, on the mechanism of CNP activation in bone growth. MeSH (Medical Subject Headings) was applied to select articles in this review process. In PubMed search,

we have used the keywords of “C-Type Natriuretic Peptide bone growth”, “C-Type Natriuretic Peptide”, “CNP bone”, and “C-Type Natriuretic Peptide mechanism bone”. A total of approximately 40 articles were found under the CNP activating bone mechanism. We have also searched the clinical trials via <https://clinicaltrials.gov/> (accessed on 4 April 2022) to prepare Table 1.

2. C-Type Natriuretic Peptide and Nitric Oxide as Bone Growth Regulators

CNP as a bone growth regulator was first mentioned in 1995 [93], where CNP was found to induce bone resorption. The production of CNP can be induced by cytokines (such as IL-1 α , IL-1 β , and TNF α), thus affecting osteoclast resorption. It is unclear if CNP acts directly on osteoclasts or not. When CNP was added to the culture, cGMP production increased (as well as bone resorption), meaning that the receptor for CNP (NPR-B) is present in the bone marrow culture cells. Adding the CNP inhibitor to the culture decreased the efficiency of bone marrow resorption in CNP-treated and untreated cells, indicating the bone marrow released CNP. Nevertheless, it is unclear what kind of cells secreted CNP peptide, as bone marrow is a heterogeneous mixture of the cells [93]. Not only resorption of osteoclasts but also proliferation and differentiation of osteoblasts are regulated by CNP peptides. Production of cGMP, induced by CNP, leads to bone formation in osteoblast-like cells. CNP activation increased the activities of alkaline phosphatase (ALP) and osteocalcin and the mineralization of nodules in the cell culture [94]. Similarly, CNP upregulated bone turnover biomarkers, both osteoblastic (osteocalcin, procollagen type I, total ALP, and bone-specific alkaline phosphatase) and osteolytic (tartrate-resistant acid phosphatase-TRAP and cross-linked C-terminal telopeptide of type I collagen- CTX-I) in osteoblast-like cells [91].

Another molecule in bone growth regulation is nitric oxide (NO). Mice deficient in the eNOS show bone abnormalities, while inducible NOS (iNOS) deficient mice show imbalances in bone osteogenesis and abnormalities in bone healing [95–97]. iNOS is synthesized in response to inflammatory stimulation, producing NO, thereby inducing bone loss. As NO is a highly reactive molecule, molecular bone targets are not fully understood [98]. Nevertheless, NO inhibits bone resorption by inducing cGMP synthesis (the same as CNP) [99]. Thus, CNP can affect bone remodeling [93].

Research on the interactions of NO and NPTs has shown that only ANP can inhibit NO through the NPR-A receptor in macrophages [100]. Even though all natriuretic receptors (with two types of NPR-B receptor) are produced in macrophages, CNP still does not inhibit NO. Receptor for CNP exists in two NPR-B receptors that differ in structure [101], while CNP is a ligand for both. However, one of the forms is shorter, without the ability to induce cGMP production by CNP binding [100]. NO is synthesized from L-arginine by inducible nitric-oxide synthase (iNOS) [102]. CNP neither inhibits the induction of iNOS nor induces L-arginine transport, which is critical for NO production [103].

Both NO and CNP stimulate the production of cGMP in cells. An additional product of the cGMP forming reaction could be 8-nitro-cGMP (Figure 1). The level of 8-nitro-cGMP increases in the presence of CNP in bone culture *in vitro*. Like cGMP, 8-nitro-cGMP stimulates the proliferation of cells in the growth plate as the bone grows. These results show that NO and CNP activation mechanisms are more complicated, activating cGMP and other molecules, which may work synergistically in the bone growth effect [101].

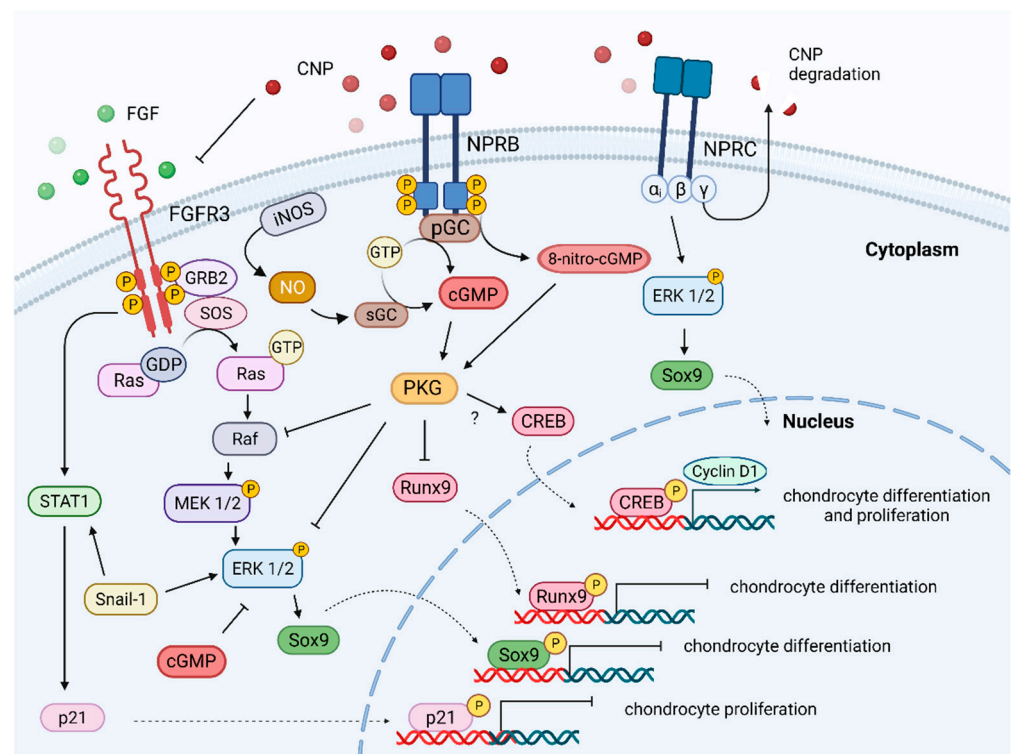


Figure 1. Signaling pathways activated or inhibited by CNP in the bone growth plate region. The cellular effects of CNP action are mediated through the NPR-B receptor, stimulating intracellular molecule cGMP production, which further results in the protein kinase G (PKG) activation. PKG activation by CNP results in the MAPK signaling pathway, which results in chondrocyte proliferation and differentiation. NPR-C receptor degrades CNP; additionally, Gi protein of the receptor modulates the level of ERK1/2 inside the cell. ?- it is not confirmed if CREB is activated by PKG.

3. CNP/NPR-B/cGMP Pathway

The signaling pathway of the chondroprotective effects with CNP is mediated by the NPR-B receptor, enhancing the activation and synthesis of cGMP. As a result, PKGII is activated, leading to the elevation of ECM (collagen II, aggrecan) and bone mineralization (ALP), finally inducing bone growth. Additionally, the activation of the NPR-B receptor inhibits the MEK/ERK signaling pathway, stopping cartilage degradation (Figure 1). However, this pathway can be stimulated by other factors (not only CNP) that either enhance or reduce bone growth. Aging and inflammation are some processes affecting reduced bone growth [104]. Thus, skeletal dysplasia should be treated at an early age of patients. There are also different CNP/NPR-B/cGMP signaling pathway inhibitors. One of the first described inhibitors was lysophosphatidic acid (LPA), which causes a decrease in cGMP concentration that was not correlated with the receptor loss. While previous research showed that PKC could be involved in the dephosphorylation of the NPR-B receptor at the Ser-523 residue [105], in this case, the activity of PKC was not changed. According to the authors, this response increases the response of fibroblasts to the wound-healing process [106]. Those investigations showed that CNP activation and different agents could regulate the NPR-B receptor. cGMP is converted from guanosine triphosphate in reactions catalyzed by various enzymes (guanyl, guanylyl, or guanylate cyclases). Guanylate cyclases are activated by different factors such as guanylin, uroguanylin, guanylyl cyclase-activating proteins, NO, as well as NPTs. Activation of the second intracellular messenger (cGMP) stimulates or modulates different pathways within the cell, depending on what receptor was activated (NPR-A, -B, or C). Processes that are activated by cGMP include platelet aggregation, blood pressure neurotransmission, sexual arousal, gut peristalsis, long bone

growth, intestinal fluid secretion, lipolysis, phototransduction, cardiac hypertrophy, and even oocyte maturation [107].

Guanylyl cyclases are ubiquitous enzymes with two classes occurring in mammals: soluble cytoplasmic guanylyl cyclase and single membrane-spanning forms (NPR-/GC-A, -B, -C, -D, -E, -F, and -G) that can be produced in different tissues. The localization within the body of these two guanylyl cyclases classes is different, as well as their ligands. ANP and BNP ligands activate NPR-A, produced in lung, kidney, adrenal, vascular smooth muscle, endothelium, heart, and adipose. Inactivation of NPR-A leads to heart-related problems (hypertension, cardiac fibrosis, and hypertrophy). The NPR-B, activated by CNP, is produced in bones, vascular smooth muscle, lung, brain, heart, liver, uterus, and follicles [108]. ATP increases the enzyme activity of NPR-B [109]. The degradation receptor for the NPTs is synthesized in the intestinal epithelium, stimulated by bacterial heat-stable enterotoxin, guanylin, and uroguanylin. Impaired production of GC-C leads to increased proliferation of colonic epithelial cells without a change in blood pressure [107].

4. CNP/NPR-B/cGMP/MAPK Pathway

The CNP/NPR-B/cGMP pathway activates endochondral ossification and induces bone growth in different models. FGFs are soluble or cell surface proteoglycans (family of 22 members [110] that activate FGFR-3 tyrosine receptors on the subphase of chondrocytes [111]. Activating mutations of FGFR3 are associated with skeletal diseases like achondroplasia, hypochondroplasia, or thanatophoric dysplasia [112]. Signal transduction of the FGFR-3 phosphorylates ERK1/2, a protein kinase of the MAPK signaling pathway [113]. Constantly phosphorylated ERK1/2 is associated with achondroplasia [114]. On the other side, the FGFs family is associated with slowing long bone growth. Intracellular interactions of FGFs/FGFR-3/MAPK and CNP/CG B/cGMP pathways were studied in mouse chondrogenic cell lines [115]. CNP signaling activation of cGMP was reduced by FGF-2 and FGF-18, while expression of the cGMP itself was not FGFs-dependent (Figure 1). CNP and cGMP inhibited the activation of pERK1/2 by FGFs/FGFR-3. CNP did not affect STAT-1 phosphorylation by FGFs/FGFR-3, another signaling pathway that could be activated (Figure 1). CNP treatment of fetal mouse tibias induced longitudinal bone growth, increasing in size and the number of chondrocytes. This effect was attenuated when FGF18 was added to the culture [115]. Crosstalk was visible between those two pathways, with evidence of the CNP influence on bone growth.

Further research confirmed the interaction of CNP signaling pathway inhibition of FGF-2 by both direct and indirect mechanisms [116]. CNP inhibited phosphorylation and activation of ERK protein kinase induced by the FGF-2 pathway in the rat chondrocyte model. CNP blocks the ERK mitogen pathway at the level of Raf-1, but not Ras or FRS2. To inhibit Raf-1, protein kinase G (PGK) is required because the inhibited CNP pathway was not able to block the ERK/MAPK pathway. The FGF-2 pathway without CNP induces degradation of chondrocyte ECM in a rat cell model of chondrosarcoma. With CNP, FGF-2 was partially inhibited, leading to the expression, activation, and release of ECM molecules and proteins (including matrix metalloproteinase 2 (MMP2), -3, -9, -10, and MMP13). Moreover, CNP induced matrix-mediated production independently of FGF-2 [116] (Figure 2).

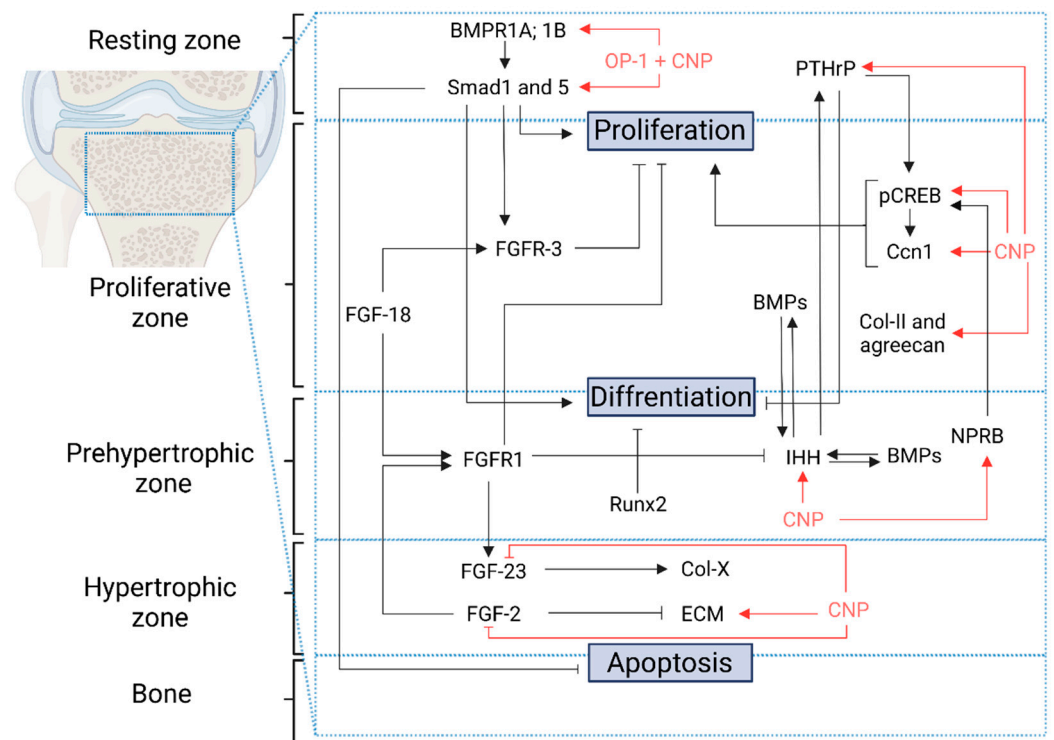


Figure 2. CNP and related bone growth involved protein expression patterns in the growth plate. BMPR1A; 1B: Bone morphogenetic protein receptors; Smad1; 5: Suppressor of Mothers against Decapentaplegic; PTHrP: Parathyroid hormone-related peptide; pCREB: phosphorylated cAMP-response element-binding protein; Ccn1: Cyclin 1 gene; Col-II: Collagen type 2; BMPs: Bone morphogenetic proteins; IHH: Indian Hedgehog; NPRB: NTP Receptor Type B; FGF: Fibroblast growth factor; FGFR: Fibroblast growth factor receptor; Runx2: Runt-related transcription factor 2; Col-X: Collagen type X; ECM: Extracellular Matrix Proteins; CNP: C-type natriuretic peptide. Red arrows and lines means accordingly activation or inhibition by CNP.

None of the previous studies show the direct influence of CNP on the FGF-23 expression. FGF-23 negatively regulates the expression of a gene coding for collagen-X [117] and disturbs collagen X metabolism [118]. Collagen X is produced primarily on the hypertrophic zone in the growth plate of cartilage, although it is involved in calcifying the cartilage [119]. Collagen II and aggrecan are primarily produced in the proliferative zone. One of the most recent reports describing studies on the primary rat osteoblast-like cells showed that CNP stimulates osteoblast proliferation with increased collagen-X levels. While CNP downregulated FGF-23 production, its receptor FGFR-1/Klotho was not changed. These results suggest that CNP can stimulate collagen X production through FGF-23 inhibition [91].

5. CNP/NPR-B/cGMP/pCREB Pathway

Mutations in either the NPPC gene encoding CNP [88] or the NPR2 gene coding for the CNP receptor called NPR-B [120] result in marked dwarfism with skeletal defects. Further studies confirmed acromesomelic dysplasia Maroteaux-type syndrome (MIM #602875) with a mutation in NPR2 [121]. Very recent studies on the Maroteaux syndrome revealed a different mechanism caused by the mutations in the NPR2 gene. Three different mutations p.Leu314Arg), p.Arg371*, and p.Arg1032* lead to variable phenotypes in the patients. These mutations affect the activation and function of the guanylate cyclase: binding of the CNP (ligand) to the NPR-B homodimer; depletion of the three domains in the receptor (transmembrane, protein kinase, and guanylate cyclase); and the deterioration of the guanylate cyclase domain. Those results indicated that the critical function of the NPR-B receptor is the activation of the cGMP in the cell [122].

Interestingly, in epiphyseal chondrodysplasia, Miura type (ECDM; OMIM #615923) disease with the heterozygous NPR2 pathogenic variant caused opposite symptoms to those in the homozygous mutation. So far, only four families with this disease have been reported. These activating mutations in NPR2 cause tall stature, long bones, scoliosis, and elongated toes and fingers in patients. The heterozygous variant (c.2647G>A (p.Val883Met)) is characterized by amino acid alternation localized in one of the domains in the NPR-B receptor-carboxyl-terminal guanylyl cyclase domain [123].

A mouse model with a gain of function mutation in the NPR2 gene exhibited skeletal overgrowth with a thick hypertrophic zone in the cartilage growth plate (higher level of the collagen type X than WT) [124]. The same pattern was not visible in the proliferating zone (similar collagen type II and aggrecan levels to WT mice). Moreover, there was no difference in apoptotic cells in the growth plate when comparing WT with *Npr2* mice. Those results suggest that the NPRB receptor regulates chondrocyte maturation at later stages of development in the hypertrophic layer. It was possible to screen for molecular pathway activation using a cell model for endochondral ossification (ATDC5). Cells were cultured for several weeks (0–8) and treated with CNP to activate the NPRB receptor. Several genes were checked to determine at which stage the chondrocytes are. The main transcription factors critical for chondrocyte gene expression are Runx2, Sox9, and MEF2C [125]. Sox9 is a transcription factor involved in chondrocyte differentiation [126], Sox9 was increased after two weeks of culturing, then declined in untreated cells once cells reached the mature stage (hypertrophic cells) [124]. On the other hand, Runx2 is expressed during chondrocyte hypertrophy [127], did not decline after two weeks, and stayed at the same level. CNP treatment did not affect the expression of both genes, Sox9 and Runx2 [124], while genes encoding CNP and its receptor NPRB peaked at two weeks. The expression level of the cell proliferation gene *Ccnd1*, encoding Cyclin D1 responsible for the progression of the cell cycle in the G1-phase [128], was the highest at four weeks of chondrogenic induction and decreased after that time [124]. When treated with CNP, a similar effect was obtained even if CNP was added at a different time (six or eight weeks), upregulating the expression of *Ccnd1*. Bone growth is regulated by the parathyroid hormone that is present at the end of long bones and delays chondrocytes hypotrophy [129], thus the expression of the genes coding for a parathyroid hormone-related protein (*Pthrp*) and its receptor parathyroid hormone 1 receptor (*Pth1r*) were measured in cell culture. Expression of both *Col2a1* and *Pthrp* was upregulated after CNP treatment, as was *Pth1r* even six weeks after treatment with CNP. Moreover, NPR-B was active when CNP was added to the ATDC5 cells due to the markedly increased production of cGMP [124].

Treatment of hypertrophic chondrocytes with cell-permeable cGMP resulted in increased phosphorylation of CREB, the transcription factor stimulating the production of the Cyclin D1, thus, showing chondrocyte activation through the NPRB-mediated molecular pathway [124]. Those experiments were also confirmed in cartilage isolated from WT neonates and treated with CNP (increased phosphorylation of CREB and Cyclin D1 expression). Contrary to previous research [130], ERK1/2 was not phosphorylated in the primary chondrocytes [124]. In the FGFR-MAPK pathway, FGFR3 is produced in the proliferating and pre-hypertrophic zone of the growth plate, not in the hypertrophic zone [131]. Thus, the CNP pathway can activate and regulate chondrocytes in different ways.

The expression of the *Npr3* gene, encoding the NPR-C receptor, was elevated after CNP treatment, which is consistent with previous research with the organ culture [132]. In the primary chondrocyte cell culture, Sox9, *Prhrp*, and *Ihh* (Indian hedgehog) expressions were increased after CNP treatment, suggesting CNP involvement in both proliferation and differentiation of the cells. Moreover, when cells were treated with CNP, cell numbers increased. With the addition of the inhibitor for either CREB or cyclin D1, CNP-induced NPRB activation was abolished, suggesting the apparent involvement of CREB and cyclin D1 in skeletal overgrowth [124]. The action of parathyroid hormone and its receptor is mediated through cAMP/protein kinase A (PKA)/CREB, regulating chondrocytes by keeping them in the proliferation stage [129]. Nevertheless, CNP treatment increased

cGMP production in the primary chondrocytes, with no cAMP effect. CNP induced phosphorylation of CREB even with PKA inhibitor treatment while it suppressed the phosphorylation of CREB by PTHrP [129]. The same pattern of CREB phosphorylation through NPRB independent of PKA was demonstrated recently [124].

Similarly, when protein kinase-G II (PKGII), downregulated by CNP, is removed from cartilage, cartilage matrix production and chondrocyte proliferation were disturbed in mice [133]. The overexpression of CNP and activating mutations in the *Npr2* gene positively affects cartilage matrix production and chondrocyte proliferation. In a previous experiment, a systemic knockout of the CNP gene was made. The generation of cartilage-specific knockout (using Cre recombinase (Cre)-loxP) of the genes revealed differences in endochondral bone growth in the growth plate between CNP and its receptor [88]. Knockout in the NPR-B receptor resulted in shorter mice than CNP knockout mice. There are several explanations for why it happened. First, and most likely, secretion of CNP from other than cartilage tissues (like blood vessels) causes its binding to the receptor, resulting in lower impairment of growth. Second, there is a higher ligand (CNP) amount than its receptor (NPR-B). When the receptor is missing and the ligand is still present, the general effect on endochondral growth could be more substantial if there is a knockout in the receptor rather than the ligand itself. Furthermore, the sensitivity of the NPR-B receptor could increase due to the absence of CNP. Additionally, the clearance system of the peptides could not work correctly because of the downregulation of the NPR-C receptor [134] or an increased level of osteocrin, a natural ligand for the NPR-C receptor [135]. Due to osteocrin's attachment to the NPR-C receptor, the clearance system of the NPTs is not working. If NPTs cannot be cleared, they will be ligands to receptors that they generally do not activate. The NPR-B receptor may be activated by other ligands, such as ANP or BNP (normally reacting with the NPR-A receptor) [88]. In both models, hypertrophic chondrocytes in the growth plate were drastically reduced with chondrocytes proliferation [88].

While inhibition of the MEK1/2-ERK1/2 pathway stimulates bone growth, p38 MAPK is one of the mediators in the CNP signaling pathway [136]. p38 inhibits stimulation of endochondral bone growth and delays mineralization in tibia organ culture by CNP. These studies confirmed that CNP targets hypertrophic chondrocytes in the growth plate rather than other zones. Even though the CNP receptor is present in all three zones at a similar level, CNP signaling pathway kinases (PKG-I and -II) are primarily produced in the hypertrophic cells. This can potentially explain the spatial distribution of CNP effects. Moreover, CNP induces the expression of NPR2 and NPR3, suggesting the existence of a feedback loop to limit CNP signaling. CNP also regulates bone morphogenic proteins (BMP) signaling and cell adhesion processes [136].

6. C-Type Natriuretic Peptide as Extracellular Matrix Regulator

CNP is engaged in the intracellular processes required for bone growth and the extracellular matrix (ECM) [137]. CNP increases the number of chondrogenic condensations in the micro mass culture of mouse embryonic limb cells. Production of N-cadherin, a cell adhesion molecule, increased after treatment with CNP peptide. Glycosaminoglycan synthesis (chondroitin sulfate) was also stimulated, probably through increased levels of the enzyme (xylosyltransferases I) necessary to produce cartilage glycosaminoglycans. On the other hand, chondrogenic transcription factors (Sox9, -5, and -6), modulators of ECM, as well as ECM building proteins (collagen II and aggrecan) were not changed by CNP [137]. Another study investigated CNP and the formation of the nodules with biglycan (BGN), a small proteoglycan involved with bone formation in osteoblasts. BGN mRNA expression increased with CNP, which shows CNP's ability to regulate gene expression to be closely correlated with bone mineralization [138].

7. Synergic Effect of OP-1 and CNP

Mutation in the gene coding for the growth hormone-insulin like growth factor-I (IGF-1) leads to prenatal and postnatal growth failure. Interaction of growth hormone with

IGF-1 regulates endochondral bone growth. IGF-1 modulates bone growth through the paracrine mechanism rather than systematically. The synergic mechanism of osteoblast differentiation and proliferation by IGF-1 and osteogenic protein-1 (OP-1) was observed when both agents were added to the rat osteoblastic cell culture [139].

Bone morphogenetic proteins (BMPs) are growth factors that induce bone growth, and the main downstream molecules for BMPs are Smads. Activated Smad5 plays an important role in BMP target gene activation. After phosphorylation, Smad5 interacts with Smad4, making a complex translocated to the nucleus, activating BMP target genes [140]. OP-1 activated Smad5 through phosphorylation of the C-terminal region.

Similarly, the synergic mechanism of OP-1 and CNP was observed in the phosphorylation of the Smad5 transcription factor responsible for bone morphogenetic protein gene activation [141]. While CNP has been added alone to the primarily osteoblastic cells, activation of Smad5 was not observed. Alkaline phosphatase (ALP) induction by OP-1 was enhanced by CNP, leading to the mineralization of bone nodules. CNP+OP-1 also enhanced the protein expression level of bone morphogenetic protein receptors IB and II (BMPR-IB; -II), compared to OP-1 alone. CNP induces the expression of genes involved in the bone mineralization process. Nevertheless, the Runx2 protein level was not enhanced by CNP but was elevated after treatment with OP-1 alone, and it was slightly reduced by the combination treatment [141].

8. Survival of Animals with C-Type Natriuretic Peptide

The survival rate of the mice with total CNP knockout was around 40% [142], which was due to severe malocclusion [88]. Mice with the CNP knockout could not eat by themselves; however, when food was pulverized, the survival rate increased to ~70% [88]. The cartilage specific CNP knockout mice survival rate was almost the same as total CNP knockout mice (75.0%). The survival rate of about ~70% is caused by their impaired skeletal growth [88]. As the mice could have higher mortality, it was impossible to analyze them in adult age. For this reason, a generation of a rat model with CNP knockout was performed. The phenotype of the rats was similar to that of the mouse model, manifesting short stature with endochondral bone growth retardation. Compared to the mice model, rats survived for over one year without malocclusions visible in the mouse model. Interestingly, only bones were affected by CNP deficiency in histological analysis, and no other tissues studied were changed compared to WT littermates. Growth plate width in the bone of CNP knockout rats (mainly hypertrophic chondrocyte layer) was lower together with reduced proliferation of growth plate chondrocytes [143]. On the other hand, crossing animals with circulating CNP peptide (SAP-Nppc-Th mice) with chondrodysplastic CNP-depleted mice leads to increased survival. Moreover, circulation of CNP recovers chondrodysplastic CNP-depleted animals from impaired endochondral bone growth, together with increased body weight [87].

9. C-Type Natriuretic Peptide as a Treatment

Achondroplasia is one of the most common diseases leading to dwarfism (1:25,000) by the mutation in a single gene FGFR3 coding for fibroblast growth factor receptor 3). In 80% of the cases, de novo dominant mutation occurs in the egg or sperm that forms the embryo [144]. Parents with new mutations usually do not have a growth deficit. The gene mutation probability increases if the father is more than 35 years old. It is the most common disease in the group of growth defects diseases. Symptoms include dwarfism, midfacial hypoplasia, incorrect torso length, excessive lordosis of the lumbar spine, narrowing of the spinal stricture, small cubic vertebral bodies, prominent forehead, collapsed nose bridge, micromelia (small hands), with normal intellectual development [112]. FGFR3 inhibits long bone growth through different pathways. Activation of phosphorylation of STAT-1 regulated by FGFR3 inhibited chondrocyte proliferation. Moreover, in the MAPK pathway regulated by FGFR3, phosphorylation of ERK1/2 inhibited chondrocyte differen-

tiation. Overall, activation of FGFR3 seems to inhibit the proliferation and differentiation of chondrocytes [130].

The mechanism of CNP in achondroplasia shows that CNP inhibits the MAPK pathway, through decreasing FGF-2 activated level of pERK1/2, what results in animals' normal length [145]. However, CNP did not affect the level of phosphoSTAT-1 in the cartilage of neonatal mice [145]. The achondroplasia mouse model, with FGFR3 mutation leading to jaw deformities, was crossed with mouse overexpressing CNP [146]. Fgfr3ach/SAP-Nppc-Tg mice had significantly improved the craniofacial region comparing symptoms to the Fgfr3ach mouse model. The thickness of synchondrosis was noticed, with increased chondrocytes proliferation within the craniofacial cartilage. Moreover, enhanced endochondral bone growth in the combined mouse model ameliorated the foramen magnum stenosis compared to Fgfr3ach only mice [146]. CNP induces endochondral ossification in the long bones and helps restore craniofacial bones in the achondroplasia mouse model.

Achondroplasia is the most common growth retardation disorder. However, growth retardation can also be a side effect of glucocorticoid-based drug administration [147]. Recent studies showed that high doses of glucocorticoid inhaled by children with asthma correlate with growth retardation [148]. The mechanism of glucocorticoids directly act on chondrocytes within the growth plate, including proliferation and differentiation, together inhibiting bone growth [147]. Growth hormone therapy to restore growth retardation connected to glucocorticoid-based drugs is ineffective [149]. Exogenous CNP-53 is a stable molecular form of intrinsic CNP peptide. It was administered to mice with induced glucocorticoid drug growth retardation [147]. Glucocorticoid-based drug (dexamethasone; DEX) and CNP-53 (dose 0.5 mg/kg/day) were injected into four- to eight-week-old mice by subcutaneous injection. The effect of CNP depended on age, as it was more effective in four-week-old mice. The molecular mechanism of this effect is not based on the action of DEX on cGMP level induction by CNP but instead on the reduction of Erk1/2 phosphorylation by combined treatment [147].

In another study, four-week-old CNP-knockout (CNP-KO) and WT rats were subcutaneously infused with 0.15 or 0.5 mg/kg CNP-53 peptide daily for four weeks. There was no significant difference in plasma bone turnover markers between WT and CNP-KO rats. The short stature of the CNP-knockout mice was restored with circulating CNP peptide administration, where CNP-KO rats were more sensitive to the treatment than WT rats [150]. In acceptance with previous research [101], gene enrichment analysis using fetal rat tibia confirmed that CNP negatively influences the MAPK pathway in chondrocytes [150].

An essential part of mechanism regulation is the feedback loop. In the case of CNP, it remains unclear how it is regulated in the systemic feedback regulation. Several factors indicate that CNP can be regulated in a systemic feedback manner.

Administration of exogenous CNP (CNP-53) to four-week-old rats (0.5 mg/kg/day) for three consecutive days did not alter the blood level of CNP [151]. However, this administration decreased mRNA expression in cartilage tissues. Interestingly, female rats were more sensitive to CNP administration, with a greater decrease in mRNA level. The influence of exogenous administration on endogenous CNP levels in tibia culture and chondrogenic cell lines did not show direct autoregulation. Thus, cartilage tissue is not directly regulated by CNP administration [151].

10. Discussion

CNP is a paracrine growth factor widely expressed in various tissues [152]. Diverse functions include the regulation of endochondral bone growth. The most critical role in humans is recognized as the hormone in skeletal growth related to growth plate proliferation. Studies in mice show that the local production of CNP within the growth plate determines physiological endochondral bone growth [88]. The dynamic role of CNP in bone growth remains a challenge due to the rapid clearance of CNP and low concentrations in the blood. An inactive portion of the synthesized product in the growth plate (amino-terminal propeptide CNP; NTproCNP) is not subject to clearance or rapid degradation. NTproCNP

is an equimolar product of CNP biosynthesis, which is easily measured in plasma. Its level in blood correlates to linear growth velocity throughout growth in both children and mouse models [153]. CNP and NTproCNP levels for both sexes were high in infancy, lower in early childhood, rising during puberty, and then falling to low adult levels. Peak levels of NTproCNP are coincident with the age of peak height velocity. Thus, CNP synthesis (as measured by NTproCNP levels in plasma) is closely related to linear growth in healthy children at all ages, resulting in an excellent biomarker of linear growth [154].

CNP products in plasma were elevated in skeletal dysplasia with profound short stature due to a disruption of the CNP receptor (NPR-B) (acromesomelic dysplasia type Maroteux), activation of the MEK/ERK MAPK pathway inhibiting NPR-B signaling, activating mutations of *FGFR3* (thanatophoric dysplasia, achondroplasia, and hypochondroplasia) [1]. Two reports support those activating mutations of NPR-B cause skeletal overgrowth [155,156], reducing plasma NTproCNP. Little is known about the factors that regulate CNP expression and translation; the details of this feedback loop require further study.

The relation between the MEK/ERK MAPK and CNP/cGMP pathways was investigated in chondrogenic cells and organ culture. Phosphorylated MEK1/2 and/or ERK1/2 inhibit cGMP generation by NPR-B. Meanwhile, NPR-B-generated cGMP inhibits MEK/ERK activation by inhibiting RAF1. Thus, overactivation of the MEK/ERK MAPK pathway leads to resistance to CNP [115]. The finding of elevated CNP levels in a population with severe short stature suggests that these individuals may also have resistance to CNP.

It is noteworthy that patients with achondroplasia affecting the CNP pathway activity have elevated plasma NTproCNP concentrations, while intracellular CNP activity is reduced [116,145,157]. In achondroplasia, the normal reciprocal antagonism between *FGFR3* (inhibiting endochondral bone growth) and CNP signaling (stimulating bone growth) is disregarded by a gain of function mutation in *FGR3* [115]. CNP production is subject to feedback regulation. Endogenous CNP remains subject to regulation during the administration of growth-promoting doses of the CNP analog in achondroplasia. With the restraining impact of the genetic mutation on CNP signaling, baseline levels of CNP products in plasma are elevated. During periods of accelerating long bone growth induced by the CNP analog, endogenous CNP is reduced in keeping with indirect negative feedback. Direct inhibition of CNP by exogenous CNP occurs in proportion to the overall level of hormone resistance. Unusual high values of plasma NTproCNP in adolescent years with achondroplasia patients receiving the CNP analog are unexplained and require future study [115].

Take-home message;

1. CNP produced in the growth plate is a potent positive regulator of linear growth.
2. Reduced intracellular CNP pathway activity may increase CNP production; a negative feedback loop regulates CNP
3. In a group of skeletal dysplasias, elevated plasma levels of NTproCNP indicate the presence of tissue resistance to CNP.
4. Long-term CNP therapy for achondroplasia and other skeletal disorders remains unknown.
5. The interaction between the CNP/NPR-B pathway and other pathways should be explored to elucidate the bone growth.

11. Conclusions

When organs were cultured, several mechanisms were found to be stimulated by CNP, including chondrocyte proliferation, cell hypertrophy, cartilage matrix production, and ECM activation. When the only CNP stimulation (cGMP) product was added to the culture, the same stimulation of longitudinal growth and glycosaminoglycan synthesis was observed. Nevertheless, cGMP only could not induce the proliferation of chondrocytes without an effect on cell hypertrophy. The second messenger for CNP (cGMP) could reproduce some of the CNP effects but not all, indicating that CNP activation is a more complex mechanism [158]. The signaling pathway of the CNP peptide has not been fully

understood. Thus, this review has discussed known mechanisms at present, as summarized in Figures 1 and 2.

Author Contributions: Conceptualization, E.R., S.T.; writing—original draft preparation, E.R.; writing—review and editing, E.R., G.W., T.F., S.T.; visualization, E.R.; supervision, G.W., S.T.; project administration, S.T.; funding acquisition, S.T. All authors have read and agreed to the published version of the manuscript.

Funding: This work was also supported by grants from Austrian MPS society, A Cure for Robert, Inc., The Carol Ann Foundation, Angelo R. Cali & Mary V. Cali Family Foundation, Inc., The Vain and Harry Fish Foundation, Inc., The Bennett Foundation, Jacob Randall Foundation, and Nemours Funds. S.T. was supported by an Institutional Development Award from the Eunice Kennedy Shriver National Institute of Child Health & Human Development of the National Institutes of Health (NICHD) (1R01HD102545-01A1).

Institutional Review Board Statement: There is no involvement of human subjects.

Informed Consent Statement: Not applicable.

Conflicts of Interest: The authors declare that they have no conflict of interest.

References

1. Long, F.; Ornitz, D.M. Development of the Endochondral Skeleton. *Cold Spring Harb. Perspect. Biol.* **2013**, *5*, a008334. [[CrossRef](#)] [[PubMed](#)]
2. Salhotra, A.; Shah, H.N.; Levi, B.; Longaker, M.T. Mechanisms of Bone Development and Repair. *Nat. Rev. Mol. Cell Biol.* **2020**, *21*, 696–711. [[CrossRef](#)] [[PubMed](#)]
3. Santhekadur, P.K.; Kumar, D.P.; Seneshaw, M.; Mirshahi, F.; Sanyal, A.J. The Multifaceted Role of Natriuretic Peptides in Metabolic Syndrome. *Biomed. Pharmacother.* **2017**, *92*, 826–835. [[CrossRef](#)] [[PubMed](#)]
4. Sonnenberg, H.; Chong, C.K.; Veress, A.T. Cardiac Atrial Factor—an Endogenous Diuretic? *Can. J. Physiol. Pharmacol.* **1981**, *59*, 1278–1279. [[CrossRef](#)]
5. Nakagawa, Y.; Nishikimi, T.; Kuwahara, K. Atrial and Brain Natriuretic Peptides: Hormones Secreted from the Heart. *Peptides* **2019**, *111*, 18–25. [[CrossRef](#)]
6. Collins, S. A Heart–Adipose Tissue Connection in the Regulation of Energy Metabolism. *Nat. Rev. Endocrinol.* **2014**, *10*, 157–163. [[CrossRef](#)]
7. Berglund, H.; Nyquist, O.; Beermann, B.; Jensen-Urstad, M.; Theodorsson, E. Influence of Angiotensin Converting Enzyme Inhibition on Relation of Atrial Natriuretic Peptide Concentration to Atrial Pressure in Heart Failure. *Heart* **1994**, *72*, 521–527. [[CrossRef](#)]
8. Kotby, A.A.; Taman, K.H.; Sedky, H.T.A.; Habeeb, N.M.; El-Hadidi, E.S.; Yosseif, H.S. Atrial Natriuretic Peptide as a Marker of Heart Failure in Children with Left Ventricular Volume Overload. *J. Paediatr. Child Health* **2013**, *49*, 43–47. [[CrossRef](#)]
9. Asakura, M.; Jiyoong, K.; Minamino, T.; Shintani, Y.; Asanuma, H.; Kitakaze, M.; The J-WIND Investigators. Rationale and Design of a Large-Scale Trial Using Atrial Natriuretic Peptide (ANP) as an Adjunct to Percutaneous Coronary Intervention for ST-Segment Elevation Acute Myocardial Infarction—Japan-Working Groups of Acute Myocardial Infarction for the Reduction of Necrotic Damage by ANP (J-WIND-ANP). *Circ. J.* **2004**, *68*, 95–100. [[CrossRef](#)]
10. Nishikimi, T.; Mori, Y.; Ishimura, K.; Tadokoro, K.; Yagi, H.; Yabe, A.; Horinaka, S.; Matsuoka, H. Association of Plasma Atrial Natriuretic Peptide, n-Terminal Proatrial Natriuretic Peptide, and Brain Natriuretic Peptide Levels with Coronary Artery Stenosis in Patients with Normal Left Ventricular Systolic Function. *Am. J. Med.* **2004**, *116*, 517–523. [[CrossRef](#)]
11. Hui, D.; Naberhuis, J.; Dibaj, S.; Naqvi, M.; Liu, D.; Bruera, E. Association Between Plasma Brain Natriuretic Peptide and Overall Survival in Patients With Advanced Cancer: Preliminary Findings. *J. Pain Symptom Manag.* **2019**, *58*, 465–471. [[CrossRef](#)] [[PubMed](#)]
12. Moore, K.B.; McKenna, K.; Osman, M.; Tormey, W.P.; McDonald, D.; Thompson, C.J. Atrial Natriuretic Peptide Increases Urinary Albumin Excretion in People with Normoalbuminuric Type-2 Diabetes. *Ir. J. Med. Sci.* **2007**, *176*, 67–73. [[CrossRef](#)] [[PubMed](#)]
13. Pedersen, E.B.; Bacevicius, E.; Bech, J.N.; Solling, K.; Pedersen, H.B. Abnormal Rhythmic Oscillations of Atrial Natriuretic Peptide and Brain Natriuretic Peptide in Chronic Renal Failure. *Clin. Sci.* **2006**, *110*, 491–501. [[CrossRef](#)] [[PubMed](#)]
14. Katan, M.; Fluri, F.; Schuetz, P.; Morgenthaler, N.G.; Zweifel, C.; Bingisser, R.; Kappos, L.; Steck, A.; Engelter, S.T.; Müller, B.; et al. Midregional Pro-Atrial Natriuretic Peptide and Outcome in Patients With Acute Ischemic Stroke. *J. Am. Coll. Cardiol.* **2010**, *56*, 1045–1053. [[CrossRef](#)]
15. Zois, N.E.; Terzic, D.; Færch, K.; Plomgaard, P.; Hansen, J.S.; Rossing, P.; Goetze, J.P. Effect of Pancreatic Hormones on Pro-Atrial Natriuretic Peptide in Humans. *EBioMedicine* **2017**, *17*, 88–94. [[CrossRef](#)]
16. Jujić, A.; Nilsson, P.M.; Persson, M.; Holst, J.J.; Torekov, S.S.; Lyssenko, V.; Groop, L.; Melander, O.; Magnusson, M. Atrial Natriuretic Peptide in the High Normal Range Is Associated With Lower Prevalence of Insulin Resistance. *J. Clin. Endocrinol. Metab.* **2016**, *101*, 1372–1380. [[CrossRef](#)]

17. Parcha, V.; Patel, N.; Gutierrez, O.M.; Li, P.; Gamble, K.L.; Musunuru, K.; Margulies, K.B.; Cappola, T.P.; Wang, T.J.; Arora, G.; et al. Chronobiology of Natriuretic Peptides and Blood Pressure in Lean and Obese Individuals. *J. Am. Coll. Cardiol.* **2021**, *77*, 2291–2303. [[CrossRef](#)]
18. Molina, C.R.; Fowler, M.B.; Mccrory, S.; Peterson, C.; Myers, B.D.; Schroeder, J.S.; Murad, F. Hemodynamic, Renal and Endocrine Effects of Atrial Natriuretic Peptide Infusion in Severe Heart Failure. *J. Am. Coll. Cardiol.* **1988**, *12*, 175–186. [[CrossRef](#)]
19. Tanaka, T.; Tsutamoto, T.; Sakai, H.; Nishiyama, K.; Fujii, M.; Yamamoto, T.; Horie, M. Effect of Atrial Natriuretic Peptide on Adiponectin in Patients with Heart Failure. *Eur. J. Heart Fail.* **2008**, *10*, 360–366. [[CrossRef](#)]
20. Valsson, F.; Lundin, S.; Kirno, K.; Hedner, T.; Houltz, E.; Saito, Y.; Ricksten, S.-E. Atrial Natriuretic Peptide Attenuates Pacing-Induced Myocardial Ischemia During General Anesthesia in Patients with Coronary Artery Disease. *Anesth. Analg.* **1999**, *88*, 279–285. [[CrossRef](#)]
21. Nojiri, T.; Yamamoto, K.; Maeda, H.; Takeuchi, Y.; Funakoshi, Y.; Inoue, M.; Okumura, M. Effect of Low-Dose Human Atrial Natriuretic Peptide on Postoperative Atrial Fibrillation in Patients Undergoing Pulmonary Resection for Lung Cancer: A Double-Blind, Placebo-Controlled Study. *J. Thorac. Cardiovasc. Surg.* **2012**, *143*, 488–494. [[CrossRef](#)] [[PubMed](#)]
22. Kitakaze, M.; Asakura, M.; Kim, J.; Shintani, Y.; Asanuma, H.; Hamasaki, T.; Seguchi, O.; Myoishi, M.; Minamino, T.; Ohara, T.; et al. Human Atrial Natriuretic Peptide and Nicorandil as Adjuncts to Reperfusion Treatment for Acute Myocardial Infarction (J-WIND): Two Randomised Trials. *Lancet* **2007**, *370*, 1483–1493. [[CrossRef](#)]
23. Sezai, A.; Wakui, S.; Akiyama, K.; Hata, M.; Yoshitake, I.; Unosawa, S.; Shiono, M.; Hirayama, A. Myocardial Protective Effect of Human Atrial Natriuretic Peptide in Cardiac Surgery—“HANP Shot” in Clinical Safety Trial. *Circ. J.* **2011**, *75*, 2144–2150. [[CrossRef](#)] [[PubMed](#)]
24. Nojiri, T.; Yamamoto, H.; Hamasaki, T.; Onda, K.; Ohshima, K.; Shintani, Y.; Okumura, M.; Kangawa, K. A Multicenter Randomized Controlled Trial of Surgery Alone or Surgery with Atrial Natriuretic Peptide in Lung Cancer Surgery: Study Protocol for a Randomized Controlled Trial. *Trials* **2017**, *18*, 183. [[CrossRef](#)]
25. Hayashida, N.; Chihara, S.; Kashikie, H.; Tayama, E.; Yokose, S.; Akasu, K.; Aoyagi, S. Effects of Intraoperative Administration of Atrial Natriuretic Peptide. *Ann. Thorac. Surg.* **2000**, *70*, 1319–1326. [[CrossRef](#)]
26. Park, K.; Itoh, H.; Yamahara, K.; Sone, M.; Miyashita, K.; Oyamada, N.; Sawada, N.; Taura, D.; Inuzuka, M.; Sonoyama, T.; et al. Therapeutic Potential of Atrial Natriuretic Peptide Administration on Peripheral Arterial Diseases. *Endocrinology* **2008**, *149*, 483–491. [[CrossRef](#)]
27. Groban, L.; Cowley, A.W.; Ebert, T.J. Atrial Natriuretic Peptide Augments Forearm Capillary Filtration in Humans. *Am. J. Physiol.-Heart Circ. Physiol.* **1990**, *259*, H258–H263. [[CrossRef](#)]
28. Kasama, S.; Toyama, T.; Hatori, T.; Sumino, H.; Kumakura, H.; Takayama, Y.; Ichikawa, S.; Suzuki, T.; Kurabayashi, M. Effects of Intravenous Atrial Natriuretic Peptide on Cardiac Sympathetic Nerve Activity and Left Ventricular Remodeling in Patients With First Anterior Acute Myocardial Infarction. *J. Am. Coll. Cardiol.* **2007**, *49*, 667–674. [[CrossRef](#)]
29. Moriyama, T.; Hagihara, S.; Shiramomo, T.; Nagaoka, M.; Iwakawa, S.; Kanmura, Y. The Protective Effect of Human Atrial Natriuretic Peptide on Renal Damage during Cardiac Surgery. *J. Anesth.* **2017**, *31*, 163–169. [[CrossRef](#)]
30. Mitaka, C.; Ohnuma, T.; Murayama, T.; Kunimoto, F.; Nagashima, M.; Takei, T.; Iguchi, N.; Tomita, M. Effects of Low-Dose Atrial Natriuretic Peptide Infusion on Cardiac Surgery–Associated Acute Kidney Injury: A Multicenter Randomized Controlled Trial. *J. Crit. Care* **2017**, *38*, 253–258. [[CrossRef](#)]
31. Rahman, S.N.; Kim, G.E.; Mathew, A.S.; Goldberg, C.A.; Allgren, R.; Schrier, R.W.; Conger, J.D. Effects of Atrial Natriuretic Peptide in Clinical Acute Renal Failure. *Kidney Int.* **1994**, *45*, 1731–1738. [[CrossRef](#)] [[PubMed](#)]
32. Swärd, K.; Valsson, F.; Odencrants, P.; Samuelsson, O.; Ricksten, S.-E. Recombinant Human Atrial Natriuretic Peptide in Ischemic Acute Renal Failure: A Randomized Placebo-Controlled Trial*. *Crit. Care Med.* **2004**, *32*, 1310–1315. [[CrossRef](#)] [[PubMed](#)]
33. Mitaka, C.; Kudo, T.; Jibiki, M.; Sugano, N.; Inoue, Y.; Makita, K.; Imai, T. Effects of Human Atrial Natriuretic Peptide on Renal Function in Patients Undergoing Abdominal Aortic Aneurysm Repair*. *Crit. Care Med.* **2008**, *36*, 745–751. [[CrossRef](#)]
34. Koda, M.; Sakamoto, A.; Ogawa, R. Effects of Atrial Natriuretic Peptide at a Low Dose on Water and Electrolyte Metabolism during General Anesthesia. *J. Clin. Anesth.* **2005**, *17*, 3–7. [[CrossRef](#)]
35. Swärd, K.; Valson, F.; Ricksten, S.-E. Long-Term Infusion of Atrial Natriuretic Peptide (ANP) Improves Renal Blood Flow and Glomerular Filtration Rate in Clinical Acute Renal Failure. *Acta Anaesthesiol. Scand.* **2001**, *45*, 536–542. [[CrossRef](#)] [[PubMed](#)]
36. Takahashi, H.; Takeda, T.; Nishizawa, Y.; Ogino, T.; Miyoshi, N.; Matsuda, C.; Yamamoto, H.; Mizushima, T.; Doki, Y.; Eguchi, H. Phase I Study of the Administration of Low-Dose Perioperative Human Atrial Natriuretic Peptide in Patients With Resectable Colorectal Cancer. *Anticancer Res.* **2020**, *40*, 5301–5307. [[CrossRef](#)]
37. van der Zander, K. Effects of Brain Natriuretic Peptide on Forearm Vasculature: Comparison with Atrial Natriuretic Peptide. *Cardiovasc. Res.* **1999**, *44*, 595–600. [[CrossRef](#)]
38. Mori, Y.; Kamada, T.; Ochiai, R. Reduction in the Incidence of Acute Kidney Injury after Aortic Arch Surgery with Low-Dose Atrial Natriuretic Peptide. *Eur. J. Anaesthesiol.* **2014**, *31*, 381–387. [[CrossRef](#)]
39. Moro, C.; Polak, J.; Hejnova, J.; Klimcakova, E.; Crampes, F.; Stich, V.; Lafontan, M.; Berlan, M. Atrial Natriuretic Peptide Stimulates Lipid Mobilization during Repeated Bouts of Endurance Exercise. *Am. J. Physiol.-Endocrinol. Metab.* **2006**, *290*, E864–E869. [[CrossRef](#)]
40. Cargill, R.I.; Lipworth, B.J. Pulmonary Vasorelaxant Activity of Atrial Natriuretic Peptide and Brain Natriuretic Peptide in Humans. *Thorax* **1995**, *50*, 183–185. [[CrossRef](#)]

41. Mukoyama, M.; Nakao, K.; Saito, Y.; Ogawa, Y.; Hosoda, K.; Suga, K.; Shirakami, G.; Jougasaki, M.; Imura, H. Increased Human Brain Natriuretic Peptide in Congestive Heart Failure. *N. Engl. J. Med.* **1990**, *323*, 757–758. [[CrossRef](#)] [[PubMed](#)]
42. Mukoyama, M.; Nakao, K.; Hosoda, K.; Suga, S.; Saito, Y.; Ogawa, Y.; Shirakami, G.; Jougasaki, M.; Obata, K.; Yasue, H. Brain Natriuretic Peptide as a Novel Cardiac Hormone in Humans. Evidence for an Exquisite Dual Natriuretic Peptide System, Atrial Natriuretic Peptide and Brain Natriuretic Peptide. *J. Clin. Investig.* **1991**, *87*, 1402–1412. [[CrossRef](#)] [[PubMed](#)]
43. Maisel, A.S.; Krishnaswamy, P.; Nowak, R.M.; McCord, J.; Hollander, J.E.; Duc, P.; Omland, T.; Storrow, A.B.; Abraham, W.T.; Wu, A.H.B.; et al. Rapid Measurement of B-Type Natriuretic Peptide in the Emergency Diagnosis of Heart Failure. *N. Engl. J. Med.* **2002**, *347*, 161–167. [[CrossRef](#)] [[PubMed](#)]
44. Maisel, A.; Barnard, D.; Jaski, B.; Frivold, G.; Marais, J.; Azer, M.; Miyamoto, M.I.; Lombardo, D.; Kelsay, D.; Borden, K.; et al. Primary Results of the HABIT Trial (Heart Failure Assessment With BNP in the Home). *J. Am. Coll. Cardiol.* **2013**, *61*, 1726–1735. [[CrossRef](#)]
45. Maisel, A.S.; Shah, K.S.; Barnard, D.; Jaski, B.; Frivold, G.; Marais, J.; Azer, M.; Miyamoto, M.I.; Lombardo, D.; Kelsay, D.; et al. How B-Type Natriuretic Peptide (BNP) and Body Weight Changes Vary in Heart Failure With Preserved Ejection Fraction Compared With Reduced Ejection Fraction: Secondary Results of the HABIT (HF Assessment With BNP in the Home) Trial. *J. Card. Fail.* **2016**, *22*, 283–293. [[CrossRef](#)]
46. Liu, Q.; Yang, J.; Bolun, Z.; Pei, M.; Ma, B.; Tong, Q.; Yin, H.; Zhang, Y.; You, L.; Xie, R. Comparison of Cardiac Function between Left Bundle Branch Pacing and Right Ventricular Outflow Tract Septal Pacing in the Short-Term: A Registered Controlled Clinical Trial. *Int. J. Cardiol.* **2021**, *322*, 70–76. [[CrossRef](#)]
47. Passino, C.; del Ry, S.; Severino, S.; Gabutti, A.; Prontera, C.; Clerico, A.; Giannessi, D.; Emdin, M. C-Type Natriuretic Peptide Expression in Patients with Chronic Heart Failure: Effects of Aerobic Training. *Eur. J. Cardiovasc. Prev. Rehabil.* **2008**, *15*, 168–172. [[CrossRef](#)]
48. Mann, D.L.; Greene, S.J.; Givertz, M.M.; Vader, J.M.; Starling, R.C.; Ambrosy, A.P.; Shah, P.; McNulty, S.E.; Mahr, C.; Gupta, D.; et al. Sacubitril/Valsartan in Advanced Heart Failure With Reduced Ejection Fraction. *JACC Heart Fail.* **2020**, *8*, 789–799. [[CrossRef](#)]
49. Zhang, W.; Wang, X.; Li, J.; Xu, M.; Ren, X.; Liu, H.; Xu, L.; Shao, J. Astragaloside IV Reduces OxLDL-Induced BNP Overexpression by Regulating HDAC. *J. Healthc. Eng.* **2021**, *2021*, 3433615. [[CrossRef](#)]
50. Morbach, C.; Buck, T.; Rost, C.; Peter, S.; Günther, S.; Störk, S.; Prettin, C.; Erbel, R.; Ertl, G.; Angermann, C.E. Point-of-Care B-Type Natriuretic Peptide and Portable Echocardiography for Assessment of Patients with Suspected Heart Failure in Primary Care: Rationale and Design of the Three-Part Handheld-BNP Program and Results of the Training Study. *Clin. Res. Cardiol.* **2018**, *107*, 95–107. [[CrossRef](#)]
51. Hu, J.; Wan, Q.; Zhang, Y.; Zhou, J.; Li, M.; Jiang, L.; Yuan, F. Efficacy and Safety of Early Ultrafiltration in Patients with Acute Decompensated Heart Failure with Volume Overload: A Prospective, Randomized, Controlled Clinical Trial. *BMC Cardiovasc. Disord.* **2020**, *20*, 447. [[CrossRef](#)] [[PubMed](#)]
52. Bristow, M.R.; Silva Enciso, J.; Gersh, B.J.; Grady, C.; Rice, M.M.; Singh, S.; Sopko, G.; Boineau, R.; Rosenberg, Y.; Greenberg, B.H. Detection and Management of Geographic Disparities in the TOPCAT Trial. *JACC Basic Transl. Sci.* **2016**, *1*, 180–189. [[CrossRef](#)] [[PubMed](#)]
53. Karlström, P.; Dahlström, U.; Boman, K.; Alehagen, U. Responder to BNP-Guided Treatment in Heart Failure. The Process of Defining a Responder. *Scand. Cardiovasc. J.* **2015**, *49*, 316–324. [[CrossRef](#)] [[PubMed](#)]
54. Mueller, C.; Scholer, A.; Laule-Kilian, K.; Martina, B.; Schindler, C.; Buser, P.; Pfisterer, M.; Perruchoud, A.P. Use of B-Type Natriuretic Peptide in the Evaluation and Management of Acute Dyspnea. *N. Engl. J. Med.* **2004**, *350*, 647–654. [[CrossRef](#)]
55. Motamed, H.; Forouzan, A.; Heybar, H.; Khorasani, M.J.; Hesam, S. Bronchodilatory Effects of B-Type Natriuretic Peptide in Acute Asthma Attacks: A Randomized Controlled Clinical Trial. *Adv. Respir. Med.* **2020**, *88*, 531–538. [[CrossRef](#)]
56. Ogawa, S.; Takeuchi, K.; Ito, S. Plasma BNP Levels in the Treatment of Type 2 Diabetes with Pioglitazone. *J. Clin. Endocrinol. Metab.* **2003**, *88*, 3993–3996. [[CrossRef](#)]
57. Stavrakis, S.; Pakala, A.; Thadani, U.; Thomas, J.; Chaudhry, M.A. Obesity, Brain Natriuretic Peptide Levels and Mortality in Patients Hospitalized With Heart Failure and Preserved Left Ventricular Systolic Function. *Am. J. Med. Sci.* **2013**, *345*, 211–217. [[CrossRef](#)]
58. Pitt, B.; Kober, L.; Ponikowski, P.; Gheorghide, M.; Filippatos, G.; Krum, H.; Nowack, C.; Kolkhof, P.; Kim, S.-Y.; Zannad, F. Safety and Tolerability of the Novel Non-Steroidal Mineralocorticoid Receptor Antagonist BAY 94-8862 in Patients with Chronic Heart Failure and Mild or Moderate Chronic Kidney Disease: A Randomized, Double-Blind Trial. *Eur. Heart J.* **2013**, *34*, 2453–2463. [[CrossRef](#)]
59. Koomen, J.; Stevens, J.; Bakris, G.; Correa-Rotter, R.; Hou, F.F.; Kitzman, D.W.; Kohan, D.; Makino, H.; McMurray, J.J.; Parving, H.; et al. Inter-individual Variability in Atrasentan Exposure Partly Explains Variability in Kidney Protection and Fluid Retention Responses: A Post Hoc Analysis of the SONAR Trial. *Diabetes Obes. Metab.* **2021**, *23*, 561–568. [[CrossRef](#)]
60. Qin, W.; Bai, W.; Liu, K.; Liu, Y.; Meng, X.; Zhang, K.; Zhang, M. Clinical Course and Risk Factors of Disease Deterioration in Critically Ill Patients with COVID-19. *Hum. Gene Ther.* **2021**, *32*, 310–315. [[CrossRef](#)]
61. Inohara, T.; Kim, S.; Pieper, K.; Blanco, R.G.; Allen, L.A.; Fonarow, G.C.; Gersh, B.J.; Ezekowitz, M.D.; Kowey, P.R.; Reiffel, J.A.; et al. B-Type Natriuretic Peptide, Disease Progression and Clinical Outcomes in Atrial Fibrillation. *Heart* **2018**, *105*, 370–377. [[CrossRef](#)] [[PubMed](#)]

62. Sugiyama, M.; Hazama, T.; Nakano, K.; Urae, K.; Moriyama, T.; Ariyoshi, T.; Kurokawa, Y.; Kodama, G.; Wada, Y.; Yano, J.; et al. Effects of Reducing L-Carnitine Supplementation on Carnitine Kinetics and Cardiac Function in Hemodialysis Patients: A Multicenter, Single-Blind, Placebo-Controlled, Randomized Clinical Trial. *Nutrients* **2021**, *13*, 1900. [[CrossRef](#)] [[PubMed](#)]
63. Seki, N.; Matsumoto, T.; Fukazawa, M. Relationship Between the Brain Natriuretic Peptide (BNP) Level and Prognosis of Diabetic Nephropathy with Microalbuminuria: A 7-Year Follow-Up Study. *Horm. Metab. Res.* **2018**, *50*, 389–396. [[CrossRef](#)] [[PubMed](#)]
64. Lok, D.J.; Klip, I.T.; Voors, A.A.; Lok, S.I.; Bruggink-André de la Porte, P.W.; Hillege, H.L.; Jaarsma, T.; van Veldhuisen, D.J.; van der Meer, P. Prognostic Value of N-Terminal pro C-Type Natriuretic Peptide in Heart Failure Patients with Preserved and Reduced Ejection Fraction. *Eur. J. Heart Fail.* **2014**, *16*, 958–966. [[CrossRef](#)]
65. Fudim, M.; Sayeed, S.; Xu, H.; Matsouaka, R.A.; Heidenreich, P.A.; Velazquez, E.J.; Yancy, C.W.; Fonarow, G.C.; Hernandez, A.F.; DeVore, A.D. Representativeness of the PIONEER-HF Clinical Trial Population in Patients Hospitalized With Heart Failure and Reduced Ejection Fraction. *Circ. Heart Fail.* **2020**, *13*, e006645. [[CrossRef](#)]
66. Mortensen, S.A.; Rosenfeldt, F.; Kumar, A.; Dolliner, P.; Filipiak, K.J.; Pella, D.; Alehagen, U.; Steurer, G.; Littarru, G.P. The Effect of Coenzyme Q 10 on Morbidity and Mortality in Chronic Heart Failure. *JACC Heart Fail.* **2014**, *2*, 641–649. [[CrossRef](#)]
67. Pellicori, P.; Ferreira, J.P.; Mariottoni, B.; Brunner-La Rocca, H.; Ahmed, F.Z.; Verdonschot, J.; Collier, T.; Cuthbert, J.J.; Petutschnigg, J.; Mujaj, B.; et al. Effects of Spironolactone on Serum Markers of Fibrosis in People at High Risk of Developing Heart Failure: Rationale, Design and Baseline Characteristics of a Proof-of-concept, Randomised, Precision-medicine, Prevention Trial. The Heart OMics in AGING (HOMAGE) Trial. *Eur. J. Heart Fail.* **2020**, *22*, 1711–1723. [[CrossRef](#)]
68. Pfisterer, M.; Buser, P.; Rickli, H.; Gutmann, M.; Erne, P.; Rickenbacher, P.; Vuillomenet, A.; Jeker, U.; Dubach, P.; Beer, H.; et al. BNP-Guided vs Symptom-Guided Heart Failure Therapy. *JAMA* **2009**, *301*, 383. [[CrossRef](#)]
69. Khan, A.; Johnson, D.K.; Carlson, S.; Hocum-Stone, L.; Kelly, R.F.; Gravely, A.A.; Mbai, M.; Green, D.L.; Santilli, S.; Garcia, S.; et al. NT-Pro BNP Predicts Myocardial Injury Post-Vascular Surgery and Is Reduced with CoQ10: A Randomized Double-Blind Trial. *Ann. Vasc. Surg.* **2020**, *64*, 292–302. [[CrossRef](#)]
70. Walford, G.A.; Ma, Y.; Christophi, C.A.; Goldberg, R.B.; Jarolim, P.; Horton, E.; Mather, K.J.; Barrett-Connor, E.; Davis, J.; Florez, J.C.; et al. Circulating Natriuretic Peptide Concentrations Reflect Changes in Insulin Sensitivity over Time in the Diabetes Prevention Program. *Diabetologia* **2014**, *57*, 935–939. [[CrossRef](#)]
71. Wolsk, E.; Claggett, B.; Pfeiffer, M.A.; Diaz, R.; Dickstein, K.; Gerstein, H.C.; Lawson, F.C.; Lewis, E.F.; Maggioni, A.P.; McMurray, J.J.; et al. Role of B-Type Natriuretic Peptide and N-Terminal Prohormone BNP as Predictors of Cardiovascular Morbidity and Mortality in Patients With a Recent Coronary Event and Type 2 Diabetes Mellitus. *J. Am. Heart Assoc.* **2017**, *6*, e004743. [[CrossRef](#)] [[PubMed](#)]
72. Buckley, L.F.; Canada, J.M.; del Buono, M.G.; Carbone, S.; Trankle, C.R.; Billingsley, H.; Kadariya, D.; Arena, R.; van Tassel, B.W.; Abbate, A. Low NT-ProBNP Levels in Overweight and Obese Patients Do Not Rule out a Diagnosis of Heart Failure with Preserved Ejection Fraction. *ESC Heart Fail.* **2018**, *5*, 372–378. [[CrossRef](#)] [[PubMed](#)]
73. Fontes-Carvalho, R.; Sampaio, F.; Teixeira, M.; Gama, V.; Leite-Moreira, A.F. The Role of a Structured Exercise Training Program on Cardiac Structure and Function after Acute Myocardial Infarction: Study Protocol for a Randomized Controlled Trial. *Trials* **2015**, *16*, 90. [[CrossRef](#)]
74. Hillock, R.J.; Frampton, C.M.; Yandle, T.G.; Troughton, R.W.; Lainchbury, J.G.; Richards, A.M. B-Type Natriuretic Peptide Infusions in Acute Myocardial Infarction. *Heart* **2008**, *94*, 617–622. [[CrossRef](#)] [[PubMed](#)]
75. Hubers, S.A.; Schirger, J.A.; Sangaralingham, S.J.; Chen, Y.; Burnett, J.C., Jr.; Hodge, D.; Chen, H.H. B-Type Natriuretic Peptide and Cardiac Remodelling after Myocardial Infarction: A Randomised Trial. *Heart* **2021**, *107*, 396–402. [[CrossRef](#)] [[PubMed](#)]
76. Kalra, P.R.; Clague, J.R.; Bolger, A.P.; Anker, S.D.; Poole-Wilson, P.A.; Struthers, A.D.; Coats, A.J. Myocardial Production of C-Type Natriuretic Peptide in Chronic Heart Failure. *Circulation* **2003**, *107*, 571–573. [[CrossRef](#)]
77. Yuan, X.; Zhiya, D.; Wenli, L.; Xiuming, W.; Wenxin, S.; Defen, W.; Jihong, N.; Fengsheng, C.; Junqi, W.; Wei, W. Measurement of Amino-Terminal Propeptide of C-Type Natriuretic Peptide in Patients with Idiopathic Short Stature or Isolated Growth Hormone Deficiency. *J. Pediatr. Endocrinol. Metab.* **2011**, *24*, 989–994. [[CrossRef](#)]
78. Kawakami, R.; Lee, C.Y.W.; Scott, C.; Bailey, K.R.; Schirger, J.A.; Chen, H.H.; Benike, S.L.; Cannone, V.; Martin, F.L.; Sangaralingham, S.J.; et al. A Human Study to Evaluate Safety, Tolerability, and Cyclic GMP Activating Properties of Cenderitide in Subjects With Stable Chronic Heart Failure. *Clin. Pharmacol. Ther.* **2018**, *104*, 546–552. [[CrossRef](#)]
79. Igaki, T.; Itoh, H.; Suga, S.; Hama, N.; Ogawa, Y.; Komatsu, Y.; Mukoyama, M.; Sugawara, A.; Yoshimasa, T.; Tanaka, I.; et al. C-Type Natriuretic Peptide in Chronic Renal Failure and Its Action in Humans. *Kidney Int. Suppl.* **1996**, *55*, S144–S147.
80. Barletta, G.; Lazzeri, C.; Vecchiarino, S.; del Bene, R.; Messeri, G.; dello Sbarba, A.; Mannelli, M.; la Villa, G. Low-Dose C-Type Natriuretic Peptide Does Not Affect Cardiac and Renal Function in Humans. *Hypertension* **1998**, *31*, 802–808. [[CrossRef](#)]
81. Savarirayan, R.; Irving, M.; Bacino, C.A.; Bostwick, B.; Charrow, J.; Cormier-Daire, V.; le Quan Sang, K.-H.; Dickson, P.; Harmatz, P.; Phillips, J.; et al. C-Type Natriuretic Peptide Analogue Therapy in Children with Achondroplasia. *N. Engl. J. Med.* **2019**, *381*, 25–35. [[CrossRef](#)] [[PubMed](#)]
82. Savarirayan, R.; Tofts, L.; Irving, M.; Wilcox, W.R.; Bacino, C.A.; Hoover-Fong, J.; Font, R.U.; Harmatz, P.; Rutsch, F.; Bober, M.B.; et al. Safe and Persistent Growth-Promoting Effects of Vosoritide in Children with Achondroplasia: 2-Year Results from an Open-Label, Phase 3 Extension Study. *Genet. Med.* **2021**, *23*, 2443–2447. [[CrossRef](#)] [[PubMed](#)]
83. Kellner, M.; Yassouridis, A.; Hua, Y.; Wendrich, M.; Jahn, H.; Wiedemann, K. Intravenous C-Type Natriuretic Peptide Augments Behavioral and Endocrine Effects of Cholecystokinin Tetrapeptide in Healthy Men. *J. Psychiatr. Res.* **2002**, *36*, 1–6. [[CrossRef](#)]

84. Potter, L.R.; Yoder, A.R.; Flora, D.R.; Antos, L.K.; Dickey, D.M. Natriuretic Peptides: Their Structures, Receptors, Physiologic Functions and Therapeutic Applications. In *cGMP: Generators, Effectors and Therapeutic Implications*; Springer: Berlin/Heidelberg, Germany, 2009; pp. 341–366.
85. Sudoh, T.; Minamino, N.; Kangawa, K.; Matsuo, H. C-Type Natriuretic Peptide (CNP): A New Member of Natriuretic Peptide Family Identified in Porcine Brain. *Biochem. Biophys. Res. Commun.* **1990**, *168*, 863–870. [[CrossRef](#)]
86. Moyes, A.J.; Hobbs, A.J. C-Type Natriuretic Peptide: A Multifaceted Paracrine Regulator in the Heart and Vasculature. *Int. J. Mol. Sci.* **2019**, *20*, 2281. [[CrossRef](#)]
87. Fujii, T.; Komatsu, Y.; Yasoda, A.; Kondo, E.; Yoshioka, T.; Nambu, T.; Kanamoto, N.; Miura, M.; Tamura, N.; Arai, H.; et al. Circulating C-Type Natriuretic Peptide (CNP) Rescues Chondrodysplastic CNP Knockout Mice from Their Impaired Skeletal Growth and Early Death. *Endocrinology* **2010**, *151*, 4381–4388. [[CrossRef](#)]
88. Nakao, K.; Osawa, K.; Yasoda, A.; Yamanaka, S.; Fujii, T.; Kondo, E.; Koyama, N.; Kanamoto, N.; Miura, M.; Kuwahara, K.; et al. The Local CNP/GC-B System in Growth Plate Is Responsible for Physiological Endochondral Bone Growth. *Sci. Rep.* **2015**, *5*, 10554. [[CrossRef](#)]
89. Breinholt, V.M.; Rasmussen, C.E.; Mygind, P.H.; Kjølgaard-Hansen, M.; Faltinger, F.; Bernhard, A.; Zettler, J.; Hersel, U. TransCon CNP, a Sustained-Release C-Type Natriuretic Peptide Prodrug, a Potentially Safe and Efficacious New Therapeutic Modality for the Treatment of Comorbidities Associated with Fibroblast Growth Factor Receptor 3–Related Skeletal Dysplasias. *J. Pharmacol. Exp. Ther.* **2019**, *370*, 459–471. [[CrossRef](#)]
90. Yamashita, T.; Fujii, T.; Yamauchi, I.; Ueda, Y.; Hirota, K.; Kanai, Y.; Yasoda, A.; Inagaki, N. C-Type Natriuretic Peptide Restores Growth Impairment Under Enzyme Replacement in Mice With Mucopolysaccharidosis VII. *Endocrinology* **2020**, *161*, bqaa008. [[CrossRef](#)]
91. Chen, W.X.; Liu, H.H.; Li, R.X.; Mammadov, G.; Wang, J.J.; Liu, F.F.; Samadli, S.; Wu, Y.F.; Zhang, D.D.; Luo, H.H.; et al. C-Type Natriuretic Peptide Stimulates Osteoblastic Proliferation and Collagen-X Expression but Suppresses Fibroblast Growth Factor-23 Expression in Vitro. *Pediatr. Rheumatol.* **2020**, *18*, 46. [[CrossRef](#)] [[PubMed](#)]
92. Yip, C.Y.Y.; Blaser, M.C.; Mirzaei, Z.; Zhong, X.; Simmons, C.A. Inhibition of Pathological Differentiation of Valvular Interstitial Cells by C-Type Natriuretic Peptide. *Arterioscler. Thromb. Vasc. Biol.* **2011**, *31*, 1881–1889. [[CrossRef](#)]
93. Holliday, L.S.; Dean, A.D.; Greenwald, J.E.; Gluck, S.L. C-Type Natriuretic Peptide Increases Bone Resorption in 1,25-Dihydroxyvitamin D₃-Stimulated Mouse Bone Marrow Cultures. *J. Biol. Chem.* **1995**, *270*, 18983–18989. [[CrossRef](#)] [[PubMed](#)]
94. Hagiwara, H.; Inoue, A.; Yamaguchi, A.; Yokose, S.; Furuya, M.; Tanaka, S.; Hirose, S. CGMP Produced in Response to ANP and CNP Regulates Proliferation and Differentiation of Osteoblastic Cells. *Am. J. Physiol.-Cell Physiol.* **1996**, *270*, C1311–C1318. [[CrossRef](#)] [[PubMed](#)]
95. Teixeira, C.C.; Agoston, H.; Beier, F. Nitric Oxide, C-Type Natriuretic Peptide and CGMP as Regulators of Endochondral Ossification. *Dev. Biol.* **2008**, *319*, 171–178. [[CrossRef](#)]
96. Armour, K.E.; Armour, K.J.; Gallagher, M.E.; Gödecke, A.; Helfrich, M.H.; Reid, D.M.; Ralston, S.H. Defective Bone Formation and Anabolic Response to Exogenous Estrogen in Mice with Targeted Disruption of Endothelial Nitric Oxide Synthase**This Study Was Supported by Grants from the Arthritis Research Campaign (UK) and the Medical Research Council (UK). *Endocrinology* **2001**, *142*, 760–766. [[CrossRef](#)] [[PubMed](#)]
97. Aguirre, J.; Buttery, L.; O’Shaughnessy, M.; Afzal, F.; Fernandez de Marticorena, I.; Hukkanen, M.; Huang, P.; MacIntyre, I.; Polak, J. Endothelial Nitric Oxide Synthase Gene-Deficient Mice Demonstrate Marked Retardation in Postnatal Bone Formation, Reduced Bone Volume, and Defects in Osteoblast Maturation and Activity. *Am. J. Pathol.* **2001**, *158*, 247–257. [[CrossRef](#)]
98. van’T Hof, R.J.; Ralston, S.H. Nitric Oxide and Bone. *Immunology* **2001**, *103*, 255–261. [[CrossRef](#)]
99. Mancini, L.; Moradi-Bidhendi, N.; Becherini, L.; Martinetti, V.; MacIntyre, I. The Biphasic Effects of Nitric Oxide in Primary Rat Osteoblasts Are CGMP Dependent. *Biochem. Biophys. Res. Commun.* **2000**, *274*, 477–481. [[CrossRef](#)]
100. Kierner, A.K.; Vollmar, A.M. Effects of Different Natriuretic Peptides on Nitric Oxide Synthesis in Macrophages¹. *Endocrinology* **1997**, *138*, 4282–4290. [[CrossRef](#)]
101. Hoshino, M.; Kaneko, K.; Miyamoto, Y.; Yoshimura, K.; Suzuki, D.; Akaike, T.; Sawa, T.; Ida, T.; Fujii, S.; Ihara, H.; et al. 8-Nitro-CGMP Promotes Bone Growth through Expansion of Growth Plate Cartilage. *Free Radic. Biol. Med.* **2017**, *110*, 63–71. [[CrossRef](#)] [[PubMed](#)]
102. Meyerhoff, M.E.; Howland, J.L. Methods in Nitric Oxide Research. *Biochem. Educ.* **1997**, *25*, 184–185. [[CrossRef](#)]
103. Kierner, A.K.; Angelika, M. Vollmar Induction of L-Arginine Transport Is Inhibited by Atrial Natriuretic Peptide: A Peptide Hormone as a Novel Regulator of Inducible Nitric-Oxide Synthase Substrate Availability. *Mol. Pharmacol.* **2001**, *60*, 421–426. [[PubMed](#)]
104. Peake, N.J.; Hobbs, A.J.; Pinguan-Murphy, B.; Salter, D.M.; Berenbaum, F.; Chowdhury, T.T. Role of C-Type Natriuretic Peptide Signalling in Maintaining Cartilage and Bone Function. *Osteoarthr. Cartil.* **2014**, *22*, 1800–1807. [[CrossRef](#)] [[PubMed](#)]
105. Potter, L.R.; Hunter, T. Activation of Protein Kinase C Stimulates the Dephosphorylation of Natriuretic Peptide Receptor-B at a Single Serine Residue. *J. Biol. Chem.* **2000**, *275*, 31099–31106. [[CrossRef](#)]
106. Abbey, S.E.; Potter, L.R. Lysophosphatidic Acid Inhibits C-Type Natriuretic Peptide Activation of Guanylyl Cyclase-B. *Endocrinology* **2003**, *144*, 240–246. [[CrossRef](#)]
107. Potter, L.R. Guanylyl Cyclase Structure, Function and Regulation. *Cell. Signal.* **2011**, *23*, 1921–1926. [[CrossRef](#)]

108. Schulz, S.; Singh, S.; Bellet, R.A.; Singh, G.; Tubb, D.J.; Chin, H.; Garbers, D.L. The Primary Structure of a Plasma Membrane Guanylate Cyclase Demonstrates Diversity within This New Receptor Family. *Cell* **1989**, *58*, 1155–1162. [[CrossRef](#)]
109. Antos, L.K.; Abbey-Hosch, S.E.; Flora, D.R.; Potter, L.R. ATP-Independent Activation of Natriuretic Peptide Receptors. *J. Biol. Chem.* **2005**, *280*, 26928–26932. [[CrossRef](#)]
110. Ornitz, D.M.; Itoh, N. Fibroblast Growth Factors. *Genome Biol.* **2001**, *2*, reviews3005.1. [[CrossRef](#)]
111. Wilke, T.A.; Gubbels, S.; Schwartz, J.; Richman, J.M. Expression of Fibroblast Growth Factor Receptors (FGFR1, FGFR2, FGFR3) in the Developing Head and Face. *Dev. Dyn.* **1997**, *210*, 41–52. [[CrossRef](#)]
112. Ornitz, D.M.; Legeai-Mallet, L. Achondroplasia: Development, Pathogenesis, and Therapy. *Dev. Dyn.* **2017**, *246*, 291–309. [[CrossRef](#)] [[PubMed](#)]
113. Kanai, M.; Göke, M.; Tsunekawa, S.; Podolsky, D.K. Signal Transduction Pathway of Human Fibroblast Growth Factor Receptor 3. *J. Biol. Chem.* **1997**, *272*, 6621–6628. [[CrossRef](#)]
114. Su, N.; Sun, Q.; Li, C.; Lu, X.; Qi, H.; Chen, S.; Yang, J.; Du, X.; Zhao, L.; He, Q.; et al. Gain-of-Function Mutation in FGFR3 in Mice Leads to Decreased Bone Mass by Affecting Both Osteoblastogenesis and Osteoclastogenesis. *Hum. Mol. Genet.* **2010**, *19*, 1199–1210. [[CrossRef](#)]
115. Ozasa, A.; Komatsu, Y.; Yasoda, A.; Miura, M.; Sakuma, Y.; Nakatsuru, Y.; Arai, H.; Itoh, N.; Nakao, K. Complementary Antagonistic Actions between C-Type Natriuretic Peptide and the MAPK Pathway through FGFR-3 in ATDC5 Cells. *Bone* **2005**, *36*, 1056–1064. [[CrossRef](#)] [[PubMed](#)]
116. Krejci, P.; Masri, B.; Fontaine, V.; Mekikian, P.B.; Weis, M.; Prats, H.; Wilcox, W.R. Interaction of Fibroblast Growth Factor and C-Natriuretic Peptide Signaling in Regulation of Chondrocyte Proliferation and Extracellular Matrix Homeostasis. *J. Cell Sci.* **2005**, *118*, 5089–5100. [[CrossRef](#)]
117. Liu, S.; Zhang, D.; Wu, Y.; Luo, H.; Jiang, G.; Xu, Y.; Wu, Y.; Xia, X.; Wei, W.; Hu, B.; et al. Fibroblast Growth Factor-23 May Serve as a Novel Biomarker for Renal Osteodystrophy Progression. *Int. J. Mol. Med.* **2018**, *43*, 535–546. [[CrossRef](#)]
118. Wu, Y.; Zhang, J.; Chen, F. The Effects of Elevated Fibroblast Growth Factor 23 on Mandibular Growth in Rats. *Arch. Oral Biol.* **2018**, *95*, 156–164. [[CrossRef](#)]
119. Zheng, Q.; Zhou, G.; Morello, R.; Chen, Y.; Garcia-Rojas, X.; Lee, B. Type X Collagen Gene Regulation by Runx2 Contributes Directly to Its Hypertrophic Chondrocyte-Specific Expression in Vivo. *J. Cell Biol.* **2003**, *162*, 833–842. [[CrossRef](#)]
120. Tsuji, T.; Kunieda, T. A Loss-of-Function Mutation in Natriuretic Peptide Receptor 2 (Npr2) Gene Is Responsible for Disproportionate Dwarfism in Cn/Cn Mouse. *J. Biol. Chem.* **2005**, *280*, 14288–14292. [[CrossRef](#)]
121. Pejchalova, K.; Krejci, P.; Wilcox, W.R. C-Natriuretic Peptide: An Important Regulator of Cartilage. *Mol. Genet. Metab.* **2007**, *92*, 210–215. [[CrossRef](#)] [[PubMed](#)]
122. Zeb, A.; Shinwari, N.; Shah, K.; Gilani, S.Z.T.; Khan, S.; Lee, K.W.; Raza, S.I.; Hussain, S.; Liaqat, K.; Ahmad, W.; et al. Molecular and in Silico Analyses Validates Pathogenicity of Homozygous Mutations in the NPR2 Gene Underlying Variable Phenotypes of Acromesomelic Dysplasia, Type Maroteaux. *Int. J. Biochem. Cell Biol.* **2018**, *102*, 76–86. [[CrossRef](#)]
123. Kenis, V.; Melchenko, E.; Mazunin, I.; Pekkinen, M.; Mäkitie, O. A New Family with Epiphyseal Chondrodysplasia Type Miura. *Am. J. Med. Genet. Part A* **2021**, *185*, 112–118. [[CrossRef](#)] [[PubMed](#)]
124. Yamamoto, K.; Kawai, M.; Yamazaki, M.; Tachikawa, K.; Kubota, T.; Ozono, K.; Michigami, T. CREB Activation in Hypertrophic Chondrocytes Is Involved in the Skeletal Overgrowth in Epiphyseal Chondrodysplasia Miura Type Caused by Activating Mutations of Natriuretic Peptide Receptor B. *Hum. Mol. Genet.* **2019**, *28*, 1183–1198. [[CrossRef](#)] [[PubMed](#)]
125. Mackie, E.J.; Ahmed, Y.A.; Tatarczuch, L.; Chen, K.-S.; Mirams, M. Endochondral Ossification: How Cartilage Is Converted into Bone in the Developing Skeleton. *Int. J. Biochem. Cell Biol.* **2008**, *40*, 46–62. [[CrossRef](#)]
126. Akiyama, H.; Chaboissier, M.-C.; Martin, J.F.; Schedl, A.; de Crombrughe, B. The Transcription Factor Sox9 Has Essential Roles in Successive Steps of the Chondrocyte Differentiation Pathway and Is Required for Expression of Sox5 and Sox6. *Genes Dev.* **2002**, *16*, 2813–2828. [[CrossRef](#)]
127. Yoshida, C.A.; Komori, T. Role of Runx Proteins in Chondrogenesis. *Crit. Rev. TM Eukaryot. Gene Expr.* **2005**, *15*, 243–254. [[CrossRef](#)]
128. Fu, M.; Wang, C.; Li, Z.; Sakamaki, T.; Pestell, R.G. Minireview: Cyclin D1: Normal and Abnormal Functions. *Endocrinology* **2004**, *145*, 5439–5447. [[CrossRef](#)]
129. Beier, F.; Ali, Z.; Mok, D.; Taylor, A.C.; Leask, T.; Albanese, C.; Pestell, R.G.; LuValle, P. TGF β and PTHrP Control Chondrocyte Proliferation by Activating Cyclin D1 Expression. *Mol. Biol. Cell* **2001**, *12*, 3852–3863. [[CrossRef](#)]
130. L'Hôte, C.G.M.; Knowles, M.A. Cell Responses to FGFR3 Signalling: Growth, Differentiation and Apoptosis. *Exp. Cell Res.* **2005**, *304*, 417–431. [[CrossRef](#)]
131. Ornitz, D.M.; Marie, P.J. Fibroblast Growth Factor Signaling in Skeletal Development and Disease. *Genes Dev.* **2015**, *29*, 1463–1486. [[CrossRef](#)] [[PubMed](#)]
132. Kuehl, A.; Pelisek, J.; Pongratz, J.; Eckstein, H.-H. C-Type Natriuretic Peptide and Its Receptors in Atherosclerotic Plaques of the Carotid Artery of Clinically Asymptomatic Patients. *Eur. J. Vasc. Endovasc. Surg.* **2012**, *43*, 649–654. [[CrossRef](#)] [[PubMed](#)]
133. Miyazawa, T.; Ogawa, Y.; Chusho, H.; Yasoda, A.; Tamura, N.; Komatsu, Y.; Pfeifer, A.; Hofmann, F.; Nakao, K. Cyclic GMP-Dependent Protein Kinase II Plays a Critical Role in C-Type Natriuretic Peptide-Mediated Endochondral Ossification. *Endocrinology* **2002**, *143*, 3604–3610. [[CrossRef](#)]

134. Kake, T.; Kitamura, H.; Adachi, Y.; Yoshioka, T.; Watanabe, T.; Matsushita, H.; Fujii, T.; Kondo, E.; Tachibe, T.; Kawase, Y.; et al. Chronically Elevated Plasma C-Type Natriuretic Peptide Level Stimulates Skeletal Growth in Transgenic Mice. *Am. J. Physiol.-Endocrinol. Metab.* **2009**, *297*, E1339–E1348. [[CrossRef](#)] [[PubMed](#)]
135. Moffatt, P.; Thomas, G.; Sellin, K.; Bessette, M.-C.; Lafrenière, F.; Akhouayri, O.; St-Arnaud, R.; Lanctôt, C. Osteocrin Is a Specific Ligand of the Natriuretic Peptide Clearance Receptor That Modulates Bone Growth. *J. Biol. Chem.* **2007**, *282*, 36454–36462. [[CrossRef](#)]
136. Agoston, H.; Khan, S.; James, C.G.; Gillespie, J.R.; Serra, R.; Stanton, L.-A.; Beier, F. C-Type Natriuretic Peptide Regulates Endochondral Bone Growth through P38 MAP Kinase-Dependent and—Independent Pathways. *BMC Dev. Biol.* **2007**, *7*, 18. [[CrossRef](#)]
137. Woods, A.; Khan, S.; Beier, F. C-Type Natriuretic Peptide Regulates Cellular Condensation and Glycosaminoglycan Synthesis during Chondrogenesis. *Endocrinology* **2007**, *148*, 5030–5041. [[CrossRef](#)]
138. Inoue, A.; Hayakawa, T.; Otsuka, E.; Kamiya, A.; Suzuki, Y.; Hirose, S.; Hagiwara, H. Correlation between Induction of Expression of Biglycan and Mineralization by C-Type Natriuretic Peptide in Osteoblastic Cells. *J. Biochem.* **1999**, *125*, 103–108. [[CrossRef](#)]
139. Yeh, L.-C.C.; Adamo, M.L.; Olson, M.S.; Lee, J.C. Osteogenic Protein-1 and Insulin-Like Growth Factor I Synergistically Stimulate Rat Osteoblastic Cell Differentiation and Proliferation¹. *Endocrinology* **1997**, *138*, 4181–4190. [[CrossRef](#)]
140. Chen, D.; Zhao, M.; Mundy, G.R. Bone Morphogenetic Proteins. *Growth Factors* **2004**, *22*, 233–241. [[CrossRef](#)]
141. Yeh, L.-C.C.; Zavala, M.C.; Lee, J.C. C-Type Natriuretic Peptide Enhances Osteogenic Protein-1-Induced Osteoblastic Cell Differentiation via Smad5 Phosphorylation. *J. Cell. Biochem.* **2006**, *97*, 494–500. [[CrossRef](#)] [[PubMed](#)]
142. Chusho, H.; Tamura, N.; Ogawa, Y.; Yasoda, A.; Suda, M.; Miyazawa, T.; Nakamura, K.; Nakao, K.; Kurihara, T.; Komatsu, Y.; et al. Dwarfism and Early Death in Mice Lacking C-Type Natriuretic Peptide. *Proc. Natl. Acad. Sci. USA* **2001**, *98*, 4016–4021. [[CrossRef](#)] [[PubMed](#)]
143. Fujii, T.; Hirota, K.; Yasoda, A.; Takizawa, A.; Morozumi, N.; Nakamura, R.; Yotsumoto, T.; Kondo, E.; Yamashita, Y.; Sakane, Y.; et al. Rats Deficient C-Type Natriuretic Peptide Suffer from Impaired Skeletal Growth without Early Death. *PLoS ONE* **2018**, *13*, e0194812. [[CrossRef](#)] [[PubMed](#)]
144. Trotter, T.L.; Hall, J.G. Health Supervision for Children With Achondroplasia. *Pediatrics* **2005**, *116*, 771–783. [[CrossRef](#)] [[PubMed](#)]
145. Yasoda, A.; Komatsu, Y.; Chusho, H.; Miyazawa, T.; Ozasa, A.; Miura, M.; Kurihara, T.; Rogi, T.; Tanaka, S.; Suda, M.; et al. Overexpression of CNP in Chondrocytes Rescues Achondroplasia through a MAPK-Dependent Pathway. *Nat. Med.* **2004**, *10*, 80–86. [[CrossRef](#)]
146. Yamanaka, S.; Nakao, K.; Koyama, N.; Isobe, Y.; Ueda, Y.; Kanai, Y.; Kondo, E.; Fujii, T.; Miura, M.; Yasoda, A.; et al. Circulatory CNP Rescues Craniofacial Hypoplasia in Achondroplasia. *J. Dent. Res.* **2017**, *96*, 1526–1534. [[CrossRef](#)]
147. Ueda, Y.; Yasoda, A.; Hirota, K.; Yamauchi, I.; Yamashita, T.; Kanai, Y.; Sakane, Y.; Fujii, T.; Inagaki, N. Exogenous C-Type Natriuretic Peptide Therapy for Impaired Skeletal Growth in a Murine Model of Glucocorticoid Treatment. *Sci. Rep.* **2019**, *9*, 8547. [[CrossRef](#)]
148. Jackson, D.J.; Bacharier, L.B.; Mauger, D.T.; Boehmer, S.; Beigelman, A.; Chmiel, J.F.; Fitzpatrick, A.M.; Gaffin, J.M.; Morgan, W.J.; Peters, S.P.; et al. Quintupling Inhaled Glucocorticoids to Prevent Childhood Asthma Exacerbations. *N. Engl. J. Med.* **2018**, *378*, 891–901. [[CrossRef](#)]
149. Rivkees, S.A.; Danon, M.; Herrin, J. Prednisone Dose Limitation of Growth Hormone Treatment of Steroid-Induced Growth Failure. *J. Pediatr.* **1994**, *125*, 322–325. [[CrossRef](#)]
150. Hirota, K.; Furuya, M.; Morozumi, N.; Yoshikiyo, K.; Yotsumoto, T.; Jindo, T.; Nakamura, R.; Murakami, K.; Ueda, Y.; Hanada, T.; et al. Exogenous C-Type Natriuretic Peptide Restores Normal Growth and Prevents Early Growth Plate Closure in Its Deficient Rats. *PLoS ONE* **2018**, *13*, e0204172. [[CrossRef](#)]
151. Ueda, Y.; Hirota, K.; Yamauchi, I.; Hakata, T.; Yamashita, T.; Fujii, T.; Yasoda, A.; Inagaki, N. Is C-Type Natriuretic Peptide Regulated by a Feedback Loop? A Study on Systemic and Local Autoregulatory Effect. *PLoS ONE* **2020**, *15*, e0240023. [[CrossRef](#)] [[PubMed](#)]
152. Prickett, T.C.; & Espiner, E.A. Circulating products of C-type natriuretic peptide and links with organ function in health and disease. *Peptides* **2020**, *132*, 170363. [[CrossRef](#)] [[PubMed](#)]
153. Espiner, E.; Prickett, T.; Olney, R. Plasma C-Type Natriuretic Peptide: Emerging Applications in Disorders of Skeletal Growth. *Horm. Res. Paediatr.* **2018**, *90*, 345–357. [[CrossRef](#)]
154. Olney, R.C.; Permuy, J.W.; Prickett, T.C.; Han, J.C.; Espiner, E.A. Amino-terminal propeptide of C-type natriuretic peptide (NTproCNP) predicts height velocity in healthy children. *Clin. Endocrinol.* **2012**, *77*, 416–422. [[CrossRef](#)] [[PubMed](#)]
155. Miura, K.; Namba, N.; Fujiwara, M.; Ohata, Y.; Ishida, H.; Kitaoka, T.; Kubota, T.; Hirai, H.; Higuchi, C.; Tsumaki, N.; et al. An overgrowth disorder associated with excessive production of cGMP due to a gain-of-function mutation of the natriuretic peptide receptor 2 gene. *PLoS ONE* **2012**, *7*, e42180. [[CrossRef](#)] [[PubMed](#)]
156. Hannema, S.E.; van Duyvenvoorde, H.A.; Premisler, T.; Yang, R.B.; Mueller, T.D.; Gassner, B.; Oberwinkler, H.; Roelfsema, F.; Santen, G.W.; Prickett, T.; et al. An activating mutation in the kinase homology domain of the natriuretic peptide receptor-2 causes extremely tall stature without skeletal deformities. *J. Clin. Endocrinol. Metab.* **2013**, *98*, E1988–98. [[CrossRef](#)] [[PubMed](#)]

157. Hutchison, M.R. BDNF Alters ERK/p38 MAPK Activity Ratios to Promote Differentiation in Growth Plate Chondrocytes. *Mol. Endocrinol.* **2012**, *26*, 1406–1416. [[CrossRef](#)]
158. Mericq, V.; Uyeda, J.A.; Barnes, K.M.; de Luca, F.; Baron, J. Regulation of Fetal Rat Bone Growth by C-Type Natriuretic Peptide and CGMP. *Pediatr. Res.* **2000**, *47*, 189. [[CrossRef](#)]

Authors Contribution

Author Contributions

I hereby declare that my contribution in the review article:

Rintz, E., Węgrzyn, G., Fujii, T., Tomatsu, S. (2022) Molecular Mechanism of Induction of Bone Growth by the C-Type Natriuretic Peptide. *International Journal of Molecular Sciences*. 23(11):5916.

included:

- Conceptualization of the review article
- Literature review
- Figure preparation and conceptualization
- Visualization of the review article
- Writing—original draft preparation
- Writing—review and editing
- Preparation of the responses to the revision



Uniwersytet Gdański
Katedra Biologii Molekularnej

mgr Estera Rintz

Prof. dr hab. Grzegorz Węgrzyn
Katedra Biologii Molekularnej
Wydział Biologii
Uniwersytet Gdański

Gdańsk, 29.05.2024

Oświadczenie o wkładzie w publikację

Oświadczam, że mój wkład w publikację:

Rintz, E., Węgrzyn, G., Fujii, T., Tomatsu, S. (2022) Molecular mechanism of induction of bone growth by the C-type natriuretic peptide. *Int. J. Mol. Sci.* 23: 5916.

polegał na opiece naukowej nad Panią Esterą Rintz oraz udziale w przygotowaniu ostatecznej wersji manuskryptu.

KIEROWNIK
KATEDRY BIOLOGII MOLEKULARNEJ

prof. dr hab. Grzegorz Węgrzyn
prof. dr hab. Grzegorz Węgrzyn

Toshihito Fujii
Kyoto University Hospital
Kyoto city
Japan

April 28, 2024

Author Contributions

I hereby declare that my contribution in the review article:

Rintz, E., Węgrzyn, G., Fujii, T., Tomatsu, S. (2022) Molecular Mechanism of Induction of Bone Growth by the C-Type Natriuretic Peptide. *International Journal of Molecular Sciences*. 23(11):5916.

included:

- Comments to original draft of the manuscript
- Writing—review and editing

Signature

Toshihito Fujii

Name, Surname: Shunji Tomatsu, MD PhD
Institution name: Nemours Children's Health
City: Wilmington, DE
Country: USA

Wilmington, May.13.2024

Author Contributions

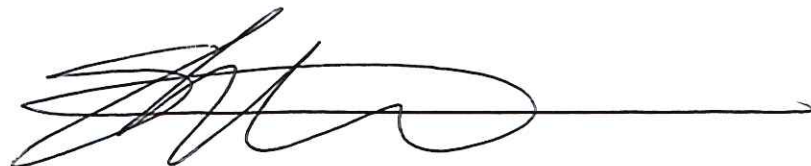
I hereby declare that my contribution in the review article:

Rintz, E., Węgrzyn, G., Fujii, T., Tomatsu, S. (2022) Molecular Mechanism of Induction of Bone Growth by the C-Type Natriuretic Peptide. *International Journal of Molecular Sciences*. 23(11):5916.

included:

- Conceptualization of the review article
- Funding acquisition
- Writing—review and editing
- Supervision and administration of the project
- Submission of the final version of the manuscript
- Handling manuscript as corresponding author
- Preparation of the responses to the revision

Signature: Shunji Tomatsu MD PhD

A handwritten signature in black ink, consisting of several overlapping loops and a long horizontal stroke extending to the right.

Rintz, E., Herreño-Pachón, A.M., Celik, B., Nidhi, F., Khan, S.,
Benincore-Flórez, E., Tomatsu, S. (2023)
Bone Growth Induction in Mucopolysaccharidosis IVA Mouse.
International Journal of Molecular Sciences. 24(12):9890.

Impact Factor = 5.6 (2023)

MNISW Punctuation = 140



Article

Bone Growth Induction in Mucopolysaccharidosis IVA Mouse

Ester Rintz ^{1,2} , Angélica María Herreño-Pachón ^{1,3}, Betül Celik ^{1,3} , Fnu Nidhi ^{1,3}, Shaukat Khan ^{1,4}, Eliana Benincore-Flórez ¹ and Shunji Tomatsu ^{1,3,4,*}

¹ Nemours Children's Health, Wilmington, DE 19803, USA; estera.rintz@ug.edu.pl (E.R.); angelicamaria.herrenopachon1@nemours.org (A.M.H.-P.); betul.celik@nemours.org (B.C.); fnu.nidhi@nemours.org (F.N.); shaukat.khan@nemours.org (S.K.); elianapatria.benincoreflores@nemours.org (E.B.-F.)

² Department of Molecular Biology, Faculty of Biology, University of Gdansk, 80-308 Gdansk, Poland

³ Faculty of Arts and Sciences, University of Delaware, Newark, DE 19716, USA

⁴ Department of Pediatrics, Thomas Jefferson University, Philadelphia, PA 19144, USA

* Correspondence: shunji.tomatsu@nemours.org

Abstract: Mucopolysaccharidosis IVA (MPS IVA; Morquio A syndrome) is caused by a deficiency of the N-acetylgalactosamine-6-sulfate-sulfatase (GALNS) enzyme, leading to the accumulation of glycosaminoglycans (GAG), keratan sulfate (KS) and chondroitin-6-sulfate (C6S), mainly in cartilage and bone. This lysosomal storage disorder (LSD) is characterized by severe systemic skeletal dysplasia. To this date, none of the treatment options for the MPS IVA patients correct bone pathology. Enzyme replacement therapy with elosulfase alpha provides a limited impact on bone growth and skeletal lesions in MPS IVA patients. To improve bone pathology, we propose a novel gene therapy with a small peptide as a growth-promoting agent for MPS IVA. A small molecule in this peptide family has been found to exert biological actions over the cardiovascular system. This work shows that an AAV vector expressing a C-type natriuretic (CNP) peptide induces bone growth in the MPS IVA mouse model. Histopathological analysis showed the induction of chondrocyte proliferation. CNP peptide also changed the pattern of GAG levels in bone and liver. These results suggest the potential for CNP peptide to be used as a treatment in MPS IVA patients.

Keywords: C-type natriuretic peptide; Morquio A syndrome; ossification; AAV gene therapy



Citation: Rintz, E.; Herreño-Pachón, A.M.; Celik, B.; Nidhi, F.; Khan, S.; Benincore-Flórez, E.; Tomatsu, S.

Bone Growth Induction in Mucopolysaccharidosis IVA Mouse.

Int. J. Mol. Sci. **2023**, *24*, 9890.

<https://doi.org/10.3390/ijms24129890>

ijms24129890

Academic Editor: Giacomina Brunetti

Received: 17 April 2023

Revised: 17 May 2023

Accepted: 5 June 2023

Published: 8 June 2023



Copyright: © 2023 by the authors. Licensee MDPI, Basel, Switzerland. This article is an open access article distributed under the terms and conditions of the Creative Commons Attribution (CC BY) license (<https://creativecommons.org/licenses/by/4.0/>).

1. Introduction

Genetic skeletal dysplasia conditions account for 5% of all birth defects, and only some of those diseases have bone-targeted treatment [1]. Morquio A syndrome (mucopolysaccharidosis type IV A; MPS IVA) is one of the skeletal dysplasia caused by the accumulation of glycosaminoglycans (GAGs), keratan sulfate (KS) and chondroitin-6-sulfate (C6S). These GAGs accumulated in the growth plate of patients' bones play a critical role in growth impairment [2,3]. MPS IVA is an inherited autosomal recessive disorder caused by a deficiency of the N-acetylgalactosamine-6-sulfate-sulfatase (GALNS) enzyme (responsible for the degradation of KS and C6S). Symptoms of the disease include systemic skeletal dysplasia, marked short stature, hypoplasia of the odontoid process, tracheal obstruction, pectus carinatum (restrictive lung), kyphoscoliosis, genu valgum, and laxity of joints. Most patients eventually are wheelchair bounded from their teenage years and do not survive the third decade of life [4,5]. Effects of severe dysplasia on the quality of life include respiratory failure, instability of the cervical region causing spinal injury [4,6], and high risk of anesthetic procedures due to the narrowed airway [7]. Patients undergo several surgical interventions throughout their life due to ongoing skeletal dysplasia [8].

One of the current treatments resolves bone dysplasia in MPS IVA patients. Available therapies for the patients include enzyme replacement therapy (ERT) and hematopoietic stem cell transplantation (HSCT), in companion with supportive treatment and surgical

interventions. ERT approach has several limitations as a treatment for MPS IVA: (1) no impact on bone lesions due to its avascular cartilage region, thus not correcting bone lesions in patients [9], (2) an expensive treatment (costs around \$578,000 per year for 25 kg patient) [10], (3) time-consuming treatment (weekly infusions for 4–6 h) [9,11], (4) no improvement of bone growth even if the treatment was started within two months old [9,12], and (5) production of antibodies against the enzyme that leads to immune response [13,14]. Moreover, the administration of ERT to the MPS IVA mouse model also did not improve bone pathology, even though it was tested in newborn mice [15]. HSCT as a treatment may be more effective for MPS IVA patients (benefits on heart, bone mineral density, and joint laxity [16]) but still have limitations; (1) risk of mortality and morbidity (risk of graft versus host disease) (2) difficulty in obtaining a donor for every patient, (3) complications after transplantation (4) limited impact to bone growth [10,16,17]. Both ERT and HSCT therapies are based on the cross-correction mechanism of enzyme secretion into the bloodstream. The mechanism of this phenomenon is based on the ability of lysosomal enzyme-expressing cells to correct other enzyme-deficient cells through the mannose-6-phosphate receptor pathway [18]. Although the enzyme is secreted and distributed throughout the body with the vascular system, penetrating the bone cartilage remains an unmet challenge [17]. There is a high demand for the bone-penetrating agent to treat avascular bone lesions in MPS IVA patients and induce bone ossification. A small molecule, C-type natriuretic peptide (CNP), induced bone growth in animal and human disease models. The CNP peptide activates bone growth through the natriuretic peptide receptor B (NPR-B) on both proliferative and pre-hypertrophic chondrocytes [19]. Stimulation of the intracellular molecule cGMP production by CNP activates multiple pathways, resulting in bone growth (in detail in [20]). Studies suggested that CNP has therapeutic potential for skeletal dysplasia, such as achondroplasia, a genetic disorder characterized by short stature and abnormal bone development [21]. However, the short half-life of natural CNP and the need for repeated injections of modified CNP currently limit the efficacy and convenience of CNP-based therapies [22]. As a result, ongoing research is focused on developing new CNP-based therapies with longer half-lives and improved efficacy. TransCon CNP has a longer half-life and requires only weekly injections, but repeated injections are still necessary to keep the treatment effective [23]. Therefore, there is a need to develop more effective and convenient treatments for skeletal dysplasia that can provide sustained therapeutic benefits without repeated injections.

To address this issue, we propose a therapeutic approach for progressive skeletal dysplasia in the MPS IVA mouse model. The use of CNP peptide as a potential treatment for MPS IVA has not been previously tested for this condition. Our proposed therapy utilizes an AAV vector as a one-time treatment to express CNP peptides. This novel approach is advantageous because it eliminates the need for frequent administration. A single treatment with CNP delivered through a viral vector expression cassette could be a promising therapeutic approach for treating progressive skeletal dysplasia in MPS IVA patients.

2. Results

2.1. Growth Induction in MPS IVA Mice after CNP Peptide Gene Therapy

To establish the effects of CNP peptide gene therapy on the MPS IVA mouse model, we injected intravenously AAV8 vector expressing human NPPC gene peptide under housekeeping promoter CAG into 4-week-old mice (dose 3.5×10^{13} GC/kg) (Figure 1). MPS IVA mice did not have GALNS enzyme activity in both plasma and tissues (Figure S1).

Mice were measured weekly for weight and length (nose to tail and nose to anus). Additionally, we took pictures on the autopsy day to compare the mice (Figure 2a). The body weights of MPS IVA and WT mice were significantly different only in week 4 (Figure 2b). In the AAV8-NPPC group, the weight significantly differed over 10 weeks starting at week 7 (Figure 2b). During the experiment, mice grew in both length parameters from week 5

(Figure 2b,c). A significant difference was observed between treated (AAV8-NPPC) and untreated MPS IVA or WT mice.

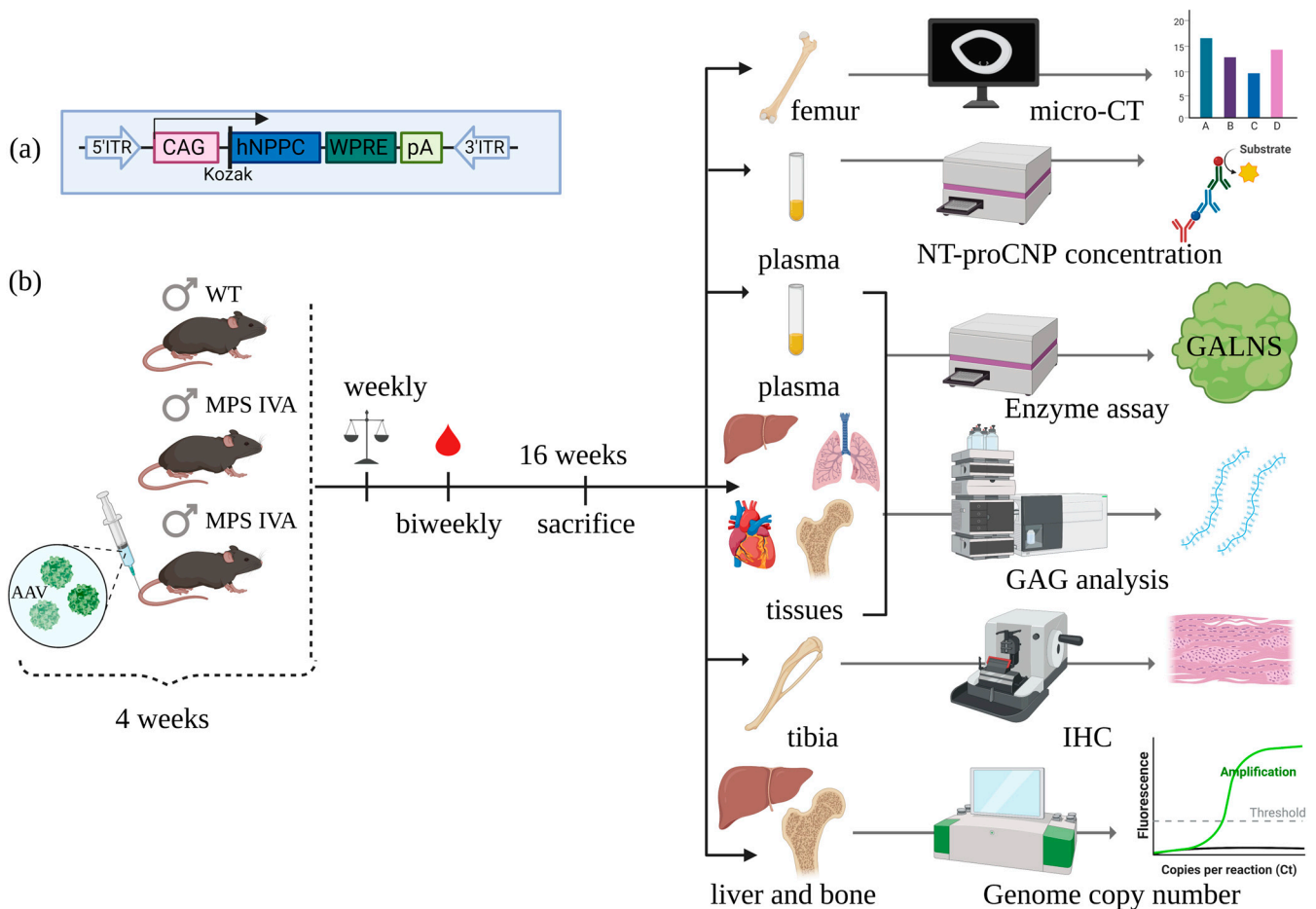


Figure 1. Experimental design. (a) A viral vector expressing cassette. (b) Experiments started at four weeks old. We have three experimental groups: untreated MPS IVA, wild-type control (WT), and treated MPS IVA with the AAV8 vector expressing CNP peptide (AAV8-NPPC). During the experiments, mice were measured weekly for body weight, nose-tail length, and nose-anus length, with biweekly blood collection. Mice were euthanized at the age of 16 weeks. After that, the analysis was made. This figure was prepared using [BioRender.com](https://www.biorender.com).

Additionally, in the final week of the experiment, we performed gait analysis in the MPS IVA mouse model to see the progression of the disease [24–26]. We did not observe changes in gait patterns even though CNP-treated mice had higher bony lengths (Figure S2).

2.2. Induction of Chondrocyte Proliferation by the Delivery of AAV8-NPPC Vector

Knee joint lesions were analyzed by toluidine blue staining 12 weeks after injection of the AAV8-NPPC vector into MPS IVA mice. Untreated MPS IVA mice showed GAG storage vacuoles in the growth plate of the tibia (Figure 3c), articular disc, and meniscus (Figure 3b) region. The growth plate region was also disorganized with vacuolated chondrocytes (Figure 3a,c). After treatment of MPS IVA mice with the AAV8-NPPC vector, the number of chondrocytes increased (Figure 3i) together with a more organized structure (Figure 3i). As previously described [2], we measured the volume of cells to assess the vacuolization of chondrocytes in the tibia growth plate region. The size of the chondrocytes decreased after the treatment of the CNP peptide (Figure 3j). Furthermore, we evaluated the improvement of vacuoles and disorganized column structures in knee joints of MPS IVA mice using pathological scores, which showed a tendency of improvement in MPS IVA mice treated

with the AAV vector compared to untreated mice. The pathological score of MPS IVA mice treated with AAV8-NPPC was significantly lower for vacuolization of chondrocytes in the articular cartilage area compared to those treated with MPSIVA, but not as low as the WT level (as shown in Table 1). Regarding other parameters, we observed a decrease, but it was not statistically significant.

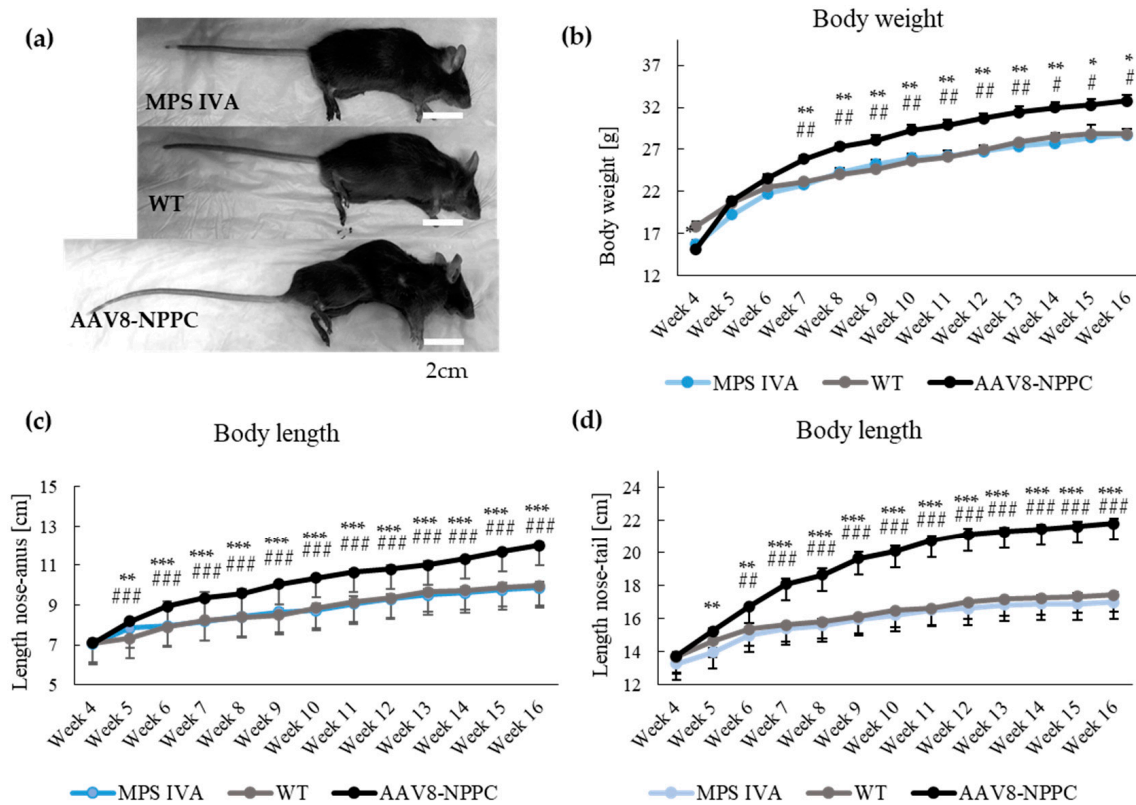


Figure 2. Establishment of CNP peptide growth induction in MPS IVA mouse model. (a) Picture of mice at week 16. (b) Body weight of mice during the experiment. (c) Body length measurement from nose to anus of mice during the experiment. (d) Body length measurement from nose to tail of mice during the experiment. Results are shown as mean values \pm SEM ($n = 5$). The following statistical symbols were used to denote as follows. AAV8-CNP group vs. WT group, *** $p \leq 0.001$, ** $p \leq 0.01$, * $p \leq 0.05$; AAV8-CNP group vs. untreated MPS IVA group, ### $p \leq 0.001$, ## $p \leq 0.01$, # $p \leq 0.05$.

Table 1. Pathological scores in bones of mucopolysaccharidosis type IVA (MPS IVA) mice treated with AAV8-NPPC vector.

Bone	Structure	Finding	MPS IVA	WT	AAV8-NPPC
Tibia	Growth plate	Vacuolization	2.9 \pm 0.1	0.0	2.8 \pm 0.2
		Column structure	2.8 \pm 0.2	0.0	2.3 \pm 0.3
	Articular cartilage	Vacuolization	2.9 \pm 0.1	0.0	2.6 \pm 0.1 #
Femur	Growth plate	Column structure	2.8 \pm 0.2	0.0	2.6 \pm 0.1
		Vacuolization	2.8 \pm 0.2	0.0	2.6 \pm 0.2
	Articular cartilage	Column structure	2.8 \pm 0.2	0.0	2.6 \pm 0.2
		Vacuolization	2.9 \pm 0.1	0.0	2.9 \pm 0.2
	Ligament	Column structure	2.9 \pm 0.1	0.0	2.7 \pm 0.4
	Meniscus	Vacuolization	3.0 \pm 0.0	0.0	2.4 \pm 0.3
		Vacuolization	2.9 \pm 0.1	0.0	2.6 \pm 0.2

Twelve weeks post-injection of the AAV8 vector, pathological scores were evaluated in femurs, tibias, ligaments, and meniscus from MPS IVA mice. Levels of storage materials and degrees of disoriented columns were scored. “No storage or very slight” was 0 (–), “slight but obvious” was 1 (+), “moderate” was 2 (++), and “marked” was 3 (+++). Each pathological slide was assessed in a double-blind manner three times. $n = 4$ –8. Data are presented as means \pm SDs. # $p < 0.05$ versus untreated MPS IVA.

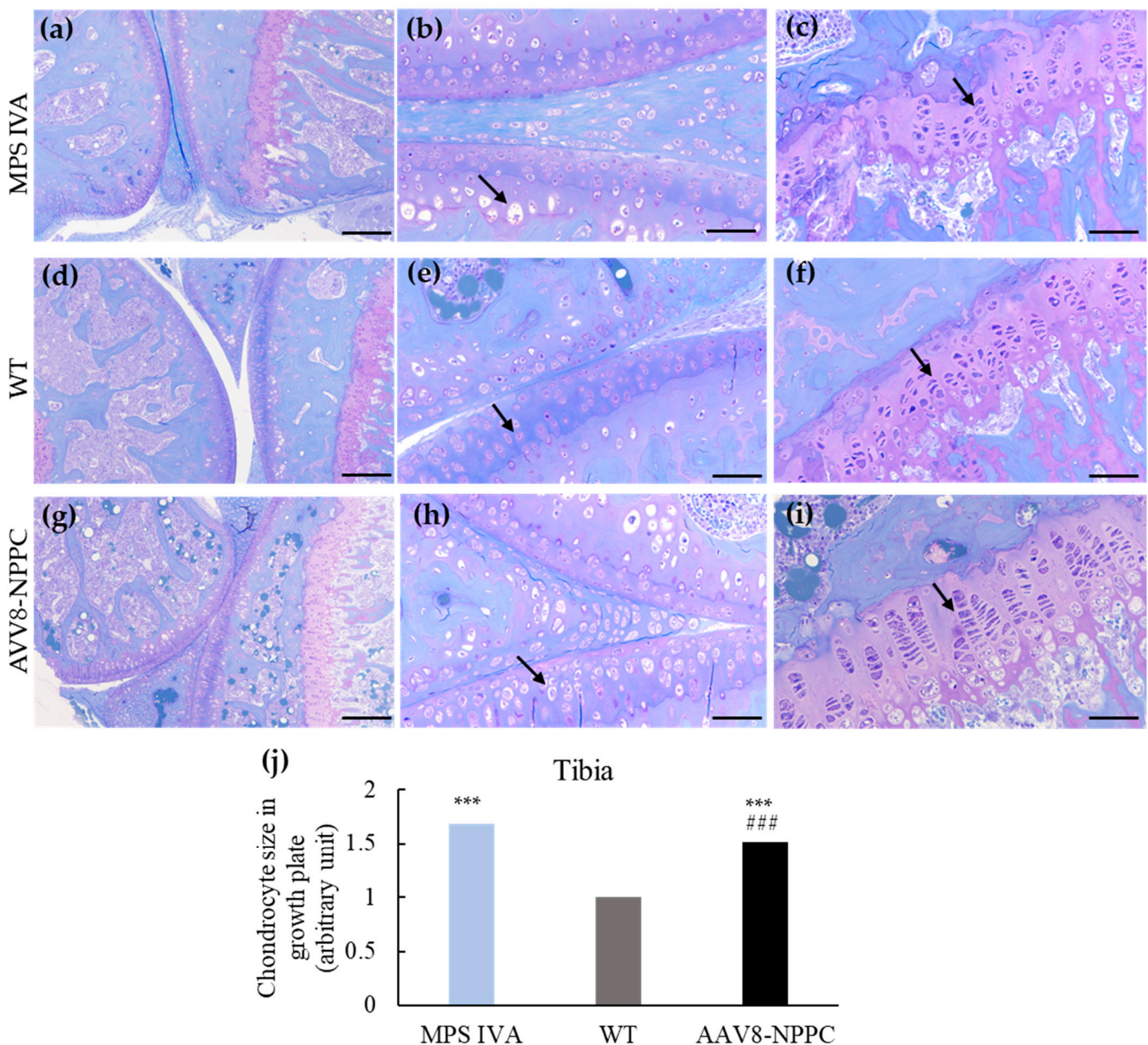


Figure 3. Correction of bone pathology in MPS IVA mice treated with AAV8-NPPC vector assessed by toluidine blue staining analysis using light microscopy. Knee joint and articular cartilage of untreated MPS IVA (a), WT (d), and MPS IVA mouse treated with AAV8-NPPC vector (g) (10× magnification and scale 200 μm). Articular disc in the knee joint of MPS IVA (b), WT (e), and MPS IVA mouse treated with AAV8-NPPC vector (h) (40× magnification and 50 μm). Growth plate region of MPS IVA (c), WT (f), and MPS IVA mouse treated with AAV8-NPPC vector (i) (40× magnification and 50 μm). Chondrocyte cell size in growth plates of the tibia (j). Data expressed fold change from the WT group ($n = 3$). Arrows indicate chondrocytes. The following statistical symbols were used to denote as follows. AAV8-CNP group vs. WT group, *** $p \leq 0.001$; AAV8-CNP group vs. untreated MPS IVA group, ### $p \leq 0.001$.

2.3. AAV Vector Biodistribution and CNP Expression

To establish if the one-time administration of vector expressing CNP affects CNP expression during the study, we measured the plasma level of human NT-proCNP as a marker of CNP expression. The expression level of NT-proCNP increased to the level of 1860.8 ± 584.6 pmol/L just four weeks after the injection (Figure 4a). Over time (weeks 12 and 16), the levels of the NT-proCNP increased, but it was not statistically different from

the 8-week-old measurement. In the case of WT and untreated MPS IVA mice, human NT-proCNP was not detected. In addition, we measured the biodistribution of the vector in the liver and bone (humerus). The vector was detected in both liver (Figure 4b) and bone (Figure 4c).

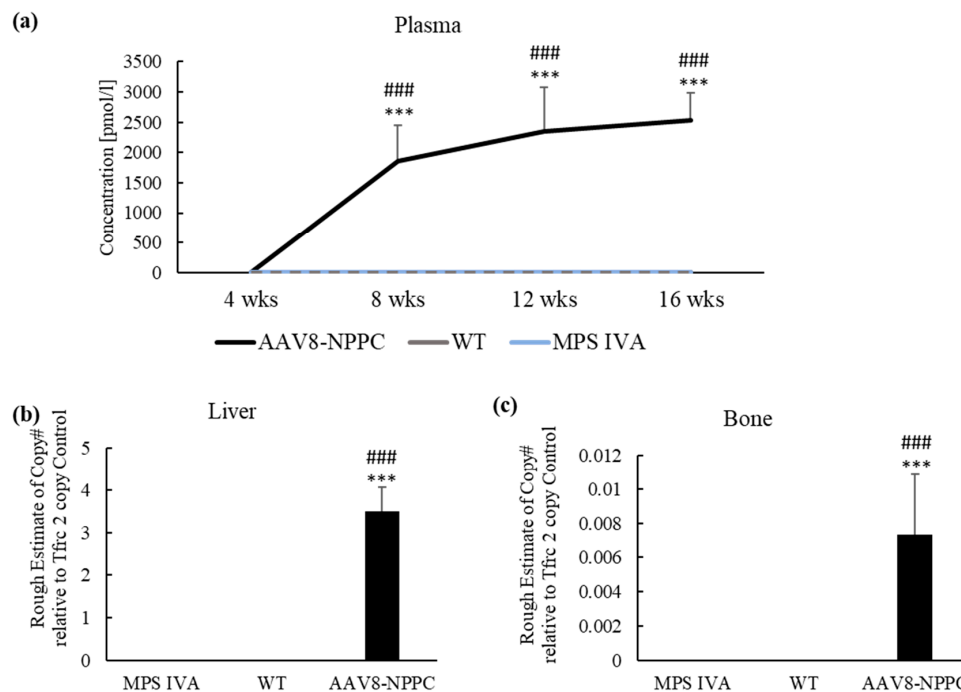


Figure 4. AAV vector Biodistribution and NT-proCNP expression and vector copy number at 12 weeks post-treatment. **(a)** Plasma; Marker for CNP expression, NT-proCNP, increased over the 12 weeks of treatment in the MPS IVA mouse model with significant differences to WT and untreated MPS IVA mice. **(b)** Liver and **(c)** bone; vector copy number at 12 weeks post-treatment. Results are shown as mean values \pm SEM ($n = 5$). The following statistical symbols were used to denote as follows. AAV8-CNP group vs. WT group, *** $p \leq 0.001$; AAV8-CNP group vs. untreated MPS IVA group, ### $p \leq 0.001$.

We performed immunohistochemistry staining to investigate the presence of CNP peptide in the liver and bone growth plate. However, we did not detect CNP in the bone growth plate samples, possibly because the peptide was secreted by the cells. In the liver samples, immunohistochemistry staining showed no significant difference in the expression levels between the mouse groups. These results could be associated with antibodies that cross-react with the murine NPPC gene.

In addition, we performed a Western blot to quantify the expression of the CNP protein in the liver, as its distribution level was over three-fold higher than in WT mice. We detected CNP expression in all groups, including MPS IVA, WT, and AAV8-NPPC (shown in Figure S3). The antibody used detected both human and mouse CNP; however, we observed the highest expression in AAV8-NPPC-treated mice due to the expression of both human and endogenous mouse CNP.

2.4. GAG Levels in the Blood and Tissues

At the autopsy, we measured mono-sulfated KS, the major KS component, in both plasma and tissues (liver, heart, lung, and bone). The levels of mono-sulfated KS are shown in Figure 5. KS was accumulated in plasma and all tissues except the heart (Figure 5c) of the MPS IVA mouse model. After treatment with CNP expressing vector, plasma KS level statistically decreased compared to untreated mice (Figure 5a). The level of KS is lower in the bone of CNP-treated mice compared to untreated MPS IVA (Figure 5c). Treatment with vector did not influence the levels of KS in the heart and lung (Figure 5c,d).

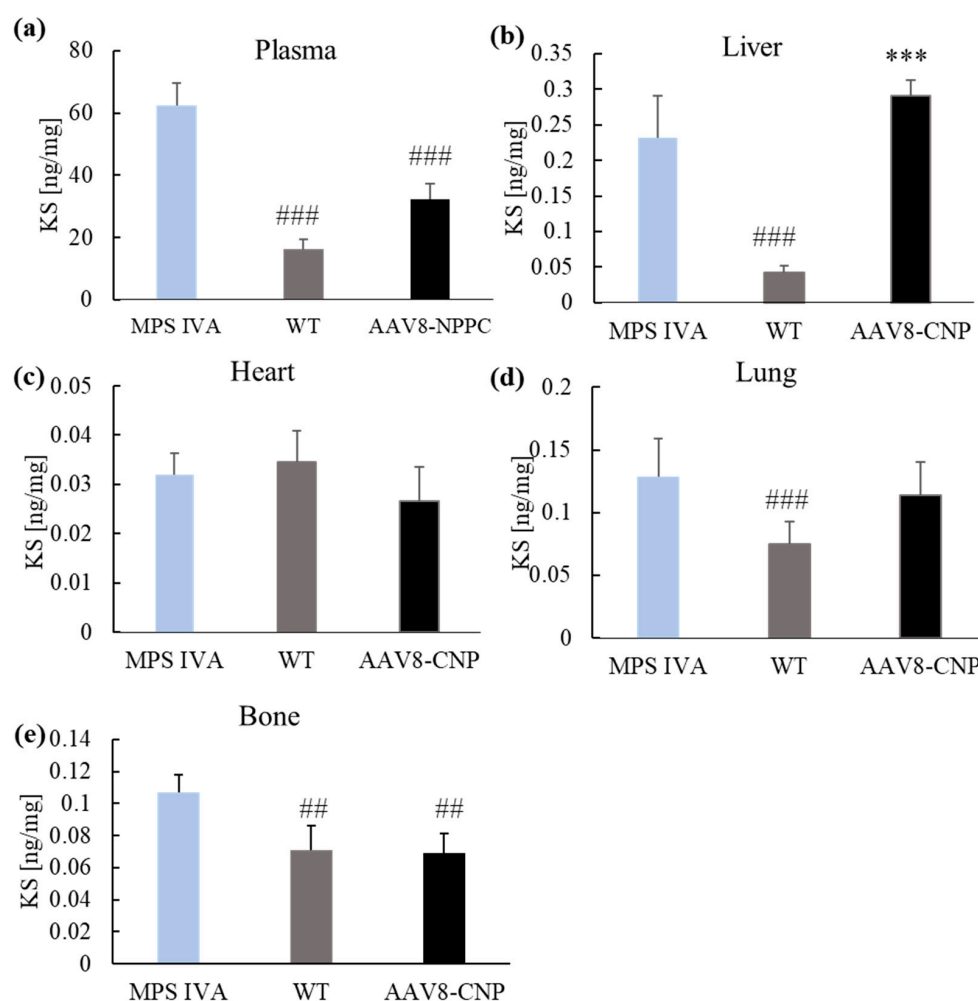


Figure 5. Mono-sulfated keratan sulfate levels. After 12 weeks post-treatment, the KS level was measured in plasma (a), liver (b), heart (c), lung (d), and bone (e). Results are shown as mean values \pm SEM ($n = 5$). The following statistical symbols were used to denote as follows. AAV8-CNP group vs. WT group, *** $p \leq 0.001$; AAV8-CNP group vs. untreated MPS IVA group, ### $p \leq 0.001$, ## $p \leq 0.01$.

Additionally, we measured the levels of other GAG in the tissues and plasma; Di-sulfated KS (Di S KS), Chondroitin disaccharide (Di 4S), O-sulfated heparan sulfate, and low sulfated heparan sulfate. We did not observe significant differences between the groups in the di-sulfated KS, O-sulfated heparan sulfate, and low-sulfated heparan sulfate. The chondroitin sulfates were accumulated in the liver of the MPS IVA mouse. Treatment with CNP expressing vector did not affect the GAG levels in the liver, but in the case of the lung after the treatment, we observed higher levels compared to WT and untreated MPS IVA mice.

2.5. Micro-CT

Micro-Computed Tomography (micro-CT) is an important tool for analyzing cortical and trabecular bone structure in medical applications such as treatment efficacy and bone tissue engineering. Micro-CT uses X-ray attenuation data to create a 3D representation of the specimen, providing direct 3D measurements of bone morphology and a larger volume of interest than traditional histologic evaluations. Micro-CT measurements are also faster and nondestructive, allowing other assays to be performed on the same sample [27]. To determine bone morphometry, we performed micro-CT in three experimental groups with analysis of the trabecular and the cortical bone (Figure 6).

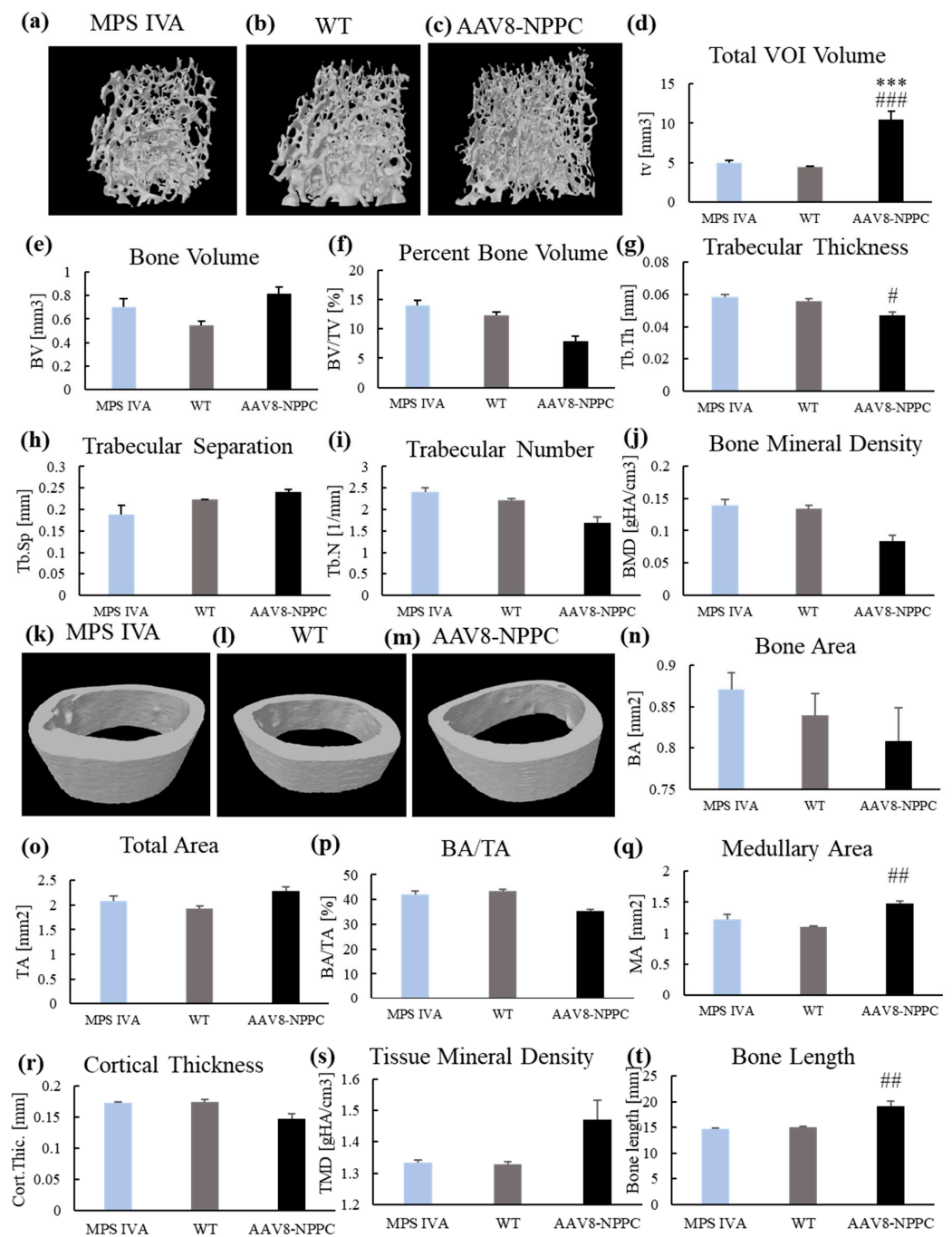


Figure 6. Trabecular and cortical morphometry after AAV vector treatment. At 12 weeks after treatment, micro-CT analysis of trabecular (a–j) and cortical (k–t) bone of three experimental groups. Trabecular analysis included ($n = 5$): trabecular bone model of MPS IVA (a), WT (b), and AAV8-NPPC (c); total trabecular volume of interest (d); trabecular bone volume (e); percent bone volume (f); trabecular thickness (g); trabecular separation (h); trabecular number (i); bone mineral density (j). Cortical analysis included (AAV8-NPPC; $n = 4$; MPS IVA, $n = 5$; WT; $n = 5$): cortical bone model of MPS IVA (k), WT (l), and AAV8-NPPC (m); Cortical bone area (n); Total area (o); Bone area/Total area (p); Medullary area (q); Cortical thickness (r); Tissue mineral density (s). Additionally, we also measured femur bone length (t). Results are shown as mean values \pm SEM. The following statistical symbols were used to denote as follows. AAV8-CNP group vs. WT group, *** $p \leq 0.001$; AAV8-CNP group vs. untreated MPS IVA group, ### $p \leq 0.001$, ## $p \leq 0.01$, # $p \leq 0.05$.

We did not see significant differences between WT and untreated MPS IVA mice, partly because of the limited number of mice (Analysis of Trabecular Bone Morphometry $n = 5$ in each group (Figure 6d–j); Cortical Bone Architecture WT; $n = 5$, MPS IVA; $n = 5$, AAV8-NPPC; $n = 4$ (Figure 6n–s). AAV8-NPPC treatment increased the trabecular volume of interest (Figure 6d) and decreased trabecular thickness (Figure 6g). In cortical bone analysis, the total cortical medullary area increased after the treatment (Figure 6q). Additionally, we measured the length of the femur used for analysis (Figure 6t). No bone length difference between untreated MPS IVA and WT mice was found. While MPS IVA mice were treated with AAV8-NPPC, femurs were longer (Figure 6t).

3. Discussion

The histological structure of the growth plate region in MPS IVA patients showed vacuolated cartilage cells with unorganized column structure and reduced calcification [28]. The short stature of MPS IVA patients is directly linked to the abnormal lysosomal storage within the chondrocytes, reducing their ability to properly proliferate and differentiate [29]. Our MPS IVA mouse model showed mono-sulfated KS accumulation in the bone (Figure 5) and an abnormal histological picture (Figure 3). Similarly, as in patients [30,31], the tibial growth plate showed an accumulation of GAG in vacuolated chondrocytes and abnormal column structure. The results were also parallel as in our other mouse models (MKC and MTOL, discussed in [2]); tibia growth plate chondrocytes were found to be more prominent in MPS IVA knockout mice than in WT (Figure 3). Furthermore, our analysis delved more deeply into the level of GAG accumulation in affected tissues. We were the first to show mono-sulfated KS accumulation in the bone of the mouse MPS IVA model, in addition to other tissues. The difference in the level of mono-KS in the liver and lung (the only tissues shown in [2]) was similar. In untreated MPS IVA, liver accumulation was 200 times higher than in WT, while in the lung, it was around 100 times more. These results are similar to our previous mouse models [2]. In the case of bone, we observed a 30% increase in mono-KS accumulation compared to WT mice (Figure 5).

As a result of a larger deletion in the GALNS gene, we did not detect the GALNS enzyme activity in any tissues and plasma samples of the MPS IVA mouse model (Figure S1). Nevertheless, with a limited number of mice analyzed, we did not observe abnormal bone growth and unique skeletal dysplasia in the new MPS IVA mouse model (Figure 2) and significant changes in the morphometry of mouse bone (Figure 6). However, there was a tendency in the MPS IVA vs. WT: higher VOI (Figure 6d), higher bone volume (Figure 6e), a higher percent of bone volume (Figure 6f), lower trabecular separation (Figure 6h), and higher bone area (Figure 6n). We will require a more significant number of mice to analyze the bone morphometry.

In an article comparing different bone lesions in MPS types I, IIIA, IVA, and VII based on micro-CT scans, it was found that MPS VII showed the highest bone abnormalities, including severe thickening of the periosteum of vertebrae and bones in the knee joint. This thickening resulted in a rough articular surface in the knee joint bones. Both plain radiographs and BMD measurements by micro-CT showed an increase in MPS VII compared to WT mice. The second most severe bone dysplasia with similar outcomes was observed in MPS I. In the case of MPS IIIA, no difference was observed in micro-CT scans compared to WT mice. While micro-CT scans of MPS IVA mice showed no significant abnormalities compared to WT mice, an abnormality in the calcaneus bone was detected on radiographs of nine-month-old MPS IVA mice, and the same anomaly was clinically evident in four other mice at six to seven months of age [32].

Overall, our experimental mouse model has similar abnormal characteristics to patients with MPS IVA [33,34], including no enzymatic activity, accumulation of GAGs, and histological changes in the bone of mice. To this date, the experimental mouse models have not shown severe skeletal phenotypes similar to that in human patients.

Many forms of mucopolysaccharidosis (MPS), such as types I, II, III, VI, and VII, have suitable animal models that accurately represent their phenotype. These models include

genetically modified animals and spontaneous mutation that occurs in feline and canine models [35]. However, for MPS IVA, no spontaneous model has been described, and to this day, the knockout mouse models have shown a limited skeletal phenotype.

In our laboratory, we have developed several mouse models with differences in the deletion size and place of the GALNS gene [2,36]. Our experience confirms that mouse models with the knockout in the GALNS gene have pathological bone phenotypes in histological analysis, along with progressive KS accumulation, which is necessary to reflect human pathology [2,36,37]. Recent studies have shown a rat model of MPS IVA generated using CRISPR/Cas9 technology. In comparison to the current mouse models, the rat model showed skeletal alterations that more closely resemble those of human patients [38].

The application of recombinant AAV (rAAV) vectors in gene therapy to address MPS is highly valuable due to their efficient infection of various cell types, capacity to persist as episomes, and minimal risk of causing insertional mutagenesis or genotoxicity. The AAV vector transduction is a multistep mechanism with crucial steps such as cellular internalization, endo-lysosomal vesicle uptake to the cell center, capsid processing for the nuclear AAV capsid entry following uncoating and AAV replication with the expression of the transgene [39]. AAV vectors have several serotypes; to date, 12 of the primate serotypes have been described (AAV1-12) [40–45]. Each serotype differs in capsid sequences and determines its tissue tropism and antigenic properties [45,46]. This study used an AAV8 vector with liver and heart tropism [47]. As the AAV8 vector internalized to the cell, the expression of the NPPC gene started in the nucleus to produce CNP peptide outside the cell membrane. The synthesis of the CNP peptide is a process started in the nucleus, where the transcribed sequence is cleaved by the enzyme furin to be secreted outside the nucleus in the propeptide CNP form. The CNP propeptide (103 amino acids) was cleaved to biologically form active CNP and inactive N-terminal proCNP (NT-proCNP) peptides, and those forms are secreted outside the cell [48,49]. As NT-proCNP has a longer life with a significant correlation to the biologically active CNP concentration, this molecule indicates CNP expression [50]. We detected increased expression of human NT-proCNP in the circulation of mice (Figure 4a); however, we did not detect CNP expression in the bone of treated mice following IHC staining. This finding suggests that CNP peptide was expressed from the AAV cassette, attached to the NPR-B receptor on the top of the cell, and activated a cascade of molecular reaction that resulted in the growth induction in mice [more on the mechanism of bone growth induction: 20]. CNP also regulates cellular condensation and GAG synthesis during the chondrogenesis process in the *in vitro* culture [51,52]. CNP increases the expression of enzymes involved in chondroitin sulfate synthesis, which is necessary for cartilage GAGs. In this study, authors did not see the change in other genes responsible for the extracellular matrix (Sox9, -5, -6, nor collagen II) [51]. Similar studies also showed an increase in GAG synthesis based on the Alcian staining; in that case, it was highly dose-dependent (10^{-8} M and 10^{-7} M CNP increased GAGs, while 10^{-6} M CNP did not affect) [52]. Our results showed decreased KS accumulation in bone compared to the untreated MPS IVA (Figure 5e). There is no direct explanation for why CNP could decrease KS in bone. Pathology slides showed a smaller size and increased number of chondrocytes after CNP treatment (Figure 3). We hypothesize that smaller chondrocytes cannot store as many KS as ballooned chondrocytes in the MPS IVA mouse model, which can indirectly explain the decreased accumulation of KS in bone tissue after CNP treatment. However, we have a limited number of animals in the pathology assessment. The overexpression of CNP previously confirmed its role in the bone ossification process by inducing bone growth in transgenic mice [53]. This research showed a decrease in bone mineral density [53]. We observed a decrease after the treatment, but it was not statistically significant (Figure 6). Natural CNP has a short lifetime of 2–3 min with a rapid degradation process that results in the ineffective long-term treatment of achondroplasia. One of the first studies to use CNP as a potential treatment for skeletal dysplasia was done in a mouse model of achondroplasia, the most common form of dwarfism caused by mutations in the fibroblast growth factor receptor 3 (FGFR3) gene. The study found that CNP could act as a negative regulator of

FGFR3, inhibiting mitogen-activated protein kinase (MAPK). After administration of the CNP analog to the mouse model of achondroplasia, the mice were much longer than their affected littermates. The mouse growth plates showed an increase in chondrocytes, and immunohistochemistry showed that after CNP treatment, the growth plates were partially normalized, together with enlargement of the epiphysis, to the level of wild-type mice. Both the proliferative and hypertrophic zones of the growth plate showed an increase in height after CNP treatment [54]. These results are similar to our histological analysis of the MPS IVA mouse model after CNP expression (Figure 3).

As a continuum of the mouse research in achondroplasia clinical trial for the Vortosite was done. In the phase 2 clinical trial, treatment with vosoritide for one year resulted in a statistically significant increase in growth velocity compared to placebo in children with achondroplasia. The most common adverse events associated with vosoritide were injection site reactions and mild hypotension, which were generally well-tolerated. Currently, Vortosite is accepted as a treatment for achondroplasia patients aged \geq two years whose epiphyses are not closed. Nevertheless, patients must receive subcutaneous injections daily to sustain CNP activity [21]. What may result in long-term side effects is not shown. As a result, another modified CNP therapeutic, TransCon, is tested in clinical trials for longer-half life (weekly injection) and efficacy [23]. Repeated injections are still necessary to keep the treatment effective; therefore, there is a need to develop more effective and convenient treatments for skeletal dysplasia that can provide sustained therapeutic benefits without the need for repeated injections.

Our study tested the potential of CNP in the expression cassette of AAV for the first time.

While our study provides valuable insights into the potential therapeutic use of CNP for progressive skeletal dysplasia in MPS IVA, several limitations exist. Firstly, our study used a small sample size, which could affect the statistical power and significance of the conclusions drawn. Further studies with larger sample sizes may be necessary to confirm the effectiveness of CNP delivered through an AAV vector expression cassette. It should also be noted that the animal model we used did not exhibit the typical phenotype of MPS IVA patients. While none of the existing mouse models fully replicate the phenotype of human MPS IVA, our study used a model closer to growth plate pathology. Lastly, our study only evaluated the short-term effects of CNP treatment and did not assess potential toxicity or long-term outcomes. Further toxicity and long-term effects analysis will be necessary before CNP is delivered through an AAV vector expression cassette, which can be considered a viable therapeutic approach for progressive skeletal dysplasia in MPS IVA patients.

Overall, we tested for the first-time usage of CNP in an AAV cassette in the MPS IVA. The administration of AAV8 expressing CNP peptide into the MPS IVA mouse model resulted in (1) high secretion of CNP peptide into circulation, (2) induction of bone growth, (3) proliferation of chondrocytes, (4) improvement in bone pathology, and (5) changes in the levels of GAGs.

4. Materials and Methods

4.1. Experimental Design

All procedures for this study were approved by the Institutional Animal Care and Use Committee at Nemours Children's Health (IACUC; RSP19-12482-001). Mice were housed in a 12/12 h light/dark cycle with food and water provided ad libitum. The experimental design is shown in Figure 1b, with three experimental groups ($n = 5$, unless stated otherwise): (1) MPS IVA mice treated with CNP expressing vector, (2) WT mice (WT), and (3) untreated MPS IVA mice (UT). Four-week-old male mice were injected intravenously with an AAV vector expressing CNP peptide at a dose of 3.5×10^{13} GC/kg in PBS (Vector Builder). After AAV gene therapy, length, and weight were measured weekly for the mice, and blood was collected biweekly for 12 constitutive weeks. At 16 weeks old, mice were euthanized in a CO₂ chamber and perfused with 10 mL of 0.9% saline. Tissues were collected for GALNS enzyme activity assay, GAG analysis, and immunohistology staining.

4.2. Expression Vector

Adeno-associated virus vector used to overexpress the human native NPPC gene in our study, pAAV[Exp]-CAG > hNPPC[NM_024409.4]:WPRE, was constructed and packaged by VectorBuilder (Figure 1a). Briefly, for the recombinant AAV manufacturing, the transfer plasmid carrying the gene of interest (GOI) was co-transfected with the proprietary Rep-cap plasmid and helper plasmid encoding adenovirus genes (E4, E2A, and VA) that mediate AAV replication into HEK293T packaging cells. After a short incubation period, viral particles were harvested from cell lysate or supernatant depending on serotype and concentrated by PEG precipitation. For ultra-purified AAV (in vivo grade), viral particles were further purified and concentrated by cesium chloride (CsCl) gradient ultracentrifugation. We used a qPCR-based approach to measure AAV titer.

4.3. MPS IVA Mouse Model

MPS IVA knockout mice (MKC2; C57BL/6 background) were generated with a larger deletion site than the previously described murine model of MPS IVA [55]. Two pairs of sgRNAs were cleaved together to generate a large deletion (~6300 bp) between the two target sites (up- and downstream of the GALNS gene) (Figure S4). GALNS enzyme activity is not detectable in tissues and blood (Figure S1). Due to GALNS deficiency, mice accumulate storage material in tissues (liver, heart, lung, bone). KS level and consequent pathology are widely used in mouse models to evaluate the severity of the patient's phenotype and improvement of the treatments [36,56]. Genotyping for the experimental cohorts was done by PCR on day 20. Primers are flanking each sgRNA site designed to test individual nonhomologous DNA end joining (NHEJ) activity, as well as paired together to screen for deletion mutations between the two target sites.

4.4. GALNS Enzyme Activity Assay

GALNS enzyme activity was determined in plasma and tissues [2]. Frozen tissues were homogenized by Bead Mill Homogenizer (OMNI International, Kennesaw, GA, USA) in 25 mmol/L Tris-HCl (pH 7.2) and 1 mmol/L phenylmethylsulphonyl fluoride. Then, homogenates were centrifuged for 30 min at 4 °C, and the supernatant was collected to a new tube and assayed for enzyme activity. Either tissue lysate or plasma (2 µL) was used for the enzymatic reaction with 22 mM 4-methylumbelliferyl-β-galactopyranoside-6-sulfate (Research Products International, Mount Prospect, IL, USA) in 0.1 M NaCl/0.1 M sodium acetate (pH 4.3) and incubated at 37 °C for 16 h. After incubation, 10 mg/mL β-galactosidase from *Aspergillus oryzae* (Sigma-Aldrich, St. Louis, MO, USA) in 0.1 M NaCl/0.1 M sodium acetate (pH 4.3) was added and incubated for additional 2 h at 37 °C. The reaction was stopped with 1 M glycine NaOH (pH 10.5) solution and read at excitation 366 nm and emission 450 nm by FLUOstar Omega plate reader (BMG LABTECH Inc., Cary, NC, USA). Activity is shown as nanomoles of 4-methylumbelliferone released per hour per microliter of plasma or milligram of protein. Protein concentration was determined by a bicinchoninic acid (BCA) protein assay kit (Thermo Fisher Scientific, Waltham, MA, USA).

4.5. Glycosaminoglycans Quantification

GAG assay was determined in plasma and tissues as previously described [2].

4.6. Gait Analysis

Gait analysis was performed as described previously [57]. Briefly, mouse feet from forelimbs were painted with orange paint, and feet from hindlimbs were painted with green paint. After that, we used paper to track animal footprints. We defined stride length as the distance between two sequential footprints of hindlimbs created by the same foot (called one stride). To stride width, we measured the distance between the left and right hindlimbs.

4.7. Bone Pathological Assessments

Tissue staining and analysis were performed as described by Tomatsu et al. [2]. Briefly, knee joints were collected from 16-week-old MPS IVA and WT mice to evaluate levels of storage granules by light microscopy. Tissues were fixed in 2% paraformaldehyde and 4% glutaraldehyde in PBS, post-fixed in osmium tetroxide and embedded in Spurr's resin. Then, toluidine blue-stained 0.5- μm -thick sections were examined. To evaluate chondrocyte cell size (vacuolization) in the growth plates of the femur or tibia, approximately 300 chondrocytes in the proliferative area were measured in each mouse by Image J 1.53t software, and results were expressed as folds-change from the wild-type group. Pathological slides from knee joints of treated and untreated MPS IVA and wild-type mice were evaluated for reduced vacuolization and improved column orientation in growth plates (Table 1). The number of storage materials and the degree of disoriented columns were scored. "No storage or very slight" was 0 (–), "slight but obvious" was 1 (+), "moderate" was 2 (++), and "marked" was 3 (+++) [2]. Each pathological slide was assessed in a double-blind manner three times. We then averaged the scores in a group of mice per section of bone (growth plate, articular disc, meniscus, and ligament).

4.8. Trabecular and Cortical Morphometry

Trabecular and Cortical Morphometry was performed by micro-CT scans (a Bruker SkyScan 1275 scanner (Bruker, Billerica, MA, USA). Before analysis, the right femur of 16-week-old mice was fixed with 96% ethanol. For analysis, the femur was wrapped in 0.9% NaCl gauze and scanned. Quantitative analysis was performed in Bruker CTan software (v1.21.1.0). The volumes of interest (VOI) of trabecular bone were identified using the distal epiphyseal plate. The volumes of interest (VOI) of cortical bone were determined based on the distal epiphyseal plate start mark and the highest point in the proximal greater trochanter; between those two landmarks, we could obtain the total length of the bone.

4.9. AAV Vector Genome Biodistribution

DNA vector biodistribution was determined as previously described [2]. Briefly, DNA was purified from the liver using the Gentra Puregene kit according to the instruction manual (QIAGEN, Germantown, MD, USA). Before purification, the bone was homogenized by Bead Mill Homogenizer (OMNI International, GA, USA) and purified according to manufacturer instructions (QIAGEN, Germantown, MD, USA). Digital PCR (dPCR) analysis on genomic DNA extracted from liver and bone samples of mice was performed using specific primers and probe sequences for NPPC gene, which are as follows: forward primer, AAC GCG CGC AAA TAC AAA G, reverse primer, GGA ATT CCC ACT TTG TAC AAG AAA, and probe 5'6-FAM /TG AGC GGC C/ZEN/T GGG ATG TTA GAC CCA/3'IABkFQ. Genomic DNA was tested non-fragmented and fragmented using enzymatic digestion or an M220 Focused-ultrasonicator (Covaris, Woburn, MA, USA). The NPPC TaqMan assay (FAM-labeled) (Thermo Fisher Scientific, Waltham, MA, USA) was used for quantitative dPCR analysis of the AAV CNP expressing vector. The concentration of DNA for the AAV chip for the liver and bone samples processed was between 0.5 and 2 ng per 16-mL reaction, dependent on the DNA concentration needed to bring the AAV copies/mL into the detectable range of the instrument. The TfrC TaqMan copy number reference assay (VIC labeled) was obtained from Thermo Fisher Scientific. 40 ng of genomic DNA per 16-mL reaction was used for TfrC dPCR. Each reaction was loaded onto a separate QuantStudio chip (QuantStudio 3D digital PCR 20 K chip kit v2, A26316; Thermo Fisher Scientific, Waltham, MA, USA). The PCR amplification profile was conducted with an ABI GeneAmp 9700 PCR thermal cycler with dual flat blocks (Applied Biosystems, Waltham, MA, USA). Then, chips were read on the QuantStudio 3D instrument to obtain the number of wells positive for the VIC and FAM channels and the number of wells without DNA and empty wells. Data analysis and chip quality were assessed using the QuantStudio 3D analysis suite. All chips were between 25% and 75% empty wells, ensuring suitability for quantitation. Copies/mL for both TfrC and AAV were determined and normalized using

the dilution factor for AAV sample input. Using Tfrc results as a reference for two copies, the number of copies of AAV per mouse genome was calculated.

4.10. ELISA for NT-proCNP

The detection of NT-proCNP in mice was done according to manufacturer instructions (Biomedica Medizinprodukte, Wien, Austria). Sample preparation included blood collected from mice and then centrifuged $8000\times g$ at $4\text{ }^{\circ}\text{C}$ for 10 min to collect the plasma sample in another tube and stored at $-20\text{ }^{\circ}\text{C}$ until further analysis. Plasma used for NT-proCNP detection was diluted 1:100 in the assay buffer provided in the ELISA kit.

4.11. Western Blot

Protein lysate was isolated from both the liver and arm bone, as described in Section 4.4. After lysis and determination of protein concentration, the protein extracts were separated by electrophoresis. However, we did not obtain a sufficient protein concentration in the arm tissue for further analysis. Therefore, only the liver tissue was analyzed for protein expression. After electrophoresis, the proteins were transferred onto a nitrocellulose membrane. The membrane was blocked with 5% nonfat dry milk in a TBST buffer and then incubated with primary antibodies overnight at $4\text{ }^{\circ}\text{C}$ (anti-CNP antibody from MyBioSource, San Diego, CA, USA, and beta-actin from Sigma-Aldrich, USA). The membrane was subsequently incubated with secondary antibodies at room temperature for 1 h, treated with a solution of substrates for HRP detection, and read with a C-DiGiT Blot Scanner Licor Machine. As CNP and beta-actin have similar protein weights, the membrane was stripped after performing analysis for the CNP protein, and beta-actin analysis was performed starting from the blocking step. The intensities of bands were analyzed using the QuantityOne 29.0 software.

4.12. Statistical Analysis

The normal distribution was found using the Kolmogorov-Smirnov test (K-S) and homogeneity of variance with the Leven test. Depending on the results, analysis of variance (two-way ANOVA) with Tukey's post-hoc test was performed if the distribution was normal. When the assumptions of the normality of the distribution and the homogeneity of variance were unmet, the nonparametric Kruskal-Wallis test, followed by Dunnett's test, was performed. Statistical analyses were performed using GraphPad Prism 9 software. Statistical significance was set at $p > 0.05$. Error bars represent SEM, as indicated in legends.

Supplementary Materials: The following supporting information can be downloaded at: <https://www.mdpi.com/article/10.3390/ijms24129890/s1>.

Author Contributions: Conceptualization, E.R., S.T.; methodology, E.R., S.K., F.N.; validation, E.R.; formal analysis, E.R.; investigation, E.R.; resources, S.T.; data curation, E.R., A.M.H.-P., B.C., S.K., F.N., E.B.-F.; writing—original draft preparation, E.R.; writing—review and editing, S.T.; visualization, E.R.; supervision, S.T.; project administration, S.T.; funding acquisition, S.T. All authors have read and agreed to the published version of the manuscript.

Funding: This work was also supported by grants from the Austrian MPS society, A Cure for Robert, Inc., The Carol Ann Foundation, Angelo R. Cali & Mary V. Cali Family Foundation, Inc., The Vain and Harry Fish Foundation, Inc., The Bennett Foundation, Jacob Randall Foundation, and Nemours Funds. S.T. was supported by an Institutional Development Award from the Eunice Kennedy Shriver National Institute of Child Health & Human Development of the National Institutes of Health (NICHD) (1R01HD102545-01A1).

Institutional Review Board Statement: Not applicable.

Informed Consent Statement: Not applicable.

Data Availability Statement: All data are available upon request.

Acknowledgments: We would like to thank Yasuhiko Ago, Sampurna Saikia, José Víctor Álvarez González, Therese Kokas, and Deborah Stabley for their support during the experiments.

Conflicts of Interest: The authors declare no conflict of interest.

References

1. Sabir, A.; Irving, M. Clinical trials in skeletal dysplasia: A paradigm for treating rare diseases. *Br. Med. Bull.* **2021**, *139*, 16–35. [[CrossRef](#)]
2. Sawamoto, K.; Karumuthil-Melethil, S.; Khan, S.; Stapleton, M.; Bruder, J.T.; Danos, O.; Tomatsu, S. Liver-Targeted AAV8 Gene Therapy Ameliorates Skeletal and Cardiovascular Pathology in a Mucopolysaccharidosis IVA Murine Model. *Mol. Ther. Methods Clin. Dev.* **2020**, *18*, 50–61. [[CrossRef](#)]
3. Khan, S.A.; Mason, R.W.; Giugliani, R.; Orii, K.; Fukao, T.; Suzuki, Y.; Yamaguchi, S.; Kobayashi, H.; Orii, T.; Tomatsu, S. Glycosaminoglycans analysis in blood and urine of patients with mucopolysaccharidosis. *Mol. Genet. Metab.* **2018**, *125*, 44–52. [[CrossRef](#)]
4. Tomatsu, S.; Montaña, A.M.; Oikawa, H.; Smith, M.; Barrera, L.; Chinen, Y.; Thacker, M.M.; Mackenzie, W.G.; Suzuki, Y.; Orii, T. Mucopolysaccharidosis type IVA (Morquio A disease): Clinical review and current treatment. *Curr. Pharm. Biotechnol.* **2011**, *12*, 931–945. [[CrossRef](#)] [[PubMed](#)]
5. Khan, S.; Alméciga-Díaz, C.J.; Sawamoto, K.; Mackenzie, W.G.; Theroux, M.C.; Pizarro, C.; Mason, R.W.; Orii, T.; Tomatsu, S. Mucopolysaccharidosis IVA and glycosaminoglycans. *Mol. Genet. Metab.* **2017**, *120*, 78–95. [[CrossRef](#)]
6. Zhou, J.; Lin, J.; Leung, W.T.; Wang, L. A basic understanding of mucopolysaccharidosis: Incidence; clinical features; diagnosis; and management. *Intractable Rare Dis. Res.* **2020**, *9*, 1–9. [[CrossRef](#)] [[PubMed](#)]
7. Moretto, A.; Bosatra, M.G.; Marchesini, L.; Tesoro, S. Anesthesiological risks in mucopolysaccharidoses. *Ital. J. Pediatr.* **2018**, *44* (Suppl. S2), 116. [[CrossRef](#)] [[PubMed](#)]
8. Tomatsu, S.; Mackenzie, W.G.; Theroux, M.C.; Mason, R.W.; Thacker, M.M.; Shaffer, T.H.; Montaña, A.M.; Rowan, D.; Sly, W.; Alméciga-Díaz, C.J.; et al. Current and emerging treatments and surgical interventions for Morquio A syndrome: A review. *Res. Rep. Endocr. Disord.* **2012**, *2012*, 65–77. [[CrossRef](#)] [[PubMed](#)]
9. Doherty, C.; Stapleton, M.; Piechnik, M.; Mason, R.W.; Mackenzie, W.G.; Yamaguchi, S.; Kobayashi, H.; Suzuki, Y.; Tomatsu, S. Effect of enzyme replacement therapy on the growth of patients with Morquio A. *J. Hum. Genet.* **2019**, *64*, 625–635. [[CrossRef](#)]
10. Taylor, M.; Khan, S.; Stapleton, M.; Wang, J.; Chen, J.; Wynn, R.; Yabe, H.; Chinen, Y.; Boelens, J.J.; Mason, R.W.; et al. Hematopoietic Stem Cell Transplantation for Mucopolysaccharidoses: Past; Present; and Future. *Biol. Blood Marrow Transplant.* **2019**, *25*, e226–e246. [[CrossRef](#)] [[PubMed](#)]
11. Qi, Y.; Musson, D.G.; Schweighardt, B.; Tompkins, T.; Jesaitis, L.; Shaywitz, A.J.; Yang, K.; O'Neill, C.A. Pharmacokinetic and pharmacodynamic evaluation of elosulfase alfa: an enzyme replacement therapy in patients with Morquio A syndrome. *Clin. Pharmacokinet.* **2014**, *53*, 1137–1147. [[CrossRef](#)]
12. Politei, J.; Porrás-Hurtado, G.L.; Guelbert, N.; Fainboim, A.; Horovitz, D.D.G.; Satizábal, J.M. Enzyme replacement therapy interruption in mucopolysaccharidosis type IVA patients and its impact in different clinical outcomes. *JIMD Rep.* **2021**, *58*, 104–113. [[CrossRef](#)] [[PubMed](#)]
13. Long, B.; Tompkins, T.; Decker, C.; Jesaitis, L.; Khan, S.; Slasor, P.; Harmatz, P.; O'Neill, C.A.; Schweighardt, B. Long-term Immunogenicity of Elosulfase Alfa in the Treatment of Morquio A Syndrome: Results from MOR-005; a Phase III Extension Study. *Clin. Ther.* **2017**, *39*, 118–129.e3. [[CrossRef](#)] [[PubMed](#)]
14. Schweighardt, B.; Tompkins, T.; Lau, K.; Jesaitis, L.; Qi, Y.; Musson, D.G.; Farmer, P.; Haller, C.; Shaywitz, A.J.; Yang, K.; et al. Immunogenicity of Elosulfase Alfa, an Enzyme Replacement Therapy in Patients with Morquio A Syndrome: Results from MOR-004, a Phase III Trial. *Clin. Ther.* **2015**, *37*, 1012–1021.e6. [[CrossRef](#)]
15. Tomatsu, S.; Montaña, A.M.; Ohashi, A.; Gutierrez, M.A.; Oikawa, H.; Oguma, T.; Dung, V.C.; Nishioka, T.; Orii, T.; Sly, W.S. Enzyme replacement therapy in a murine model of Morquio A syndrome. *Hum. Mol. Genet.* **2008**, *17*, 815–824. [[CrossRef](#)]
16. Sawamoto, K.; Álvarez González, J.V.; Piechnik, M.; Otero, F.J.; Couce, M.L.; Suzuki, Y.; Tomatsu, S. Mucopolysaccharidosis IVA: Diagnosis, Treatment; and Management. *Int. J. Mol. Sci.* **2020**, *21*, 1517. [[CrossRef](#)] [[PubMed](#)]
17. Tomatsu, S.; Sawamoto, K.; Alméciga-Díaz, C.J.; Shimada, T.; Bober, M.B.; Chinen, Y.; Yabe, H.; Montaña, A.M.; Giugliani, R.; Kubaski, F.; et al. Impact of enzyme replacement therapy and hematopoietic stem cell transplantation in patients with Morquio A syndrome. *Drug Des. Devel Ther.* **2015**, *9*, 1937–1953. [[CrossRef](#)] [[PubMed](#)]
18. Biffi, A. Hematopoietic Stem Cell Gene Therapy for Storage Disease: Current and New Indications. *Mol. Ther.* **2017**, *25*, 1155–1162. [[CrossRef](#)] [[PubMed](#)]
19. Bartels, C.F.; Bükülmez, H.; Padayatti, P.; Rhee, D.K.; van Ravenswaaij-Arts, C.; Pauli, R.M.; Mundlos, S.; Chitayat, D.; Shih, L.Y.; Al-Gazali, L.I.; et al. Mutations in the transmembrane natriuretic peptide receptor NPR-B impair skeletal growth and cause acromesomelic dysplasia, type Maroteaux. *Am. J. Hum. Genet.* **2004**, *75*, 27–34. [[CrossRef](#)]
20. Rintz, E.; Węgrzyn, G.; Fujii, T.; Tomatsu, S. Molecular Mechanism of Induction of Bone Growth by the C-Type Natriuretic Peptide. *Int. J. Mol. Sci.* **2022**, *23*, 5916. [[CrossRef](#)]
21. Duggan, S. Vosoritide: First Approval. *Drugs* **2021**, *81*, 2057–2062. [[CrossRef](#)] [[PubMed](#)]
22. Savarirayan, R.; Irving, M.; Bacino, C.A.; Bostwick, B.; Charrow, J.; Cormier-Daire, V.; Le Quan Sang, K.H.; Dickson, P.; Harmatz, P.; Phillips, J.; et al. C-Type Natriuretic Peptide Analogue Therapy in Children with Achondroplasia. *N. Engl. J. Med.* **2019**, *381*, 25–35. [[CrossRef](#)] [[PubMed](#)]

23. Breinholt, V.M.; Rasmussen, C.E.; Mygind, P.H.; Kjølgaard-Hansen, M.; Faltinger, F.; Bernhard, A.; Zettler, J.; Hersel, U. TransCon CNP, a Sustained-Release C-Type Natriuretic Peptide Prodrug; a Potentially Safe and Efficacious New Therapeutic Modality for the Treatment of Comorbidities Associated with Fibroblast Growth Factor Receptor 3-Related Skeletal Dysplasias. *J. Pharmacol. Exp. Ther.* **2019**, *370*, 459–471. [[CrossRef](#)] [[PubMed](#)]
24. Peracha, H.; Sawamoto, K.; Averill, L.; Kecskemethy, H.; Theroux, M.; Thacker, M.; Nagao, K.; Pizarro, C.; Mackenzie, W.; Kobayashi, H.; et al. Molecular genetics and metabolism; special edition: Diagnosis, diagnosis and prognosis of Mucopolysaccharidosis IVA. *Mol. Genet. Metab.* **2018**, *125*, 18–37. [[CrossRef](#)]
25. Dhawale, A.A.; Church, C.; Henley, J.; Holmes, L., Jr.; Thacker, M.M.; Mackenzie, W.G.; Miller, F. Gait pattern and lower extremity alignment in children with Morquio syndrome. *J. Pediatr. Orthop. B* **2013**, *22*, 59–62. [[CrossRef](#)]
26. Salazar-Torres, J.J.; Church, C.; Shields, T.; Shrader, M.W.; Fisher, L.; Mackenzie, W.G.; Mackenzie, W.G.S. Evaluation of Gait Pattern and Lower Extremity Kinematics of Children with Morquio Syndrome (MPS IV). *Diagnostics* **2021**, *11*, 1350. [[CrossRef](#)]
27. Bouxsein, M.L.; Boyd, S.K.; Christiansen, B.A.; Guldberg, R.E.; Jepsen, K.J.; Müller, R. Guidelines for assessment of bone microstructure in rodents using micro-computed tomography. *J. Bone Miner Res.* **2010**, *7*, 1468–1486. [[CrossRef](#)]
28. McClure, J.; Smith, P.S.; Sorby-Adams, G.; Hopwood, J. The histological and ultrastructural features of the epiphyseal plate in Morquio type A syndrome (mucopolysaccharidosis type IVA). *Pathology* **1986**, *18*, 217–221. [[CrossRef](#)]
29. Zustin, J. Morquio disease: The role of cartilage canals in the pathogenesis of chondrogenic dwarfism. *Med. Hypotheses* **2010**, *6*, 642–644. [[CrossRef](#)]
30. De Franceschi, L.; Roseti, L.; Desando, G.; Facchini, A.; Grigolo, B. A molecular and histological characterization of cartilage from patients with Morquio syndrome. *Osteoarthr. Cartil.* **2007**, *15*, 1311–1317. [[CrossRef](#)]
31. Bank, R.A.; Groener, J.E.; van Gemund, J.J.; Maaswinkel, P.D.; Hoeben, K.A.; Schut, H.A.; Everts, V. Deficiency in N-acetylgalactosamine-6-sulfate sulfatase results in collagen perturbations in cartilage of Morquio syndrome A patients. *Mol. Genet. Metab.* **2009**, *97*, 196–201. [[CrossRef](#)] [[PubMed](#)]
32. Rowan, D.J.; Tomatsu, S.; Grubb, J.H.; Montañó, A.M.; Sly, W.S. Assessment of bone dysplasia by micro-CT and glycosaminoglycan levels in mouse models for mucopolysaccharidosis type I, IIIA, IVA, and VII. *J. Inherit. Metab. Dis.* **2013**, *2*, 235–246. [[CrossRef](#)]
33. Fujitsuka, H.; Sawamoto, K.; Peracha, H.; Mason, R.W.; Mackenzie, W.; Kobayashi, H.; Yamaguchi, S.; Suzuki, Y.; Orii, K.; Orii, T.; et al. Biomarkers in patients with mucopolysaccharidosis type II and IV. *Mol. Genet. Metab. Rep.* **2019**, *19*, 100455. [[CrossRef](#)]
34. Martell, L.; Lau, K.; Mei, M.; Burnett, V.; Decker, C.; Foehr, E.D. Biomarker analysis of Morquio syndrome: Identification of disease state and drug responsive markers. *Orphanet J. Rare Dis.* **2011**, *6*, 84. [[CrossRef](#)] [[PubMed](#)]
35. Haskins, M.E. Animal models for mucopolysaccharidosis disorders and their clinical relevance. *Acta Paediatr.* **2007**, *455*, 56–62. [[CrossRef](#)]
36. Tomatsu, S.; Gutierrez, M.; Nishioka, T.; Yamada, M.; Yamada, M.; Tosaka, Y.; Grubb, J.H.; Montañó, A.M.; Vieira, M.B.; Trandafirescu, G.G.; et al. Development of MPS IVA mouse (Galnstm(hC79S.mC76S)slu) tolerant to human N-acetylgalactosamine-6-sulfate sulfatase. *Hum. Mol. Genet.* **2005**, *14*, 3321–3335. [[CrossRef](#)] [[PubMed](#)]
37. Tomatsu, S.; Vogler, C.; Montañó, A.M.; Gutierrez, M.; Oikawa, H.; Dung, V.C.; Orii, T.; Noguchi, A.; Sly, W.S. Murine model (Galns(tm(C76S)slu)) of MPS IVA with missense mutation at the active site cysteine conserved among sulfatase proteins. *Mol. Genet. Metab.* **2007**, *3*, 251–258. [[CrossRef](#)]
38. Bertolin, J.; Sánchez, V.; Ribera, A.; Jaén, M.L.; Garcia, M.; Pujol, A.; Sánchez, X.; Muñoz, S.; Marcó, S.; Pérez, J.; et al. Treatment of skeletal and non-skeletal alterations of Mucopolysaccharidosis type IVA by AAV-mediated gene therapy. *Nat. Commun.* **2021**, *12*, 5343. [[CrossRef](#)]
39. Berry, G.E.; Asokan, A. Cellular transduction mechanisms of adeno-associated viral vectors. *Curr. Opin. Virol.* **2016**, *21*, 54–60. [[CrossRef](#)]
40. Schultz, B.R.; Chamberlain, J.S. Recombinant adeno-associated virus transduction and integration. *Mol. Ther.* **2008**, *16*, 1189–1199. [[CrossRef](#)]
41. Xiao, W.; Chirmule, N.; Berta, S.C.; McCullough, B.; Gao, G.; Wilson, J.M. Gene therapy vectors based on adeno-associated virus type 1. *J. Virol.* **1999**, *73*, 3994–4003. [[CrossRef](#)] [[PubMed](#)]
42. Samulski, R.J.; Srivastava, A.; Berns, K.I.; Muzyczka, N. Rescue of adeno-associated virus from recombinant plasmids: Gene correction within the terminal repeats of AAV. *Cell* **1983**, *33*, 135–143. [[CrossRef](#)] [[PubMed](#)]
43. Chiorini, J.A.; Kim, F.; Yang, L.; Kotin, R.M. Cloning and characterization of adeno-associated virus type 5. *J. Virol.* **1999**, *73*, 1309–1319. [[CrossRef](#)]
44. Chiorini, J.A.; Yang, L.; Liu, Y.; Safer, B.; Kotin, R.M. Cloning of adeno-associated virus type 4 (AAV4) and generation of recombinant AAV4 particles. *J. Virol.* **1997**, *71*, 6823–6833. [[CrossRef](#)]
45. Mori, S.; Wang, L.; Takeuchi, T.; Kanda, T. Two novel adeno-associated viruses from cynomolgus monkey: Pseudotyping characterization of capsid protein. *Virology* **2004**, *330*, 375–383. [[CrossRef](#)]
46. Hauck, B.; Xiao, W. Characterization of tissue tropism determinants of adeno-associated virus type 1. *J. Virol.* **2003**, *77*, 2768–2774. [[CrossRef](#)]
47. Wu, Z.; Asokan, A.; Samulski, R.J. Adeno-associated virus serotypes: Vector toolkit for human gene therapy. *Mol. Ther.* **2006**, *14*, 316–327. [[CrossRef](#)] [[PubMed](#)]
48. Prickett, T.C.; Espiner, E.A. Circulating products of C-type natriuretic peptide and links with organ function in health and disease. *Peptides* **2020**, *132*, 170363. [[CrossRef](#)] [[PubMed](#)]

49. Wu, C.; Wu, F.; Pan, J.; Morser, J.; Wu, Q. Furin-mediated processing of Pro-C-type natriuretic peptide. *J. Biol. Chem.* **2003**, *278*, 25847–25852. [[CrossRef](#)] [[PubMed](#)]
50. Keng, B.M.H.; Gao, F.; Tan, R.S.; Ewe, S.H.; Teo, L.L.Y.; Xie, B.Q.; Goh, G.B.B.; Koh, W.P.; Koh, A.S. N-Terminal pro C-Type Natriuretic Peptide (NTproCNP) and myocardial function in ageing. *PLoS ONE* **2018**, *13*, e0209517. [[CrossRef](#)] [[PubMed](#)]
51. Woods, A.; Khan, S.; Beier, F. C-type natriuretic peptide regulates cellular condensation and glycosaminoglycan synthesis during chondrogenesis. *Endocrinology* **2007**, *148*, 5030–5041. [[CrossRef](#)] [[PubMed](#)]
52. Tezcan, B.; Serter, S.; Kiter, E.; Tufan, A.C. Dose dependent effect of C-type natriuretic peptide signaling in glycosaminoglycan synthesis during TGF- β 1 induced chondrogenic differentiation of mesenchymal stem cells. *J. Mol. Histol.* **2010**, *41*, 247–258. [[CrossRef](#)] [[PubMed](#)]
53. Kake, T.; Kitamura, H.; Adachi, Y.; Yoshioka, T.; Watanabe, T.; Matsushita, H.; Fujii, T.; Kondo, E.; Tachibe, T.; Kawase, Y.; et al. Chronically elevated plasma C-type natriuretic peptide level stimulates skeletal growth in transgenic mice. *Am. J. Physiol. Endocrinol. Metab.* **2009**, *297*, E1339–E1348. [[CrossRef](#)] [[PubMed](#)]
54. Lorget, F.; Kaci, N.; Peng, J.; Benoist-Lasselien, C.; Mugniery, E.; Oppeneer, T.; Wendt, D.J.; Bell, S.M.; Bullens, S.; Bunting, S.; et al. Evaluation of the therapeutic potential of a CNP analog in a Fgfr3 mouse model recapitulating achondroplasia. *Am. J. Hum. Genet.* **2012**, *6*, 1108–1114. [[CrossRef](#)] [[PubMed](#)]
55. Tomatsu, S.; Orii, K.O.; Vogler, C.; Nakayama, J.; Levy, B.; Grubb, J.H.; Gutierrez, M.A.; Shim, S.; Yamaguchi, S.; Nishioka, T.; et al. Mouse model of N-acetylgalactosamine-6-sulfate sulfatase deficiency (Galns^{-/-}) produced by targeted disruption of the gene defective in Morquio A disease. *Hum. Mol. Genet.* **2003**, *12*, 3349–3358. [[CrossRef](#)] [[PubMed](#)]
56. Tomatsu, S.; Montaña, A.M.; Dung, V.C.; Ohashi, A.; Oikawa, H.; Oguma, T.; Orii, T.; Barrera, L.; Sly, W.S. Enhancement of drug delivery: Enzyme-replacement therapy for murine Morquio A syndrome. *Mol. Ther.* **2010**, *18*, 1094–1102. [[CrossRef](#)]
57. Wertman, V.; Gromova, A.; La Spada, A.R.; Cortes, C.J. Low-Cost Gait Analysis for Behavioral Phenotyping of Mouse Models of Neuromuscular Disease. *J. Vis. Exp.* **2019**, *18*, e59878.

Disclaimer/Publisher's Note: The statements, opinions and data contained in all publications are solely those of the individual author(s) and contributor(s) and not of MDPI and/or the editor(s). MDPI and/or the editor(s) disclaim responsibility for any injury to people or property resulting from any ideas, methods, instructions or products referred to in the content.

Supplementary materials

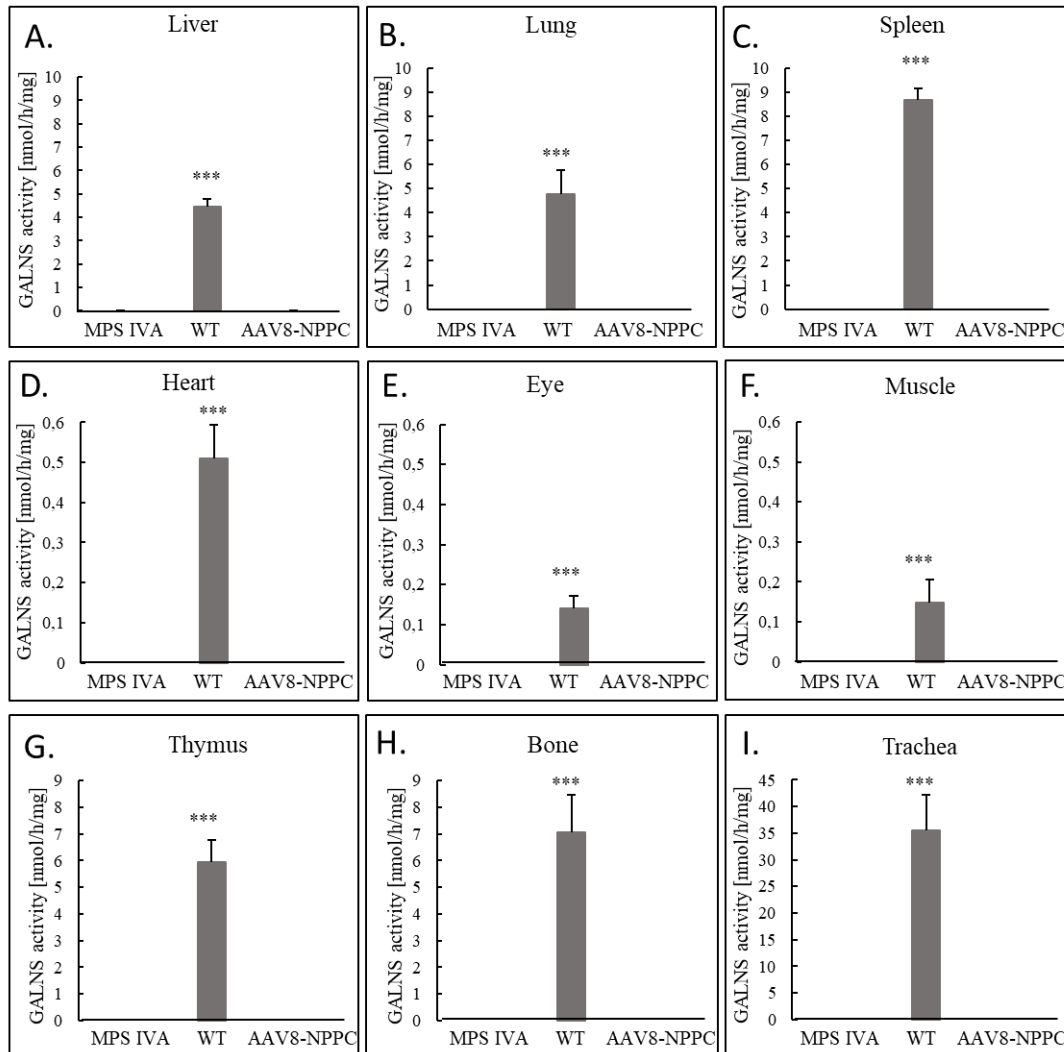


Figure S1. GALNS enzyme assay activity. After 12 weeks post-treatment, we measured GALNS enzyme assay activity in tissues: liver (A), lung (B), spleen (C), heart (D), eye (E), muscle (F), thymus (G), bone (H), trachea (I). Results are shown as mean values \pm SEM (n=5). The following statistical symbols were used to denote as follows. AAV8-CNP group vs. WT group, *** $p \leq 0.001$.

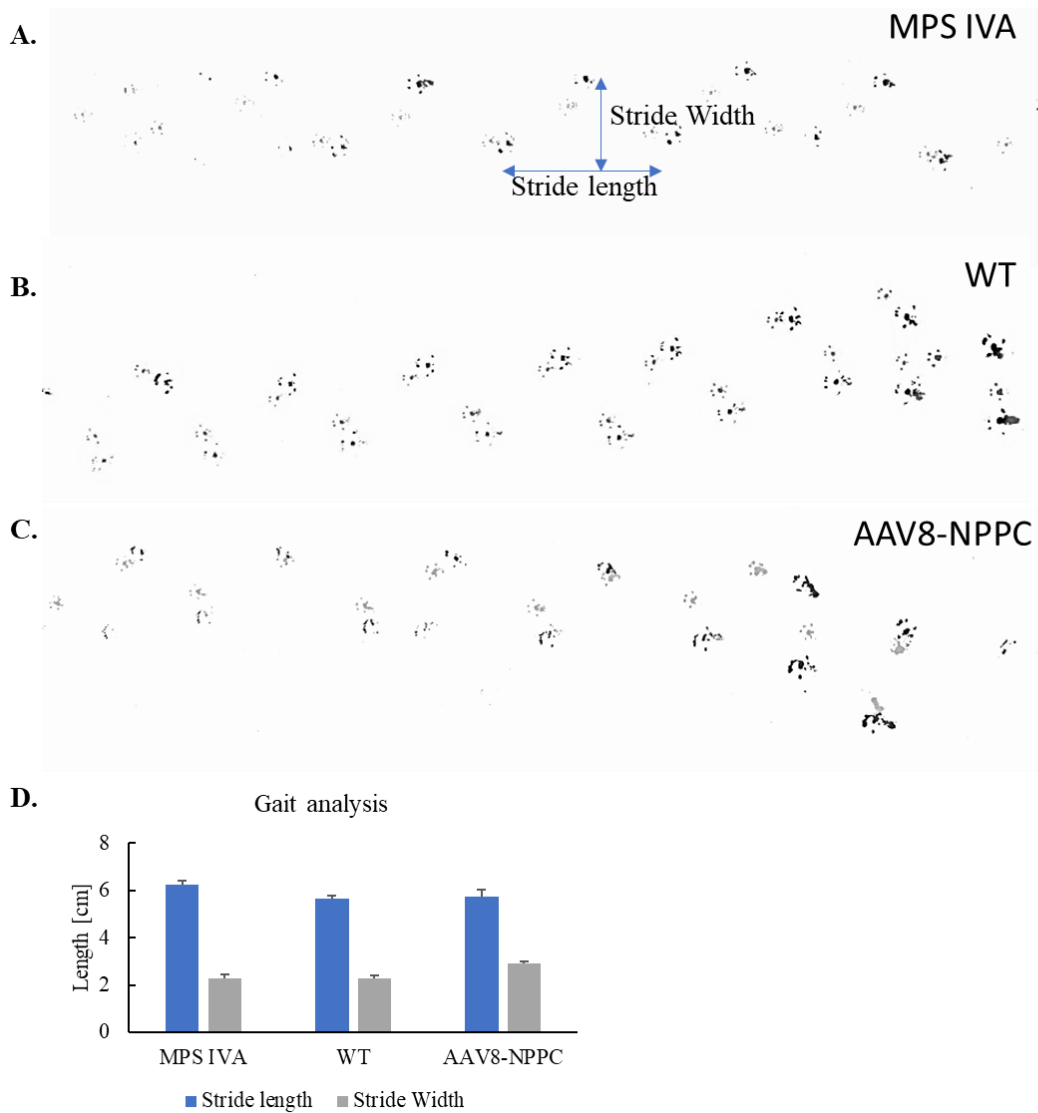


Figure S2. Gait analysis. To analyze the walking pattern of mice, we performed a gait analysis on the final week before the autopsy. Representation of the walking pattern of MPS IVA (A), WT (B), and AAV8-NPPC (C), calculation of stride length and width (D). Results are shown as mean values \pm SEM (n=5). No significant difference was observed between the groups.

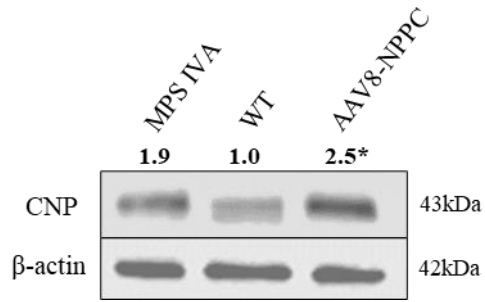


Figure S3. CNP protein expression in the liver tissue. Relative levels of the proteins were measured using the Western-blotting procedure. Representative blots are shown and data were quantitated by densitometry. The following statistical symbols were used to denote as follows. AAV8-CNP group vs. WT group, * $p \leq 0.05$.

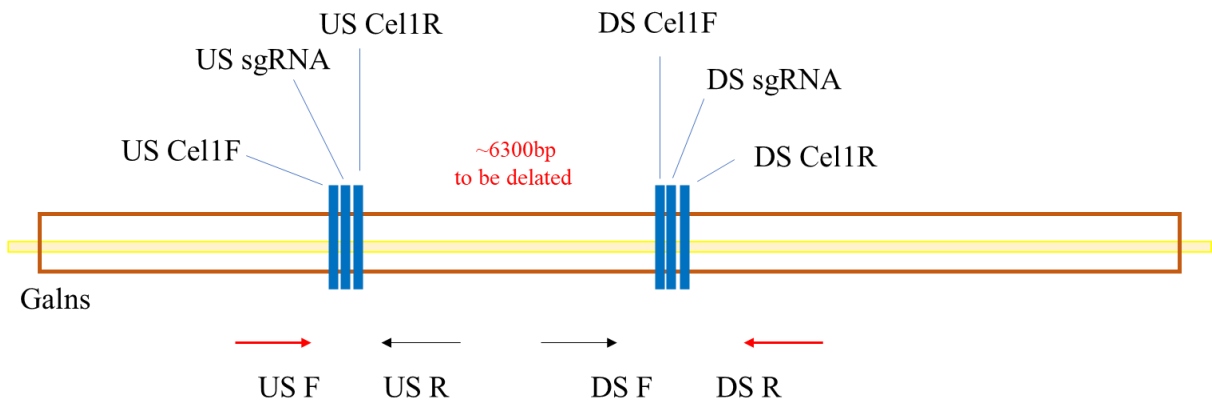


Figure S4. Construct of the GALNS gene deletions. Two pairs of sgRNAs cleaved together to generate a large deletion between two target sites. Primers flanking each sgRNA site were designed to test individual NHEJ activity, as well as paired together (red arrows) to screen for deletion mutations between the two target sites. All mutations were sequence verified. US-upstream, DS-downstream

Authors Contribution

Author Contributions

I hereby declare that my contribution in the research article:

Rintz E, Herreño-Pachón AM, Celik B, Nidhi F, Khan S, Benincore-Flórez E, Tomatsu S. Bone Growth Induction in Mucopolysaccharidosis IVA Mouse. *Int J Mol Sci.* 2023 Jun 8;24(12):9890. doi: 10.3390/ijms24129890. PMID: 37373036; PMCID: PMC10298227.

included:

- Experimental plan
- Animal handling – autopsies, blood collection, measurements, injections of the vector
- Enzyme assay performance and analysis of tissues and plasma
- Analysis and preparation of pathological slides
- ELISA performance and analysis of results
- Genome copy number experiment preparation and analysis
- Glycosaminoglycans level performance and analysis of results
- Micro-CT preparation and analysis of results
- Statistical analysis of all data included in the manuscript
- All Figures preparation and conceptualization
- Literature review
- Visualization of the manuscript
- Writing—original draft preparation
- Writing—review and editing
- Preparation of the responses to the revision



Uniwersytet Gdański
Katedra Biologii Molekularnej
mgr Estera Rintz

Angelica Maria Herreño-Pachón
Nemours Hospital for Children
Wilmington, DE
United States

Wilmington, 10 May 2024

Author Contributions

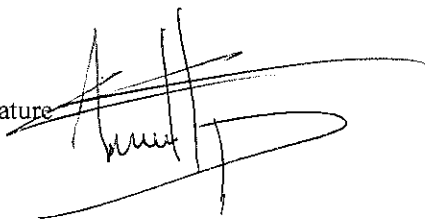
I hereby declare that my contribution in the research article:

Rintz E, Herreño-Pachón AM, Celik B, Nidhi F, Khan S, Benincore-Flórez E, Tomatsu S. Bone Growth Induction in Mucopolysaccharidosis IVA Mouse. Int J Mol Sci. 2023 Jun 8;24(12):9890. doi: 10.3390/ijms24129890. PMID: 37373036; PMCID: PMC10298227.

included:

- Literature review for the project
- Application for the funding – preparing draft for the project
- Participating in the Animal handling – taking part in autopsies, blood collection

Signature

A handwritten signature in black ink, appearing to be 'Angelica Herreño-Pachón', written over a horizontal line. The signature is stylized and includes a large, sweeping flourish at the end.

Shaukat Khan
Nemours Hospital for Children
Wilmington, DE
United States

Wilmington, 5 May 2024

Author Contributions

I hereby declare that my contribution in the research article:

Rintz E, Herreño-Pachón AM, Celik B, Nidhi F, Khan S, Benincore-Flórez E, Tomatsu S. Bone Growth Induction in Mucopolysaccharidosis IVA Mouse. *Int J Mol Sci.* 2023 Jun 8;24(12):9890. doi: 10.3390/ijms24129890. PMID: 37373036; PMCID: PMC10298227.

included:

- Performing LC/MS/MS analysis



Signature

Eliana Benincore-Flórez
Nemours Hospital for Children
Wilmington, DE
United States

Wilmington, 5 May 2024

Author Contributions

I hereby declare that my contribution in the research article:

Rintz E, Herreño-Pachón AM, Celik B, Nidhi F, Khan S, Benincore-Flórez E, Tomatsu S. Bone Growth Induction in Mucopolysaccharidosis IVA Mouse. *Int J Mol Sci.* 2023 Jun 8;24(12):9890. doi: 10.3390/ijms24129890. PMID: 37373036; PMCID: PMC10298227.

included:

- Participating in the analysis of pathology slides

Signature



Name, Surname: Shunji Tomatsu, MD PhD
Institution name: Nemours Children's Health
City: Wilmington, DE
Country: USA

Wilmington, May.13.2024

Author Contributions

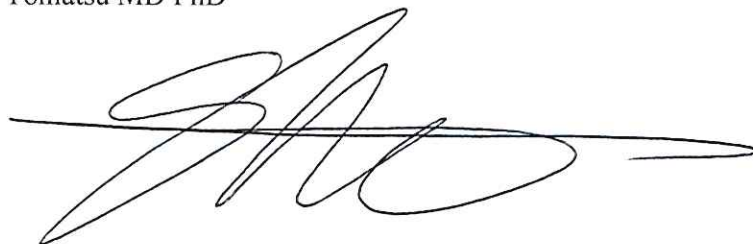
I hereby declare that my contribution in the research article:

Rintz E, Herreño-Pachón AM, Celik B, Nidhi F, Khan S, Benincore-Flórez E, Tomatsu S. Bone Growth Induction in Mucopolysaccharidosis IVA Mouse. Int J Mol Sci. 2023 Jun 8;24(12):9890. doi: 10.3390/ijms24129890. PMID: 37373036; PMCID: PMC10298227.

included:

- Conceptualization of the project
- Writing—review and editing
- Supervision and administration of the project
- Pathology scoring
- Funding acquisition
- Submission of the final version of the manuscript
- Handling manuscript as corresponding author
- Preparation of the responses to the revision

Signature: Shunji Tomatsu MD PhD

A handwritten signature in black ink, consisting of stylized, overlapping loops and a long horizontal stroke extending to the right.

**Rintz, E., Celik, B., Nidhi, F., Herreño-Pachón, A.M., Khan, S.,
Benincore-Flórez, E., Tomatsu, S. (2024)**

Adeno-associated virus-based gene therapy delivering combinations of two growth associated genes to MPS IVA mice. *Molecular Therapy and Nucleic Acids*. 35(2):102211 doi.org/10.1016/j.omtn.2024.102211

Impact Factor = 8.8 (2024)

MNISW Punctuation = 140

Adeno-associated virus-based gene therapy delivering combinations of two growth-associated genes to MPS IVA mice

Estera Rintz,^{1,2} Betul Celik,^{1,3} Nidhi Fnu,^{1,3} Angélica María Herreño-Pachón,^{1,3} Shaukat Khan,^{1,4} Eliana Benincore-Flórez,¹ and Shunji Tomatsu^{1,3,4}

¹Nemours Children's Health, Wilmington, DE 19803, USA; ²Department of Molecular Biology, Faculty of Biology, University of Gdansk, 80-308 Gdansk, Poland; ³Faculty of Arts and Sciences, University of Delaware, Newark, DE 19716, USA; ⁴Department of Pediatrics, Thomas Jefferson University, Philadelphia, PA 19144, USA

Mucopolysaccharidosis type IVA (MPS IVA) is caused by a deficiency of the galactosamine (N-acetyl)-6-sulfatase (GALNS) enzyme responsible for the degradation of specific glycosaminoglycans (GAGs). The progressive accumulation of GAGs leads to various skeletal abnormalities (short stature, hypoplasia, tracheal obstruction) and several symptoms in other organs. To date, no treatment is effective for patients with bone abnormalities. To improve bone pathology, we propose a novel combination treatment with the adeno-associated virus (AAV) vectors expressing GALNS enzyme and a natriuretic peptide C (CNP; NPPC gene) as a growth-promoting agent for MPS IVA. In this study, an MPS IVA mouse model was treated with an AAV vector expressing GALNS combined with another AAV vector expressing NPPC gene, followed for 12 weeks. After the combination therapy, bone growth in mice was induced with increased enzyme activity in tissues (bone, liver, heart, lung) and plasma. Moreover, there were significant changes in bone morphology in CNP-treated mice with increased CNP activity in plasma. Delivering combinations of CNP and GALNS gene therapies enhanced bone growth in MPS IVA mice more than in GALNS gene therapy alone. Enzyme expression therapy alone fails to reach the bone growth region; our results indicate that combining it with CNP offers a potential alternative.

INTRODUCTION

The mucopolysaccharidoses (MPS) are a group of rare inherited lysosomal storage disorders with a total incidence of 1 in 25,000 births.¹ The low incidence of MPS is also caused by the poor prenatal and birth diagnosis of the patients.² MPS group is classified into eight types based on the defective enzyme in the lysosome.^{3,4} When a lysosomal enzyme is defective, it loses its ability to efficiently break down its enzyme substrates, glycosaminoglycans (GAGs). As a result, GAGs build up inside the cell and throughout the entire organism. The symptoms of MPS vary depending on the specific type of the disorder, the defective enzyme, and the accumulated specific GAGs.³

Most symptoms are connected to the GAG accumulation within the body, such as organomegaly, heart dysfunction, hernias, and neuro-

logical and skeletal symptoms.³ Currently, there is no cure for MPS. Treatment options for the MPS include enzyme replacement therapy (ERT) and hematopoietic stem cell transplantation (HSCT). ERT has several limitations: high cost, immune response, weekly administration, and ineffectiveness for bone and brain treatment. HSCT has the limitations of finding a suitable donor, transplant rejection, transplant age limits, invasive procedures, limited correction of the CNS, and skeletal symptoms.^{5,6} Additionally, patients need constant supportive or palliative care that includes rehabilitation, surgical interventions, or medications that can control musculoskeletal, respiratory, ophthalmological, and neurological manifestations.⁷

The most severe symptoms of MPS occur when there is dysfunction in the CNS or skeletal abnormalities.⁸ Novel therapies primarily targeting the CNS are under clinical or preclinical studies and will be available to patients soon. These therapies include receptor-mediated transport of the enzyme (RMT)⁹ or gene therapy.¹⁰ RMT is the direct enzyme modification that targets specific receptors, helping to transport ligands through barriers such as blood-brain barrier. RMT therapy was assessed in several MPS types: MPS I,^{11–13} MPS II,^{14,15} MPS III,^{16,17} and MPS VII.¹⁸ Some of these therapies are approved or in clinics: MPS I (NCT04227600, NCT03053089, NCT02371226) and MPS II (NCT04573023, NCT04251026) (Database: [ClinicalTrials.gov](https://clinicaltrials.gov)). Similarly, our study used a receptor-based approach targeting natriuretic peptide C (CNP) receptors with CNP, which induces bone growth. Gene therapy is extensively studied for MPS patients. It can be distinguished into two main categories depending on the way of vector administration: *in vivo* and *ex vivo* gene therapy. *In vivo* gene therapy is a direct transfer of the viral vector to the organism; it can be through intravenous, intracerebral, or other direct administration routes. *Ex vivo* gene therapy includes more steps: collecting the cells from patients (e.g., stem cells), transduction with the vector of interest, and re-administration of the transduced cells to the patient.¹⁰ Both approaches are studied

Received 13 February 2024; accepted 3 May 2024;
<https://doi.org/10.1016/j.omtn.2024.102211>.

Correspondence: Shunji Tomatsu, Nemours Children's Health, Wilmington, DE 19803, USA.

E-mail: shunji.tomatsu@nemours.org



for the MPS patients in clinics (Table S1). Most potential gene therapies focus on the cross-correction mechanism of the enzyme in the blood flow. The enzyme is expressed in the cell of interest and secreted through the bloodstream to other cells in the body. High expression of the enzyme from viral vector helps to reach hard-to-treat tissues, such as brain or bone.¹⁹ However, elevated transgene expression could potentially impact the organism, leading to a heightened immune response.

Available treatments for MPS can help to manage specific symptoms and extend life expectancy.²⁰ However, individuals with MPS still experience significant challenges due to skeletal abnormalities, including kyphosis, scoliosis, genu valgum, trachea obstruction, joint pain, and severe short stature. Additional therapeutic approaches are needed to address skeletal dysfunction in these disorders, including inflammation reduction and pain management.^{21,22}

The type of accumulated GAGs in the bones determines the specific cells affected. In MPS types I, II, and VI, dermatan sulfate accumulates mostly in bone cells like osteocytes, osteoblasts, and osteoclasts, leading to an imbalance in bone formation. Imbalances in bone formation can result in abnormal bone ossification, growth, and strength, with a consequent risk of osteoporosis.^{23–25} In MPS IVA (Morquio A syndrome), keratan sulfate (KS) accumulates mainly in the bone cartilage. Targeting chondrocyte cells, responsible for cartilage formation in avascular regions of the bone, poses significant challenges in treatment.²⁶ Consequently, additional treatment approaches are necessary to address avascular cartilage tissue and alleviate the burden of skeletal-related symptoms in MPS IVA patients.

Numerous investigations utilize adeno-associated virus (AAV) vectors in bone research, both for delivering a transgene of interest^{27–29} and in more recent studies employing AAV vectors for base editing in the treatment of bone fragility.³⁰ Our prior studies have demonstrated the effectiveness of AAV vectors expressing the galactosamine (N-acetyl)-6-sulfatase (GALNS) enzyme in treating MPS IVA in the mouse model.^{31,32} Our analysis revealed increased enzyme activity and decreased chondrocyte volume due to a cross-correction mechanism.³² However, we did not observe an increased proliferation of chondrocytes. Thus, to address the bone, we used an AAV8 vector expressing the peptide that previously showed bone growth induction in the MPS IVA mice.³³ CNP, a potential bone-penetrating agent, stimulates bone growth by activating the natriuretic peptide receptor B on chondrocytes. Despite its therapeutic promise for skeletal dysplasia, the short half-life of natural CNP and the need for repeated injections of modified CNP currently limit its effectiveness. Our previous results showed that CNP effectively targets chondrocytes, activating its proliferation and differentiation in the growth plate of MPS IVA mice.³³

In this article, our objective was to evaluate a combined therapy in a mouse model of MPS IVA. This therapeutic strategy involved gene therapy applying two different transgenes.

We focused on two primary issues observed in MPS IVA patients: KS and C6S accumulation and bone growth failure. To achieve this goal,

we administered AAV vectors co-expressing two transgenes, the GALNS enzyme and the bone growth-inducing peptide, CNP. AAV9 has a broader targeting range within the body, affecting tissues such as striated muscles, liver, bone, and the CNS, potentially leading to greater expression of the vector; thus, we used this serotype for GALNS expression.^{34–37} AAV8 also has a broad range of targeted tissues when delivered locally,^{38–43} with the greatest transduction efficacy in hepatocytes out of all AAV serotypes in different models.^{37,38} Considering our familiarity with AAV vectors, we opted for AAV8 as the expression vector for CNP, which will be expressed more in liver. This choice was made to prevent potential overexpression in one particular tissue. Also, we avoided antibodies against one specific serotype raised, causing more immune reactions and adverse effects. Our experiments highlight the significance of carefully controlling the dosage of CNP to avoid unintended immune reactions.

RESULTS

Growth induction in MPS IVA by combination therapy is dose dependent

To establish the effects of combination therapy gene therapy with CNP and GALNS enzyme on the MPS IVA mouse model, we injected intravenously vectors according to Figure 1 under housekeeping promoter CAG into 4-week-old mice.

Mice were measured weekly for weight and length (nose to tail and nose to anus). Additionally, pictures were obtained on the autopsy day to observe physiological differences (anatomical) among treated mice (Figure 2A). The body weights of MPS IVA and wild-type (WT) mice were significantly different only at week 4 (Figure 2B). In the combination therapy, we observed a difference only in group 7 treated with two vectors AAV9-hGALNS and AAV8-hNPPC (dose 4×10^{13} GC/kg + 4×10^{13} GC/kg) starting from week 4 in comparison to WT mice and at weeks 9, 10, and 12 in comparison with the untreated MPS IVA mice. Weight differences were insignificant in any other groups during the experiment. We measured growth patterns in all experimental groups weekly. There was no difference between untreated MPS IVA and WT groups. During the experiment, mice in groups 5–7 were injected with two vectors (NPPC and GALNS) separately, and mice in group 4 received dual AAV vectors with two tandem genes (Figures 2C and 2D). There was no difference in growth parameters in the group injected with only the AAV9-hGALNS vector compared with the WT or untreated MPS IVA mouse group. We saw significant differences between groups in the growth pattern. Mice in group 7 were treated with two vectors, AAV9-hGALNS and AAV8-hNPPC (dose 4×10^{13} GC/kg + 4×10^{13} GC/kg), which had the highest dose of CNP and their rapid growth pattern. The difference was significant in the first week after the injection, with more than 2 cm in both measurements (nose to tail and nose to anus) compared with the WT and MPS IVA mice. Growth was stabilized around week 11; however, mice started to have abnormal motion and were terminated at week 13. Due to overgrowth, we decreased the dose of the injected AAV8-NPPC in the next groups. Mice injected with the lowest dose of the CNP-expressing vector showed slight differences in weeks 7 and 9–12; we did not

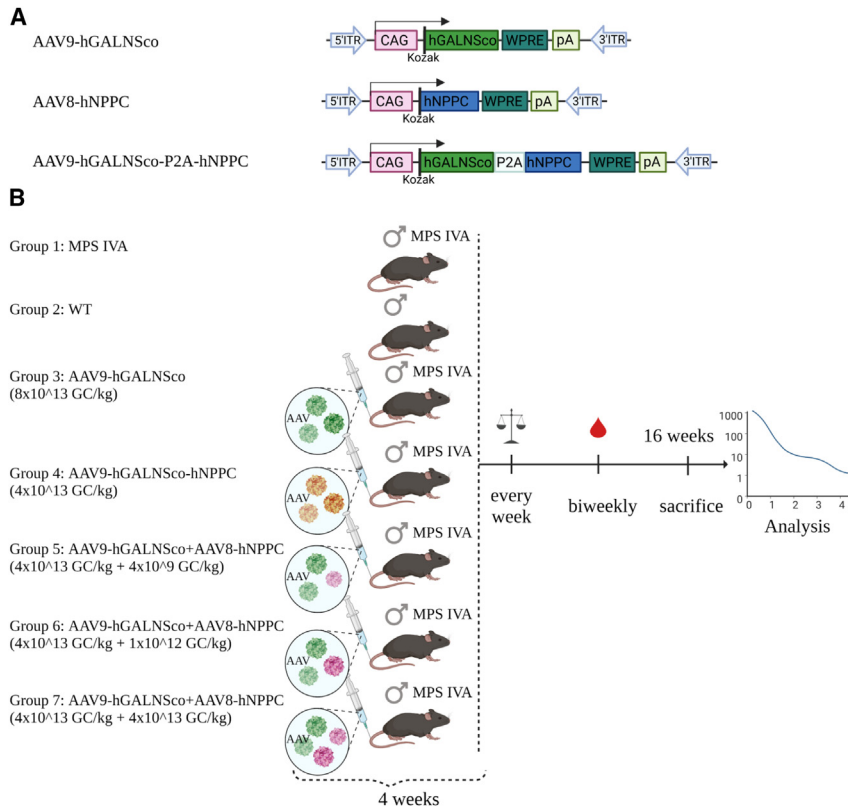


Figure 1. Experimental design

(A) An AAV vector construct. We used three AAV vectors containing synthetic ubiquitous CAG promoter. (B) Experiments started at 4 weeks of age. We have seven experimental groups: (1) untreated MPS IVA; (2) WT control (WT); (3) MPS IVA mice AAV9 vector expressing human GALNS enzyme (AAV9-hGALNS); (4) MPS IVA mice AAV9 vector expressing two transgenes-human GALNS enzyme and human CNP (AAV9-hGALNSco-hNPPC); and three groups (5, 6, and 7) of combination therapy with the same vectors with different dosage (AAV9-hGALNS+ AAV8-hNPPC). During the experiments, mice were measured weekly for body weight, nose-tail length, and nose-anus length, with biweekly blood collection. Mice were euthanized at 16 weeks (except group 7, which was euthanized at 13 weeks). After that, the analysis was undertaken. This figure was prepared using [BioRender.com](https://www.biorender.com).

see a difference in growth pattern in the other weeks. As the difference in the lowest dose was minimal in comparison with WT and MPS IVA mice, we administered the middle dose of the AAV8-NPPC injected with two vectors AAV9-hGALNS and AAV8-hNPPC (dose 4×10^{13} GC/kg + 1×10^{12} GC/kg) (group 6). In group 6, we saw a significant difference in the growth pattern, starting at week 5 and stabilizing at week 9. Group 4, with two tandem transgenes, showed a higher growth pattern than group 7. In group 4, the difference in growth started at week 7 compared with WT and MPS IVA mice.

AAV9-hGALNS delivery increases GALNS activity

Before performing *in vivo* experiments, we evaluated the transduction efficacy of the AAV9-hGALNS vector in human fibroblast cell lines (either healthy or MPS IVA patients). At 48 h after transduction with the vector, we saw an elevation of the GALNS enzyme activity in MPS IVA patient's cell lines using a multiplicity of infection (MOI) (10^5 and 10^6). We did not see a difference in the enzyme activity between MOIs, and neither MOI reached the activity level of cells from healthy individuals (Figure S1). Therefore, we used a high dose of AAV9-hGALNS in a mouse model of MPS IVA. The mouse model used in this study was the MPS IVA knockout mice (MKC2; C57BL/6 background), as described previously.³³ These mice lack GALNS enzyme activity, resulting in the accumulation of storage material (KS) in various tissues and plasma. These biomarkers (enzyme activity and substrate accumulation) were extensively used to assess the severity of the phenotype and measure the effectiveness

of various therapeutic approaches in MPS IVA patients and animal models.^{44–47} We collected several tissues (liver, bone, trachea, muscle, spleen, heart, lung, eye, thymus, and brain) (Figure 3A) to evaluate the enzyme activity. Additionally, we evaluated plasma GALNS enzyme activity every other week to see the progression of the therapy (Figure 3B). We saw increased GALNS enzyme activity in tissues collected in all treated groups. In group 3, which was treated with only AAV9-hGALNSco, we saw a supraphysiological level of GALNS enzyme activity in every tissue, except trachea and brain. Plasma enzyme activity showed increased expression starting from week 6 and gradually increased until week 16. Group 4, which was treated with dual AAV vector expressing tandem genes, GALNS and CNP, showed that the enzyme activities in liver and heart were similar to those of WT; in other tissues, the activity was either not detected or was on the lower level. Plasma enzyme activity in group 4 was not detected during the experiment. Combination therapy of two separately injected vectors (groups 5–7) showed that the GALNS activity exceeded WT expression in all tissues except trachea and brain. The same pattern was seen in the plasma GALNS activity.

Additionally, we quantified the GALNS protein by western blot to evaluate the possible outcome of lower enzyme activity in group 4 injected with AAV9-hGALNS-hNPPC. We saw a higher level of liver GALNS protein in group 4 compared with WT mice, consistent with the enzyme activity (Figure 4A). All groups had significantly higher GALNS protein levels than the WT mouse group. As the protein concentration and enzyme activity were synchronized, we also measured anti-GALNS antibodies in the final week (Figure 4B). Based on our previous results,³¹ we anticipated an increase in antibody levels throughout the weeks of the experiment, peaking around the final weeks. Therefore, we drew our conclusions on the antibody levels from the final week, correlating them with the enzyme activity. In group 4, no GALNS enzyme activity was seen in plasma

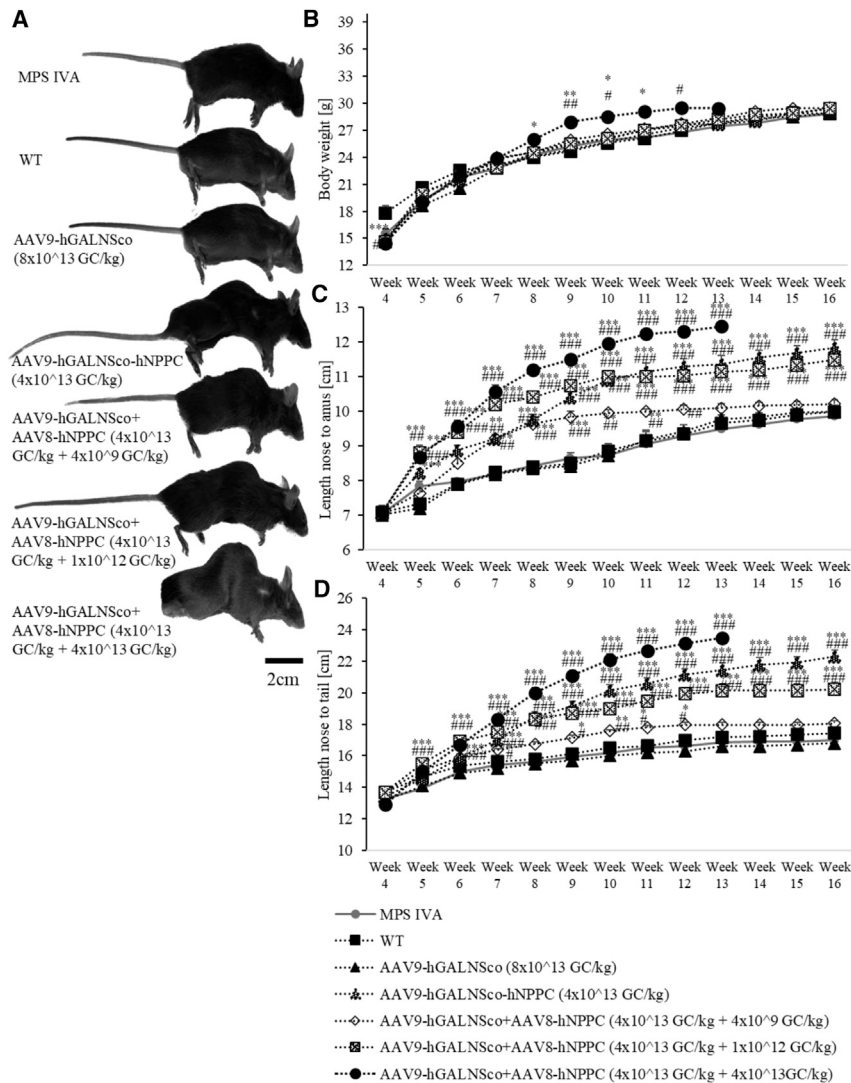


Figure 2. Dose-dependent growth induction in MPS IVA mice

Seven experimental groups are presented: (1) untreated MPS IVA; (2) WT control (WT); (3) MPS IVA mice AAV9 vector expressing human GALNS enzyme (AAV9-hGALNS); (4) MPS IVA mice AAV9 vector expressing two transgenes-human GALNS enzyme and human CNP (AAV9-hGALNSco-hNPPC); and three groups (5, 6, and 7) of combination therapy with the same vectors with different dosages (AAV9-hGALNS+ AAV8-hNPPC). (A) Picture of mice on the day week of the experiment. (B) Body weight of mice during the experiment. (C) Body length measurement from nose to anus of mice during the experiment. (D) Body length measurement from nose to tail of mice during the experiment. Results are shown as mean values \pm SEM (n = 5). The following statistical symbols were used to denote the following vs. WT group, ***p \leq 0.001, **p \leq 0.01, *p \leq 0.05; vs. untreated MPS IVA group, ###p \leq 0.001, ##p \leq 0.01, #p \leq 0.05.

throughout all the checkpoints (weeks 4–16), while we saw the highest anti-GALNS antibodies in the final week. Moreover, even though group 7 had high antibodies, the expression of the GALNS was high enough not to clear the enzyme from the bloodstream.

GAGs in blood and tissues decreased as a result of AAV-GALNS delivery

To measure the effectiveness of the AAV vector therapy at autopsy, we measured mono-sulfated KS, the major KS component, and dermatan sulfate (DS; Di4S) in both plasma and tissues (liver, bone, heart, and lung). The levels of these two GAGs are shown in Figure 5. KS was accumulated in plasma and all tissues except the heart (Figure 5A) of the MPS IVA mouse model. After treatment with any vector, we saw a decrease in KS levels in plasma and all tissues except heart. We saw the accumulation of the DS only in liver samples of MPS IVA compared with the WT mice (Figure 5B). After treatment with any vector, we saw decreased Di4S (DS) accumulation in the

liver. We did not detect differences in bone samples. Additionally, we measured the level of other GAGs in the tissues and plasma: O-sulfated heparan sulfate (DiHS-0S) and N-sulfated heparan sulfate (DiHS-NS) (Figure S2). We did not observe significant differences between the MPS IVA and WT mice in the measured GAGs. For the DiHS-0S (Figure S2B), we only saw an increase in plasma for groups 6 and 7 compared with both WT and MPS IVA mice. The only increase in the DiHS-NS (Figure S2C) was in groups 6 and 7 in lungs.

AAV vector biodistribution and expression

To establish the biodistribution of the vectors, we performed digital PCR (dPCR) in bone and liver during the study (Figure 6). Both vectors (expressing human GALNS and NPPC) were undetected in bone and liver in WT and untreated MPS IVA groups. GALNS was detected in all groups in both bone (Figure 6A) and liver (Figure 6B). The highest vector copy number for the GALNS was detected in group 3, which was injected with only the AAV9-hGALNS vector in bone; other groups had similar copy numbers. In the case of NPPC, the biodistribution of the dual vector with two transgenes (group 4) was the highest in both bone and liver (Figures 6C and 6D) compared with other groups. For the vector with the lowest dose of NPPC (group 5), the NPPC vector was undetectable in both bone and liver. In the middle dose (group 6), it was undetectable in bone and with minimal detection in liver (Figures 6C and 6D). In the highest dose of combination therapy (group 7), the NPPC vector was detected in both bone and liver, but it was lower than in group 5 (Figures 6C and 6D).

Additionally, we measured the plasma level of human NT-proCNP as a marker of CNP expression (Figure 6E). Human NT-proCNP was

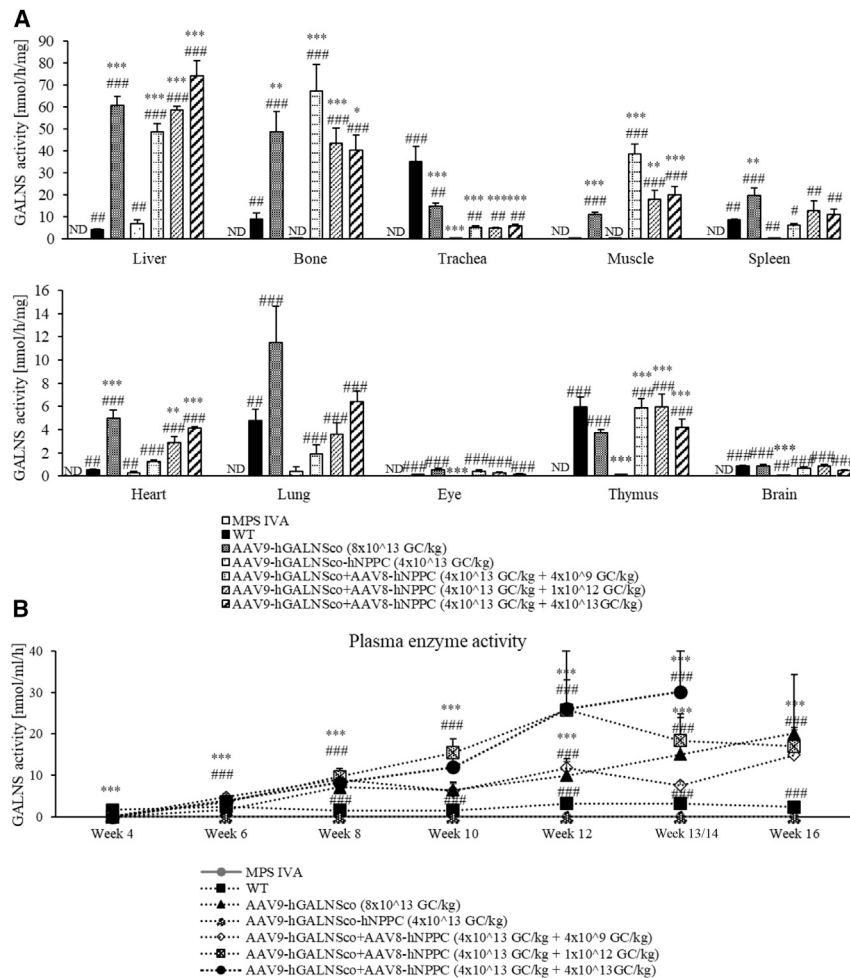


Figure 3. GALNS enzyme activity in MPS IVA mice treated with AAV9-hGALNS vector

Seven experimental groups are presented: (1) untreated MPS IVA; (2) WT control (WT); (3)MPS IVA mice AAV9 vector expressing human GALNS enzyme (AAV9-hGALNS); (4) MPS IVA mice AAV9 vector expressing two transgenes-human GALNS enzyme and human CNP (AAV9-hGALNSco-hNPPC); and three groups (5, 6, and 7) of combination therapy with the same vectors with different dosages (AAV9-hGALNS+ AAV8-hNPPC). (A) GALNS activity in tissues (liver, bone, trachea, muscle, spleen, heart, lung, eye, thymus, and brain). (B) Plasma GALNS activity during the experiment. The figure represents week 13/14 because group 7 was terminated in week 13, while other groups had blood collected at week 14. Results are shown as mean values ± SEM (n = 5). The following statistical symbols were used to denote the following vs. WT group, ***p ≤ 0.001, **p ≤ 0.01, *p ≤ 0.05; vs. untreated MPS IVA group, ###p ≤ 0.001, ##p ≤ 0.01, #p ≤ 0.05.

detected at the highest level in group 7 in comparison with other groups. It was undetectable in group 5, and minimal detection was observed in group 4 injected with two transgenes (Figure 6E).

We performed immunohistochemistry staining to investigate the presence of the GALNS enzyme in the bone growth plate (Figure S3). The expression of GALNS in WT and AAV9-hGALNSco was on the same level. We did not detect any bone GALNS expression in the AAV9-hGALNSco-hNPPC vector. In the combination therapy group, the GALNS expression level was similar to the highest expression in the bone marrow region of the bone (Figures S3E–S3G).

Micro-computed tomography

We analyzed cortical and trabecular bone structure by using micro-computed tomography (micro-CT). Micro-CT created a 3D representation of the specimen using X-ray attenuation data, enabling direct measurements of bone morphology. We used micro-CT to examine bone morphometry in seven experimental groups, focusing on both trabecular and cortical bone (Figure 7). We did not see significant differences between WT and untreated MPS IVA mice. Treatment with

AAV9-hGALNSco significantly increased trabecular separation (Figure 7E), compared with WT and MPS IVA mice. AAV9-hGALNSco-hNPPC and AAV9-hGALNSco+AAV8-hNPPC (group 5) treatments were not significantly different, while treatment with AAV9-hGALNSco+AAV8-hNPPC (group 6) increased bone area (Figure 7J) and cortical thickness (Figure 7N) compared with both WT and MPS IVA. In group 7 with a high dose of combination therapy, an increase of values was seen in trabecular volume of interest (Figure 7A), total area (Figure 7I), and medullary area (Figure 7L), while a decrease was seen in the percent bone volume (Figure 7C), trabecular thickness (Figure 7F), bone mineral density (Figure 7G), BA/TA (Figure 7K), and cortical thickness (Figure 7N).

Induction of chondrocyte proliferation

Knee joint lesions were assessed using toluidine blue staining 12 weeks after the administration of AAV vectors in MPS IVA mice. In untreated MPS IVA mice, GAG storage vacuoles were observed in the growth plate and articular cartilage of the tibia (Figure 8), as well as in the articular disc and growth plate of femur and meniscus region (Figures S5 and S6). The growth plate region was also disorganized, characterized by chondrocytes with vacuolation (Figures 8 and S4–S6).

We evaluated the improvement of vacuoles and disorganized column structures in knee joints of MPS IVA mice using pathological scores, which showed a tendency of improvement in MPS IVA mice treated with the combination therapy of AAV vector expressing GALNS and CNP compared with untreated mice. The pathological score of MPS IVA mice treated with groups AAV9-hGALNSco+AAV8-hNPPC

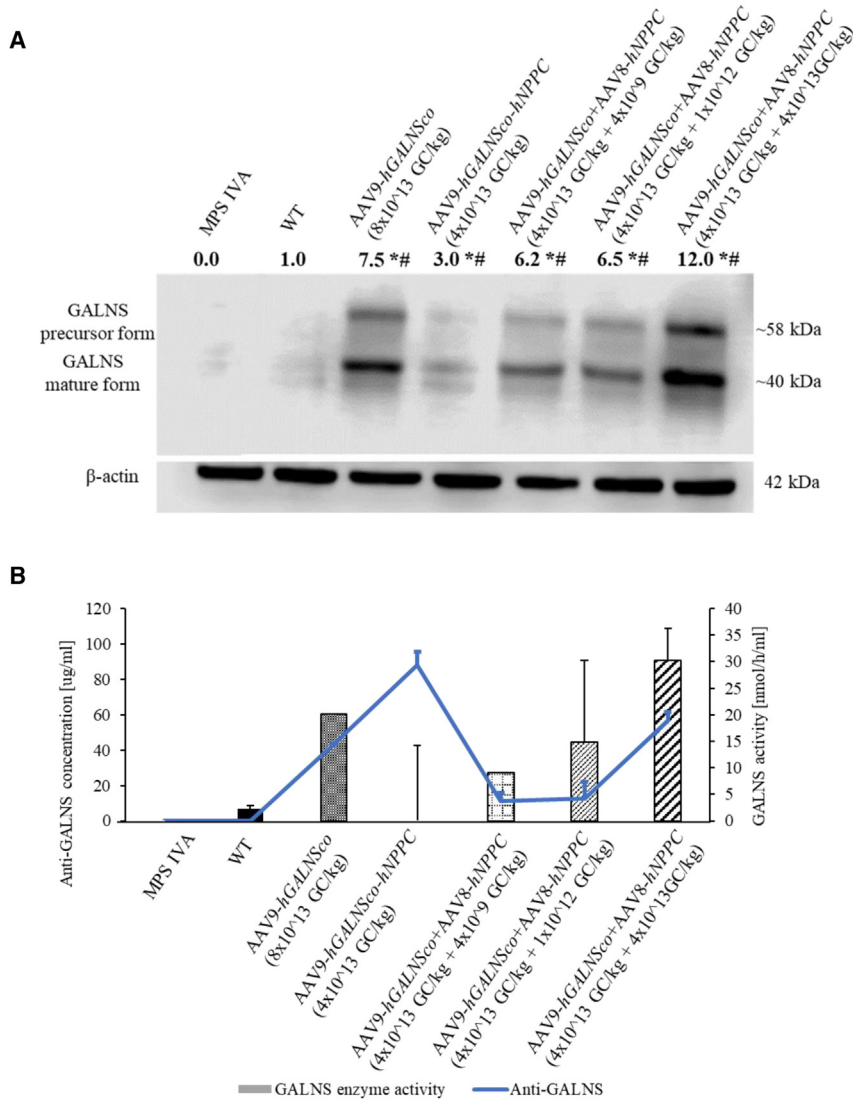


Figure 4. GALNS expression and anti-GALNS antibodies

Seven experimental groups are presented: (1) untreated MPS IVA; (2) WT control (WT); (3) MPS IVA mice AAV9 vector expressing human GALNS enzyme (AAV9-hGALNS); (4) MPS IVA mice AAV9 vector expressing two transgenes-human GALNS enzyme and human CNP (AAV9-hGALNSco-hNPPC); and three groups (5, 6, and 7) of combination therapy with the same vectors with different dosages (AAV9-hGALNS+ AAV8-hNPPC). (A) Liver GALNS protein level measured by western blot; calculated analysis of the mature form of the GALNS protein. (B) Correlation of plasma enzyme activity with GALNS clearance antibodies. Results are shown as mean values \pm SEM (n = 5). The following statistical symbols were used to denote the following vs. WT group, * $p \leq 0.001$; vs. untreated MPS IVA group, # $p \leq 0.001$.

AAV9-hGALNSco + AAV8-hNPPC (groups 6 and 7), was lower than in the untreated MPS IVA group. None of the treatments reached the WT level in the score pathology analysis.

DISCUSSION

MPS IVA exerts its most profound impact on the skeletal system, leading to skeletal dysplasia and restricted endurance. This dysplasia significantly decreases mobility and often necessitates multiple surgeries on the hip, legs, trachea, and spine. During the lifetime of the patients, the length of the trachea outgrows skeletal growth, leading to airway obstruction, one of the most life-threatening conditions for the patients.^{48–50} Therapeutic interventions in patients address skeletal (mostly surgeries) and non-skeletal symptoms (ERT and HSCT). ERT improved endurance, lung capacity, and walking ability.⁵¹ Nevertheless, long-term evaluations have shown that pulmonary function decreased over time.⁵¹ Even when patients received ERT before 2 years of age, their growth did not improve.⁵² MPS IVA patients also face life-threatening cardiovascular issues, leading to high morbidity and mortality. In MPS IVA, the small size of the left ventricle decreases stroke volume and increases heart rate, while impaired diastolic filling arises from thickened left ventricle and heart valves. After ERT, cardiovascular function did not change for older patients.⁵¹ Early implementation of ERT stabilizes cardiac hypertrophy, but valvular heart disease may take several years to stabilize.⁵³ ERT for MPS IVA patients decreases KS levels (decreased organomegaly) and improves endurance; however, it has a minor to no effect on the skeletal, pulmonary, and cardiac problems attributed to a considerable part of the mortality rate in MPS IVA patients.⁵⁴ HSCT showed better improvement than ERT in skeletal abnormalities. Ten years after transplantation, patients showed a decreased need for surgical intervention and delayed progression of skeletal dysmorphia.

(groups 6 and 7) was significantly lower for the column structure of chondrocytes in the growth plate area of tibia and femur bone compared with those treated with MPSIVA, but not as low as the WT level (as shown in Table 1). The vacuolization of chondrocytes in the articular cartilage area was compared with those treated with MPSIVA. The WT level was lower than in the treated groups (groups 6 and 7). The column structure of chondrocytes in the articular cartilage area of tibia was improved after combination treatment AAV9-hGALNSco+AAV8-hNPPC (groups 5, 6, and 7), as well as in the AAV9-hGALNSco (group 3) alone. However, a notably lower score compared with untreated MPS IVA was explicitly observed in the columnar structure of chondrocytes within the articular cartilage region of the femur. This effect was evident only after treatment with a higher dose of CNP in the combination therapy AAV9-hGALNSco+AAV8-hNPPC (group 7). Regarding the vacuolization of chondrocytes in the ligament area, the score in two groups,

(groups 6 and 7) was significantly lower for the column structure of chondrocytes in the growth plate area of tibia and femur bone compared with those treated with MPSIVA, but not as low as the WT level (as shown in Table 1). The vacuolization of chondrocytes in the articular cartilage area was compared with those treated with MPSIVA. The WT level was lower than in the treated groups (groups 6 and 7). The column structure of chondrocytes in the articular cartilage area of tibia was improved after combination treatment AAV9-hGALNSco+AAV8-hNPPC (groups 5, 6, and 7), as well as in the AAV9-hGALNSco (group 3) alone. However, a notably lower score compared with untreated MPS IVA was explicitly observed in the columnar structure of chondrocytes within the articular cartilage region of the femur. This effect was evident only after treatment with a higher dose of CNP in the combination therapy AAV9-hGALNSco+AAV8-hNPPC (group 7). Regarding the vacuolization of chondrocytes in the ligament area, the score in two groups,

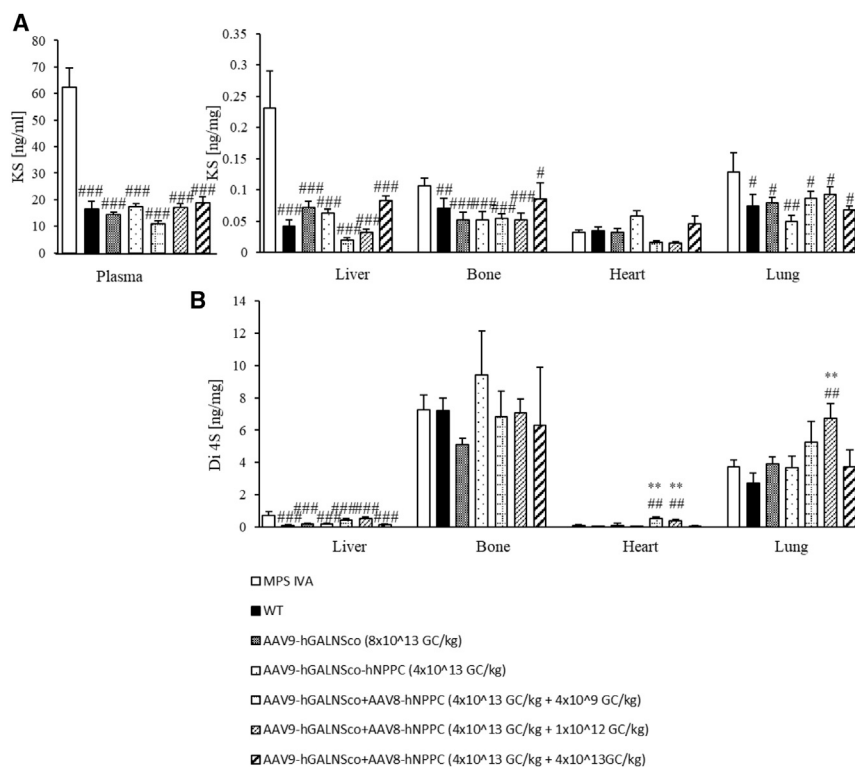


Figure 5. GAG levels in MPS IVA mice treated with AAV vectors

Seven experimental groups are presented: (1) untreated MPS IVA; (2) WT control (WT); (3) MPS IVA mice AAV9 vector expressing human GALNS enzyme (AAV9-hGALNS); (4) MPS IVA mice AAV9 vector expressing two transgenes—human GALNS enzyme and human CNP (AAV9-hGALNSco-hNPPC); and three groups (5, 6, and 7) of combination therapy with the same vectors with different dosages (AAV9-hGALNS+ AAV8-hNPPC). At 12 weeks after treatment, the level of GAG was measured: Mono-sulfated KS levels (A) plasma, liver, bone, heart, and lung; chondroitin disaccharide (Di 4S) levels in (B) liver, bone, heart, and lung. Results are shown as mean values \pm SEM ($n = 5$). The following statistical symbols were used to denote the following vs. WT group, *** $p \leq 0.001$, ** $p \leq 0.01$, * $p \leq 0.05$; vs. untreated MPS IVA group, ### $p \leq 0.001$, ## $p \leq 0.01$, # $p \leq 0.05$. See also Figure S2.

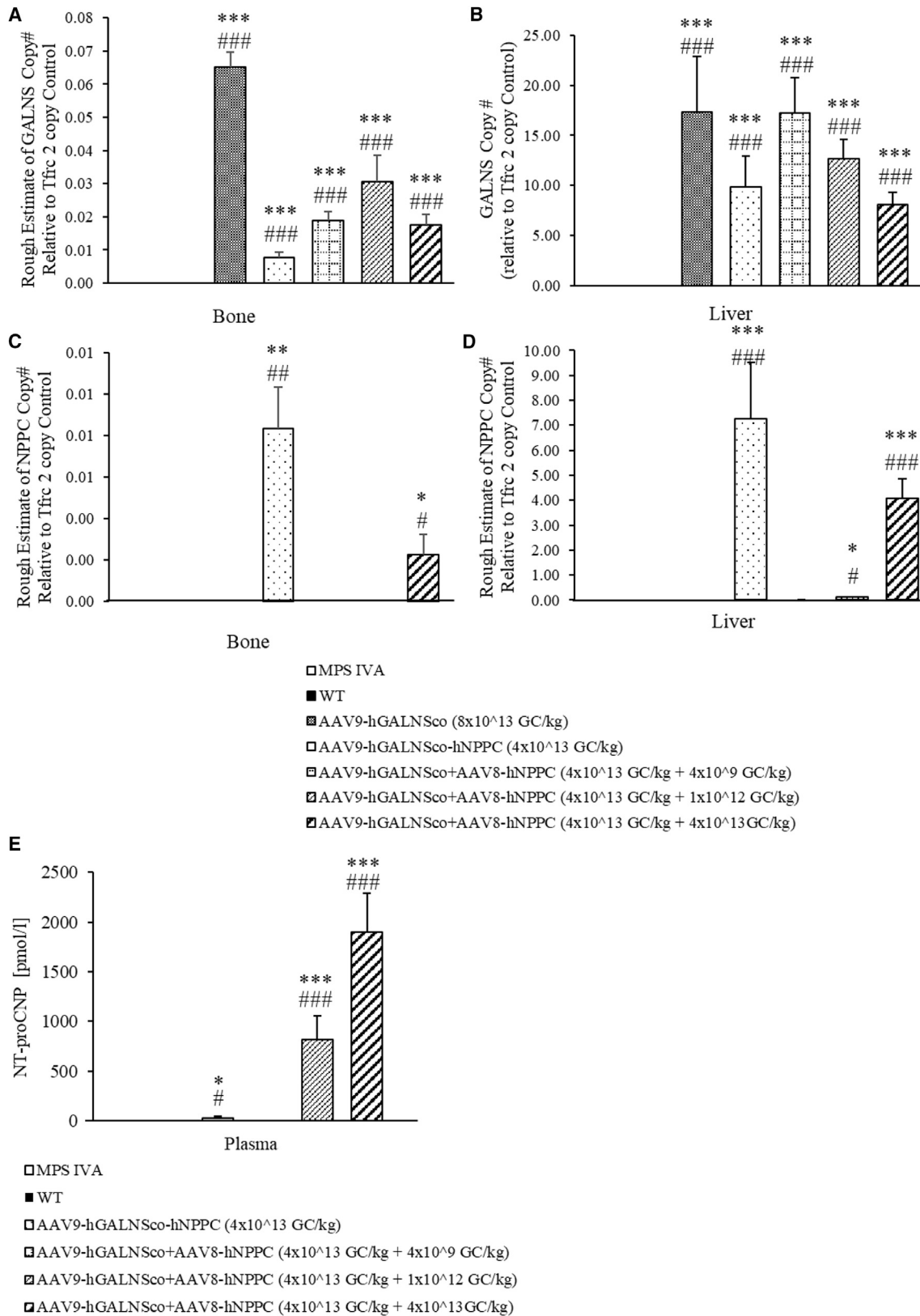
However, HSCT still has a minor effect on bone-related issues, although we need to increase the number of patients who undergo HSCT at an earlier stage (<2 years of age).⁵⁵ Despite these benefits, HSCT has various drawbacks, including finding a suitable donor, the risk of graft-versus-host disease, and procedure-related complications.

None of the currently available treatment options for MPS IVA patients improve bone growth. CNP maintains cartilage homeostasis and facilitates endochondral bone formation. In a mouse model, when the NPPC gene responsible for CNP production was inactivated, bone growth, birth rate, and skull size were decreased. However, no significant differences were observed in other organs or body weight.^{56–59} Inducing bone growth through CNP involves binding to the Npr3 receptor located on the cell surface, followed by the downstream activation of cyclic GMP-dependent protein kinase II (discussed in Rintz et al.⁶⁰). In our earlier experiments, we examined the effectiveness of incorporating the CNP into the AAV8 vector expression cassette for the first time. When MPS IVA mice were treated with this CNP-containing AAV vector, we observed a notable increase in growth, accompanied by consistent maintenance of body weight,³³ similar to other studies.^{61–64} Furthermore, we observed a more organized chondrocyte structure within the growth plate, characterized by enhanced proliferation and differentiation.³³

In this study, combining two distinct vectors in MPS IVA mice revealed different responses while yielding positive outcomes. Analysis

of combination therapy revealed how two distinct vectors can express separate transgenes that work synergistically. The mechanism of AAV transduction in the cell starts with binding to the cell surface receptors (1), then vector encapsulated by the endosome (2), then escaping (3), entering the nucleus after uncoating the viral ssDNA (4), transcription with the use of host polymerases (5), and transgene released to the cytoplasm and going through translation (6).⁶⁵ The GALNS enzyme will go through further processing in the Golgi apparatus to be an active form of the enzyme that can act both locally and be secreted outside the cell.¹⁹ As for CNP, after translation, it is further cleaved by cytoplasmic enzymes to an active form of the peptide.^{66,67}

The treatment approach resulted in the sustained elevation of GALNS activity in the bloodstream and notable GALNS activity in crucial target tissues, such as bone, heart, and liver. Furthermore, there was a significant decrease in the accumulation of KS both in the blood and tissues, leading to improvements in bone pathology and the promotion of bone growth in a dose-dependent manner. The experiment involved injecting two separate vectors, each expressing a different transgene or a single vector expressing both transgenes (CNP and GALNS). Initially, an equal dose of AAV expressing human GALNS and AAV expressing human NPPC (group 7) was administered. The high dose of both transgenes increased GALNS enzyme and CNP expression. However, the experiment had to be terminated at 13 weeks of age due to the overexpression of the CNP, which led to excessive growth in the mice (Figure 2). Consequently, the mice faced difficulties in movement, indicating that CNP effects are dose dependent. Thus, we decreased the dose of the CNP-expressing vector, decreasing the mouse growth to a minimum (group 6). With the middle dose of the CNP, the growth was linear without a negative outcome (group 5). We also evaluated the effect of the growth pattern in the mice after



(legend on next page)

injecting one vector with two transgenes (group 4) separated with a P2A sequence. The P2A sequence enables the co-expression of multiple proteins from a single mRNA transcript by inducing ribosomal skipping during translation.⁶⁸ The growth was linear without overgrowth in this group (Figure 2). In conclusion, the bone growth seen in our study is not due to GALNS, but rather CNP. It is also critical to have the optimal CNP vector dose to avoid excessive growth. Decreasing the accumulated KS in the bone and tissues is one of the primary goals in the MPS IVA patient treatment. The KS level corresponds with the disease's clinical severity.^{54,69} In humans, ERT does not change blood KS levels and skeletal symptoms⁷⁰ while improving urine KS accumulation.^{71,72} Thus, circulating KS in the bloodstream might indicate better therapeutic efficacy for the skeletal symptoms.^{69,73} We evaluated the efficacy of the GALNS-expressing AAV gene therapy. After administration of the AAV-containing GALNS cDNA, the enzyme activity increased in most groups 2 weeks after injection into untreated MPS IVA mice. We did not detect enzyme activity in mice treated with AAV9-hGALNS-hNPPC (group 4) (Figure 3B). In other groups, GALNS enzyme activity in plasma correlated with plasma KS level reduction at the final week of treatment. In group 4, no GALNS activity was detected. However, we observed the same decrease in the KS level as in other groups (Figure 5A). The tissue enzyme activity showed that combination therapy (groups 5–7) with two separate vectors had higher activity than one vector containing two transgenes (group 4) (Figure 3A). The greatest amount of enzyme expression was seen in the liver, but we also detected overexpression in bone, heart, and other tissues. Overexpression in the tissues correlated with the decrease in the KS level. In group 4, we did not detect the enzyme activity in bone, although GALNS activity reached the WT level in liver and heart. This might be due to the P2A sequence being too close to the GALNS sequence, leading to a change in the protein conformation P2A peptides lead to relatively high levels of downstream protein expression compared with other strategies for multigene co-expression, and they are small in size, thus bearing a lower risk of interfering with the function of co-expressed genes. Several different groups have successfully employed P2A peptides for polycistronic and bi-cistronic multigene expression.^{74–80} Therefore, it is possible to have a high level of CNP downstream, although it impacts GALNS gene upstream because of the instability of the GALNS protein with the additional amino acid at the C-terminal. In the final week, we also detected high anti-GALNS activity in group 4, which may neutralize the GALNS activity (Figure 4B). Additionally, the GALNS protein level in liver was lower than in the other combination groups (Figure 4A). In group 4, the level of transgene expression in tissues and blood effectively decreased

KS accumulation in tissues and plasma, including bones, despite there being no GALNS enzyme activity.

The biodistribution of the vectors showed that the vector expressing GALNS was present in both bone and liver for all tested groups (Figures 6A and 6B). In group 4, which was treated with a single vector containing two transgenes, we detected the GALNS protein in both bone and liver, although we did not detect GALNS activity in bone despite a decreased KS level in bone. A small residual activity of GALNS or cross-correction may account for this decrease. For the NPPC biodistribution, we detected it (Figures 6C and 6D) in groups 4, 6, and 7, which exhibit growth induction (Figure 2). Furthermore, we assessed the expression of human NT-proCNP as a reliable indicator of CNP expression (Figure 6E). Its extended lifespan demonstrated a noteworthy correlation with the biologically active CNP concentration, making it a valuable marker for evaluating CNP expression levels.⁸¹ We saw a correlation between increased NT-proCNP and growth induction after treatment. Improvement of bone pathology with two vectors of a high dose of AAV8-hNPPC and AAV9-hGALNS was observed. CNP also increased the size and the number of chondrocytes in the articular cartilage and growth plate; in addition, the vacuoles decreased. It remains unknown why the high-dose group impacts the vacuolization in chondrocytes.

The bone-targeted therapy was evaluated by measuring GALNS protein expression in bone. Our findings demonstrated that a small fraction of GALNS can be provided in bone through cross-correction and direct bone targeting, as depicted in the vector biodistribution (Figure 6). Significant GALNS expression was observed primarily in bone marrow (Figure S3), with the highest levels detected in the group receiving a combination of two vectors (groups 5–7). As for the AAV9-hGALNS-injected group, the GALNS detection level was similar to the WT level (Figure S3C). Conversely, in the group receiving only one vector (group 4), GALNS staining was not detected (Figure S3D). Regarding bone pathology, micro-CT assessment did not reveal significant differences in most parameters among the various groups (Figure 7). The lack of significant differences can be attributed to challenges in mouse imaging studies, including small bone size, critical voxel size choices, potential site heterogeneity, and age-related bone loss, making subtle variations harder to detect. However, the group receiving the highest dose of the NPPC-expressing vector in combination (group 7) exhibited the most noticeable changes, which correlated with the visible alterations in the skeleton (Figure 2A). We performed bone staining with toluidine blue to

Figure 6. AAV vector biodistribution and NT-proCNP expression

Seven experimental groups are presented: (1) untreated MPS IVA; (2) WT control (WT); (3) MPS IVA mice AAV9 vector expressing human GALNS enzyme (AAV9-hGALNS); (4) MPS IVA mice AAV9 vector expressing two transgenes-human GALNS enzyme and human CNP (AAV9-hGALNSco-hNPPC); and three groups (5, 6, and 7) of combination therapy with the same vectors with different dosages (AAV9-hGALNS+ AAV8-hNPPC). Bone (A) and liver (B) GALNS vector copy number at 12 weeks after treatment; bone (C) and liver (D) NPPC vector copy number at 12 weeks after treatment. Marker for CNP expression in plasma (NT-proCNP) is higher in groups 4, 6, and 7 compared with WT and untreated MPS IVA groups (E). Results are shown as mean values \pm SEM (n = 5). The following statistical symbols were used to denote comparison with ***p \leq 0.001, **p \leq 0.01, *p \leq 0.05 significant differences compared with the WT group; ###p \leq 0.001, ##p \leq 0.01, #p \leq 0.05 significant differences compared with the untreated MPS IVA group.

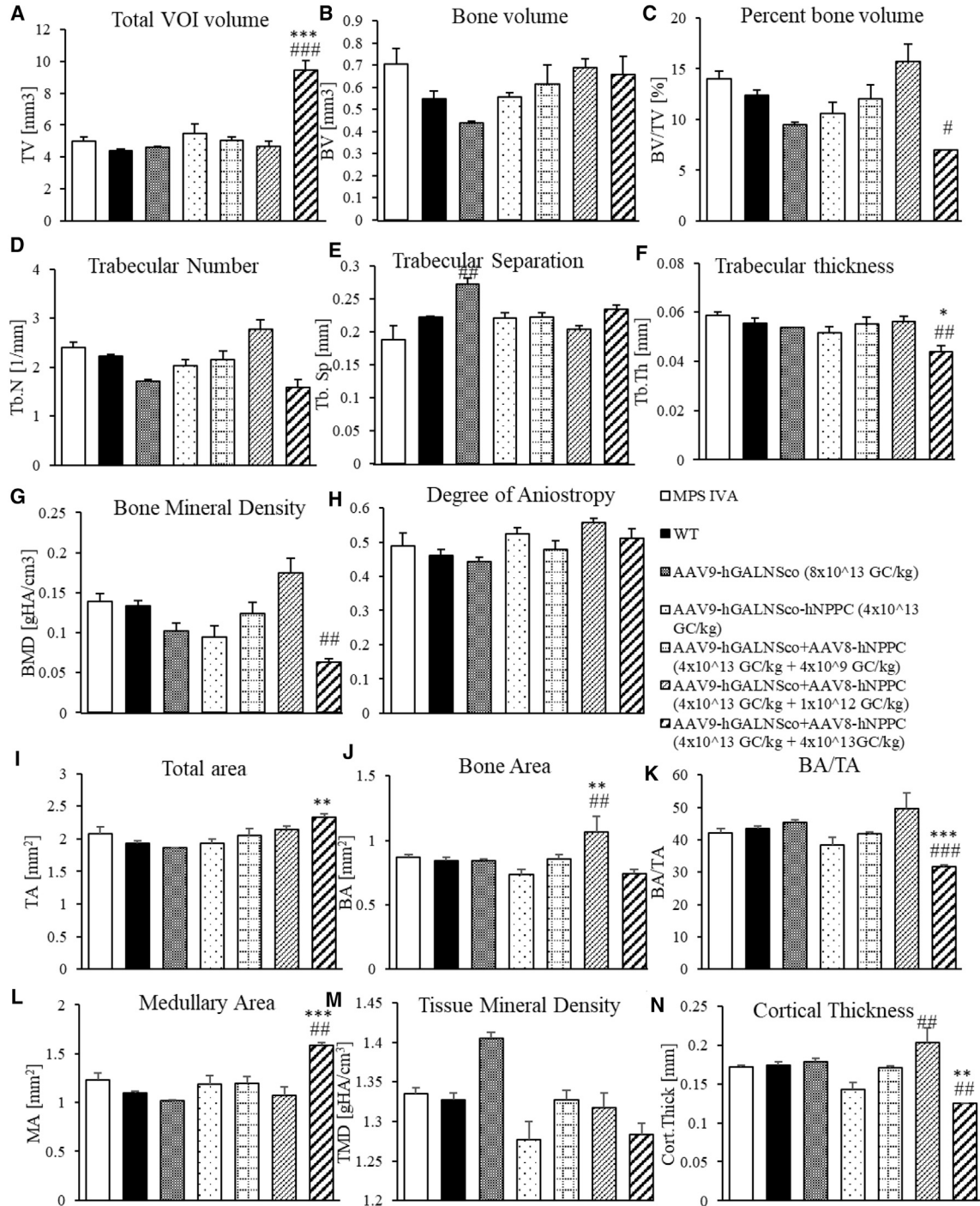


Figure 7. Trabecular and cortical morphometry after AAV vector treatment

Seven experimental groups are presented: (1) untreated MPS IVA; (2) WT control (WT); (3) MPS IVA mice AAV9 vector expressing human GALNS enzyme (AAV9-hGALNS); (4) MPS IVA mice AAV9 vector expressing two transgenes-human GALNS enzyme and human CNP (AAV9-hGALNSco-hNPPC); and three groups (5, 6, and 7) of combination therapy with the same vectors with different dosages (AAV9-hGALNS+ AAV8-hNPPC). At 12 weeks after treatment, micro-CT analysis of trabecular (A–H) and cortical (I–N) bone of seven experimental groups was performed. Trabecular analysis included (n = 5; except group 7 that was n = 3): total trabecular volume of interest (A); trabecular bone

(legend continued on next page)

evaluate the effectiveness of AAV treatment. Bone pathology revealed significant differences in the score calculation of chondrocytes (Table 1). The untreated MPS IVA chondrocytes are vacuolated with a disorganized structure (Figures 8 and S4–S6). After combination therapy of the AAV vector with CNP, we saw improvements in growth plate organization and decreased vascularization of treated chondrocytes. Our study has offered valuable insights into the potential therapeutic use of CNP for progressive skeletal dysplasia in MPS IVA. However, we must acknowledge certain limitations. First, the small sample size used in our study may affect the statistical power and the significance of the conclusions. Thus, more extensive studies are necessary to validate the effectiveness of CNP delivered through an AAV vector expression cassette in combination with the GALNS enzyme as a potential combination therapy.

Patients with MPS IVA cannot catabolize two molecules—chondroitin sulfate and KS—due to a lack of GALNS enzyme activity. As these two molecules are the main GAGs in the cartilage, their excessive accumulation in MPS IVA patients damaged cartilage tissues, including growth plates, leading to various skeletal symptoms. The growth plate region of the bone is an avascular structure, and ERT is not an accessible option for patients.²² Earlier investigations involving the combined administration of CNP and ERT in a MPS VII mouse model demonstrated favorable results for treatment, surpassing the outcomes of individual monotherapies. This combined approach enhanced bone growth and increased enzyme activity.⁸² Nonetheless, the constraints associated with ERT remain a challenge. Consequently, we propose a potentially superior long-term solution: an AAV therapy to facilitate continuous enzyme expression.

In conclusion, bone growth with high GALNS enzyme activity is proven with co-expression of GALNS and CNP genes, especially in separate cassette vectors. It is recommended that the optimal dose of the CNP vector is defined with a more significant number of mice to eliminate undesired overgrowth and adverse effects, moving forward to a clinical trial. It may be considered to add a microRNA system^{83,84} to stop the CNP gene expression when we observe the excessive growth.

MATERIALS AND METHODS

Expression vector

To overexpress the human native NPPC gene and/or codon-optimized human GALNS enzyme gene, three AAV vectors were used: pAAV[Exp]-CAG>hNPPC[NM_024409.4]:WPRE; pAAV[Exp]-CAG>{hGALNSco}:WPRE; pAAV[Exp]-CAG>hGALNS[NM_001323544.2](ns):P2A:hNPPC[NM_024409.4]:WPRE (VectorBuilder, Chicago, IL, USA).

Experimental design

All procedures for this study were approved by the Institutional Animal Care and Use Committee of Nemours Children's Health. Mice were housed in a 12/12h light/dark cycle with food and water provided *ad libitum*. The experimental design is shown in Figure 1B, with seven experimental groups (n = 5, unless stated otherwise), two control groups (WT and untreated MPS IVA), and five treated groups (groups 3–7). We injected 4-week-old male mice intravenously with one or two of the AAV vector(s) (Figure 1A) depending on the experimental group, as shown in Figure 1B. In the case of groups 3 and 4, mice were injected with one vector. As for groups 5–7, mice were injected with two vectors; the AAV9-hGALNS vector was injected with the same dose of 4×10^{13} GC/kg, while the dosage of the AAV8-hNPPC differs in the groups (group 5: 4×10^9 GC/kg; group 6: 1×10^{12} GC/kg; and group 7: 4×10^{13} GC/kg). Mice were measured (length and weight) weekly, and blood was collected biweekly for 12 constitutive weeks. At 16 weeks of age, mice were euthanized in a CO₂ chamber and perfused with 10 mL 0.9% saline, except for group 7, which was euthanized at 13 weeks. Tissues were collected for further analysis.

MPS IVA mouse model

This study used a previously described mouse model of the MPS IVA knockout mice (MKC2; C57BL/6 background).³³ Mice did not have GALNS enzyme activity and showed an accumulation of storage material in many tissues and plasma. We performed genotyping at 20 days of age by PCR. Primers were designed to flank each single guide RNA site, allowing for the evaluation of individual nonhomologous DNA end-joining activity and screening for deletion mutations between the two target sites when paired.

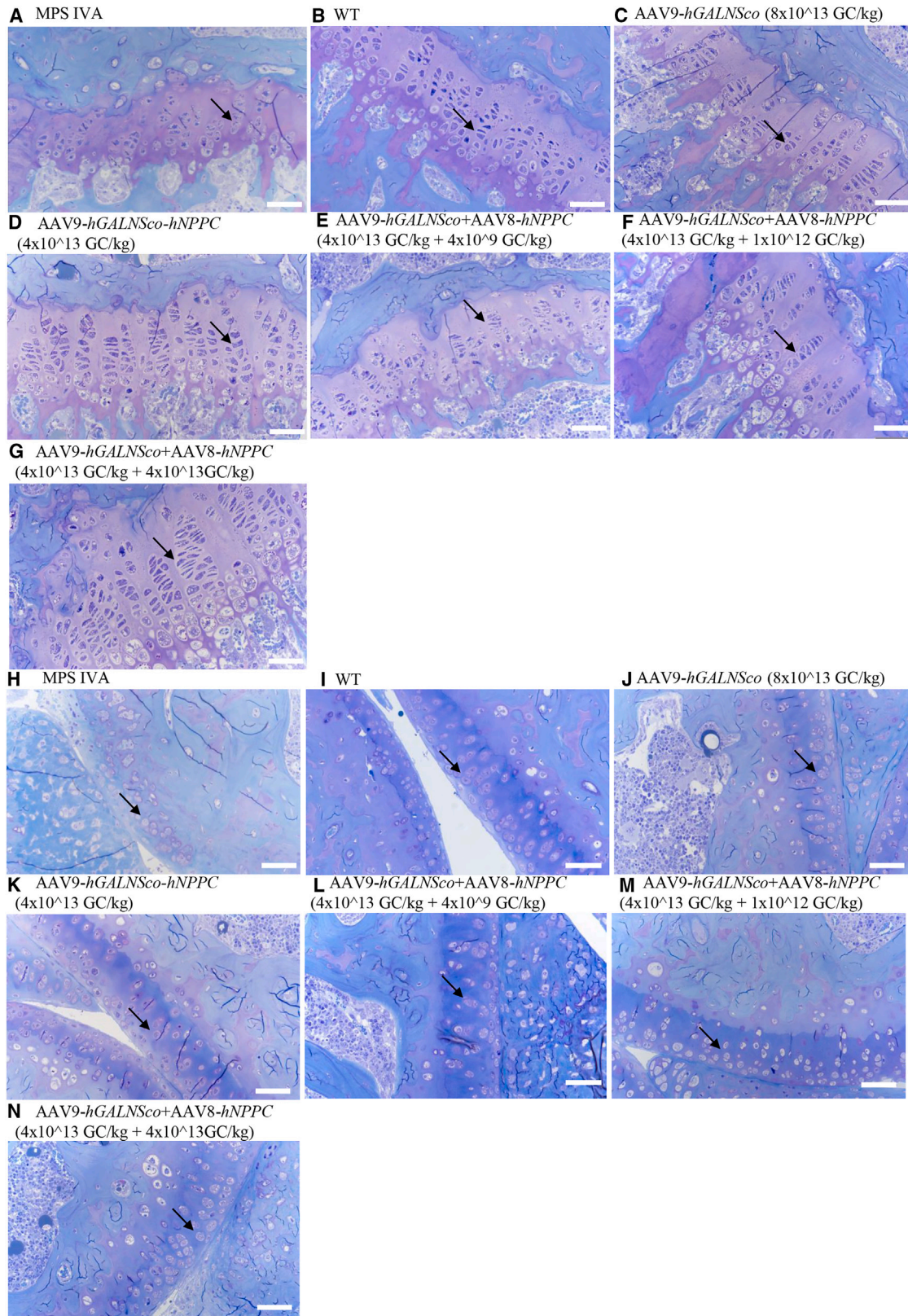
Cell lines

Human fibroblasts (either a healthy patient or MPS IVA patient) were plated onto six-well plates (3×10^5 cells/well) and incubated overnight at 37°C in a humidified 5% CO₂ incubator before transduction. After incubation, cells were transduced with the AAV9-hGALNS vector at MOI 10⁵/well and 10⁶/well. The next day, we changed the medium of the cells. At 48 h after transduction, we collected cells for GALNS enzyme assay measurement.

GALNS enzyme activity assay

A GALNS enzyme activity assay was performed as previously described.³³ Human fibroblast pellets were lysed with the lysis buffer (25 mM/L Tris-HCl (pH 7.2) and 1 mM/L phenylmethylsulphonyl fluoride). Then, lysed cells were centrifuged for 30 min at 4°C, and the supernatant was collected in a new tube and assayed for enzyme activity. Tissues were homogenized with Bead Mill Homogenizer (OMNI International, Kennesaw, GA, USA) supernatant was used

volume (B), percent bone volume (C), trabecular number (D), trabecular separation (E), trabecular thickness (F), bone mineral density (G), and degree of anisotropy (H). Cortical analysis included (n = 5; except group 7, n = 3): Total area (I), cortical bone area (J), bone area/total area (K), medullary area (L), tissue mineral density (M), and cortical thickness (N). Results are shown as mean values ± SEM. The following statistical symbols were used to denote comparison with ***p ≤ 0.001, **p ≤ 0.01, *p ≤ 0.05 significant differences compared with the WT group; ###p ≤ 0.001, ##p ≤ 0.01, #p ≤ 0.05 significant differences compared with the untreated MPS IVA group.



(legend on next page)

for the assay. Either tissue/cell lysate or plasma (2 μ L) was used for the enzymatic reaction with 22 mM 4-methylumbelliferyl- β -galactopyranoside-6-sulfate (Research Products International, Mount Prospect, IL, USA) and incubated at 37°C for 16 h. After incubation, 10 mg/mL β -galactosidase from *Aspergillus oryzae* (Sigma-Aldrich, St. Louis, MO, USA) was added and incubated for 2 h at 37°C. To stop the reaction, a 1 M glycine NaOH solution (pH 10.5) was used, and the resulting mixture was subjected to measurement using a FLUOstar Omega plate reader (BMG LABTECH Inc., Cary, NC, USA) at an excitation wavelength of 366 nm and an emission wavelength of 450 nm. The enzyme activity is expressed as nanomoles of 4-methylumbelliferone released per hour per microliter of plasma or milligram of protein. The protein concentration in the samples was determined using a bicinchoninic acid protein assay kit (Thermo Fisher Scientific, Waltham, MA, USA).

GAGs quantification

GAG assay was determined in plasma and tissues as previously described.³²

Bone pathological assessments

Tissue staining and analysis were performed as described previously.^{32,33} Briefly, knee joints were collected from 16-week-old MPS IVA and WT mice to evaluate levels of storage granules by light microscopy. Tissues were fixed in 2% paraformaldehyde and 4% glutaraldehyde in PBS, post-fixed in osmium tetroxide, and embedded in Spurr's resin. Then, toluidine blue-stained 0.5- μ m-thick sections were examined. To evaluate chondrocyte cell size (vacuolization) in the growth plates of femur or tibia, approximately 300 chondrocytes in the proliferative area were measured in each mouse by ImageJ software, and results were expressed as folds-change from the WT group. Pathological slides from knee joints of treated and untreated MPS IVA and WT mice were evaluated for reduced vacuolization and improved column orientation in growth plates (Table 1). The amount of storage materials and the degree of disoriented columns were scored. No storage or very slight was 0 (–), slight but obvious was 1 (+), moderate was 2 (++), and marked was 3 (+++). Each pathological slide was assessed in a double-blind manner three times.³³ We then averaged the scores in a group of mice per section of bone (growth plate, articular disc, meniscus, and ligament).

Trabecular and cortical morphometry

Trabecular and cortical morphometry measurements were carried out using micro-CT scans performed with a Bruker SkyScan 1275

scanner (Bruker, Billerica, MA, USA) as previously described.³³ To prepare the samples, the right femur from 16-week-old mice was fixed using 96% ethanol. Prior to analysis, the femur was carefully wrapped in gauze soaked in 0.9% NaCl and subjected to scanning. Quantitative analysis was conducted using Bruker CTan software (v1.21.1.0). The regions of interest (ROIs) for trabecular bone were identified by focusing on the distal epiphyseal plate. As for cortical bone, the ROIs were determined based on the starting point of the distal epiphyseal plate and the highest point in the proximal greater trochanter. The total length of the bone was obtained by considering the area between these two landmarks.

AAV vector genome biodistribution

dPCR was performed to assess the biodistribution of DNA vectors. For this purpose, DNA was extracted from the liver with the Genra Puregene kit, following the manufacturer's instructions (-QIAGEN, Germantown, MD, USA). As for the bone, prior to purification, it was homogenized using the Bead Mill Homogenizer (OMNI International), and subsequently purified according to the provided guidelines (QIAGEN). To perform dPCR analysis, specific primers and probe sequences targeting either the NPPC or GALNS gene (Table S2) were used to amplify genomic DNA obtained from liver and bone samples of mice. Genomic DNA was tested in both non-fragmented and fragmented forms, the latter achieved through enzymatic digestion or an M220 Focused-ultrasonicator (Covaris, Woburn, MA, USA). Quantitative dPCR analysis of the AAV CNP-expressing vector was conducted using the TaqMan assay (FAM-labeled) (Thermo Fisher Scientific, Waltham, MA, USA). The DNA concentration for the AAV chip in the liver and bone samples ranged between 0.5 and 2 ng per 16-mL reaction, depending on the required DNA concentration to ensure detectability on the instrument. The Tfrc TaqMan copy number reference assay (VIC labeled) was acquired from Thermo Fisher Scientific. For the Tfrc dPCR, 40 ng genomic DNA per 16-mL reaction was utilized. Each reaction was loaded onto a separate QuantStudio chip (QuantStudio 3D digital PCR 20K chip kit v2, A26316; Thermo Fisher Scientific). PCR amplification was carried out using an ABI GeneAmp 9700 PCR thermal cycler with dual flat blocks (Applied Biosystems, Waltham, MA, USA). The QuantStudio 3D instrument was employed to read the chips, enabling the determination of the number of wells positive for the VIC and FAM channels, as well as the number of wells without DNA and empty wells. Subsequent data analysis and chip quality assessment were performed using the QuantStudio 3D

Figure 8. Correction of bone pathology in MPS IVA mice treated with AAV vectors assessed by toluidine blue staining analysis using light microscopy

Seven experimental groups are presented: (1) untreated MPS IVA; (2) WT control (WT); (3) MPS IVA mice AAV9 vector expressing human GALNS enzyme (AAV9-hGALNS); (4) MPS IVA mice AAV9 vector expressing two transgenes-human GALNS enzyme and human CNP (AAV9-hGALNSco-hNPPC); and three groups (5, 6, and 7) of combination therapy with the same vectors with different dosages (AAV9-hGALNS+ AAV8-hNPPC). Tibia growth plate of untreated MPS IVA (A), WT (B), AAV9-hGALNSco (8×10^{13} GC/kg) (C), AAV9-hGALNSco-hNPPC (4×10^{13} GC/kg) (D), AAV9-hGALNSco+AAV8-hNPPC (4×10^{13} GC/kg + 4×10^9 GC/kg) (E), AAV9-hGALNSco+AAV8-hNPPC (4×10^{13} GC/kg + 1×10^{12} GC/kg) (F), and AAV9-hGALNSco+AAV8-hNPPC (4×10^{13} GC/kg + 4×10^{13} GC/kg) (G). Tibia articular cartilage of untreated MPS IVA (H), WT (I), AAV9-hGALNSco (8×10^{13} GC/kg) (J), AAV9-hGALNSco-hNPPC (4×10^{13} GC/kg) (K), AAV9-hGALNSco + AAV8-hNPPC (4×10^{13} GC/kg + 4×10^9 GC/kg) (L), AAV9-hGALNSco + AAV8-hNPPC (4×10^{13} GC/kg + 1×10^{12} GC/kg) (M), and AAV9-hGALNSco+AAV8-hNPPC (4×10^{13} GC/kg + 4×10^{13} GC/kg) (N). Original magnification $\times 40$, with 500- μ m scale bar. Arrows show chondrocytes. See also Figures S4–S6.

Table 1. Pathological scores in bone of MPS IVA mice treated with AAV vectors

			MPS IVA	WT	AAV9-hGALNSco	AAV9-hGALNSco-hNPPC	AAV9-hGALNSco+ AAV8-hNPPC	AAV9-hGALNSco+ AAV8-hNPPC	AAV9-hGALNSco+ AAV8-hNPPC
Bone	Structure	Finding	-	-	8×10^{13} GC/kg	4×10^{13} GC/kg	4×10^{13} GC/kg $+4 \times 10^9$ GC/kg	4×10^{13} GC/kg $+1 \times 10^{12}$ GC/kg	4×10^{13} GC/kg $+4 \times 10^{13}$ GC/kg
	growth plate	vacuolization	2.9 ± 0.1	0.0	2.8 ± 0.1	2.9 ± 0.1	2.9 ± 0.1	2.4 ± 0.2	2.4 ± 0.3 #
		column structure	2.8 ± 0.1	0.0	2.5 ± 0.1	2.6 ± 0.2	2.7 ± 0.1	2.1 ± 0.2 #	2.2 ± 0.2 #
Tibia	articular cartilage	vacuolization	2.9 ± 0.1	0.0	2.8 ± 0.1	2.9 ± 0.1	2.7 ± 0.1 #	2.7 ± 0.1 #	2.6 ± 0.1 #
		column structure	2.9 ± 0.2	0.0	2.7 ± 0.1 #	2.8 ± 0.1	2.7 ± 0.1 #	2.5 ± 0.1 #	2.4 ± 0.1 #
	growth plate	vacuolization	2.8 ± 0.2	0.0	2.9 ± 0.1	3.0 ± 0.1	3.0 ± 0.1	2.7 ± 0.1	2.2 ± 0.1 #
		column structure	3.0 ± 0.1	0.0	2.8 ± 0.1	2.8 ± 0.1	3.0 ± 0.1	2.5 ± 0.1 #	2.1 ± 0.3 #
Femur	articular cartilage	vacuolization	2.9 ± 0.1	0.0	2.8 ± 0.1	2.8 ± 0.1	2.8 ± 0.1	2.6 ± 0.1 #	2.3 ± 0.2 #
		column structure	2.9 ± 0.1	0.0	2.6 ± 0.1	2.8 ± 0.1	2.8 ± 0.1	2.5 ± 0.1	2.2 ± 0.1 #
Ligament		vacuolization	3.0 ± 0.0	0.0	N/A	3.0 ± 0.0	2.7 ± 0.2	2.3 ± 0.1 #	2.0 ± 0.1 #
Meniscus		vacuolization	2.9 ± 0.1	0.0	2.7 ± 0.2	3.0 ± 0.0	2.7 ± 0.2	2.7 ± 0.1	2.6 ± 0.2

Results are shown as mean values \pm SEM (n = 4–7). The following statistical symbols were used to denote comparison with #p \leq 0.01, significant differences to untreated MPS IVA group.
N/A, not available.

analysis suite. All chips contained between 25% and 75% empty wells, ensuring their suitability for quantitation. Copies per milliliter for both Tfrc and AAV were calculated and normalized using the dilution factor for the AAV sample input. The number of AAV copies per mouse genome was calculated by employing the Tfrc results as a reference for two copies.

ELISA

NT-proCNP was detected in mice according to manufacturer instructions (Biomedica Medizinprodukte, Vienna, Austria). Sample preparation included blood collected from mice to be centrifuged at $8,000 \times g$ at 4°C for 10 min to collect plasma sample to another tube and stored at -20°C until further analysis. Plasma used for NT-proCNP detection was diluted 1:100 in the assay buffer provided in the ELISA kit.

Anti-GALNS IgG and IgE antibodies was detected by indirect ELISA in treated and untreated mice according to a previously published paper.⁸⁵ Ninety-six-well polystyrene microplates were coated with $2 \mu\text{g/L}$ rh galactosamine (N-acetyl)-6-sulfatase/GALNS; lot#DDJU0319021 (R&D Systems, Minneapolis, MN, USA) ($0.2 \mu\text{g/well}$) diluted in coating buffer (15 mM Na_2CO_3 , 35 mM NaHCO_3 , 0.02% NaN_3 , pH = 9.6) and incubated overnight at 4°C . After overnight incubation, the plate was washed with TBST buffer (TBS-Tween: 10 mM Tris pH = 7.5, 150 mM NaCl, 0.05% Tween 20). The plate was blocked for 1 h with 3% bovine serum. Plasma (1:100 dilution in TBST) or standard (GALNS Polyclonal rabbit antibodies cat#PA5-22098; 1 mg/mL; 100 μL) was added and incubated for 2.5 h at 37°C . After incubation, the plate was washed $4 \times$ with TBST, and then 100 μL peroxidase substrate TMB (3,3',5,5'-tetramethylbenzidine; Thermo Fisher Scientific) was added and incubated for 30 min at RT on moving rotor. The reaction was stopped with 1N HCl. The plate was read at 450 nm, and the

OD was measured using a FLUOstar Omega plate reader (BMG LABTECH Inc.).

Immunohistology staining

Tibia was collected in the final week and fixed in 10% formalin. Formalin-fixed paraffin-embedded samples were processed from fixed tissue. The samples were cut at $5 \mu\text{m}$ on a Leica RM2255 microtome (Leica, Buffalo Grove, IL, USA) and floated onto Superfrost Plus slides (Thermo Fisher Scientific, Fremont, CA, USA). The sections were heat immobilized for 60 min in a 60°C oven. Slides were deparaffinized on a Sakura (Torrance, CA, USA) Stainer using xylene, 100% ETOH, 95% ETOH, and 80% ETOH. Antigen retrieval was performed by adding slides to Bond ER 2 solution (Leica) in a 60°C oven overnight, cooled down, and then rinsed in de-ionized water, after which the slides were stained using the Novolink Min Polymer Detection System (Leica Biosystems-RE7290-K). The slides were rinsed in Bond Wash (Leica-AR-9590), and then briefly placed into peroxidase block, rinsed in bond wash, then incubated in their prospective antibody: rabbit anti-GALNS (Creative Biolabs, Shirley, NY, USA) for 30 min. The slides were then rinsed in bond wash solution and incubated in the polymer. After additional rinses of bond wash, the slides were developed in the DAB kit, rinsed, and then counterstained with hematoxylin from the kit. The slides were rinsed in de-ionized water and then placed on the Sakura Tissue-Tek Prisma Automated Stainer/Coverslipper (Sakura, Torrance, CA, USA), dehydrated, cleared, and then mounted in Tissue Tek Glas mounting media (Sakura). The area of CNP expression was calculated with ImageJ software.

Western blot

Protein lysate was isolated from both the liver and arm bone, as described in the "GALNS enzyme activity assay" section. After lysis

and determination of protein concentration, the protein extracts were separated by electrophoresis. However, we did not obtain a sufficient protein concentration in the bone tissue for further analysis. Therefore, only the liver tissue was analyzed for protein expression. After electrophoresis, the proteins were transferred onto a nitrocellulose membrane. The membrane was blocked with 5% nonfat dry milk in TBST buffer and then incubated with primary antibodies overnight at 4°C (rabbit anti-GALNS [Creative Biolabs] and beta-actin [Sigma-Aldrich, St. Louis, MO, USA]). The membrane was subsequently incubated with secondary antibodies at room temperature for 1 h, treated with a solution of substrates for horseradish peroxidase detection, and read with a C-DiGiT Blot Scanner Licor Machine. As CNP and beta-actin have similar protein weights, the membrane was stripped after performing analysis for the CNP protein, and beta-actin analysis was performed starting from the blocking step. The intensities of bands were analyzed using the QuantityOne software.

Statistical analysis

The normal distribution was found using the Kolmogorov-Smirnov test and homogeneity of variance with the Leven test. Depending on the results, analysis of variance (two-way ANOVA) with Tukey's *post hoc* test was performed if the distribution was normal. When the assumptions of the normality of the distribution and the homogeneity of variance were unmet, the nonparametric Kruskal-Wallis test, followed by Dunnett's test, was performed. Statistical analyses were performed using GraphPad Prism 9 software. Statistical significance was set at a *p* value of >0.05. Error bars represent SEM, as indicated in legends.

DATA AND CODE AVAILABILITY

The data that support the findings of this study are available on request from the corresponding author (S.T.).

SUPPLEMENTAL INFORMATION

Supplemental information can be found online at <https://doi.org/10.1016/j.omtn.2024.102211>.

ACKNOWLEDGMENTS

This work was also supported by grants from the Austrian MPS society, A Cure for Robert, Inc., The Carol Ann Foundation, Angelo R. Cali & Mary V. Cali Family Foundation, Inc., The Vain and Harry Fish Foundation, Inc., The Bennett Foundation, Jacob Randall Foundation, and Nemours Funds. S.T. was supported by an Institutional Development Award from the Eunice Kennedy Shriver National Institute of Child Health & Human Development of the National Institutes of Health (NICHD) (1R01HD102545-01A1).

AUTHOR CONTRIBUTIONS

Conceptualization, E.R., S.T.; methodology, E.R., S.K., and F.N.; validation, E.R.; formal analysis, E.R.; investigation, E.R.; resources, S.T.; data curation, E.R., A.M.H.-P., B.C., S.K., F.N., and E.B.-F.; writing—original draft preparation, E.R.; writing—review and editing, S.T.; visualization, E.R.; supervision, S.T.; project administration, S.T.;

funding acquisition, S.T. All authors have read and agreed to the published version of the manuscript.

DECLARATION OF INTERESTS

The authors declare no conflict of interest.

REFERENCES

- Çelik, B., Tomatsu, S.C., Tomatsu, S., and Khan, S.A. (2021). Epidemiology of Mucopolysaccharidoses Update. *Diagnostics* 11, 273. <https://doi.org/10.3390/diagnostics11020273>.
- Kubaski, F., de Oliveira Poswar, F., Michelin-Tirelli, K., Burin, M.G., Rojas-Málaga, D., Brusius-Facchin, A.C., Leistner-Segal, S., and Giugliani, R. (2020). Diagnosis of Mucopolysaccharidoses. *Diagnostics* 10, 172. <https://doi.org/10.3390/diagnostics10030172>.
- Giugliani, R. (2012). Mucopolysaccharidoses: From understanding to treatment, a century of discoveries. *Genet. Mol. Biol.* 35, 924–931. <https://doi.org/10.1590/s1415-47572012000600006>.
- Verheyen, S., Blatterer, J., Speicher, M.R., Bhavani, G.S., Boons, G.J., Ilse, M.B., Andrae, D., Sproß, J., Vaz, F.M., Kircher, S.G., et al. (2022). Novel subtype of mucopolysaccharidosis caused by arylsulfatase K (ARSK) deficiency. *J. Med. Genet.* 59, 957–964. <https://doi.org/10.1136/jmedgenet-2021-108061>.
- Nagpal, R., Goyal, R.B., Priyadarshini, K., Kashyap, S., Sharma, M., Sinha, R., and Sharma, N. (2022). Mucopolysaccharidosis: A broad review. *Indian J. Ophthalmol.* 70, 2249–2261. https://doi.org/10.4103/ijo.IJO_425_22.
- Rintz, E., Pierzynowska, K., Podlacha, M., and Węgrzyn, G. (2020). Has resveratrol a potential for mucopolysaccharidosis treatment? *Eur. J. Pharmacol.* 888, 173534. <https://doi.org/10.1016/j.ejphar.2020.173534>.
- Nan, H., Park, C., and Maeng, S. (2020). Mucopolysaccharidoses I and II: Brief Review of Therapeutic Options and Supportive/Palliative Therapies. *BioMed Res. Int.* 2020, 2408402. <https://doi.org/10.1155/2020/2408402>.
- Stapleton, M., Arunkumar, N., Kubaski, F., Mason, R.W., Tadao, O., and Tomatsu, S. (2018). Clinical presentation and diagnosis of mucopolysaccharidoses. *Mol. Genet. Metabol.* 125, 4–17. <https://doi.org/10.1016/j.ymgme.2018.01.003>.
- Zhang, W., Liu, Q.Y., Haqqani, A.S., Leclerc, S., Liu, Z., Fauteux, F., Baumann, E., Delaney, C.E., Ly, D., Star, A.T., et al. (2020). Differential expression of receptors mediating receptor-mediated transcytosis (RMT) in brain microvessels, brain parenchyma and peripheral tissues of the mouse and the human. *Fluids Barriers CNS* 17, 47. <https://doi.org/10.1186/s12987-020-00209-0>.
- Sawamoto, K., Chen, H.H., Alméciga-Díaz, C.J., Mason, R.W., and Tomatsu, S. (2018). Gene therapy for Mucopolysaccharidoses. *Mol. Genet. Metabol.* 123, 59–68. <https://doi.org/10.1016/j.ymgme.2017.12.434>.
- Acosta, W., Ayala, J., Dolan, M.C., and Cramer, C.L. (2015). RTB Lectin: a novel receptor-independent delivery system for lysosomal enzyme replacement therapies. *Sci. Rep.* 5, 14144. <https://doi.org/10.1038/srep14144>.
- Boado, R.J., Zhang, Y., Zhang, Y., Xia, C.F., Wang, Y., and Pardridge, W.M. (2008). Genetic engineering of a lysosomal enzyme fusion protein for targeted delivery across the human blood-brain barrier. *Biotechnol. Bioeng.* 99, 475–484. <https://doi.org/10.1002/bit.21602>.
- Kida, S., Koshimura, Y., Yoden, E., Yoshioka, A., Morimoto, H., Imakiire, A., Tanaka, N., Tanaka, S., Mori, A., Ito, J., et al. (2023). Enzyme replacement with transferrin receptor-targeted α -L-iduronidase rescues brain pathology in mucopolysaccharidosis I mice. *Mol. Ther. Methods Clin. Dev.* 29, 439–449. <https://doi.org/10.1016/j.omtn.2023.05.010>.
- Lu, J.Z., Hui, E.K.W., Boado, R.J., and Pardridge, W.M. (2010). Genetic engineering of a bifunctional IgG fusion protein with iduronate-2-sulfatase. *Bioconjugate Chem.* 21, 151–156. <https://doi.org/10.1021/bc90382q>.
- Sonoda, H., Morimoto, H., Yoden, E., Koshimura, Y., Kinoshita, M., Golovina, G., Takagi, H., Yamamoto, R., Minami, K., Mizoguchi, A., et al. (2018). A Blood-Brain-Barrier-Penetrating Anti-human Transferrin Receptor Antibody Fusion Protein for Neuronopathic Mucopolysaccharidosis II. *Mol. Ther.* 26, 1366–1374. <https://doi.org/10.1016/j.ymthe.2018.02.032>.

16. Kan, S.H., Troitskaya, L.A., Sinow, C.S., Haitz, K., Todd, A.K., Di Stefano, A., Le, S.Q., Dickson, P.I., and Tippin, B.L. (2014). Insulin-like growth factor II peptide fusion enables uptake and lysosomal delivery of α -N-acetylglucosaminidase to mucopolysaccharidosis type IIIB fibroblasts. *Biochem. J.* 458, 281–289. <https://doi.org/10.1042/BJ20130845>.
17. Boado, R.J., Lu, J.Z., Hui, E.K.W., Lin, H., and Pardridge, W.M. (2016). Insulin Receptor Antibody- α -N-Acetylglucosaminidase Fusion Protein Penetrates the Primate Blood-Brain Barrier and Reduces Glycosaminoglycans in Sanfilippo Type B Fibroblasts. *Mol. Pharm.* 13, 1385–1392. <https://doi.org/10.1021/acs.molpharmaceut.6b00037>.
18. Boado, R.J., and Pardridge, W.M. (2010). Genetic engineering of IgG-glucuronidase fusion proteins. *J. Drug Target.* 18, 205–211. <https://doi.org/10.3109/10611860903353362>.
19. Leal, A.F., Benincore-Florez, E., Rintz, E., Herreño-Pachón, A.M., Celik, B., Ago, Y., Alméciga-Díaz, C.J., and Tomatsu, S. (2022). Mucopolysaccharidoses: Cellular Consequences of Glycosaminoglycans Accumulation and Potential Targets. *Int. J. Mol. Sci.* 24, 477. <https://doi.org/10.3390/ijms24010477>.
20. Hampe, C.S., Wesley, J., Lund, T.C., Orchard, P.J., Polgreen, L.E., Eisengart, J.B., McLoon, L.K., Cureoglu, S., Schachern, P., and McIvor, R.S. (2021). Mucopolysaccharidosis Type I: Current Treatments, Limitations, and Prospects for Improvement. *Biomolecules* 11, 189. <https://doi.org/10.3390/biom11020189>.
21. Schmidt, M., Breyer, S., Löbel, U., Yarar, S., Stücker, R., Ullrich, K., Müller, I., and Muschol, N. (2016). Musculoskeletal manifestations in mucopolysaccharidosis type I (Hurler syndrome) following hematopoietic stem cell transplantation. *Orphanet J. Rare Dis.* 11, 93. <https://doi.org/10.1186/s13023-016-0470-7>.
22. Sawamoto, K., Álvarez González, J.V., Piechnik, M., Otero, F.J., Couce, M.L., Suzuki, Y., and Tomatsu, S. (2020). Mucopolysaccharidosis IVA: Diagnosis, Treatment, and Management. *Int. J. Mol. Sci.* 21, 1517. <https://doi.org/10.3390/ijms21041517>.
23. Gatto, F., Redaelli, D., Salvadè, A., Marzorati, S., Sacchetti, B., Ferina, C., Roobrouck, V.D., Bertola, F., Romano, M., Villani, G., et al. (2012). Hurler disease bone marrow stromal cells exhibit altered ability to support osteoclast formation. *Stem Cell. Dev.* 21, 1466–1477. <https://doi.org/10.1089/scd.2011.0555>.
24. Fung, E.B., Johnson, J.A., Madden, J., Kim, T., and Harmatz, P. (2010). Bone density assessment in patients with mucopolysaccharidosis: A preliminary report from patients with MPS II and VI. *J. Pediatr. Rehabil. Med.* 3, 13–23.
25. Nur, B.G., Nur, H., and Mihci, E. (2017). Bone mineral density in patients with mucopolysaccharidosis type III. *J. Bone Miner. Metabol.* 35, 338–343. <https://doi.org/10.1007/s00774-016-0762-y>.
26. Khan, S., Alméciga-Díaz, C.J., Sawamoto, K., Mackenzie, W.G., Theroux, M.C., Pizarro, C., Mason, R.W., Orii, T., and Tomatsu, S. (2017). Mucopolysaccharidosis IVA and glycosaminoglycans. *Mol. Genet. Metabol.* 120, 78–95. <https://doi.org/10.1016/j.ymgme.2016.11.007>.
27. Gafni, Y., Pelled, G., Zilberman, Y., Turgeman, G., Apparailly, F., Yotvat, H., Galun, E., Gazit, Z., Jorgensen, C., and Gazit, D. (2004). Gene therapy platform for bone regeneration using an exogenously regulated, AAV-2-based gene expression system. *Mol. Ther.* 9, 587–595. <https://doi.org/10.1016/j.ymthe.2003.12.009>.
28. Dai, J., and Rabie, A.B.M. (2007). The use of recombinant adeno-associated virus for skeletal gene therapy. *Orthod. Craniofac. Res.* 10, 1–14. <https://doi.org/10.1111/j.1601-6343.2007.00381.x>.
29. Yang, Y.S., Xie, J., Chaugule, S., Wang, D., Kim, J.M., Kim, J., Tai, P.W.L., Seo, S.K., Gravalles, E., Gao, G., and Shim, J.H. (2020). Bone-Targeting AAV-Mediated Gene Silencing in Osteoclasts for Osteoporosis Therapy. *Mol. Ther. Methods Clin. Dev.* 17, 922–935. <https://doi.org/10.1016/j.omtm.2020.04.010>.
30. Yang, Y.S., Sato, T., Chaugule, S., Ma, H., Xie, J., Gao, G., and Shim, J.H. (2024). AAV-based gene editing of type I collagen mutation to treat osteogenesis imperfecta. *Mol. Ther. Nucleic Acids* 35, 102111. <https://doi.org/10.1016/j.omtm.2023.102111>.
31. Piechnik, M., Amendun, P.C., Sawamoto, K., Stapleton, M., Khan, S., Fnu, N., Álvarez, V., Pachon, A.M.H., Danos, O., Bruder, J.T., et al. (2022). Sex Difference Leads to Differential Gene Expression Patterns and Therapeutic Efficacy in Mucopolysaccharidosis IVA Murine Model Receiving AAV8 Gene Therapy. *Int. J. Mol. Sci.* 23, 12693. <https://doi.org/10.3390/ijms232012693>.
32. Sawamoto, K., Karumthil-Meethil, S., Khan, S., Stapleton, M., Bruder, J.T., Danos, O., and Tomatsu, S. (2020). Liver-Targeted AAV8 Gene Therapy Ameliorates Skeletal and Cardiovascular Pathology in a Mucopolysaccharidosis IVA Murine Model. *Mol. Ther. Methods Clin. Dev.* 18, 50–61. <https://doi.org/10.1016/j.omtm.2020.05.015>.
33. Rintz, E., Herreño-Pachón, A.M., Celik, B., Nidhi, F., Khan, S., Benincore-Florez, E., and Tomatsu, S. (2023). Bone Growth Induction in Mucopolysaccharidosis IVA Mouse. *Int. J. Mol. Sci.* 24, 9890. <https://doi.org/10.3390/ijms24129890>.
34. Chen, S.K., Hawley, Z.C.E., Zavodszky, M.I., Hana, S., Ferretti, D., Grubor, B., Hawes, M., Xu, S., Hamann, S., Marsh, G., et al. (2023). Efficacy and safety of a SOD1-targeting artificial miRNA delivered by AAV9 in mice are impacted by miRNA scaffold selection. *Mol. Ther. Nucleic Acids* 34, 102057. <https://doi.org/10.1016/j.omtm.2023.102057>.
35. Vercauteren, K., Hoffman, B.E., Zolotukhin, I., Keeler, G.D., Xiao, J.W., Basner-Tschakarjan, E., High, K.A., Ertl, H.C., Rice, C.M., Srivastava, A., et al. (2016). Superior In vivo Transduction of Human Hepatocytes Using Engineered AAV3 Capsid. *Mol. Ther.* 24, 1042–1049. <https://doi.org/10.1038/mt.2016.61>.
36. Inagaki, K., Fuess, S., Storm, T.A., Gibson, G.A., Mctiernan, C.F., Kay, M.A., and Nakai, H. (2006). Robust systemic transduction with AAV9 vectors in mice: efficient global cardiac gene transfer superior to that of AAV8. *Mol. Ther.* 14, 45–53. <https://doi.org/10.1016/j.ymthe.2006.03.014>.
37. Issa, S.S., Shaimardanova, A.A., Solovyeva, V.V., and Rizvanov, A.A. (2023). Various AAV Serotypes and Their Applications in Gene Therapy: An Overview. *Cells* 12, 785. <https://doi.org/10.3390/cells12050785>.
38. Su, J., She, K., Song, L., Jin, X., Li, R., Zhao, Q., Xiao, J., Chen, D., Cheng, H., Lu, F., et al. (2023). In vivo base editing rescues photoreceptors in a mouse model of retinitis pigmentosa. *Mol. Ther. Nucleic Acids* 31, 596–609. <https://doi.org/10.1016/j.omtm.2023.02.011>.
39. Rubin, J.D., Nguyen, T.V., Allen, K.L., Ayasoufi, K., and Barry, M.A. (2019). Comparison of Gene Delivery to the Kidney by Adenovirus, Adeno-Associated Virus, and Lentiviral Vectors After Intravenous and Direct Kidney Injections. *Hum. Gene Ther.* 30, 1559–1571. <https://doi.org/10.1089/hum.2019.127>.
40. Wang, A.Y., Peng, P.D., Ehrhardt, A., Storm, T.A., and Kay, M.A. (2004). Comparison of adenoviral and adeno-associated viral vectors for pancreatic gene delivery *in vivo*. *Hum. Gene Ther.* 15, 405–413. <https://doi.org/10.1089/104303404322959551>.
41. Zincarelli, C., Soltys, S., Rengo, G., and Rabinowitz, J.E. (2008). Analysis of AAV serotypes 1–9 mediated gene expression and tropism in mice after systemic injection. *Mol. Ther.* 16, 1073–1080. <https://doi.org/10.1038/mt.2008.76>.
42. Nam, H.J., Lane, M.D., Padron, E., Gurda, B., McKenna, R., Kohlbrenner, E., Aslanidi, G., Byrne, B., Muzyczka, N., Zolotukhin, S., and Agbandje-McKenna, M. (2007). Structure of adeno-associated virus serotype 8, a gene therapy vector. *J. Virol.* 81, 12260–12271. <https://doi.org/10.1128/JVI.01304-07>.
43. Nakai, H., Fuess, S., Storm, T.A., Muramatsu, S.I., Nara, Y., and Kay, M.A. (2005). Unrestricted hepatocyte transduction with adeno-associated virus serotype 8 vectors in mice. *J. Virol.* 79, 214–224. <https://doi.org/10.1128/JVI.79.1.214-224.2005>.
44. Tomatsu, S., Montañó, A.M., Ohashi, A., Gutierrez, M.A., Oikawa, H., Oguma, T., Dung, V.C., Nishioka, T., Orii, T., and Sly, W.S. (2008). Enzyme replacement therapy in a murine model of Morquio A syndrome. *Hum. Mol. Genet.* 17, 815–824. <https://doi.org/10.1093/hmg/ddm353>.
45. Tomatsu, S., Orii, K.O., Vogler, C., Nakayama, J., Levy, B., Grubb, J.H., Gutierrez, M.A., Shim, S., Yamaguchi, S., Nishioka, T., et al. (2003). Mouse model of N-acetylgalactosamine-6-sulfate sulfatase deficiency (Galns^{-/-}) produced by targeted disruption of the gene defective in Morquio A disease. *Hum. Mol. Genet.* 12, 3349–3358. <https://doi.org/10.1093/hmg/ddg366>.
46. Tomatsu, S., Montañó, A.M., Dung, V.C., Ohashi, A., Oikawa, H., Oguma, T., Orii, T., Barrera, L., and Sly, W.S. (2010). Enhancement of drug delivery: enzyme-replacement therapy for murine Morquio A syndrome. *Mol. Ther.* 18, 1094–1102. <https://doi.org/10.1038/mt.2010.32>.
47. Tomatsu, S., Montañó, A.M., Oikawa, H., Dung, V.C., Hashimoto, A., Oguma, T., Gutiérrez, M.L., Takahashi, T., Shimada, T., Orii, T., and Sly, W.S. (2015). Enzyme replacement therapy in newborn mucopolysaccharidosis IVA mice: early treatment rescues bone lesions? *Mol. Genet. Metabol.* 114, 195–202. <https://doi.org/10.1016/j.ymgme.2014.05.013>.

48. Averill, L.W., Kecskemethy, H.H., Theroux, M.C., Mackenzie, W.G., Pizarro, C., Bober, M.B., Ditro, C.P., and Tomatsu, S. (2021). Tracheal narrowing in children and adults with mucopolysaccharidosis type IVA: evaluation with computed tomography angiography. *Pediatr. Radiol.* 51, 1202–1213. <https://doi.org/10.1007/s00247-020-04946-0>.
49. Doherty, C., Averill, L.W., Theroux, M., Mackenzie, W.G., Pizarro, C., Mason, R.W., and Tomatsu, S. (2018). Natural history of Morquio A patient with tracheal obstruction from birth to death. *Mol. Genet. Metab. Rep.* 14, 59–67. <https://doi.org/10.1016/j.ymgmr.2017.11.005>.
50. Tomatsu, S., Averill, L.W., Sawamoto, K., Mackenzie, W.G., Bober, M.B., Pizarro, C., Goff, C.J., Xie, L., Orii, T., and Theroux, M. (2016). Obstructive airway in Morquio A syndrome, the past, the present and the future. *Mol. Genet. Metabol.* 117, 150–156. <https://doi.org/10.1016/j.ymgme.2015.09.007>.
51. Cleary, M., Davison, J., Gould, R., Geberhiwot, T., Hughes, D., Mercer, J., Morrison, A., Murphy, E., Santra, S., Jarrett, J., et al. (2021). Impact of long-term elosulfase alfa treatment on clinical and patient-reported outcomes in patients with mucopolysaccharidosis type IVA: results from a Managed Access Agreement in England. *Orphanet J. Rare Dis.* 16, 38. <https://doi.org/10.1186/s13023-021-01675-x>.
52. Doherty, C., Stapleton, M., Piechnik, M., Mason, R.W., Mackenzie, W.G., Yamaguchi, S., Kobayashi, H., Suzuki, Y., and Tomatsu, S. (2019). Effect of enzyme replacement therapy on the growth of patients with Morquio A. *J. Hum. Genet.* 64, 625–635. <https://doi.org/10.1038/s10038-019-0604-6>.
53. Lin, H.Y., Chen, M.R., Lin, S.M., Hung, C.L., Niu, D.M., Chuang, C.K., and Lin, S.P. (2018). Cardiac features and effects of enzyme replacement therapy in Taiwanese patients with Mucopolysaccharidosis IVA. *Orphanet J. Rare Dis.* 13, 148. <https://doi.org/10.1186/s13023-018-0883-6>.
54. Fujitsuka, H., Sawamoto, K., Peracha, H., Mason, R.W., Mackenzie, W., Kobayashi, H., Yamaguchi, S., Suzuki, Y., Orii, K., Orii, T., et al. (2019). Biomarkers in patients with mucopolysaccharidosis type II and IV. *Mol. Genet. Metab. Rep.* 19, 100455. <https://doi.org/10.1016/j.ymgmr.2019.100455>.
55. Yabe, H., Tanaka, A., Chinen, Y., Kato, S., Sawamoto, K., Yasuda, E., Shintaku, H., Suzuki, Y., Orii, T., and Tomatsu, S. (2016). Hematopoietic stem cell transplantation for Morquio A syndrome. *Mol. Genet. Metabol.* 117, 84–94. <https://doi.org/10.1016/j.ymgme.2015.09.011>.
56. Chusho, H., Tamura, N., Ogawa, Y., Yasoda, A., Suda, M., Miyazawa, T., Nakamura, K., Nakao, K., Kurihara, T., Komatsu, Y., et al. (2001). Dwarfism and early death in mice lacking C-type natriuretic peptide. *Proc. Natl. Acad. Sci. USA* 98, 4016–4021. <https://doi.org/10.1073/pnas.071389098>.
57. Kake, T., Kitamura, H., Adachi, Y., Yoshioka, T., Watanabe, T., Matsushita, H., Fujii, T., Kondo, E., Tachibe, T., Kawase, Y., et al. (2009). Chronically elevated plasma C-type natriuretic peptide level stimulates skeletal growth in transgenic mice. *Am. J. Physiol. Endocrinol. Metab.* 297, E1339–E1348. <https://doi.org/10.1152/ajpendo.00272.2009>.
58. Komatsu, Y., Chusho, H., Tamura, N., Yasoda, A., Miyazawa, T., Suda, M., Miura, M., Ogawa, Y., and Nakao, K. (2002). Significance of C-type natriuretic peptide (CNP) in endochondral ossification: analysis of CNP knockout mice. *J. Bone Miner. Metabol.* 20, 331–336. <https://doi.org/10.1007/s007740200048>.
59. Tsuji, T., Kondo, E., Yasoda, A., Inamoto, M., Kiyosu, C., Nakao, K., and Kunieda, T. (2008). Hypomorphic mutation in mouse Nppc gene causes retarded bone growth due to impaired endochondral ossification. *Biochem. Biophys. Res. Commun.* 376, 186–190. <https://doi.org/10.1016/j.bbrc.2008.08.139>.
60. Rintz, E., Węgrzyn, G., Fujii, T., and Tomatsu, S. (2022). Molecular Mechanism of Induction of Bone Growth by the C-Type Natriuretic Peptide. *Int. J. Mol. Sci.* 23, 5916. <https://doi.org/10.3390/ijms23115916>.
61. Ueda, Y., Yasoda, A., Hirota, K., Yamauchi, I., Yamashita, T., Kanai, Y., Sakane, Y., Fujii, T., and Inagaki, N. (2019). Exogenous C-type natriuretic peptide therapy for impaired skeletal growth in a murine model of glucocorticoid treatment. *Sci. Rep.* 9, 8547. <https://doi.org/10.1038/s41598-019-44975-w>.
62. Nakao, K., Osawa, K., Yasoda, A., Yamanaka, S., Fujii, T., Kondo, E., Koyama, N., Kanamoto, N., Miura, M., Kuwahara, K., et al. (2015). The Local CNP/GC-B system in growth plate is responsible for physiological endochondral bone growth. *Sci. Rep.* 5, 10554. <https://doi.org/10.1038/srep10554>.
63. Bükülmez, H., Khan, F., Bartels, C.F., Murakami, S., Ortiz-Lopez, A., Sattar, A., Haqqi, T.M., and Warman, M.L. (2014). Protective effects of C-type natriuretic peptide on linear growth and articular cartilage integrity in a mouse model of inflammatory arthritis. *Arthritis Rheumatol.* 66, 78–89. <https://doi.org/10.1002/art.38199>.
64. Lorget, F., Kaci, N., Peng, J., Benoist-Lassel, C., Mugniery, E., Oppeneer, T., Wendt, D.J., Bell, S.M., Bullens, S., Bunting, S., et al. (2012). Evaluation of the therapeutic potential of a CNP analog in a Fgfr3 mouse model recapitulating achondroplasia. *Am. J. Hum. Genet.* 91, 1108–1114. <https://doi.org/10.1016/j.ajhg.2012.10.014>.
65. Berry, G.E., and Asokan, A. (2016). Cellular transduction mechanisms of adeno-associated viral vectors. *Curr. Opin. Virol.* 21, 54–60. <https://doi.org/10.1016/j.coviro.2016.08.001>.
66. Wu, C., Wu, F., Pan, J., Morser, J., and Wu, Q. (2003). Furin-mediated processing of Pro-C-type natriuretic peptide. *J. Biol. Chem.* 278, 25847–25852. <https://doi.org/10.1074/jbc.M301223200>.
67. Prickett, T.C., and A Espiner, E. (2020). Circulating products of C-type natriuretic peptide and links with organ function in health and disease. *Peptides* 132, 170363. <https://doi.org/10.1016/j.peptides.2020.170363>.
68. Daniels, R.W., Rossano, A.J., Macleod, G.T., and Ganetzky, B. (2014). Expression of multiple transgenes from a single construct using viral 2A peptides in *Drosophila*. *PLoS One* 9, e100637. <https://doi.org/10.1371/journal.pone.0100637>.
69. Tomatsu, S., Okamura, K., Taketani, T., Orii, K.O., Nishioka, T., Gutierrez, M.A., Velez-Castrillon, S., Fachel, A.A., Grubb, J.H., Cooper, A., et al. (2004). Development and testing of new screening method for keratan sulfate in mucopolysaccharidosis IVA. *Pediatr. Res.* 55, 592–597. <https://doi.org/10.1203/01.PDR.0000113767.60140.E9>.
70. Khan, S.A., Mason, R.W., Giugliani, R., Orii, K., Fukao, T., Suzuki, Y., Yamaguchi, S., Kobayashi, H., Orii, T., and Tomatsu, S. (2018). Glycosaminoglycans analysis in blood and urine of patients with mucopolysaccharidosis. *Mol. Genet. Metabol.* 125, 44–52. <https://doi.org/10.1016/j.ymgme.2018.04.011>.
71. Hendriks, C.J., Burton, B., Fleming, T.R., Harmatz, P., Hughes, D., Jones, S.A., Lin, S.P., Mengel, E., Scarpa, M., Valayannopoulos, V., et al. (2014). Efficacy and safety of enzyme replacement therapy with BMN 110 (elosulfase alfa) for Morquio A syndrome (mucopolysaccharidosis IVA): a phase 3 randomised placebo-controlled study. *J. Inher. Metab. Dis.* 37, 979–990. <https://doi.org/10.1007/s10545-014-9715-6>.
72. Hendriks, C.J., Parini, R., AlSayed, M.D., Raiman, J., Giugliani, R., Solano Villarreal, M.L., Mitchell, J.J., Burton, B.K., Guelbert, N., Stewart, F., et al. (2016). Long-term endurance and safety of elosulfase alfa enzyme replacement therapy in patients with Morquio A syndrome. *Mol. Genet. Metabol.* 119, 131–143. <https://doi.org/10.1016/j.ymgme.2016.05.018>.
73. Tomatsu, S., Montaña, A.M., Oguma, T., Dung, V.C., Oikawa, H., de Carvalho, T.G., Gutiérrez, M.L., Yamaguchi, S., Suzuki, Y., Fukushi, M., et al. (2010). Validation of keratan sulfate level in mucopolysaccharidosis type IVA by liquid chromatography-tandem mass spectrometry. *J. Inher. Metab. Dis.* 33, S35–S42. <https://doi.org/10.1007/s10545-009-9013-x>.
74. Takahashi, K., Tanabe, K., Ohnuki, M., Narita, M., Ichisaka, T., Tomoda, K., and Yamanaka, S. (2007). Induction of pluripotent stem cells from adult human fibroblasts by defined factors. *Cell* 131, 861–872. <https://doi.org/10.1016/j.cell.2007.11.019>.
75. Szczczak, A.L., Workman, C.J., Wang, Y., Vignali, K.M., Diloglou, S., Vanin, E.F., and Vignali, D.A.A. (2004). Correction of multi-gene deficiency *in vivo* using a single 'self-cleaving' 2A peptide-based retroviral vector. *Nat. Biotechnol.* 22, 589–594. Erratum in: *Nat. Biotechnol.* 22(12):1590. Erratum in: *Nat. Biotechnol.* 2004 Jun;22(6):760. <https://doi.org/10.1038/nbt957>.
76. Vaseghi, H.R., Yin, C., Zhou, Y., Wang, L., Liu, J., and Qian, L. (2016). Generation of an inducible fibroblast cell line for studying direct cardiac reprogramming. *Genesis* 54, 398–406. <https://doi.org/10.1002/dvg.22947>.
77. Tang, W., Ehrlich, I., Wolff, S.B.E., Michalski, A.M., Wölfl, S., Hasan, M.T., Lüthi, A., and Sprengel, R. (2009). Faithful expression of multiple proteins via 2A-peptide self-processing: a versatile and reliable method for manipulating brain circuits. *J. Neurosci.* 29, 8621–8629. <https://doi.org/10.1523/JNEUROSCI.0359-09.2009>.
78. Verrier, J.D., Madorsky, I., Coggin, W.E., Geesey, M., Hochman, M., Walling, E., Daroszewski, D., Eccles, K.S., Ludlow, R., and Semple-Rowland, S.L. (2011).

- Bicistronic lentiviruses containing a viral 2A cleavage sequence reliably co-express two proteins and restore vision to an animal model of LCA1. *PLoS One* 6, e20553. <https://doi.org/10.1371/journal.pone.0020553>.
79. Geier, M., Fauland, P., Vogl, T., and Glieder, A. (2015). Compact multi-enzyme pathways in *P. pastoris*. *Chem. Commun.* 51, 1643–1646. <https://doi.org/10.1039/c4cc08502g>.
80. Liu, Z., Chen, O., Wall, J.B.J., Zheng, M., Zhou, Y., Wang, L., Vaseghi, H.R., Qian, L., and Liu, J. (2017). Systematic comparison of 2A peptides for cloning multi-genes in a polycistronic vector. *Sci. Rep.* 7, 2193. <https://doi.org/10.1038/s41598-017-02460-2>.
81. Woods, A., Khan, S., and Beier, F. (2007). C-type natriuretic peptide regulates cellular condensation and glycosaminoglycan synthesis during chondrogenesis. *Endocrinology* 148, 5030–5041. <https://doi.org/10.1210/en.2007-0695>.
82. Yamashita, T., Fujii, T., Yamauchi, I., Ueda, Y., Hirota, K., Kanai, Y., Yasoda, A., and Inagaki, N. (2020). C-Type Natriuretic Peptide Restores Growth Impairment Under Enzyme Replacement in Mice With Mucopolysaccharidosis VII. *Endocrinology* 161, bqaa008. <https://doi.org/10.1210/endo/bqaa008>.
83. Geisler, A., and Fehner, H. (2016). MicroRNA-regulated viral vectors for gene therapy. *World J. Exp. Med.* 6, 37–54. <https://doi.org/10.5493/wjem.v6.i2.37>.
84. Qiao, C., Yuan, Z., Li, J., He, B., Zheng, H., Mayer, C., Li, J., and Xiao, X. (2011). Liver-specific microRNA-122 target sequences incorporated in AAV vectors efficiently inhibits transgene expression in the liver. *Gene Ther.* 18, 403–410. <https://doi.org/10.1038/gt.2010.157>.
85. Sosa, A.C., Kariuki, B., Gan, Q., Knutsen, A.P., Bellone, C.J., Guzmán, M.A., Barrera, L.A., Tomatsu, S., Chauhan, A.K., Armbricht, E., and Montañó, A.M. (2020). Oral immunotherapy tolerizes mice to enzyme replacement therapy for Morquio A syndrome. *J. Clin. Invest.* 130, 1288–1300. <https://doi.org/10.1172/JCI125607>.

OMTN, Volume 35

Supplemental information

Adeno-associated virus-based gene therapy delivering combinations of two growth-associated genes to MPS IVA mice

Estera Rintz, Betul Celik, Nidhi Fnu, Angélica María Herreño-Pachón, Shaukat Khan, Eliana Benincore-Flórez, and Shunji Tomatsu

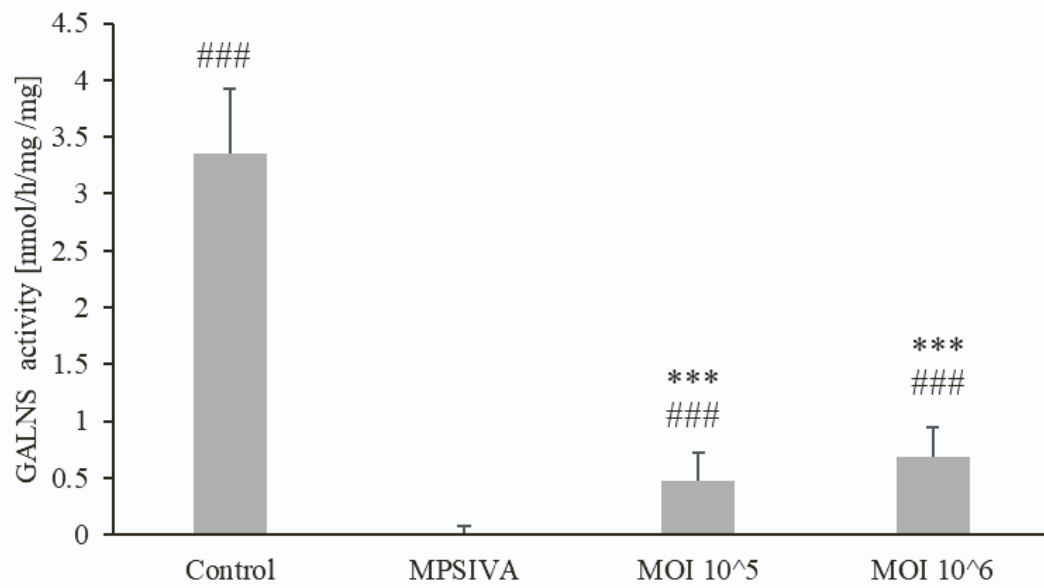


Figure S1. AAV9-hGALNS vector increase enzyme activity in human fibroblast cell lines. Control- healthy patient cells. Experiment was conducted in three individual replicates. Results are shown as mean values \pm SEM (n=3). The following statistical symbols were used to denote as follows. vs. Control group, *** $p \leq 0.001$; vs. untreated MPS IVA group, ### $p \leq 0.001$

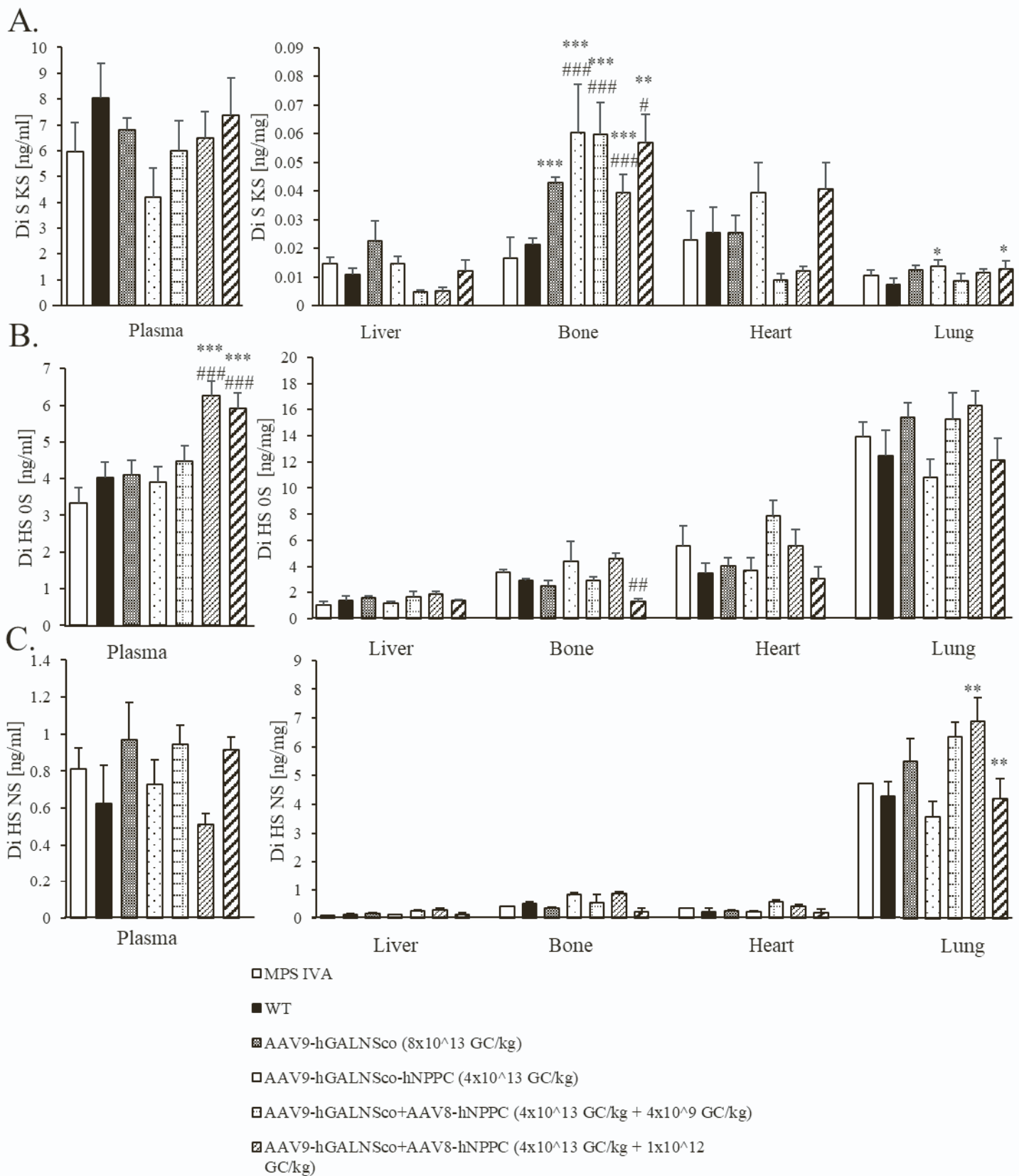


Figure S2. Glycosaminoglycans (GAGs) Levels in MPS IVA Mice Treated with AAV vectors. After 12 weeks post-treatment, the level of GAG was measured: Di-sulfated KS (Di S KS) (A), *O*-sulfated heparan sulfate (Di HS OS) (B), and *N*-sulfated heparan sulfate (Di HS NS) (C) levels in plasma, Liver, Bone, Heart, and Lung. Results are shown as mean values \pm SEM (n=5). The following statistical symbols were used to denote as follows. vs. WT group, *** $p \leq 0.001$, ** $p \leq 0.01$, * $p \leq 0.05$; vs. untreated MPS IVA group, ### $p \leq 0.001$.

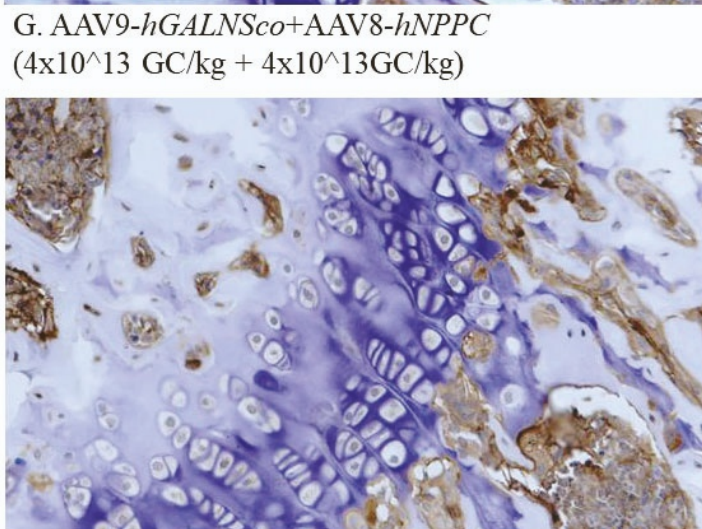
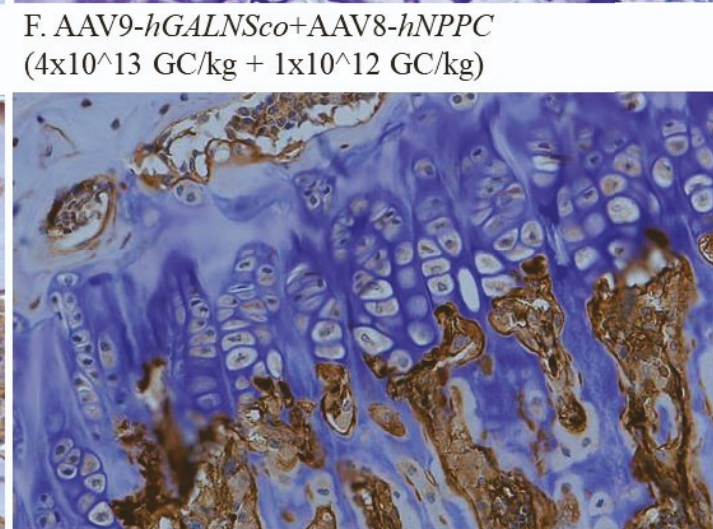
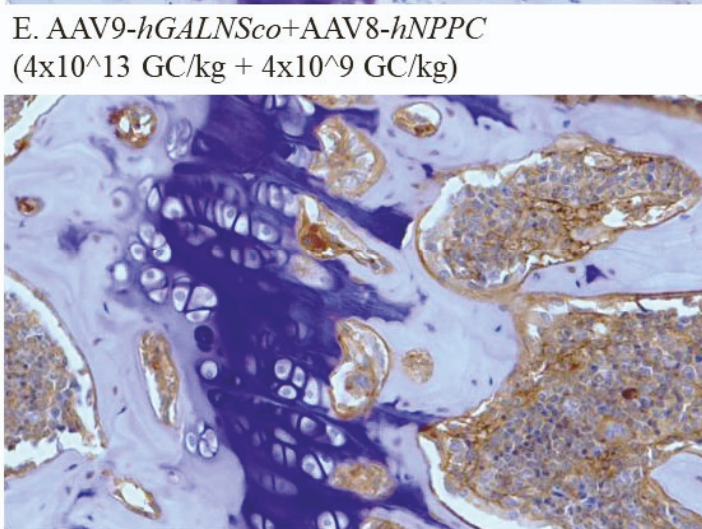
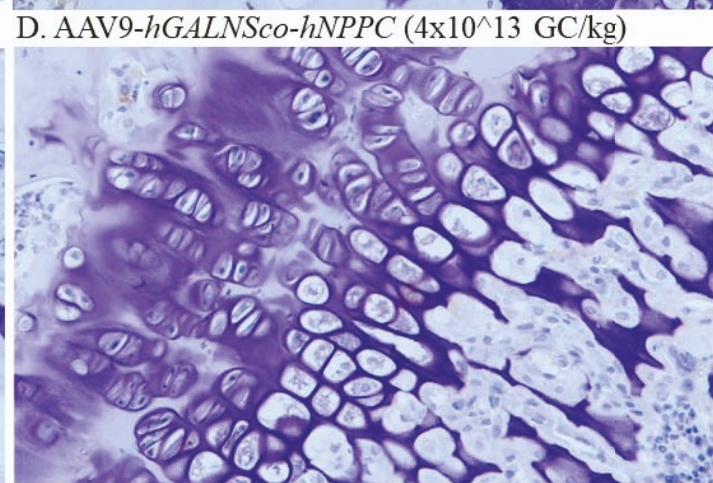
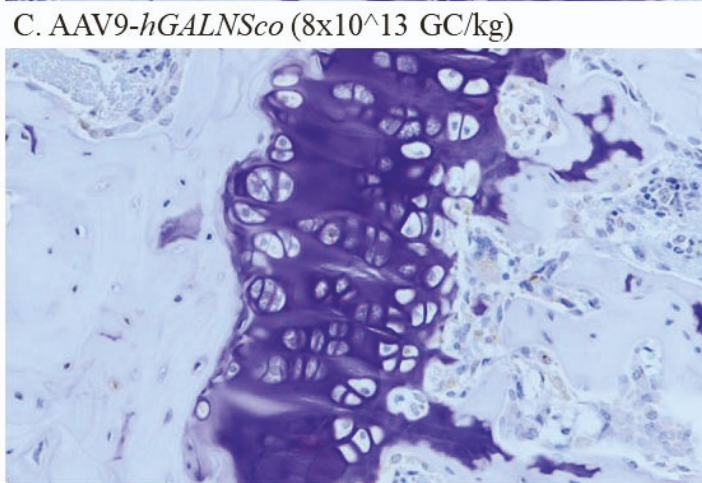
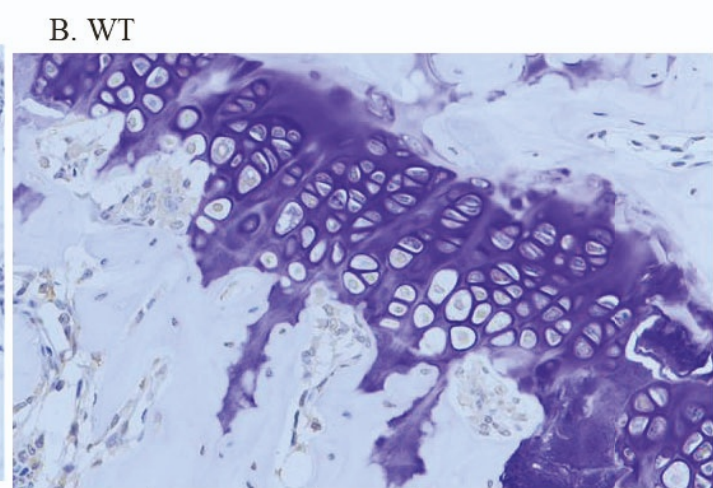
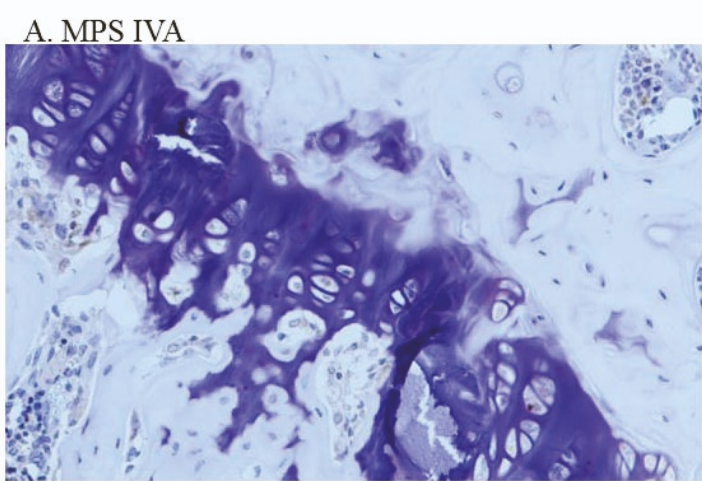
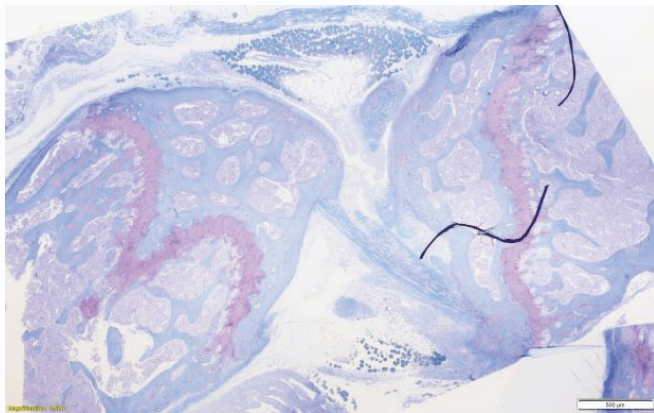
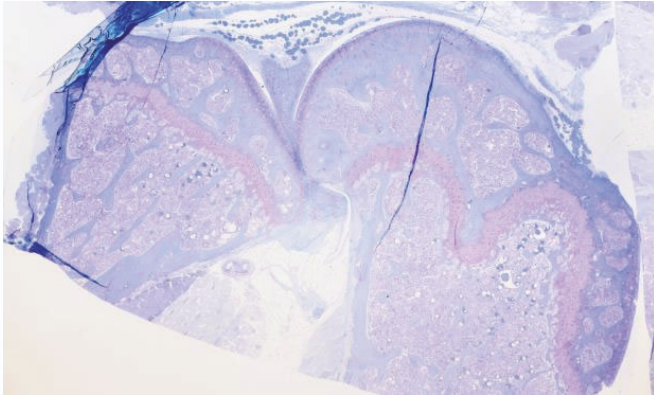


Figure S3. GALNS staining in tibia. After 12 weeks post-treatment, the level of GALNS expression in bone represented as IHC staining. Representative pictures are shown of MPS IVA (A), WT (B), AAV9-*hGALNSco* (8×10^{13} GC/kg) (C), AAV9-*hGALNSco-hNPPC* (4×10^{13} GC/kg) (D), AAV9-*hGALNSco*+AAV8-*hNPPC* (4×10^{13} GC/kg + 4×10^9 GC/kg) (E), AAV9-*hGALNSco*+AAV8-*hNPPC* (4×10^{13} GC/kg + 1×10^{12} GC/kg) (F), AAV9-*hGALNSco*+AAV8-*hNPPC* (4×10^{13} GC/kg + 4×10^{13} GC/kg) (G).

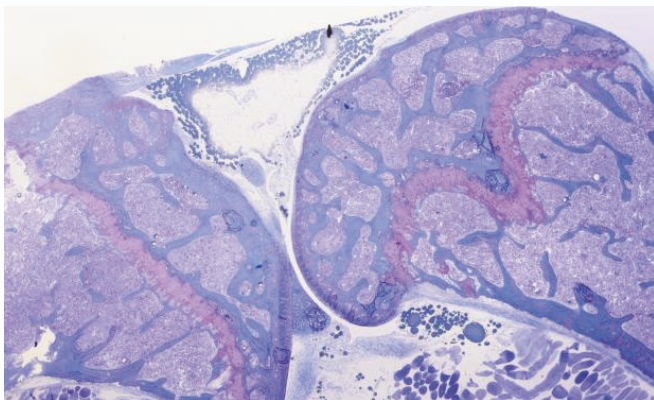
A. MPS IVA



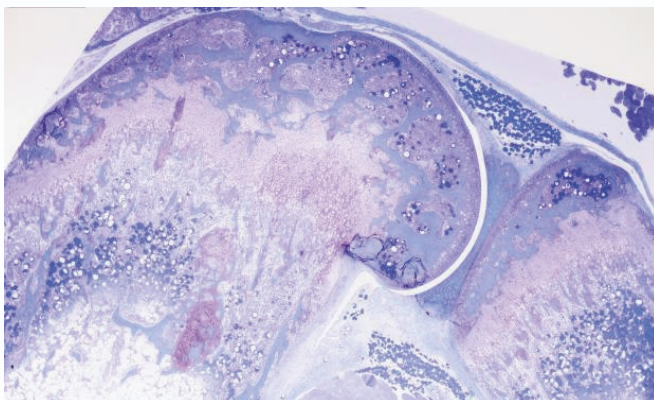
C. AAV9-*hGALNSco* (8×10^{13} GC/kg)



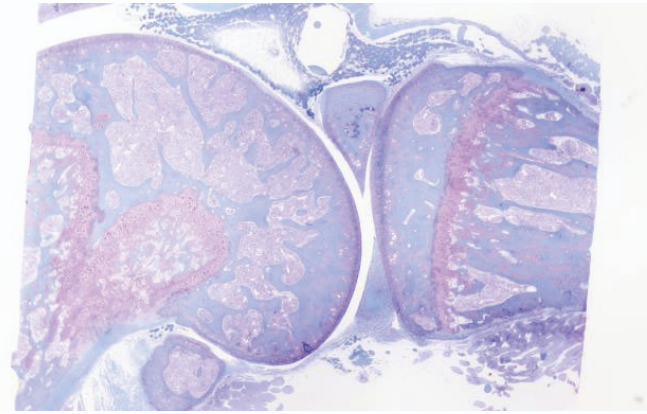
E. AAV9-*hGALNSco*+AAV8-*hNPPC*
(4×10^{13} GC/kg + 4×10^9 GC/kg)



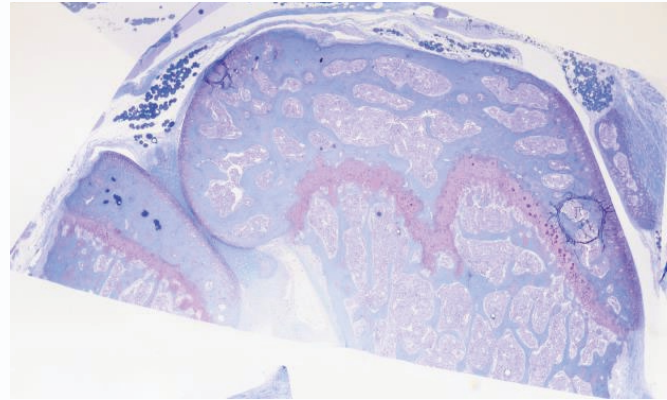
G. AAV9-*hGALNSco*+AAV8-*hNPPC*
(4×10^{13} GC/kg + 4×10^{13} GC/kg)



B. WT



D. AAV9-*hGALNSco*-*hNPPC* (4×10^{13} GC/kg)



F. AAV9-*hGALNSco*+AAV8-*hNPPC*
(4×10^{13} GC/kg + 1×10^{12} GC/kg)

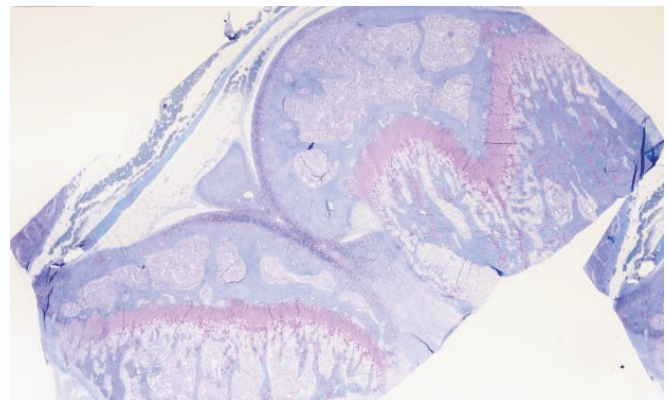
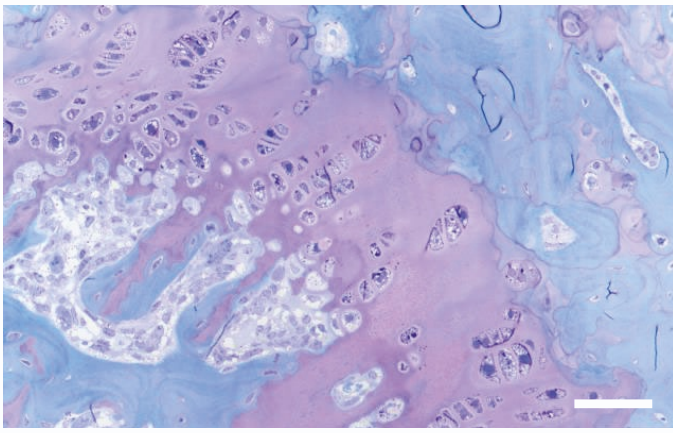
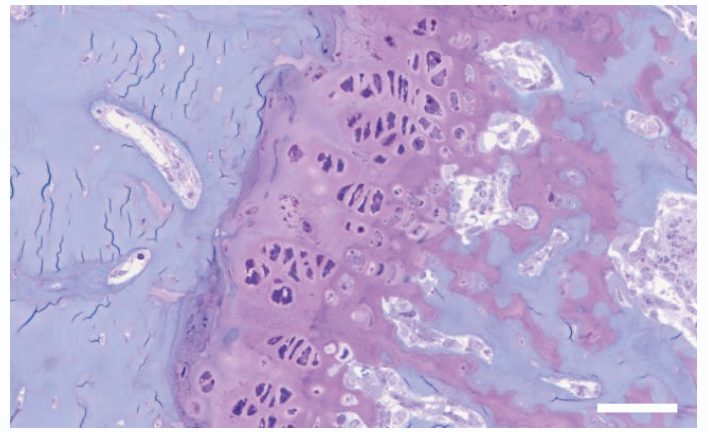


Figure S4. Correction of bone pathology in MPS IVA mice treated with AAV vectors assessed by toluidine blue staining analysis using light microscopy. Knee joint of untreated MPS IVA (A); WT (B); AAV9-*hGALNSco* (8×10^{13} GC/kg) (C); AAV9-*hGALNSco*-*hNPPC* (4×10^{13} GC/kg) (D); AAV9-*hGALNSco*+AAV8-*hNPPC* (4×10^{13} GC/kg+ 4×10^9 GC/kg) (E); AAV9-*hGALNSco*+AAV8-*hNPPC* (4×10^{13} GC/kg+ 1×10^{12} GC/kg) (F); AAV9-*hGALNSco*+AAV8-*hNPPC* (4×10^{13} GC/kg + 4×10^{13} GC/kg) (G). (4x magnification with 500 μ m scale bar).⁴

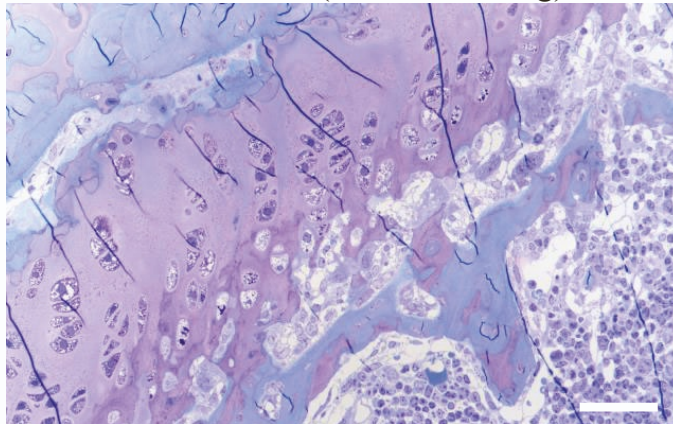
A. MPS IVA



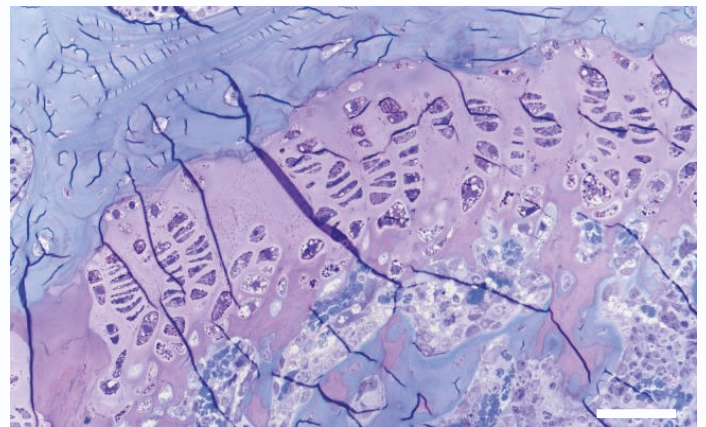
B. WT



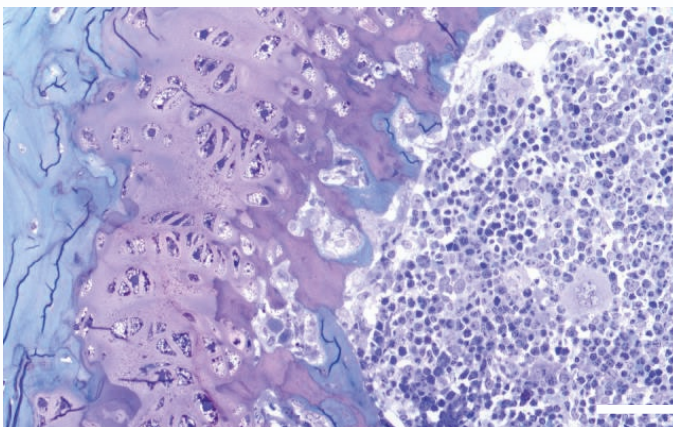
C. AAV9-*hGALNSco* (8×10^{13} GC/kg)



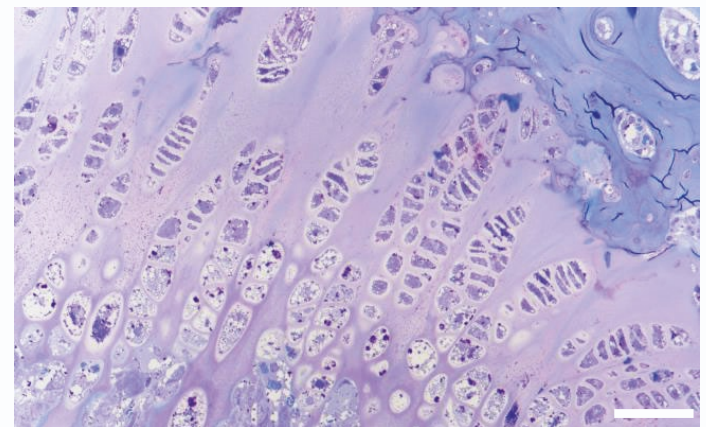
D. AAV9-*hGALNSco-hNPPC* (4×10^{13} GC/kg)



E. AAV9-*hGALNSco*+AAV8-*hNPPC*
(4×10^{13} GC/kg + 4×10^9 GC/kg)



F. AAV9-*hGALNSco*+AAV8-*hNPPC*
(4×10^{13} GC/kg + 1×10^{12} GC/kg)



G. AAV9-*hGALNSco*+AAV8-*hNPPC*
(4×10^{13} GC/kg + 4×10^{13} GC/kg)

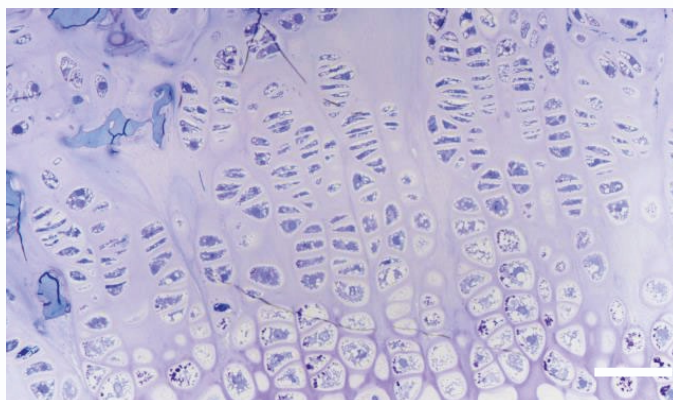
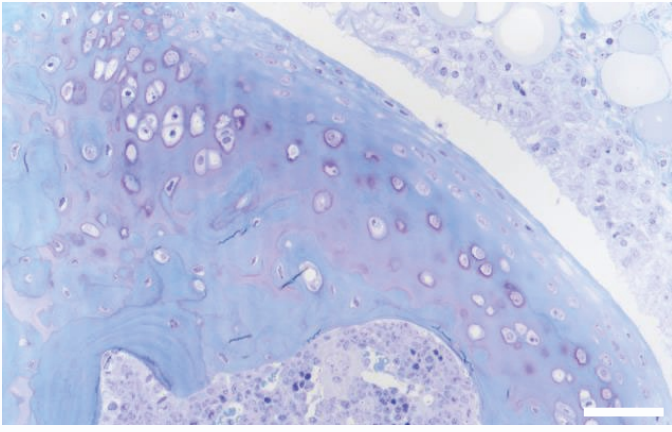
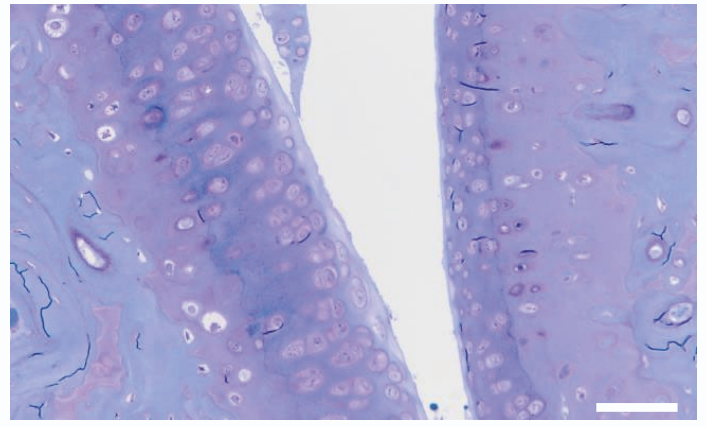


Figure S5. Correction of bone pathology in MPS IVA mice treated with AAV vectors assessed by toluidine blue staining analysis using light microscopy. Femur growth plate of untreated MPS IVA (A); WT (B); AAV9-*hGALNSco* (8×10^{13} GC/kg) (C); AAV9-*hGALNSco-hNPPC* (4×10^{13} GC/kg) (D); AAV9-*hGALNSco*+AAV8-*hNPPC* (4×10^{13} GC/kg+ 4×10^9 GC/kg) (E); AAV9-*hGALNSco*+AAV8-*hNPPC* (4×10^{13} GC/kg+ 1×10^{12} GC/kg) (F); AAV9-*hGALNSco*+AAV8-*hNPPC* (4×10^{13} GC/kg + 4×10^{13} GC/kg) (G). (40x magnification with 500 μ m scale bar).

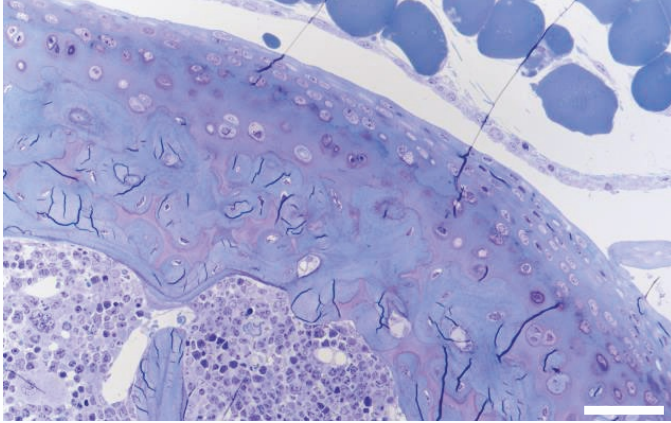
A. MPS IVA



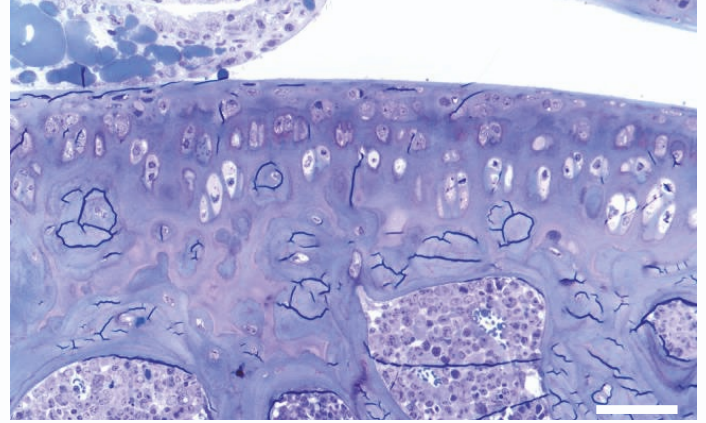
B. WT



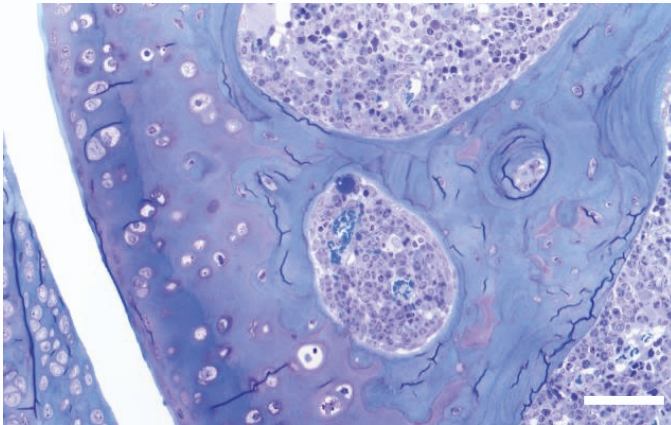
C. AAV9-*hGALNSco* (8×10^{13} GC/kg)



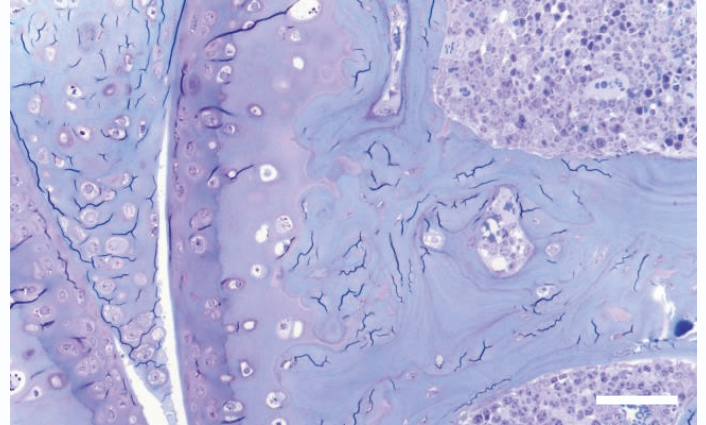
D. AAV9-*hGALNSco-hNPPC* (4×10^{13} GC/kg)



E. AAV9-*hGALNSco*+AAV8-*hNPPC*
(4×10^{13} GC/kg + 4×10^9 GC/kg)



F. AAV9-*hGALNSco*+AAV8-*hNPPC*
(4×10^{13} GC/kg + 1×10^{12} GC/kg)



G. AAV9-*hGALNSco*+AAV8-*hNPPC*
(4×10^{13} GC/kg + 4×10^{13} GC/kg)

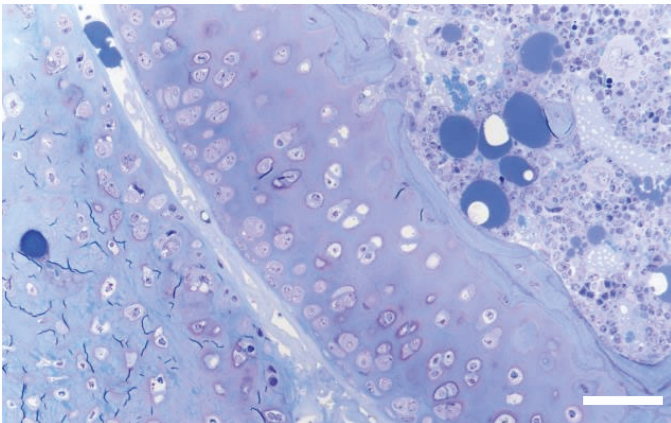


Figure S6. Correction of bone pathology in MPS IVA mice treated with AAV vectors assessed by toluidine blue staining analysis using light microscopy. Femur articular cartilage of untreated MPS IVA (A); WT (B); AAV9-*hGALNSco* (8×10^{13} GC/kg) (C); AAV9-*hGALNSco-hNPPC* (4×10^{13} GC/kg) (D); AAV9-*hGALNSco*+AAV8-*hNPPC* (4×10^{13} GC/kg+ 4×10^9 GC/kg) (E); AAV9-*hGALNSco*+AAV8-*hNPPC* (4×10^{13} GC/kg+ 1×10^{12} GC/kg) (F); AAV9-*hGALNSco*+AAV8-*hNPPC* (4×10^{13} GC/kg + 4×10^{13} GC/kg) (G). (40x magnification with 500 μ m scale bar).

Table S1. Gene therapy related clinical trials (clinicaltrials.gov, accessed 29 January 2024).

	<i>In vivo</i>	<i>Ex vivo</i>
MPS I	NCT03580083	NCT03488394
	NCT02702115	NCT05682144
	NCT06103487	
MPS II	NCT03041324	NCT00004454
	NCT04597385	NCT05665166
	NCT04571970	
	NCT03566043	
MPS IIIA	NCT03612869	NCT04201405
	NCT02716246	
	NCT04088734	
	NCT01474343	
	NCT04360265	
MPS IIIB	NCT03315182	
	NCT03300453	
	NCT04655911	
MPS VI	NCT03173521	

Table S2. Primers and probes used for the dPCR reaction.

Gene	Sequence		Tm	GC %
GALNS	Forward	AGAAGCCCTGAGCAGAATCA	63.274	50
	Reverse	CAGTTCATCACGGCCCAATTAC	63.502	50
	Probe	AGCAGCACCAAGAGGCTCTGG TTC	69.926	58.3
NPPC	Forward	AACGCGCGCAAATACAAAG	63.756	55
	Reverse	GGAATTCCCACCTTTGTACAAGA AA	63.828	55.5
	Probe	TGAGCGGCCTGGGATGTTAGA CCCA	70.543	63.6

Authors Contribution

Author Contribution

I hereby declare that my contribution in the research article:

Rintz E, Celik B, Nidhi F, Herreño-Pachón AM, Khan S, Benincore-Flórez E, Tomatsu S. Adeno-associated virus-based gene therapy delivering combinations of two growth associated genes to MPS IVA mice. 2024. Molecular Therapy and Nucleic Acids. doi.org/10.1016/j.omtn.2024.102211

included:

- Experimental plan
- Animal handling – autopsies, blood collection, measurements, injections of the vector
- Enzyme assay performance and analysis of tissues and plasma
- Analysis and preparation of pathological slides
- ELISA performance and analysis of results
- Genome copy number experiment preparation and analysis
- Glycosaminoglycans level performance and analysis of results
- Micro-CT preparation and analysis of results
- Statistical analysis of all data included in the manuscript
- All Figures preparation and conceptualization
- Literature review
- Visualization of the manuscript
- Writing—original draft preparation
- Writing—participation in review and editing
- Preparation of the responses to the revision



Uniwersytet Gdański
Katedra Biologii Molekularnej
mgr Estera Rintz

Betul Celik
Nemours Hospital for Children
Wilmington, DE
United States

Wilmington, 10 May 2024

Author Contributions

I hereby declare that my contribution in the research article:

Rintz E, Celik B, Nidhi F, Herreño-Pachón AM, Khan S, Benincore-Flórez E, Tomatsu S. Adeno-associated virus-based gene therapy delivering combinations of two growth associated genes to MPS IVA mice. 2024. Molecular Therapy and Nucleic Acids. doi.org/10.1016/j.omtn.2024.102211

included:

- Participating in the Experimental plan preparation
- Participating in the Enzyme assay performance
- Participating in the Pathology slides evaluation
- Participating in the Animal handling – taking part in autopsies, blood collection, injections



Signature

Angelica Maria Herreño-Pachón
Nemours Hospital for Children
Wilmington, DE
United States

Wilmington, 10 May 2024

Author Contributions

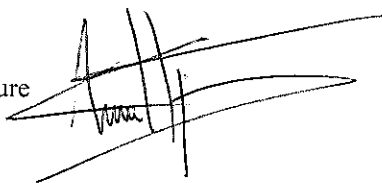
I hereby declare that my contribution in the research article:

Rintz E, Celik B, Nidhi F, Herreño-Pachón AM, Khan S, Benincore-Flórez E, Tomatsu S. Adeno-associated virus-based gene therapy delivering combinations of two growth associated genes to MPS IVA mice. 2024. Molecular Therapy and Nucleic Acids. doi.org/10.1016/j.omtn.2024.102211

included:

- Participating in the Animal handling – taking part in autopsies, blood collection

Signature

A handwritten signature in black ink, appearing to be 'A. Herreño-Pachón', written over a set of horizontal lines. The signature is stylized and somewhat obscured by the lines.

Shaukat Khan
Nemours Hospital for Children
Wilmington, DE
United States

Wilmington, 10 May 2024

Author Contributions

I hereby declare that my contribution in the research article:

Rintz E, Celik B, Nidhi F, Herreño-Pachón AM, Khan S, Benincore-Flórez E, Tomatsu S. Adeno-associated virus-based gene therapy delivering combinations of two growth associated genes to MPS IVA mice. 2024. *Molecular Therapy and Nucleic Acids*. doi.org/10.1016/j.omtn.2024.102211

included:

- Performing LC/MS/MS analysis

Shaukat Ali Khan.

Signature

Eliana Benincore-Flórez
Nemours Hospital for Children
Wilmington, DE
United States

Wilmington, 10 May 2024

Author Contributions

I hereby declare that my contribution in the research article:

Rintz E, Celik B, Nidhi F, Herreño-Pachón AM, Khan S, Benincore-Flórez E, Tomatsu S. Adeno-associated virus-based gene therapy delivering combinations of two growth associated genes to MPS IVA mice. 2024. *Molecular Therapy and Nucleic Acids*. doi.org/10.1016/j.omtn.2024.102211

included:

- Participating in the analysis of pathology slides

Signature

A handwritten signature in black ink, reading "Eliana Benincore-Flórez". The signature is written in a cursive style with a large initial 'E' and a long, sweeping underline.

Name, Surname: Shunji Tomatsu, MD PhD
Institution name: Nemours Children's Health
City: Wilmington, DE
Country: USA

Wilmington, May.13.2024

Author Contributions

I hereby declare that my contribution in the research article:

Rintz E, Celik B, Nidhi F, Herreño-Pachón AM, Khan S, Benincore-Flórez E, Tomatsu S. Adeno-associated virus-based gene therapy delivering combinations of two growth associated genes to MPS IVA mice. 2024. Molecular Therapy and Nucleic Acids. doi.org/10.1016/j.omtn.2024.102211

included:

- Conceptualization of the project
- Writing—review and editing
- Supervision and administration of the project
- Pathology scoring
- Funding acquisition
- Submission of the final version of the manuscript
- Handling manuscript as corresponding author
- Preparation of the responses to the revision

Signature: Shunji Tomatsu MD PhD

A handwritten signature in black ink, consisting of a series of loops and a long horizontal stroke extending to the right.

Funding

1. Project title: “Mechanizm degradacji glikozoaminoglikanów pod wpływem resweratrolu w mysim modelu neuronopatycznej choroby z grupy mukopolisacharydoz” (2019/35/N/NZ2/00505) financed by National Science Center in Poland in PRELUDIUM 18 program (210 000zł). Primary Investigator: Estera Rintz
2. Project title: „” financed by Sanfilippo Foundation (35 000zł) Primary Investigator: Professor Grzegorz Węgrzyn
3. Austrian MPS society, A Cure for Robert, Inc., The Carol Ann Foundation, Angelo R. Cali & Mary V. Cali Family Foundation, Inc., The Vain and Harry Fish Foundation, Inc., The Bennett Foundation, Jacob Randall Foundation, and Nemours Funds. S.T. was supported by an Institutional Development Award from the Eunice Kennedy Shriver National Institute of Child Health & Human Development of the National Institutes of Health (NICHD) (1R01HD102545-01A1).

Academic achievements

Scientific articles

1. **Rintz, E.**, Banacki, M., Ziemian, M., Kobus, B., and G. Wegrzyn. "Causes of Death in Mucopolysaccharidoses." *Molecular Genetics and Metabolism*, vol. 142, no. 3, 2024, article 108507, doi:10.1016/j.ymgme.2024.108507.
2. Cyske, Z., Gaffke, L., **Rintz, E.**, Wiśniewska, K., Wegrzyn, G., and K. Pierzynowska. "Molecular Mechanisms of the Ambroxol Action in Gaucher Disease and GBA1 Mutation-Associated Parkinson Disease." *Neurochemistry International*, 24 May 2024, article 105774, doi:10.1016/j.neuint.2024.105774.
3. **Rintz, E.**, Celik, B., Nidhi, F., Herreño-Pachón, A. M., Khan, S., Benincore-Flórez, E., and S. Tomatsu. "Adeno-Associated Virus-Based Gene Therapy Delivering Combinations of Two Growth Associated Genes to MPS IVA Mice." *Molecular Therapy and Nucleic Acids*, 2024, doi:10.1016/j.omtn.2024.102211.
4. Ago, Y., **Rintz, E.**, Musini, K. S., Ma, Z., and S. Tomatsu. "Molecular Mechanisms in Pathophysiology of Mucopolysaccharidosis and Prospects for Innovative Therapy." *International Journal of Molecular Sciences*, vol. 25, no. 3, 2024.
5. Bębnowska, D., Hryniewicz, R., Wiśniewska, K., Żabińska, M., **Rintz, E.**, Pierzynowska, K., and P. Niedźwiedzka-Rystwej. "Apoptosis Activation During Lagovirus Europaeus/GI.2 Infection in Rabbits." *Frontiers in Microbiology*, vol. 14, 2024.
6. Gaffke, L., **Rintz, E.**, Pierzynowska, K., and G. Wegrzyn. "Actin Cytoskeleton Polymerization and Focal Adhesion as Important Factors in the Pathomechanism and Potential Targets of Mucopolysaccharidosis Treatment." *Cells*, vol. 12, no. 13, 2023.
7. Gaffke, L., Firyn, N., **Rintz, E.**, Pierzynowska, K., Piotrowska, E., Mazur-Marzec, H., and G. Wegrzyn. "Therapeutic Potential of Lithium Chloride and Valproic Acid Against Neuronopathic Types of Mucopolysaccharidoses Through Induction of the Autophagy Process." *Archives of Biochemistry and Biophysics*, vol. 747, 2023.
8. Kujawa, M. J., Pierzynowska, K., Gaffke, L., Cyske, Z., **Rintz, E.**, Rąbalski, Ł., Kosiński, M., Wegrzyn, G., Mański, A., and P. Anikiej-Wiczenbach. "Clinical Presentation of 13 Children with Alkaptonuria." *Journal of Inherited Metabolic Disease*, vol. 46, no. 5, 2023, pp. 916-930.
9. Leal, A. F., Inci Orhan, K., Seyrantepe, V., **Rintz, E.**, Celik, B., Ago, Y., León, D., Suarez Diego, A., Alméciga-Díaz, C. J., and S. Tomatsu. "Molecular Trojan Horses for

- Treating Lysosomal Storage Diseases." *Molecular Genetics and Metabolism*, vol. 140, no. 3, 2023, article 107648, pp. 1-11.
10. Leal, A. F., Benincore-Flórez, E., **Rintz, E.**, Herreño-Pachón, A. M., Celik, B., Ago, Y., Alméciga-Díaz, C. J., and S. Tomatsu. "Mucopolysaccharidoses: Cellular Consequences of Glycosaminoglycans Accumulation and Potential Targets." *International Journal of Molecular Sciences*, vol. 24, no. 1, 2023, pp. 1-21.
 11. Pierzynowska, K., Gaffke, L., Żabińska, M., Cyske, Z., **Rintz, E.**, Wiśniewska, K., Podlacha, M., and G. Wegrzyn. "Roles of the Oxytocin Receptor (OXTR) in Human Diseases." *International Journal of Molecular Sciences*, vol. 24, no. 4, 2023, pp. 1-21.
 12. **Rintz, E.**, Podlacha, M., Cyske, Z., Pierzynowska, K., Wegrzyn, G., and L. Gaffke. "Activities of (Poly)Phenolic Antioxidants and Other Natural Autophagy Modulators in the Treatment of Sanfilippo Disease: Remarkable Efficacy of Resveratrol in Cellular and Animal Models." *Neurotherapeutics*, vol. 20, 2023, pp. 254-271.
 13. **Rintz, E.**, Herreño-Pachón, A. M., Celik, B., Nidhi, F., Khan, S., Benincore-Flórez, E., and S. Tomatsu. "Bone Growth Induction in Mucopolysaccharidosis IVA Mouse." *International Journal of Molecular Sciences*, vol. 24, no. 12, 2023, pp. 1-17.
 14. Żabińska, M., Gaffke, L., Bielańska, P., Podlacha, M., **Rintz, E.**, Cyske, Z., Wegrzyn, G., and K. Pierzynowska. "Decreased Levels of Chaperones in Mucopolysaccharidoses and Their Elevation as a Putative Auxiliary Therapeutic Approach." *Pharmaceutics*, vol. 15, no. 2, 2023, pp. 1-18.
 15. Pierzynowska, K., Podlacha, M., Gaffke, L., **Rintz, E.**, Wiśniewska, K., Cyske, Z., and G. Wegrzyn. "Correction of Symptoms of Huntington Disease by Genistein Through FOXO3-Mediated Autophagy Stimulation." *Autophagy*, online first, 2023.
 16. Gaffke, L., Szczudło, Z., Podlacha, M., Cyske, Z., **Rintz, E.**, Mantej, J., Krzelowska, K., Wegrzyn, G., and K. Pierzynowska. "Impaired Ion Homeostasis as a Possible Associate Factor in Mucopolysaccharidosis Pathogenesis: Transcriptomic, Cellular and Animal Studies." *Metabolic Brain Disease*, vol. 37, no. 2, 2022, pp. 299-310.
 17. Kosznik-Kwaśnicka, K., Podlacha, M., Grabowski, Ł., Stasiłojć, M., Nowak-Zaleska, A., Ciemińska, K., Cyske, Z., Dydecka, A., Gaffke, L., Mantej, J., Myślińska, D., Necel, A., Pierzynowska, K., Piotrowska, E., Radzanowska-Alenowicz, E., **Rintz, E.**, Sitko, K., and G. Wegrzyn. "Biological Aspects of Phage Therapy Versus Antibiotics Against *Salmonella Enterica* Serovar Typhimurium Infection of Chickens." *Frontiers in Cellular and Infection Microbiology*, 4 Aug. 2022, article 941867, doi:10.3389/fcimb.2022.941867.

18. **Rintz, E.**, Wegrzyn, G., Fujii, T., and S. Tomatsu. "Molecular Mechanism of Induction of Bone Growth by the C-Type Natriuretic Peptide." *International Journal of Molecular Sciences*, vol. 23, no. 11, 2022, article 5916, pp. 1-19.
19. **Rintz, E.**, Higuchi, T., Kobayashi, H., Galileo, D. S., Wegrzyn, G., and S. Tomatsu. "Promoter Considerations in the Design of Lentiviral Vectors for Use in Treating Lysosomal Storage Diseases." *Molecular Therapy-Methods & Clinical Development*, vol. 24, 2022, pp. 71-87.
20. Brokowska, J., Pierzynowska, K., Gaffke, L., **Rintz, E.**, and G. Wegrzyn. "Expression of Genes Involved in Apoptosis is Dysregulated in Mucopolysaccharidoses as Revealed by Pilot Transcriptomic Analyses." *Cell Biology International*, vol. 45, no. 7, 2021, pp. 1546-1557.
21. Gaffke, L., Pierzynowska, K., **Rintz, E.**, Cyske, Z., Giecewicz, I., and G. Wegrzyn. "Gene Expression-Related Changes in Morphologies of Organelles and Cellular Component Organization in Mucopolysaccharidoses." *International Journal of Molecular Sciences*, vol. 22, no. 5, 2021.
22. Pierzynowska, K., **Rintz, E.**, Gaffke, L., and G. Wegrzyn. "Ferroptosis and Its Modulation by Autophagy in Light of the Pathogenesis of Lysosomal Storage Diseases." *Cells*, vol. 10, no. 2, 2021.
23. Pierzynowska, K., Podlacha, M., Łuszczek, D., **Rintz, E.**, Gaffke, L., Szczudło, Z., Tomczyk, M., Smoleński, R. T., and G. Wegrzyn. "Hair Dymorphology in the R6/1 and R6/2 Mouse Models of Huntington's Disease." *Gene*, vol. 765, 2021, pp. 1-7.
24. Pierzynowska, K., Cyske, Z., Gaffke, L., **Rintz, E.**, Mantej, J., Podlacha, M., Wiśniewska, K., Żabińska, M., Sochocka, M., and P. Lorenc. "Potencjał Autofagii Indukowanej Przez Genisteinę w Leczeniu Chorób Neurodegeneracyjnych." *Postępy Biochemii*, vol. 67, no. 2, 2021, pp. 117-129.
25. Amendum, P. C., Khan, S., Yamaguchi, S., Kobayashi, H., Ago, Y., Suzuki, Y., Celik, B., **Rintz, E.**, Hossain, J., Xiao, W., and S. Tomatsu. "Glycosaminoglycans as Biomarkers for Mucopolysaccharidoses and Other Disorders." *Diagnostics (Basel)*, vol. 11, no. 9, 2021, article 1563.
26. Gaffke, L., Pierzynowska, K., Podlacha, M., Hoinkis, D., **Rintz, E.**, Brokowska, J., Cyske, Z., and G. Wegrzyn. "Underestimated Aspect of Mucopolysaccharidosis Pathogenesis: Global Changes in Cellular Processes Revealed by Transcriptomic Studies." *International Journal of Molecular Sciences*, vol. 21, no. 4, 2020, pp. 1-19.

27. Hać, A., Brokowska, J., **Rintz, E.**, Bartkowski, M., Wegrzyn, G., and A. Herman-Antosiewicz. "Mechanism of Selective Anticancer Activity of Isothiocyanates Relies on Differences in DNA Damage Repair Between Cancer and Healthy Cells." *European Journal of Nutrition*, vol. 59, no. 4, 2020, pp. 1421-1432.
28. Krause, K., Maciąg-Dorszyńska, M., Wosinski, A., Gaffke, L., Morcinek-Orłowska, J., **Rintz, E.**, Bielańska, P., Szalewska-Pałasz, A., Muskhelishvili, G., and G. Wegrzyn. "The Role of Metabolites in the Link Between DNA Replication and Central Carbon Metabolism in Escherichia Coli." *Genes*, vol. 11, no. 4, 2020, pp. 1-13.
29. Pierzynowska, K., Gaffke, L., Jankowska, E., **Rintz, E.**, Witkowska, J., Wiczerzak, E., Podlacha, M., and G. Wegrzyn. "Proteasome Composition and Activity Changes in Cultured Fibroblasts Derived from Mucopolysaccharidoses Patients and Their Modulation by Genistein." *Frontiers in Cellular and Developmental Biology*, vol. 8, 2020.
30. **Rintz, E.**, Pierzynowska, K., Podlacha, M., and G. Wegrzyn. "Has Resveratrol a Potential for Mucopolysaccharidosis Treatment?" *European Journal of Pharmacology*, vol. 888, 2020, pp. 1-10.
31. **Rintz, E.**, Gaffke, L., Podlacha, M., Brokowska, J., Cyske, Z., Wegrzyn, G., and K. Pierzynowska. "Transcriptomic Changes Related to Cellular Processes with Particular Emphasis on Cell Activation in Lysosomal Storage Diseases from the Group of Mucopolysaccharidoses." *International Journal of Molecular Sciences*, vol. 21, no. 9, 2020.
32. Pierzynowska, K., Gaffke, L., Cyske, Z., Puchalski, M., **Rintz, E.**, Bartkowski, M., Osiadły, M., Pierzynowski, M., and J. Mantej. "Autophagy Stimulation as a Promising Approach in Treatment of Neurodegenerative Diseases." *Metabolic Brain Disease*, vol. 33, no. 4, 2018, pp. 989-1008.
33. Pierzynowska, K., Podlacha, M., Brokowska, J., Gaffke, L., Mantej, J., Cyske, Z., **Rintz, E.**, Osiadły, M., and M. Bartkowski. "Molecular Mechanisms of Genistein Action in the Light of Therapies for Genetic and Immunological Diseases." *Postępy Biochemii*, vol. 64, no. 4, 2018, pp. 262-275.

Book chapters

1. Gaffke L., Pierzynowska K., Cyske Z., **Rintz E.**, Podlacha M., Mincewicz G., Węgrzyn G.: Hopes and disappointments related to the use of flavonoids in therapeutical approaches, W: Modulation of oxidative stress: biochemical, physiological and pharmacological aspects / Saso Luciano [i in.] (red.), 2023, Academic Press, ISBN 978-0-443-19247-0, s. 199-210, 50 punktów
2. **Rintz E.**, Gaffke L., Pierzynowska K., Podlacha M., Mantej J., Bednarek M., Cyske Z., Bałuch M., Bielańska P., Bilak A.: Genistein - a natural antioxidant and its use in treatment of various diseases, W: Bentham briefs in biomedicine and pharmacotherapy: oxidative stress and natural antioxidants / Kaur Pardeep [i in.] (red.), vol. 1, 2021, Bentham Science Publishers, ISBN 978-981-4998-88-8, s. 397-420, łączna liczba autorów: 12, 5 punktów
3. Pierzynowska K., **Rintz E.**, Gaffke L., Cyske Z., Podlacha M., Brokowska J., Węgrzyn G.: Mucopolysaccharidosis Type III (Sanfilippo Disease) subtypes A, B, C, D: molecular mechanism and therapeutic effect, W: Neurochemistry of metabolic diseases: lysosomal storage diseases, Phenylketonuria, and Canavan disease / Surendran Sankar (red.), 2020, NOVA Science Publishers, ISBN 978-1-53618-339-9, s. 51-101

Scientific Congress

1. Celik B., Rintz E., Nidhi F., Khan S., Tomatsu S.: Ex vivo lentiviral gene therapy for mucopolysaccharidosis type IVA, 2024, 20th Annual WORLDSymposium™ 2024, referat wygłoszony
2. Gaffke L., **Rintz E.**, Pierzynowska K., Węgrzyn G.: Actin cytoskeleton polymerization and focal adhesion as important factors in the pathomechanism and potential targets of mucopolysaccharidosis treatment, 2024, 20th Annual WORLDSymposium™ 2024, referat wygłoszony
3. **Rintz E.**, Gaffke L., Podlacha M., Pierzynowska K., Węgrzyn G.: Insights into the molecular basis of resveratrol-induced autophagy in a mouse model of sanfilippo syndrome type III B, 2024, 17th International Symposium on Mucopolysaccharidoses and Related Diseases 2024, referat wygłoszony

4. **Rintz E.**, Gaffke L., Podlacha M., Pierzynowska K., Węgrzyn G.: Molecular mechanism of resveratrol-induced autophagy in mouse model of Sanfilippo syndrome type IIIB, 2024, 20th Annual WORLDSymposium™ 2024, referat wygłoszony
5. **Rintz E.**, Gaffke L., Podlacha M., Pierzynowska K., Węgrzyn G. Resweratrol - naturalny induktor procesu autofagii w mysim modelu choroby rzadkiej, 2024, IX Ogólnopolska konferencja biologii molekularnej, referat wygłoszony
6. Węgrzyn G., **Rintz E.**, Podlacha M., Gaffke L., Wiśniewska K., Cyske Z., Pierzynowska K.: Therapeutic potential of foxo3-dependent stimulation of autophagy by 3,5,4'- trihydroxystilbene (resveratrol) or 4',5,7-trihydroxyisoflavone (genistein) in mucopolysaccharidosis type iiib and huntington disease, 2024, 17th International Symposium on Mucopolysaccharidoses and Related Diseases
7. Celik B., **Rintz E.**, Nidhi F., Khan S., Tomatsu S.: Lentiviral gene therapy for mucopolysaccharidosis type IVA, 2023, 19th Annual WORLDSymposium™ 2023, referat wygłoszony
8. Pierzynowska K., Podlacha M., Gaffke L., **Rintz E.**, Wiśniewska K., Cyske Z., Węgrzyn G.: Correction of symptoms of Huntington disease in the mouse R6/1 model by genistein through the FOXO3-mediated autophagy stimulation , 2023, 5th Congress of Polish Biosciences "Different faces of biosciences" 2023, referat wygłoszony
9. Pierzynowska K., Podlacha M., Gaffke L., **Rintz E.**, Wiśniewska K., Cyske Z., Węgrzyn G.: Stymulacja autofagii koryguje odkładanie się agregatów białkowych oraz objawy choroby Huntingtona w modelach komórkowych i zwierzęcych, 2023, XI Zjazd Polskiego Towarzystwa Genetyki Człowieka 2023, referat wygłoszony
10. Grabowski Ł., Podlacha M., **Rintz E.**, Mantej J., Myślińska D., Nowak-Zaleska A., Gaffke L., Pierzynowska K., Piotrowska E., Cyske Z.: The effect of phage therapy on the level of immunological parameters in the chicken model, 2022, Viruses of Microbes Conference 2022, poster
11. Kosznik-Kwaśnicka K., Ciemińska K., Nowak-Zaleska A., Podlacha M., Myślińska D., Pierzynowska K., Cyske Z., Gaffke L., **Rintz E.**, Mantej J.: The story of a phage cocktail: effectiveness of phage cocktail against S. Typhimurium on in vitro and in vivo models, 2022, Viruses of Microbes Conference 2022, poster
12. **Rintz E.**, Celik B., Khan S., Węgrzyn G., Tomatsu S.: Adeno-associated virus vector combination genetherapy with C-type natriuretic peptide and GALNSenzyme in Mucopolysaccharidosis IVA mousemodel, 2022, ESGCT 29th Annual Congress In collaboration with BSGCT 2022, referat wygłoszony

13. Podlacha M., **Rintz E.**, Pierzynowska K., Węgrzyn G.: Therapeutic effects of genistein on cognitive abnormalities in Huntington's disease, 2019, 17th International Conference on Rare Diseases "Don't miss a rare disease" 2019, referat wygłoszony
14. **Rintz E.**, Podlacha M., Węgrzyn G., Pierzynowska K.: A new look at treatment of Huntington's disease - therapy with the use of genistein, 2019, 17th International Conference on Rare Diseases "Don't miss a rare disease" 2019, referat wygłoszony
15. **Rintz E.**, Podlacha M., Pierzynowska K., Węgrzyn G.: The effect of genistein on anxiety related behaviors in R6 / 1 mice constituting genetically modified model of Huntington's disease, 2019, IV International Sopot Youth Conference "Where the World is heading?" 2019, referat wygłoszony
16. Węgrzyn G., Pierzynowska K., Gaffke L., Lopez-Lugo S., Cyske Z., **Rintz E.**, Pankanin D.: Genistein-mediated correction of differential defects in the cytoskeleton in cellular models of various neurodegenerative diseases, 2018, 18th European Congress On Biotechnology 2018, referat wygłoszony
17. **Rintz E.**, Podlacha M., Wrona D., Węgrzyn G.: Pobudzenie receptorów NMDA jądra przysiódkowej przegrody a reakcja neuro-immunologiczna u szczurów o odmiennej wrażliwości na stres, 2018, II Konferencja Doktorantów Pomorza "BioMed Session" 2018, poster

Research projects as a Primary Investigator

1. Project title: "Mechanizm degradacji glikozoaminoglikanów pod wpływem resweratrolu w mysim modelu neuronopatycznej choroby z grupy mukopolisacharydoz" (2019/35/N/NZ2/00505) financed by National Science Center in Poland in PRELUDIUM 18 program (210 000zł)
2. Project title: "Kombinowana terapia enzymatyczna z resweratrolem w komórkowym modelu MPS I" (533-0C20-GS17-23) financed by University of Gdansk in UGrants START 2023 program (20 000zł)
3. Project title: "Korelacja pomiędzy aktywacją autofagii a odpowiedzią immunologiczną w Mukopolisacharydozie typu IIIB" (533-0C20-GS54-24) financed by University of Gdansk in UGrants START 2024 program (20 000zł)